frontiers | Research Topics

Applied ‘model’ organisms in industrial biotechnology

Edited by
Zhi-Qiang Liu, Xiao-Jun Ji and Panagiotis Madesis

Published in
Frontiers in Bioengineering and Biotechnology

ISSN 1664-8714
ISBN 978-2-8325-2343-8
DOI 10.3389/978-2-8325-2343-8

About Frontiers

Frontiers is more than just an open access publisher of scholarly articles: it is a pioneering approach to the world of academia, radically improving the way scholarly research is managed. The grand vision of Frontiers is a world where all people have an equal opportunity to seek, share and generate knowledge. Frontiers provides immediate and permanent online open access to all its publications, but this alone is not enough to realize our grand goals.

Frontiers journal series

The Frontiers journal series is a multi-tier and interdisciplinary set of open-access, online journals, promising a paradigm shift from the current review, selection and dissemination processes in academic publishing. All Frontiers journals are driven by researchers for researchers; therefore, they constitute a service to the scholarly community. At the same time, the *Frontiers journal series* operates on a revolutionary invention, the tiered publishing system, initially addressing specific communities of scholars, and gradually climbing up to broader public understanding, thus serving the interests of the lay society, too.

Dedication to quality

Each Frontiers article is a landmark of the highest quality, thanks to genuinely collaborative interactions between authors and review editors, who include some of the world's best academicians. Research must be certified by peers before entering a stream of knowledge that may eventually reach the public - and shape society; therefore, Frontiers only applies the most rigorous and unbiased reviews. Frontiers revolutionizes research publishing by freely delivering the most outstanding research, evaluated with no bias from both the academic and social point of view. By applying the most advanced information technologies, Frontiers is catapulting scholarly publishing into a new generation.

What are Frontiers Research Topics?

Frontiers Research Topics are very popular trademarks of the *Frontiers journals series*: they are collections of at least ten articles, all centered on a particular subject. With their unique mix of varied contributions from Original Research to Review Articles, Frontiers Research Topics unify the most influential researchers, the latest key findings and historical advances in a hot research area.

Find out more on how to host your own Frontiers Research Topic or contribute to one as an author by contacting the Frontiers editorial office: frontiersin.org/about/contact

Applied 'model' organisms in industrial biotechnology

Topic editors

Zhi-Qiang Liu — Zhejiang University of Technology, China

Xiao-Jun Ji — Nanjing Tech University, China

Panagiotis Madesis — University of Thessaly, Greece

Citation

Liu, Z.-Q., Ji, X.-J., Madesis, P., eds. (2023). *Applied 'model' organisms in industrial biotechnology*. Lausanne: Frontiers Media SA. doi: 10.3389/978-2-8325-2343-8

Table of contents

frontiers in Bioengineering and Biotechnology

ORIGINAL RESEARCH
published: 22 September 2021
doi: 10.3389/fbioe.2021.720473

Obtaining Cellulose-Available Raw Materials by Pretreatment of Common Agro-Forestry Residues With *Pleurotus* spp.

*Milica Galić, Mirjana Stajić *, Jelena Vukojević and Jasmina Ćilerdžić*

Faculty of Biology, University of Belgrade, Belgrade, Serbia

The goals of the present study were to characterize the profile of ligninolytic enzymes in five *Pleurotus* species and determine their ability to delignify eight common agro-forestry residues. Generally, corn stalks were the optimal inducer of Mn-dependent peroxidase activity, but the activity peak was noted after wheat straw fermentation by *P. eryngii* (3066.92 U/L). *P. florida* was the best producer of versatile peroxidase, especially on wheat straw (3028.41 U/L), while apple sawdust induced the highest level of laccase activity in *P. ostreatus* (49601.82 U/L). Efficiency of the studied enzymes was expressed in terms of substrate dry matter loss, which was more substrate-than species-dependent. Reduction of substrate dry mass ranged between 24.83% in wheat straw and 8.83% in plum sawdust as a result of fermentation with *P. florida* and *P. pulmonarius*, respectively. The extent of delignification of the studied substrates was different, ranging from 51.97% after wheat straw fermentation by *P. pulmonarius* to 4.18% in grapevine sawdust fermented by *P. ostreatus*. *P. pulmonarius* was also characterized by the highest cellulose enrichment (6.54) and *P. ostreatus* by very low one (1.55). The tested biomass is a highly abundant but underutilized source of numerous value-added products, and a cocktail of ligninolytic enzymes of *Pleurotus* spp. could be useful for its environmentally and economically friendly transformation.

Keywords: delignification, laccase, lignocellulose, Mn-oxidizing peroxidases, white-rot fungi

OPEN ACCESS

Edited by:
Zhi-Qiang Liu,
Zhejiang University of Technology, China

Reviewed by:
Helena P. Felgueiras,
University of Minho, Portugal
Tomer Meir Salame,
Weizmann Institute of Science, Israel

****Correspondence:***
Mirjana Stajić
stajicm@bio.bg.ac.rs

Specialty section:
This article was submitted to Industrial Biotechnology, a section of the journal Frontiers in Bioengineering and Biotechnology

Received: *04 June 2021*
Accepted: *13 September 2021*
Published: *22 September 2021*

Citation:
Galić M, Stajić M, Vukojević J and Ćilerdžić J (2021) Obtaining Cellulose-Available Raw Materials by Pretreatment of Common Agro-Forestry Residues With Pleurotus *spp. Front. Bioeng. Biotechnol. 9:720473. doi: 10.3389/fbioe.2021.720473*

INTRODUCTION

Lignocellulose accounts for about 60% of the total biomass on Earth and presents promising raw material for various industrial processes, such as production of bioethanol, paper, feed, food and numerous other value-added products (Stajić et al., 2009; Rastogi and Shrivastava, 2017). However, its complex chemical structure makes its utilization extremely demanding (Bilal et al., 2017). The most challenging phase in its transformation is removal of lignin, i.e., release of cellulose and hemicellulose for subsequent enzymatic hydrolysis. Lignin is a most recalcitrant natural compound, whose physical and chemical mineralization is neither ecologically nor economically justified. Therefore, the development of biological pretreatment systems represents the current trend in biotechnology (Meehnian et al., 2017). Owing to their well developed enzymatic system, fungi are a highly effective biofactory for lignocellulose conversion to cellulose-available resources. An enzyme cocktail composed of laccases, peroxidases and numerous auxiliary enzymes, makes white-rot mushrooms the most efficient delignifiers and potential participants in numerous biotechnological

TABLE 1 | Studied *Pleurotus* species.

Species	Code	Origin
Pleurotus eryngii	HAI 193	Ukraine, Kherson Region, Chaplinka district, Askania-Nova on *Stipa* sp
Pleurotus florida	HAI 217	United States , Florida
Pleurotus ostreatus	HAI 1105	Israel, Golan Heights, Massada, on *Quercus calliprinos*
Pleurotus pulmonarius	HAI 573	Russia, Sochi
Pleurotus salignus	HAI 326	Israel, Dan Natural Reserve, Tel Dan, on *Salix* sp

processes (Stajić et al., 2009; Knežević et al., 2014; Rudakiya and Gupte, 2017). However, despite numerous studies conducted during the past few decades, there is still a need for finding the most selective lignin remover, i.e., the species whose activity will retain the cellulose intact. It is well known that species of the genus *Pleurotus* are among the most efficient and selective mineralizators of lignin in agriculture residues (Stajić et al., 2004, 2006; Dong et al., 2013; Singh and Singh, 2014; Aditiya et al., 2016; Mustafa et al., 2016; Bilal et al., 2017; Fang et al., 2018; Matrínez-Patiño et al., 2018; Alfaro et al., 2020; de Souza et al., 2020). Their remarkable degradation ability is primarily based on the synthesis of numerous highly active laccase isoforms (Martínez et al., 1994; Muñoz et al., 1997; Ćilerdžić et al., 2017). However, the number and activity of secreted isoforms are not only genetically defined, but also depend on substrate type and composition.

Wheat straw and corn stalks are the main lignocellulosics bioconverted to ethanol in Europe and North America, respectively. However, numerous other agro-forestry residues remain unexploited and present serious environmental burdens in numerous regions of the world (Ghaffar et al., 2015). Thus, in many agricultural countries, enormous amounts of cuttings from fruit production remain as environmental ballast. According to data of the Food and Agricultural Organization from 2017, apple and plum were cultures with high annual yields in the European Union (10,106,442 and 1,292,856 metric tons (t), respectively), while Italy and France were the main grape producers, with 7,169,745 and 5,915,882 t, respectively. Serbia was the leader in blackberry production in Europe (27,558 t), the fourth leading world producer of raspberry (68,500 t) and a considerable producer of apple (378,644 t), plum (330,582 t) and grape (165,568 t) in 2013. The mentioned fruit quantities are good indicators of the amount of biomass whose main part remains unused. Additionally, some of them have not yet been studied as substrates for fungal cultivation and raw materials for many industries.

Based on the presented facts, the goals of the study were to characterize the profiles of ligninolytic enzymes in five *Pleurotus* species and determine their ability to delignify eight common but unexploited agro-forestry residues.

MATERIALS AND METHODS

Organisms and Growth Conditions

Cultures of the studied *Pleurotus* spp. were obtained from the Institute of Evolution, University of Haifa, Israel (HAI) and are maintained on malt agar medium in the culture collection of the Institute of Botany, Faculty of Biology, University of Belgrade. The cultures were obtained from fruiting bodies collected in different world regions (**Table 1**).

The inoculum was obtained by inoculation of synthetic medium (glucose, 10.0 g/L; NH_4NO_3, 2.0 g/L; K_2HPO_4, 1.0 g/L; NaH_2PO_4 x H_2O, 0.4 g/L; $MgSO_4$ x $7H_2O$, 0.5 g/L; yeast extract, 2.0 g/L; pH 6.5) with mycelium of 7-day-old culture, grown at room temperature on a rotary shaker for 7 days, washing of harvested biomass with sterile distilled water (dH_2O) and its homogenization with dH_2O in a laboratory blender (Stajić et al., 2010).

Solid-state cultivation was carried out during 21 days at 25°C, in the dark, in 250 ml flasks containing 6.0 g of tested plant residues (wheat straw, corn stalks and sawdust of oak, grapevine, blackberry, raspberry, plum and apple) as the carbon source and 30.0 ml of modified synthetic medium (without glucose) to reach a relative humidity of approximately 83%andinoculated with 3.0 ml of prepared inoculum.

The control samples contained medium that was not inoculated but was treated in the same way as the inoculated samples and were used as a negative control for substrate depolymerization.

Assays of Enzyme Activity and Total Protein Production

Samples were harvested after 21 days of cultivation, and extracellular enzymes were extracted by stirring samples with 50.0 ml dH_2O on a magnetic stirrer at 4°C for 10 min. The extracts were centrifuged (at 4°C and 3000 rpm for 15 min), and the resulting supernatants were used for spectrophotometric (BioQuest CECIL CE2501, United Kingdom) determination of the activities of Mn-oxidizing peroxidases [Mn-dependent peroxidase (MnP, EC 1.11.1.13) and versatile peroxidase (VP, EC 1.11.1.16)] and laccase (EC 1.10.3.2), as well as total protein content.

The activities of Mn-oxidizing peroxidases and laccases were determined according to the methods of Ćilerdžić et al. (2016) using 3 mm phenol red (ε_{610} = 22,000 M^{-1} cm^{-1}) and 2,2'-azino-bis-[3-ethyltiazoline-6-sulfonate] (ABTS) (ε_{436} = 29,300 M^{-1} cm^{-1}), respectively, as the highly specific substrates for these enzymes. Enzymatic activity was expressed in U/L, where activity of 1U representing the amount of enzyme that transforms 1 µmol of substrate per min.

Total protein content was determined according to Silva et al. (2005) using Bradford's reagent and bovine serum albumin as the standard and expressed in mg/ml. The obtained value was used to define the specific enzyme activity (U/mg).

Electrophoresis

Laccase isoforms of the studied *Pleurotus* species cultivated on tested substrates and their isoelectric points (pIs) were determined by isoelectric focusing (IEF) using a Mini IEF Cell 111 (Bio-Rad, United States). Isoelectric focusing was carried out in 7.5% polyacrylamide gel with 5.0% ampholyte on a pH gradient from 3 to 10. Bands were visualized after gel exposure to an ABTS/phosphate buffer (pH 5.0) mixture at room temperature. After completion of focusing, the gel was fixed in trichloroacetic acid, and protein bands were detected by staining with Coomassie Brilliant Blue (CBB) (Stajić et al., 2010). An IEF marker with a pI ranged from 3.6 to 9.3 (Sigma-Aldrich, United States) was used.

Defining the Amount of Lignocellulosic Polymers

The loss of substrate dry matter (%) was determined by the formula.

(Mi–Mf)/Mi x 100, where Mi represents the initial lignocellulosic mass and Mf is the mass after fermentation by the studied species.

Contents of hemicellulose, cellulose and lignin were measured by modified versions of the methods of Kirk and Obst (1988) and Van Soest et al. (1991). The samples were dried at a 60°C to the constant mass, ground and treated with neutral detergent/Na_2SO_3 mixture under refluxing conditions to remove soluble sugars, proteins, lipids and vitamins. The obtained biomass represented neutral detergent fibers (NDF). Acidic detergent fibers (ADF) were obtained by treating the obtained samples with an acidic detergent solution, and the difference between NDF and ADF represented the amount of hemicellulose. Lignin content (LC) was defined after incubation of the samples with 72% H_2SO_4 at 30°C and its hydrolysis at 120°C and expressed as percent of the quantity present in the initial sample. Cellulose content was calculated as the difference between ADF and LC.

The efficiency of lignin degradation was expressed as the cellulose enrichment, which represents the ratio between the remaining amounts of cellulose and lignin in treated samples.

Statistical Analyses

All experiments were done in three replicates and the results were expressed as mean ± standard error. Assaying significant differences between means was performed by one-way analysis of variance (ANOVA) and Tukey's test, using STATISTICA, version 6.0 (StatSoft, Inc., Tulsa, United States). Statistical significance was declared at $p < 0.05$.

RESULTS

Characterization of Ligninolytic Enzymes of *Pleurotus* spp.

The obtained results confirmed that Mn-oxidizing peroxidases and lacasse activities depend on the species of mushroom and type of substrate. To be specific, the studied *Pleurotus* species differed significantly among themselves in their potential for secretion of enzymes on the same substrate, but also each species showed considerable variability of enzymes activities on different substrates. Thus, *P. eryngii* HAI 193 was the best producer of highly active forms of MnP on most substrates except plum and apple sawdusts, while *P. ostreatus* HAI 1105 and *P. salignus* HAI 326 were the weakest MnP producers on almost all residues (**Figure 1**).

As for the effect of substrate type, maximal MnP activity in *P. eryngii* was measured after fermentation of wheat straw (3066.92 U/L), while this activity was slightly lower on corn stalks (2848.48 U/L) and lowest on apple sawdust (308.71 U/L). However, although the highest MnP activity was noted on wheat straw, corn stalks were the optimal inducer of enzyme production in all of the other studied species, i.e., this activity in them ranged between 1888.89 U/L and 2848.48 U/L (**Figure 1**).

A different picture was observed for VP. Thus, *P. florida* HAI 217 produced highly active VP isoforms on almost all of the tested substrates with the maximal activity on wheat straw, while the lowest activity was noted in *P. salignus* HAI 326 on apple sawdust. Wheat straw and corn stalks stood out as the best substrates for production of highly active VP isoforms, with peaks of 3028.41 U/L and 2905.30 U/L noted in *P. florida* and *P. salignus*, respectively (**Figure 2**). On the other hand, apple and blackberry sawdusts were the weakest stimulators of VP activity (60.61 U/L in *P. salignus* and 128.79 U/L in *P. ostreatus*, respectively).

In the case of laccase, even three species were good producers, *P. florida*, *P. salignus*, and especially *P. ostreatus*, in which the highest activity was noted. As for the effect of the studied substrates on the activity profile, it was absolutely contrary to the situation with MnP and VP. To be specific, the tested sawdusts were good stimulators, while wheat straw and corn stalks did not induce the synthesis of highly active laccase isoforms. Thus, the highest activity was obtained in apple sawdust fermentation by *P. ostreatus* (49601.82 U/L), although grapevine, oak and raspberry sawdusts also induced laccase activity of about 40000.00 U/L in many species. The lowest activity was observed after fermentation of corn stalks by *P. salignus* (1160.42 U/L), but it was also low after fermentation of wheat straw by *P. pulmonarius* and *P. salignus* (1262.80 U/L and 1433.45 U/L, respectively) (**Figure 3**).

Regarding the purity of the enzymes, the highest specific activities of MnP (3.73 U/mg), VP (3.62 U/mg) and laccase (229.50 U/mg) were noted in *P. salignus* cultivated on wheat straw, raspberry and apple sawdust, respectively (**Figures 1–3**).

Because it showed the highest production and activity, laccase was chosen for further characterization. The number, intensity and pI of visualized laccase isoforms on the same substrate varied among the studied species, but also differed for each species on various substrates (**Figure 4**). Thus, oak, grapevine, blackberry, raspberry and plum sawdusts induced synthesis of more numerous or/and more intensive isoforms in all of the studied species. However, it should be emphasized that the number and intensity of isoforms did not coincide with the measured activity in all species and on all substrates. Although *P. ostreatus* produced the most active laccase during apple sawdust fermentation, only one isoenzyme with pI about 3.6 was visualized (**Figure 4**). On the other hand, in *P. eryngii,* whose laccase activity was moderate, several isoforms with pIs of about

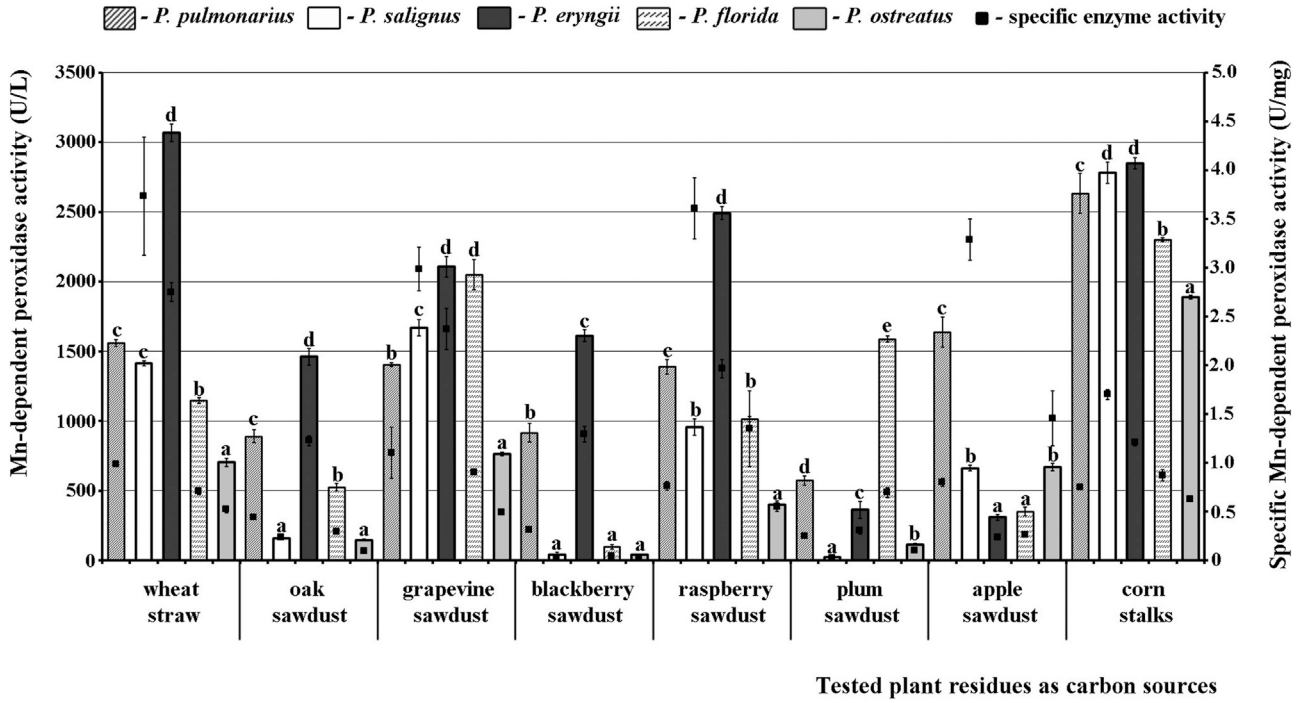

FIGURE 1 | Activity of Mn-dependent peroxidases of *Pleurotus* spp. depending on the type of agro-forestry residues. Values superscripted with the same letter in each values group (for each plant residue) are not significantly different ($p < 0.05$).

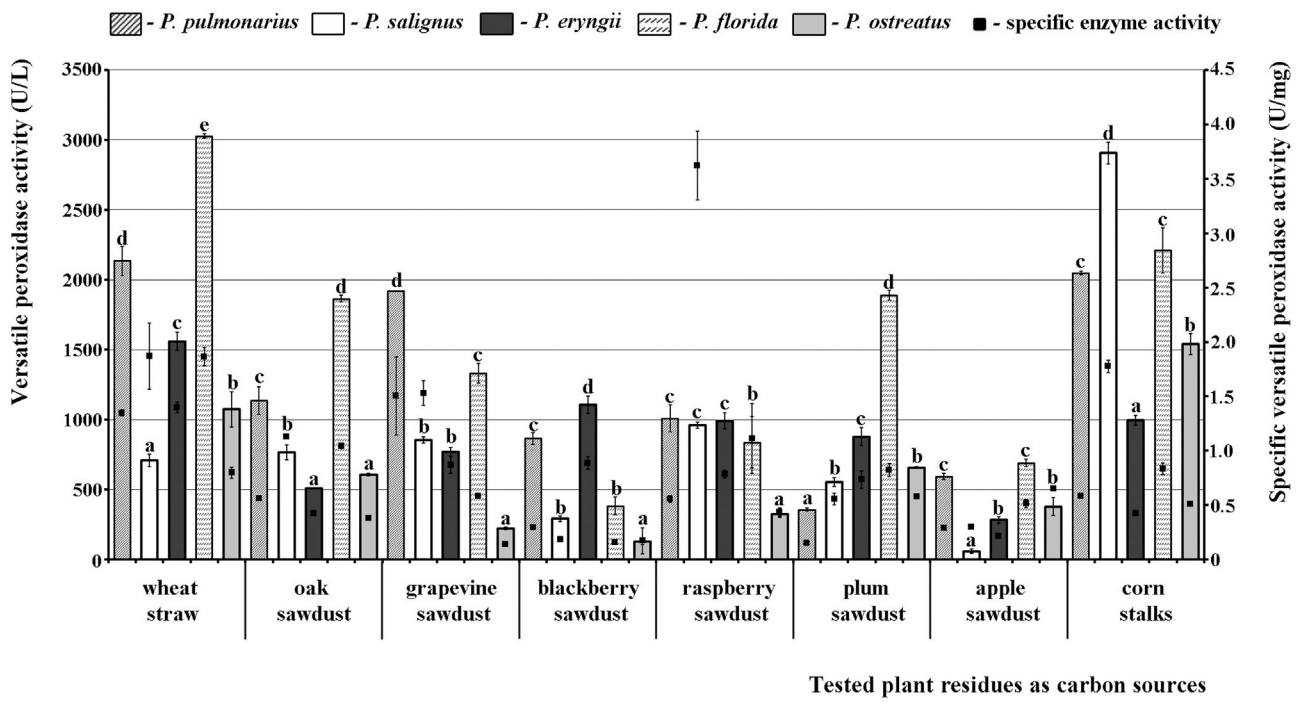

FIGURE 2 | Activity of versatile peroxidases of *Pleurotus* spp. depending on the type of agro-forestry residues. Values superscripted with the same letter in each values group (for each plant residue) are not significantly different ($p < 0.05$).

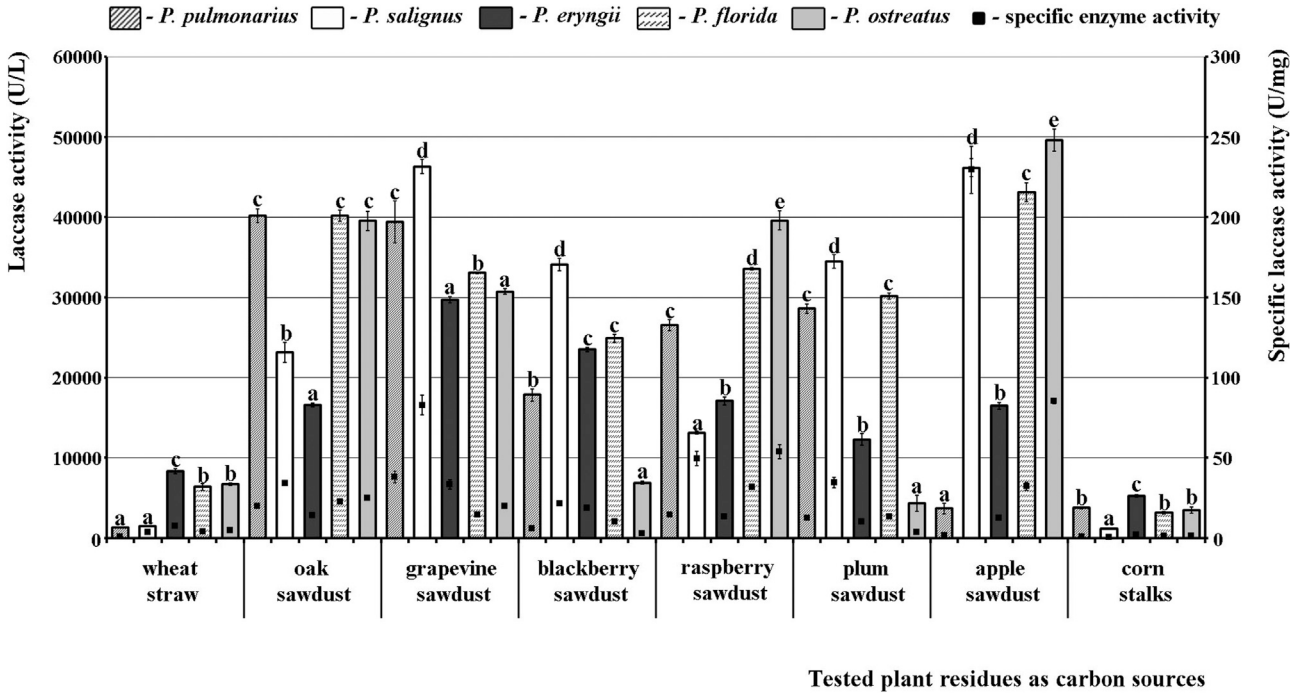

FIGURE 3 | Activity of laccases of *Pleurotus* spp. depending on the type of agro-forestry residues. Values superscripted with the same letter in each values group (for each plant residue) are not significantly different ($p < 0.05$).

3.6, 4.6 and 5.3 were visualized on all substrates except corn stalks, where *P. ostreatus* was dominant with respect to the number of isoforms, despite very low activity (**Figure 4**).

Degradation of Lignocellulosic Biomass

Generally, the percentage of dry matter loss was substrate- and species-dependent. Thus, the tested species showed significant differences in the capacity for reduction of the total dry mass of tested substrates (**Table 2**). The greatest loss of dry matter was noted for wheat straw, where the highest level of reduction (24.83%) was obtained in the case of *P. florida*. On the other hand, plum and oak sawdusts were the most resistant to the effect of *Pleurotus* spp. enzymes, and their dry matter losses were the lowest (8.83 and 9.67%, respectively, by *P. pulmonarius*). However, a low correlation between dry mass loss and MnP, VP and laccase activities was noted (R^2 = 0.06, 0.18 and 0.09, respectively).

The tested species varied with respect to the degree of lignin and cellulose degradation (**Table 2**). Thus, *P. pulmonarius* was the most effective degrader of wheat straw lignin (51.97%) and slightly weaker mineralizator of blackberry sawdust lignin (40.38%). Another member of the group of good degraders is *P. salignus*, which caused a 43.01%. reduction of lignin content in corn stalks-based substrate. On the other hand, grapevine sawdust was the most resistant to the studied ligninosomes, especially to *P. ostreatus* one, which degraded only 4.18% of this polymer. However, although *P. pulmonarius* and *P. salignus* were the best delignificators of the mentioned residues, the activities of their ligninolytic enzymes were not the highest at a given measurement point, which is confirmed by the correlation coefficients between the amount of decomposed lignin and the activity of MnP, VP and laccase (R^2 = 0.18, 0.26, 0.37, respectively), which could be explained by the dynamics of the synthesis of highly active forms of these enzymes.

Although the main aim of this study was to define the cultivation conditions for maximal lignin removal and cellulose preservation, it was found that the studied species degraded cellulose to a certain extent, depending on the substrate type. *Pleurotus florida*, *P. ostreatus* and *P. salignus* caused the maximal loss of cellulose in corn stalks (33.03, 30.33 and 29.85%, respectively), in contrast to oak sawdust, where *P. salignus* mineralized only 6.37% of cellulose (**Table 2**).

However, the degree of lignin and cellulose degradation is not a unique indicator of species and substrate applicability in various biotechnological processes. The main indicator is degradation selectivity, expressed as the ratio between remaining cellulose and lignin amounts, i.e., cellulose enrichment. Thus, the highest cellulose enrichment was noted in *P. pulmonarius* (6.54) which was the most effective degrader of wheat straw lignin but the weak mineralizator of its cellulose. On the other hand, *P. ostreatus* was the weakest delignifier of grapevine sawdust (4.18%), but good consumer of its cellulose which induced the low cellulose enrichment (1.55) (**Table 2**).

DISCUSSION

Lignocellulose-based biomass is an abundant and renewable resource for the production of bioethanol, paper, feed, food and

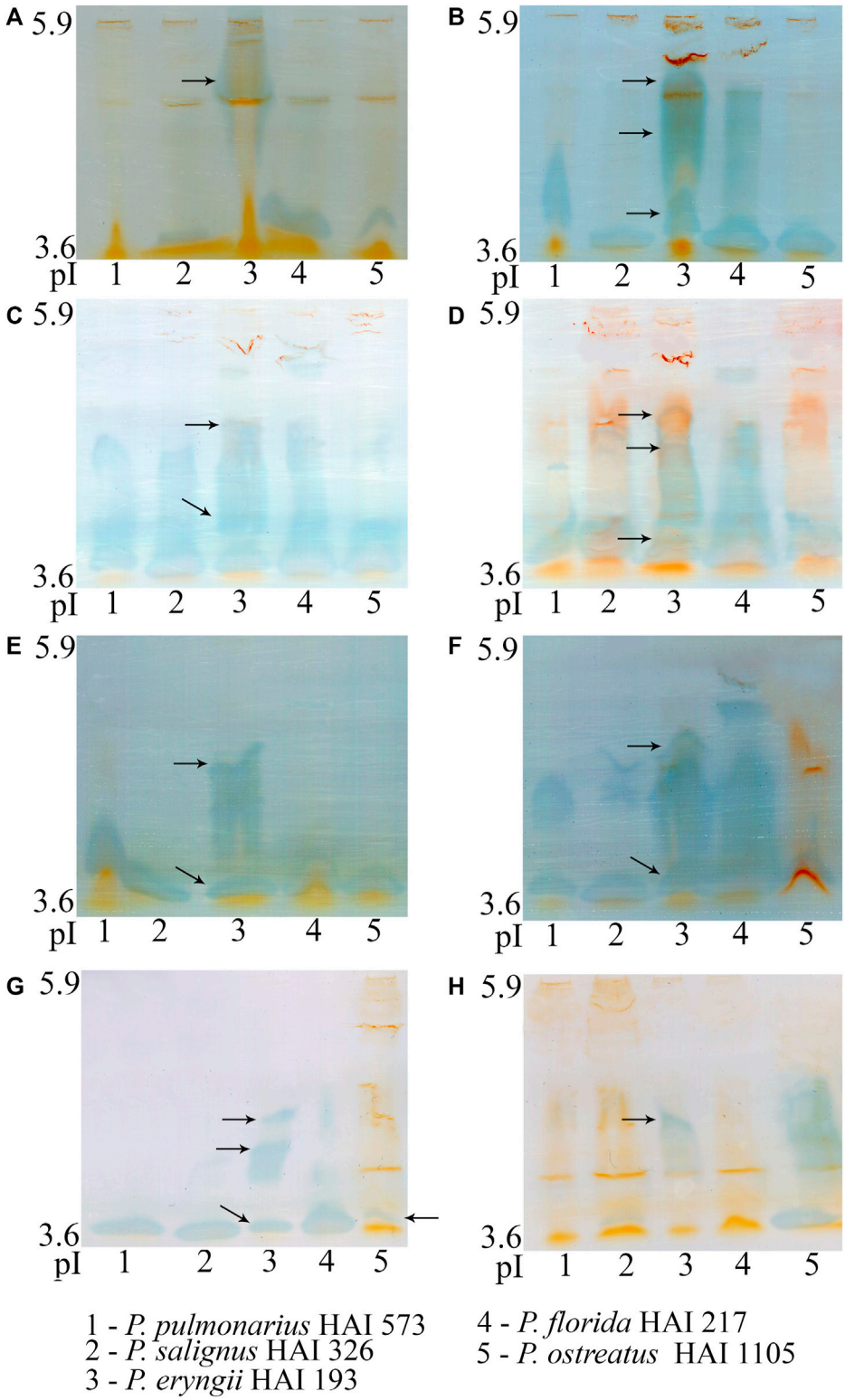

FIGURE 4 | Isoelectric focusing pattern of *Pleurotus* spp. laccases after 21 days of solid-state fermentation of wheat straw **(A)**, oak sawdust **(B)**, grapevine sawdust **(C)**, blackberry sawdust **(D)**, raspberry sawdust **(E)**, plum sawdust **(F)**, apple sawdust **(G)** and corn stalks **(H)**.

TABLE 2 | Extent of depolymerization of plant residues by *Pleurotus* spp.

Plant residue	Studied samples	Sample weight (g)	Fibres composition of samples (mg)			Dry matter loss (%)	Extent of polymers degradation (%)			Cellulose enrichment
			Lignin	Cellulose	Hemicellulose		Lignin	Cellulose	Hemicellulose	
Wheat straw	Control*	6.00	666.00	2418.00	1692.00	—	—	—	—	—
	P. pulmonarius	4.77	319.86	2091.01	1050.28	20.50^{d}	51.97^{d}	13.52^{c}	37.93^{d}	6.54^{c}
	P. salignus	4.88	434.14	2258.51	1009.75	18.67^{b}	34.81^{c}	6.60^{a}	40.32^{e}	5.20^{b}
	P. eryngii	5.16	443.85	2152.14	1269.61	14.00^{a}	33.36^{b}	11.00^{b}	24.96^{a}	4.85^{b}
	P. florida	4.51	446.79	1769.10	1119.22	24.83^{e}	32.91^{b}	26.84^{e}	33.85^{c}	3.96^{a}
	P. ostreatus	4.81	499.82	1965.65	1158.25	19.83^{c}	24.95^{a}	18.71^{d}	31.55^{b}	3.93^{a}
Oak sawdust	Control*	6.00	1530.00	2808.84	1159.97	—	—	—	—	—
	P. pulmonarius	5.42	1040.45	2454.81	1013.35	9.67^{a}	32.00^{d}	12.60^{c}	12.60^{b}	2.36^{b}
	P. salignus	5.31	1168.86	2629.94	892.58	11.50^{c}	23.60^{c}	6.37^{a}	23.05^{d}	2.25^{b}
	P. eryngii	5.38	1237.40	2383.34	1097.52	10.33^{b}	19.12^{b}	15.15^{d}	5.38^{a}	1.93^{a}
	P. florida	5.34	1174.14	2593.78	1008.69	11.00^{c}	23.26^{c}	7.66^{b}	13.04^{c}	2.21^{b}
	P. ostreatus	5.36	1253.30	2485.18	1017.64	10.67^{b}	18.08^{a}	11.52^{c}	12.27^{b}	1.98^{a}
Grapevine sawdust	Control*	6.00	1421.41	2652.00	887.08	—	—	—	—	—
	P. pulmonarius	4.93	1134.36	1898.82	695.41	17.83^{c}	20.19^{e}	28.40^{c}	21.61^{c}	1.67^{a}
	P. salignus	5.13	1283.25	2160.99	600.56	14.50^{b}	9.72^{c}	18.51^{a}	32.30^{e}	1.68^{a}
	P. eryngii	5.29	1201.74	2170.54	794.10	11.83^{a}	15.45^{d}	18.15^{a}	10.48^{a}	1.81^{b}
	P. florida	5.15	1333.07	2177.18	756.61	14.17^{b}	6.21^{b}	17.90^{a}	14.71^{b}	1.63^{a}
	P. ostreatus	5.11	1362.00	2116.78	654.46	14.83^{b}	4.18^{a}	20.18^{b}	26.22^{d}	1.55^{a}
Blackberry sawdust	Control*	6.00	1218.00	2712.00	1038.00	—	—	—	—	—
	P. pulmonarius	4.81	726.16	2183.29	706.92	19.83^{c}	40.38^{d}	19.50^{b}	31.90^{c}	3.01^{c}
	P. salignus	4.86	850.68	1968.71	709.71	19.00^{c}	30.16^{c}	27.41^{d}	31.63^{c}	2.31^{b}
	P. eryngii	5.12	834.23	2267.27	946.83	14.67^{a}	31.51^{c}	16.40^{a}	8.78^{a}	2.72^{c}
	P. florida	5.06	895.27	2169.88	723.29	15.67^{b}	26.50^{b}	19.99^{b}	30.32^{b}	2.42^{b}
	P. ostreatus	5.02	988.15	2081.64	707.26	16.33^{b}	18.87^{a}	23.24^{c}	31.86^{c}	2.04^{a}
Raspberry sawdust	Control*	6.00	1200.00	2160.00	1308.00	—	—	—	—	—
	P. pulmonarius	4.84	885.35	1940.04	619.26	19.33^{c}	26.22^{e}	10.18^{a}	52.66^{e}	2.19^{b}
	P. salignus	4.94	934.23	1823.97	726.62	17.67^{b}	22.15^{c}	15.56^{b}	44.45^{b}	1.95^{a}
	P. eryngii	5.02	903.06	1796.09	988.35	16.33^{a}	24.75^{d}	16.85^{c}	24.44^{a}	1.99^{a}
	P. florida	4.84	1026.93	1932.76	678.16	19.33^{c}	14.42^{b}	10.52^{a}	48.15^{c}	1.88^{a}
	P. ostreatus	4.99	1057.24	1924.98	658.28	16.83^{a}	11.90^{a}	10.88^{a}	49.67^{d}	1.82^{a}
Plum sawdust	Control*	6.00	1837.49	2544.00	1368.00	—	—	—	—	—
	P. pulmonarius	5.47	1509.44	2029.00	738.32	8.83^{a}	17.85^{d}	20.24^{b}	46.03^{b}	1.34^{b}
	P. salignus	5.27	1729.54	1919.37	680.22	12.17^{c}	5.87^{a}	24.55^{c}	50.28^{c}	1.11^{a}
	P. eryngii	5.34	1569.37	1868.30	848.74	11.00^{b}	14.59^{c}	26.56^{d}	37.96^{a}	1.19^{a}
	P. florida	5.22	1696.18	2155.45	594.97	13.00^{d}	7.69^{b}	15.27^{a}	56.51^{d}	1.27^{b}
	P. ostreatus	5.31	1719.79	1868.42	721.89	11.50^{b}	6.41^{a}	26.56^{d}	47.23^{b}	1.09^{a}
Apple sawdust	Control*	6.00	1158.00	2808.00	1176.00	—	—	—	—	—
	P. pulmonarius	5.01	881.58	2068.72	931.69	16.50^{b}	23.87^{d}	26.33^{c}	20.78^{b}	2.35^{b}
	P. salignus	4.80	1003.41	2290.08	691.34	20.00^{e}	13.35^{c}	18.44^{b}	41.21^{d}	2.28^{a}
	P. eryngii	5.16	862.22	2070.36	1048.09	14.00^{a}	25.54^{e}	26.27^{c}	10.88^{a}	2.40^{b}
	P. florida	4.85	1022.93	2419.15	814.46	19.17^{d}	11.66^{b}	13.85^{a}	30.74^{c}	2.36^{b}
	P. ostreatus	4.95	1043.82	2290.46	638.16	17.50^{c}	9.86^{a}	18.43^{b}	45.73^{e}	2.19^{a}
Corn stalks	Control*	6.00	594.00	2796.00	1860.43	—	—	—	—	—
	P. pulmonarius	4.93	409.52	2452.20	1036.14	17.83^{b}	31.06^{b}	12.30^{a}	44.31^{c}	5.99^{b}
	P. salignus	4.64	338.50	1961.45	1029.41	22.67^{d}	43.01^{e}	29.85^{c}	44.67^{c}	5.79^{b}
	P. eryngii	5.16	366.57	2060.04	1270.10	14.00^{a}	38.29^{d}	26.32^{b}	31.73^{a}	5.62^{b}
	P. florida	4.66	381.96	1872.52	1043.39	22.33^{d}	35.70^{c}	33.03^{d}	43.92^{c}	4.90^{a}
	P. ostreatus	4.76	423.91	1948.07	1105.02	20.67^{c}	28.64^{a}	30.33^{c}	40.60^{b}	4.60^{a}

**Uninoculated plant residue.*

[a–e]Values superscripted with the same letter in the same sub-column (for each plant residue) are not significantly different ($p < 0.05$).

numerous value-added products (Stajić et al., 2009; Rastogi and Shrivastava, 2017). Well-known shortcomings of conventional physico-chemical delignification methods have led to a growing need to find a more efficient biological pretreatment of lignocellulose in order to realize sucessful utilization. That has encouraged a huge number of studies examining fungi as the most prominent delignifiers. Although species of the genus *Pleurotus* are known as effective lignocellulosic depolymerizers, the majority of recent studies have addressed the ligninolytic potential of *P. ostreatus* with scarce data about the other species

of this genus (Stajić et al., 2004, 2006; Singh and Singh, 2014; Aditiya et al., 2016; Bilal et al., 2017; Alfaro et al., 2020). Compared to previous reports, the *Pleurotus* spp. profiled in the present research showed an encouraging ligninolytic capacity in relation to various agro-forestry residues. The tremendous influence of the lignocellulosic substrate type on laccase activity has been already shown for *Pleurotus* spp. by Stajić et al. (2006). However, in comparison with our results, those authors reported many times lower laccase activity for *P. eryngii*, *P. ostreatus* and *P. pulmonarius* strains after 7 days of fermentation of tangerine peels and grapevine sawdust. Significantly lower laccase activity (~500 U/L) was also observed after 3 weeks of sugarcane bagasse fermentation by the *P. ostreatus* strain studied by Dong et al. (2013), a value of about 35000 U/L being achieved only after 6 weeks of cultivation. Previous studies also reported an effect of substrate type on the number of visualized laccase isoforms. Thus, Muñoz et al. (1997) obtained two laccase bands after fermentation of glucose/ammonium-tartrate medium by *P. ostreatus*, Palmieri et al. (1997) obtained four bands after submerged cultivation in potato dextrose/yeast extract medium, while Stajić et al. (2006) observed expression of three isoforms on grapevine sawdust. However, there are numerous data that the activity of enzymes is not always positively correlated with the number of visualized isoforms, i.e., it often happens that the mushroom synthesizes a larger number of isoforms of lower activities or only a few or one isoform of high activity.

On the other hand, Dong et al. (2013) reported an extremely high activity of MnP, even 150000 U/L, after 3 weeks of sugarcane bagasse fermentation by *P. ostreatus*. This enzyme could be responsible for the recorded significant loss of total dry mass (8%) and lignin degradation (47%). A similar extent of delignification was also caused by the *P. ostreatus* strain studied by Asgher et al. (2014) cultivated on corn stalks and wheat straw, when 54 and 45.7% of lignin, respectively, was removed. In our study, *P. pulmonarius* and *P. salignus* caused a similar loss of dry biomass and lignin from wheat straw and corn stalks, respectively, despite low laccase activity. The high level of lignin depolymerization can be attributed to highly active Mn-oxidizing peroxidases, which have a crucial role in the initial phase of the process when a large amount of generated Mn^{3+} makes up for the decreased action of laccases due to their limited diffusion into the substrate as a result of their oversized molecules (Knežević et al., 2016; Stajić et al., 2016). A level of rice straw delignification (25%) similar to that obtained for the as strain tested in our study during cultivation on wheat straw was caused by a Chinese strain of *P. ostreatus* (Mustafa et al., 2016). However, a considerably lower delignification potential was recorded in *P. sajor-caju*, used for the pretreatment of residues collected at a co-digestion biogas plant, where only 8.7% of lignin was degraded after 6 weeks of cultivation (Fang et al., 2018). Another weak delignifier was *P. eryngii* as studied by Martínez-Patiño et al. (2018), which caused only 1.5% lignin mineralization after even 45 days of fermentation of olive tree leaves owing to extremely low MnP and laccase activities (8.0 U/g and 3.0 U/g, respectively).

Similar to the high percentage of plant raw materials delignification, a high level of its hemicellulose degradation was measured in our study, which Martínez et al. (1994) explained by the preference of white rot fungi to decompose lignin and xylan over the other polymers. Thus, even 47% of lignin and 43% of xylan loss was detected after *P. eryngii* cultivation on wheat straw which only a 14% of cellulose was degraded (Camarero et al., 1994).

The origin of strains and their genetic predisposition certainly have a very important effect on their delignification selectivity. Thus, in contrast to the *P. florida* strain tested in the present study, which showed a low cellulose enrichment, the strains studied by Rouches et al. (2016) caused highly selective delignification of wheat straw and corn stalks, successfully pretreating them for biogas production. Mustafa et al. (2016) also reported a high selectivity for a Chinese *P. ostreatus* strain during rice straw fermentation. On the other hand, extremely low selectivity was noted after fermentation of banana leaf-based waste by an Indian *P. florida* strain, which caused about 30% lignin removal and even 50–70% cellulose removal (Chanakya et al., 2015).

Generally, the obtained results clearly singled out *P. pulmonarius* HAI 573 as highly efficient and selective delignifier, especially of wheat straw, which opens new possibilities for the use of its ligninolytic cocktail in pretreatment of this raw material, as the first phase in numerous biotechnological processes, primarily in bioethanol and paper production.

CONCLUSION

The main contribution of the present study is the characterization of the ligninolytic enzyme system and lignocellulose degradation capacity of insufficiently studied *Pleurotus* species. Most of the substrates considered in the study were tested for the first time in despite their great abundance and demonstrated high potential for induction of strong ligninolytic enzymes production by *Pleurotus* spp. This opens up a huge space for future detailed studies aiming to include these lignocellulosics in a number of biotechnological processes. Pretreated with the most selective degraders, those lignocellulosics could be used for the production of more digestable feed, paper, bioethanol and other valued compounds. The present study has clearly confirmed that naturally destructive organisms such as *Pleurotus* spp., i.e., a cocktail of their ligninolytic enzymes, could be potentially employed in very useful biotechnological processes making possible the utilization of common lignocellulosic wastes. The obtained results can serve as the basis for further optimization of high-scale production of the most active enzyme isoforms for industrial utilization.

DATA AVAILABILITY STATEMENT

The original contributions presented in the study are included in the article/Supplementary Material, further inquiries can be directed to the corresponding author.

AUTHOR CONTRIBUTIONS

MG Methodology, Investigation, Writing-original draft. JC and MS Conceptualization, Writing-review and editing. JV Supervision.

FUNDING

This study was financially supported by the Ministry of Education, Science and Technological Development of the Republic of Serbia (Contract number: 451-03-9/2021-14/200178).

REFERENCES

Aditiya, H. B., Mahlia, T. M. I., Chong, W. T., Nur, H., and Sebayang, A. H. (2016). Second Generation Bioethanol Production: A Critical Review. *Renew. Sust. Energ. Rev.* 66, 631–653. doi:10.1016/j.rser.2016.07.015

Alfaro, M., Majcherczyk, A., Kües, U., Ramírez, L., and Pisabarro, A. G. (2020). Glucose Counteracts wood-dependent Induction of Lignocellulolytic Enzyme Secretion in Monokaryon and Dikaryon Submerged Cultures of the white-rot Basidiomycete *Pleurotus Ostreatus*. *Sci. Rep.* 10, 12421. doi:10.1038/s41598-020-68969-1

Asgher, M., Bashir, F., and Iqbal, H. M. N. (2014). A Comprehensive Ligninolytic Pre-treatment Approach from Lignocellulose green Biotechnology to Produce Bio-Ethanol. *Chem. Eng. Res. Des.* 92, 1571–1578. doi:10.1016/j.cherd.2013.09.003

Bilal, M., Asgher, M., Iqbal, H. M. N., Hu, H., and Zhang, X. (2017). Biotransformation of Lignocellulosic Materials into Value-Added Products-A Review. *Int. J. Biol. Macromolecules* 98, 447–458. doi:10.1016/j.ijbiomac.2017.01.133

Camarero, S., Galletti, G. C., and Martínez, A. T. (1994). Preferential Degradation of Phenolic Lignin Units by Two white Rot Fungi. *Appl. Environ. Microbiol.* 60, 4509–4516. doi:10.1128/aem.60.12.4509-4516.1994

Chanakya, H. N., Malayil, S., and Vijayalakshmi, C. (2015). Cultivation of *Pleurotus* Spp. On a Combination of Anaerobically Digested Plant Material and Various Agro-Residues. *Energ. Sust. Dev.* 27, 84–92. doi:10.1016/j.esd.2015.04.007

Ćilerdžić, J., Galić, M., Vukojević, J., Brčeski, I., and Stajić, M. (2017). Potential of Selected Fungal Species to Degrade Wheat Straw, the Most Abundant Plant Raw Material in Europe. *BMC Plant Biol.* 17 (Suppl. 2), 249. doi:10.1186/s12870-017-1196-y

Ćilerdžić, J., Stajić, M., and Vukojević, J. (2016). Degradation of Wheat Straw and Oak Sawdust by *Ganoderma Applanatum*. *Int. Biodeter. Biodegr.* 114, 39–44. doi:10.1016/j.ibiod.2016.05.024

De Souza, L., Y., M., and Shivakumar, S. (2020). Bioconversion of Lignocellulosic Substrates for the Production of Polyhydroxyalkanoates. *Biocatal. Agric. Biotechnol.* 28, 101754. doi:10.1016/j.bcab.2020.101754

Dong, X. Q., Yang, J. S., Zhu, N., Wang, E. T., and Yuan, H. L. (2013). Sugarcane Bagasse Degradation and Characterization of Three white-rot Fungi. *Bioresour. Tech.* 131, 443–451. doi:10.1016/j.biortech.2012.12.182

Fang, W., Zhang, P., Zhang, X., Zhu, X., van Lier, J. B., and Spanjers, H. (2018). White Rot Fungi Pretreatment to advance Volatile Fatty Acid Production from Solid-State Fermentation of Solid Digestate: Efficiency and Mechanisms. *Energy* 162, 534–541. doi:10.1016/j.energy.2018.08.082

Ghaffar, S. H., Fan, M., and McVicar, B. (2015). Bioengineering for Utilisation and Bioconversion of Straw Biomass into Bio-Products. *Ind. Crops Prod.* 77, 262–274. doi:10.1016/j.indcrop.2015.08.060

Kirk, T. K., and Obst, J. R. (1988). "Lignin Determination," in *Methods in Enzymology*. Editors S. P. Colowick and N. O. Kaplan (SanDiego: Academic Press), 161, 87–101. doi:10.1016/0076-6879(88)61014-7

Knežević, A., Stajić, M., Jovanović, V. M., Kovačević, V., Ćilerdžić, J., Milovanović, I., et al. (2016). Induction of Wheat Straw Delignification by *Trametes* Species. *Sci. Rep.* 6, 26529. doi:10.1038/srep26529

Knežević, A., Stajić, M., Vukojević, J., and Milovanović, I. (2014). The Effect of Trace Elements on Wheat Straw Degradation by *Trametes Gibbosa*. *Int. Biodeter. Biodegr.* 96, 152–156.

Maganhotto de Souza Silva, C. M., Soares de Melo, I., and Roberto de Oliveira, P. (2005). Ligninolytic Enzyme Production by *Ganoderma* Spp. *Enzyme Microb. Tech.* 37, 324–329. doi:10.1016/j.enzmictec.2004.12.007

Martínez, A., Camarero, S., Guillen, F., Gutiérrez, A., Muñoz, C., Varela, E., et al. (1994). Progress in Biopulping of Non-woody Materials: Chemical, Enzymatic and Ultrastructural Aspects of Wheat Straw Delignification with Ligninolytic Fungi from the Genus *Pleurotus*. *FEMS Microbiol. Rev.* 13, 265–273. doi:10.1016/0168-6445(94)90084-1

Martínez-Patiño, J. C., Lu-Chau, T. A., Gullón, B., Ruiz, E., Romero, I., Castro, E., et al. (2018). Application of a Combined Fungal and Diluted Acid Pretreatment on Olive Tree Biomass. *Ind. Crops Prod.* 121, 10–17. doi:10.1016/j.indcrop.2018.04.078

Meehnian, H., Jana, A. K., and Jana, M. M. (2017). Pretreatment of Cotton Stalks by Synergistic Interaction of *Daedalea Flavida* and *Phlebia Radiata* in Co-culture for Improvement in Delignification and Saccharification. *Int. Biodeterioration Biodegradation* 117, 68–77. doi:10.1016/j.ibiod.2016.11.022

Muñoz, C., Guillén, F., Martínez, A. T., and Martínez, M. J. (1997). Laccase Isoenzymes of Pleurotus Eryngii: Characterization, Catalytic Properties, and Participation in Activation of Molecular Oxygen and Mn2+ Oxidation. *Appl. Environ. Microbiol.* 63, 2166–2174. doi:10.1128/aem.63.6.2166-2174.1997

Mustafa, A. M., Poulsen, T. G., and Sheng, K. (2016). Fungal Pretreatment of rice Straw with *Pleurotus Ostreatus* and *Trichoderma Reesei* to Enhance Methane Production under Solid-State Anaerobic Digestion. *Appl. Energ.* 180, 661–671. doi:10.1016/j.apenergy.2016.07.135

Palmieri, G., Giardina, P., Bianco, C., Scaloni, A., Capasso, A., and Sannia, G. (1997). A Novel white Laccase from *Pleurotus Ostreatus*. *J. Biol. Chem.* 272, 31301–31307. doi:10.1074/jbc.272.50.31301

Rastogi, M., and Shrivastava, S. (2017). Recent Advances in Second Generation Bioethanol Production: An Insight to Pretreatment, Saccharification and Fermentation Processes. *Renew. Sust. Energ. Rev.* 80, 330–340. doi:10.1016/j.rser.2017.05.225

Rouches, E., Herpoël-Gimbert, I., Steyer, J. P., and Carrere, H. (2016). Improvement of Anaerobic Degradation by white-rot Fungi Pretreatment of Lignocellulosic Biomass: A Review. *Renew. Sust. Energ. Rev.* 59, 179–198. doi:10.1016/j.rser.2015.12.317

Rudakiya, D. M., and Gupte, A. (2017). Degradation of Hardwoods by Treatment of white Rot Fungi and its Pyrolysis Kinetics Studies. *Int. Biodeterioration Biodegradation* 120, 21–35. doi:10.1016/j.ibiod.2017.02.004

Singh, A. P., and Singh, T. (2014). Biotechnological Applications of wood-rotting Fungi: A Review. *Biomass and Bioenergy* 62, 198–206. doi:10.1016/j.biombioe.2013.12.013

Stajić, M., Kukavica, B., Vukojević, J., Simonić, J., Veljović-Jovanović, S., and Duletić-Laušević, S. (2010). Wheat Straw Conversion by Enzymatic System of *Ganoderma Lucidum*. *Bioresources* 5, 2362–2373.

Stajic, M., Persky, L., Cohen, E., Hadar, Y., Brceski, I., Wasser, S. P., et al. (2004). Screening of Laccase, Manganese Peroxidase, and Versatile Peroxidase Activities of the Genus Pleurotus in Media with Some Raw Plant Materials as Carbon Sources. *Abab* 117, 155–164. doi:10.1385/abab:117:3:155

Stajić, M., Persky, L., Friesem, D., Hadar, Y., Wasser, S. P., Nevo, E., et al. (2006). Effect of Different Carbon and Nitrogen Sources on Laccase and Peroxidases Activity by Selected *Pleurotus* Species. *Enzyme Microb. Tech.* 38, 65–73. doi:10.1016/j.enzmictec.2005.03.026

Stajić, M., Vukojević, J., Milovanović, I., Ćilerdžić, J., and Knežević, A. (2016). "Role of Mushroom Mn-Oxidizing Peroxidases in Biomass Conversion," in *Microbial Enzymes in Bioconversion of Biomass*. Editor V. K. Gupta (Switzerland: Springer International Publishing), 251–269.

Stajić, M., Vukojević, J., and Duletić-Laušević, S. (2009). Biology ofPleurotus Eryngiiand Role in Biotechnological Processes: a Review. *Crit. Rev. Biotechnol.* 29, 55–66. doi:10.1080/07388550802688821

Van Soest, P. J., Robertson, J. B., and Lewis, B. A. (1991). Methods for Dietary Fiber, Neutral Detergent Fiber, and Nonstarch Polysaccharides in Relation

to Animal Nutrition. *J. Dairy Sci.* 74, 3583–3597. doi:10.3168/jds.s0022-0302(91)78551-2

Conflict of Interest: The authors declare that the research was conducted in the absence of any commercial or financial relationships that could be construed as a potential conflict of interest.

Publisher's Note: All claims expressed in this article are solely those of the authors and do not necessarily represent those of their affiliated organizations, or those of the publisher, the editors and the reviewers. Any product that may be evaluated in this article, or claim that may be made by its manufacturer, is not guaranteed or endorsed by the publisher.

frontiers in Bioengineering and Biotechnology

BRIEF RESEARCH REPORT
published: 25 October 2021
doi: 10.3389/fbioe.2021.754250

Clostridium acetobutylicum atpG-Knockdown Mutants Increase Extracellular pH in Batch Cultures

Yu-Sin Jang[1], Hyeon Jeong Seong[1], Seong Woo Kwon[1], Yong-Suk Lee[1], Jung Ae Im[2], Haeng Lim Lee[1], Ye Rin Yoon[1] and Sang Yup Lee[2]**

[1]Division of Applied Life Science (BK21), Department of Applied Life Chemistry, Institute of Agriculture and Life Science (IALS), Gyeongsang National University, Jinju, South Korea, [2]Department of Chemical and Biomolecular Engineering (BK21 Plus Program), BioProcess Engineering Research Center, Institute for the BioCentury, Korea Advanced Institute of Science and Technology (KAIST), Daejeon, South Korea

ATPase, a key enzyme involved in energy metabolism, has not yet been well studied in *Clostridium acetobutylicum*. Here, we knocked down the *atpG* gene encoding the ATPase gamma subunit in *C. acetobutylicum* ATCC 824 using a mobile group II intron system and analyzed the physiological characteristics of the *atpG* gene knockdown mutant, 824-2866KD. Properties investigated included cell growth, glucose consumption, production of major metabolites, and extracellular pH. Interestingly, in 2-L batch fermentations, 824-2866KD showed no significant difference in metabolite biosynthesis or cell growth compared with the parent ATCC 824. However, the pH value in 824-2866KD cultures at the late stage of the solventogenic phase was abnormally high (pH 6.12), compared with that obtained routinely in the culture of ATCC 824 (pH 5.74). This phenomenon was also observed in batch cultures of another *C. acetobutylicum*, BEKW-2866KD, an *atpG*-knockdown and *pta-buk* double-knockout mutant. The findings reported in this study suggested that ATPase is relatively minor than acid-forming pathway in ATP metabolism in *C. acetobutylicum.*

Keywords: *Clostridium acetobutylicum*, ATPase, *atpG*, knockdown, extracellular pH

OPEN ACCESS

Edited by:
Xiao-Jun Ji,
Nanjing Tech University, China

Reviewed by:
Farshad Darvishi,
Alzahra University, Iran
Zongjie Dai,
Tianjin Institute of Industrial Biotechnology (CAS), China

****Correspondence:***
Yu-Sin Jang
jangys@gnu.ac.kr
Sang Yup Lee
leesy@kaist.ac.kr

Specialty section:
This article was submitted to Industrial Biotechnology, a section of the journal Frontiers in Bioengineering and Biotechnology

Received: *06 August 2021*
Accepted: *11 October 2021*
Published: *25 October 2021*

Citation:
Jang Y-S, Seong HJ, Kwon SW, Lee Y-S, Im JA, Lee HL, Yoon YR and Lee SY (2021) Clostridium acetobutylicum atpG-Knockdown Mutants Increase Extracellular pH in Batch Cultures. *Front. Bioeng. Biotechnol. 9:754250. doi: 10.3389/fbioe.2021.754250*

INTRODUCTION

Clostridium acetobutylicum is a strictly anaerobic, gram-positive bacterium that survives in hostile environments by producing endospores (Shao et al., 2007). *C. acetobutylicum* possesses industrially applicable metabolic properties, notably including the production of organic solvents, such as acetone, butanol, and ethanol (Kwon et al., 2020; Shin et al., 2021). *C. acetobutylicum* produces the solvents through biphasic pathway, which is divided into an acidogenic phase and a solventogenic phase (Shao et al., 2007; Im et al., 2021). During the acidogenic phase, which corresponds to the initial growth phase, most carbon sources are used to produce acetate, butyrate, and carbon dioxide (Jang et al., 2012). As cell growth enters the stationary phase, the metabolism of *C. acetobutylicum* shifts to the solventogenic phase (Lütke-Eversloh, 2014), during which organic acids are re-assimilated, and most of the carbon sources are used to produce butanol, acetone, and ethanol as final products (Jang et al., 2012).

The reason for this biphasic fermentation is closely related to the energy and redox metabolism in *C. acetobutylicum* (**Figure 1**) (Jang et al., 2014a; Lütke-Eversloh, 2014). In these bacteria, ATP is primarily produced from glucose through glycolysis (Externbrink et al., 2000). During the initial

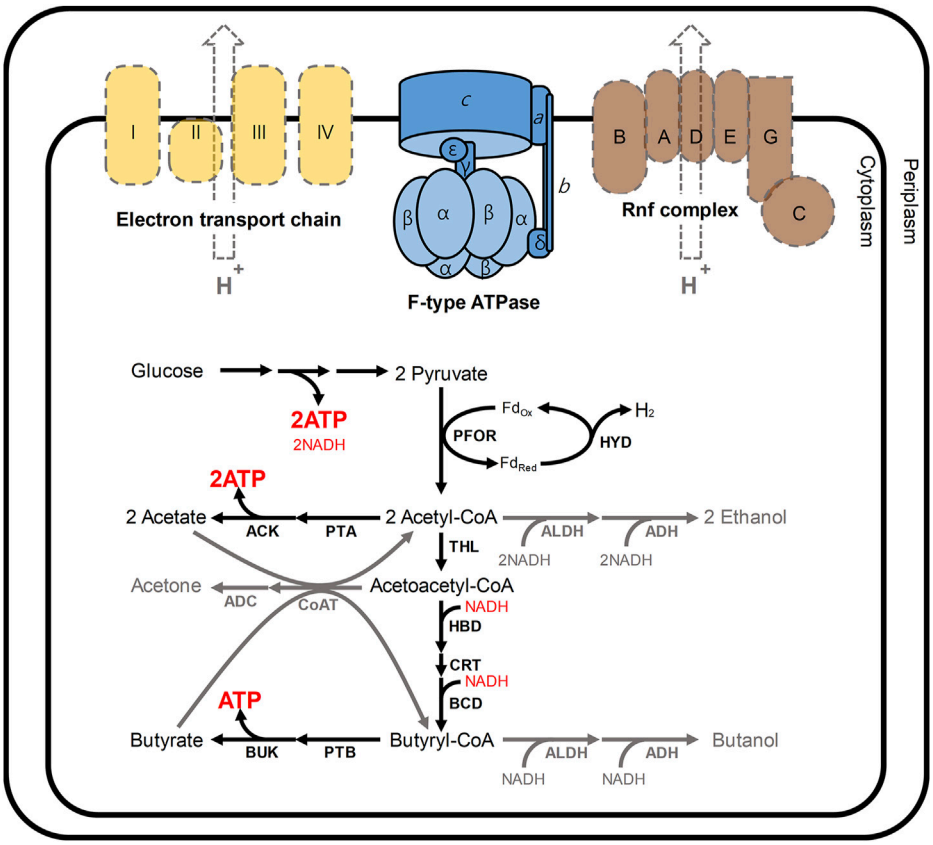

FIGURE 1 | Schematic presentation of the energy and redox metabolism in *C. acetobutylicum*. In *C. acetobutylicum*, F-type ATPase is encoded by the *atp* operon (*atp*IBEFHAGDC). In general, F-type ATPases require the proton motive force to produce ATP; however, neither the electron transport chain (yellow) nor Rnf complex (brown) has been reported in *C. acetobutylicum* (Tremblay et al., 2012). The Rnf complex is commonly reported in other clostridia such as *Clostridium beijerinkii, Clostridium saccharobutylicum* and *Clostridium saccharoperbutylacetonicum*, but it is usual that the Rnf is not found in *C. acetobutylicum* (Poehlein et al., 2017). In this situation, meanwhile, 2 mol of ATP are produced from a glucose through glycolysis. During the initial growth phase (namely, acidogenic phase), additional ATP is produced through the routes for the production of acetate and butyrate. At that time, NADH could be re-oxidized *via* two routes: 1) a cascade reaction for butyrate formation involving 3-hydroxybutyryl-CoA dehydrogenase (HBD) and butyryl-CoA dehydrogenase (BCD); 2) hydrogen production reaction catalyzed by hydrogenase (HYD) coupled with ferredoxin oxidoreductase (PFOR). During solventogenic phase (gray arrows), the function of hydrogenase is turned-off, and NAD^+ is regenerated by 4 (HBD, BCD, ALDH, and ADH) and 2 (ALDH and ADH) dehydrogenases for butanol and ethanol biosynthesis, respectively. Abbreviations: ACK, acetate kinase; ADC, acetoacetate decarboxylase; ADH, alcohol dehydrogenase; ALDH, aldehyde dehydrogenase; BUK, butyrate kinase, CoAT, CoA transferase; CRT, crotonase; THL, thiolase; PTA, phosphotransacetylase; and PTB, phosphotransbutyrylase.

growth phase in *C. acetobutylicum*, additional ATP is produced through substrate-level phosphorylation, which is coupled to the production of acetate and butyrate (Externbrink et al., 2000). At that time, to regenerate NAD^+, NADH could be oxidized *via* not only two enzymes 3-hydroxybutyryl-CoA dehydrogenase (HBD) and butyryl-CoA dehydrogenase (BCD) responsible for butyrate formation, but also hydrogenase (HYD) coupled with ferredoxin oxidoreductase (PFOR; **Figure 1**) (Du et al., 2021; Jiang et al., 2021). As the acidogenic phase progresses, the external pH is continuously lowered to nearby 4.5, and NADH also accumulates, both of which have adverse effects on *C. acetobutylicum* (Jang et al., 2012; Lütke-Eversloh, 2014). At this point, the metabolism of *C. acetobutylicum* shifts from the acidogenic phase to the solventogenic phase (Jang et al., 2012; Li et al., 2020; Thi et al., 2020). After such phase transition, the function of hydrogenase is turned-off, and NAD^+ is regenerated by 4 and 2 dehydrogenases for butanol and ethanol biosynthesis, respectively (Tremblay et al., 2012; Fast and Papoutsakis, 2018) (see **Figure 1** for details). Continuous acid re-assimilation and carbon flux toward solvent production cause the lowered external pH to rise (Kim et al., 2020; Li et al., 2020).

Despite such perfect metabolism for energy and redox regulation through biphasic fermentation, the *atp* operon encoding ATPase was reported in *C. acetobutylicum* genome (Nölling et al., 2001; Cho et al., 2017). The fully sequenced *atp* operon in *C. acetobutylicum* has been shown to include the *atp*IBEFHAGDC (F-type ATPase) (Externbrink et al., 2000). F-type ATPases, which are conjugated to the inner membrane in microbes, generally mediate ATP synthesis through oxidative phosphorylation (Externbrink et al., 2000; Mukherjee and Warshel, 2015; Zharova and Vinogradov, 2017; Kang et al., 2019). F-type ATPases require the proton motive force (PMF) to produce ATP from ADP and inorganic phosphate (Pi); however, neither the electron transport chain nor Rnf complex

has been reported in *C. acetobutylicum* (Tremblay et al., 2012; Shin et al., 2021) (**Figure 1**). Although physiological effects of disrupting ATPase have been analyzed in other organisms, such as *Escherichia coli* (Jensen and Michelsen, 1992; Causey et al., 2003; Shah and Duncan, 2015; Burger et al., 2020), *Lactococcus lactis* (Koebmann et al., 2000; Koebmann et al., 2002a), *Rhodobacter capsulatus* (Borghese et al., 1998), *Saccharomyces cerevisiae* (Weber et al., 1995; Zhang and Zhang, 2019), *Corynebacterium glutamicum* (Sekine et al., 2001; Koch-Koerfges et al., 2012), and *Bacillus subtilis* (Santana et al., 1994), the consequences of ATPase mutation in *C. acetobutylicum* ATCC 824 have not yet been investigated. Here, to reveal the main function of F-type ATPase in *C. acetobutylicum*, we constructed ATPase-knockdown strains and performed a physiological characterization of resulting ATPase-knockdown strains.

MATERIALS AND METHODS

Bacterial Strains, Plasmids, and Culture Conditions

E. coli strains and recombinants were grown in Luria-Bertani (LB) broth at 37°C (An et al., 2020; Lone et al., 2020). *C. acetobutylicum* ATCC 824 and the engineered strain BEKW and mutants were grown in clostridial growth medium (CGM) or 2X YTG agar in an anaerobic chamber (Forma Scientific, Marietta, OH, United States) under 4% hydrogen and 96% nitrogen at 37°C (Jang et al., 2012). Ampicillin (50 μg/ml), chloramphenicol (34 μg/ml), or erythromycin (40 μg/ml) was added to the medium, as required.

Construction of Knockdown Mutants

The mobile group II intron system was used to construct *atpG*-knockdown mutants of *C. acetobutylicum* (Heap et al., 2007; Shao et al., 2007; Jang et al., 2012; Jang et al., 2014b; Kim et al., 2015; Kwon et al., 2020). The *atpG*-targeted intron for knockdown was amplified by overlap extension PCR using the following primers: 2866-IBS, 5′-AAAAAAGCTTATAATTATCCTTAATAGCCGACCGTGTGCGCCCAGATAGGGTG-3′; 2866-EBS1, 5′-CAGATTGTACAAATGTGGTGATAACAGATAAGTCGACCGTGCTAACTTACCTTTCTTTGT-3′; 2866-EBS2, 5′-TGAACGCAAGTTTCTAATTTCGGTTGCTATCCGATAGAGGAAAGTGTCT-3′; EBS universal, 5′-CGAAATTAGAAACTTGCGTTCAGTAAAC-3′ (**Supplementary Table S1**). The amplified PCR fragment (~0.5 kb) was double-digested using restriction enzymes *Bsr*GI and *Hin*dIII, and then ligated into pCACYS3 (Jang et al., 2012) digested using the same enzymes, yielding the recombinant plasmid, pCAC2866KD. Plasmid pCAC2866KD was consecutively transformed into *E. coli* TOP10 (pAN1) containing the plasmid pAN1, which harbors the methyltransferase gene, *φ*3TI (Mermelstein and Papoutsakis, 1993). Thus, the recombinant plasmid, pCAC2866KD, is methylated by the methyltransferase in the resulting *E. coli* strain. *C. acetobutylicum* ATCC 824 and its *pta-buk* double mutant BEKW (Jang et al., 2012) were subsequently transformed with the methylated recombinant plasmid, yielding the *atpG*-knockdown mutant strains, 824-2866KD and BEKW-2866KD, respectively. The resulting *atp*G-knockdown mutants, in which the targeted intron was inserted in the sense strand, were validated by PCR using primers atpG-F and atpG-R (**Supplementary Table S1**). The intron insertion into the target site on the *atpG* gene was further confirmed by sequencing the DNA fragments obtained from PCR with primers atpG-seq-F and atpG-seq-R using total DNA of the mutant (**Supplementary Table S1**).

Batch Fermentation

C. acetobutylicum ATCC 824 and its mutants were inoculated into 500-ml Erlenmeyer flasks containing 200 ml CGM and then cultured anaerobically to an optical density at 600 nm (OD_{600}) of 1.0 at 37°C (Jang et al., 2012). The resulting seed cultures were transferred into a 5-L Liflus GX bioreactor (Biotron, Gyunggi-do, South Korea) containing 1.8 L CGM for fermentation. The bioreactor was set at an agitation speed of 200 rpm, a nitrogen gas flow rate of 0.25 vvm, and a temperature of 37°C. The pH was automatically maintained above 5.0 with ammonia solution but was not controlled when pH became higher than the set value. Samples were periodically withdrawn from the culture medium for analysis of cell growth and concentrations of glucose, organic acids, and organic solvents.

Analytical Methods

Samples were collected for monitoring cell growth, glucose consumption, pH, and production of metabolites, including acetate, butyrate, acetone, ethanol, and butanol. Batch fermentations of each strain were independently performed in duplicate. Cell growth was monitored by measuring OD_{600} using an Ultrospec 3000 spectrophotometer (Pharmacia Biotech, Uppsala, Sweden). The concentrations of acetate, butyrate, and glucose were determined using a high-performance liquid chromatography (HPLC) system (Prostar; Varian, Palo Alto, CA, United States) equipped with a packed column (Metacarb 87H; MetaChem Technologies, Torrance, CA, United States) and refractive index detector (RI-27; Shodex, Japan). The mobile phase consisted of 0.01 N H_2SO_4 (Im et al., 2019; Chun and Sang, 2020; Lee et al., 2020). The concentrations of acetone, butanol, and ethanol were determined using a gas chromatography system (Agilent 7890; Agilent Technologies, California, United States) equipped with a packed column (80/120 Carbopack BAW glass column; Supelco, Bellefonte, PA, United States) and flame ionization detector (Jang et al., 2012; Baek et al., 2019). Helium gas was used for the mobile phase.

RESULTS AND DISCUSSION

Construction of the *atpG*-Knockdown *C. acetobutylicum* Mutants

CAC2866 (*atp*G encoding ATPase gamma subunit), one of nine ATPase-coding genes found in *C. acetobutylicum*, is an important part of the ATPase enzyme (Externbrink et al., 2000). The ATPase gamma subunit forms the central shaft, which forms the connection between the F_0 rotary motor and the F_1 catalytic

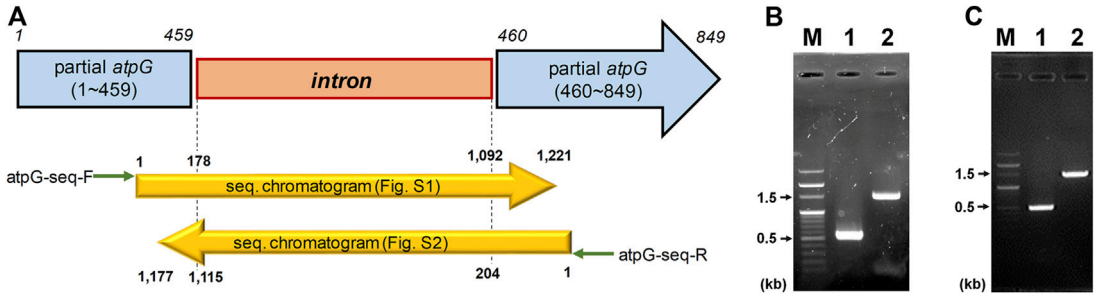

FIGURE 2 | Inactivation of *C. acetobutylicum atpG* gene by the intron insertion using mobile group II intron system. **(A)** Schematic diagram of the mutated *atpG* gene (blue) constructed by intron (orange) insertion. The intron was inserted between 459th and 460th nucleotides in the wild-type *atpG* gene, which was confirmed by sequencing using primers atpG-seq-F (green arrow) and atpG-seq-R (reverse green arrow; **Supplementary Table S1**). The mutated *atpG* gene was schematically aligned with DNA sequencing chromatograms (yellow arrows; see **Supplementary Figures S1, S2** for detailed chromatogram). **(B,C)** Validation of the *atpG* gene mutation in strains 824-2866KD **(B)** and BEKW-2866KD **(C)**. The *atp*G-knockdown mutants, 824-2866KD and BEKW-2866KD were validated by PCR using primers atpG-F and atpG-R (**Supplementary Table S1**). **(B)** M, 100-bp marker; lane #1, ATCC 824; lane #2, 824-2866KD. **(C)** M, 100-bp marker; lane #1, BEKW; lane #2, BEKW-2866KD.

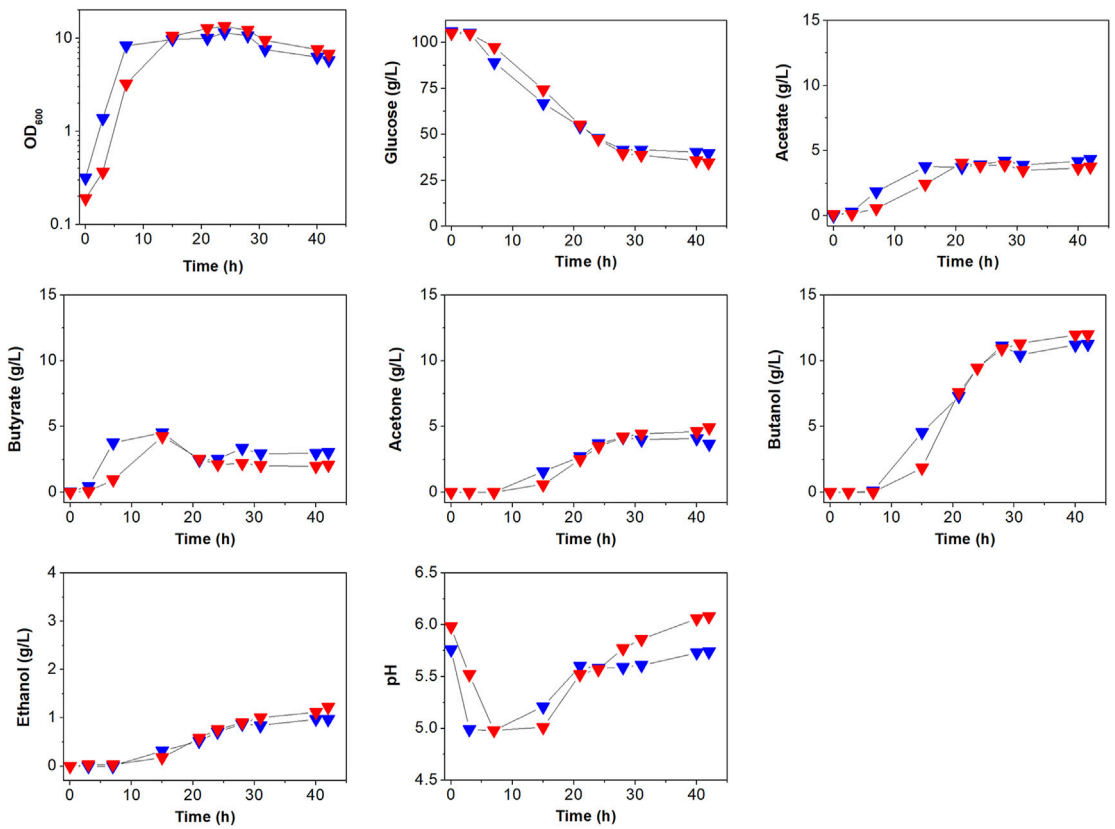

FIGURE 3 | Comparison of batch fermentation profiles between *C. acetobutylicum* ATCC 824 (blue) and its mutant 824-2866KD (red). Fermentation parameters are cell growth (OD_{600}) glucose consumption, acids (acetate and butyrate) production, and solvents (acetone, butanol, and ethanol) production. Merged version of batch fermentation profiles of *C. acetobutylicum* 824-2866KD are shown in **Supplementary Figure S3A**. Other reproduced bioreactor cultivation profiles are shown in **Supplementary Figure S3B**.

complex (**Figure 1**; Mukherjee and Warshel, 2015). Disruption of the gamma subunit of F-ATPase in other organisms decreases ATPase activity and ATP levels, resulting in cell growth inhibition and a shift in metabolism (Iwamoto et al., 1990; Shin et al., 1992; Lai-Zhang et al., 1999). Accordingly, to investigate the effects of ATPase knockdown on physiological

characteristics of *C. acetobutylicum*, we constructed *atpG*-knockdown mutant strains, 824-2866KD and BEKW-2866KD from wild-type ATCC 824 and the *pta-buk* double mutant BEKW strains, respectively, by using mobile group II intron system (**Figure 2**; **Supplementary Figures S1, S2**).

Effects of *atpG* Knockdown on Cell Growth, Glucose Consumption, and Metabolite Production

To see the effects of *atpG* knockdown on physiological characteristics, we first analyzed and compared cell growth between ATCC 824 and 824-2866KD (**Figure 3**; **Supplementary Figure S3**). There was no apparent difference in growth between ATCC 824 and 824-2866KD (**Figure 3**), even though disruption of ATPase is known to reduce ATPase activity and ATP level, which in turn inhibits cell growth in non-clostridia strains (Iwamoto et al., 1990; Ferrandiz and De La Campa, 2002; Causey et al., 2003; Cipriano et al., 2006; Kim et al., 2020).

The effects of *atpG* knockdown in *C. acetobutylicum* were also assessed by examining glucose consumption, which is known to be affected by ATP levels (Koebmann et al., 2002b; Dai et al., 2020). Glucose concentration decreased steadily during exponential and stationary phases in both ATCC 824 and 824-2866KD (**Figure 3**; **Supplementary Figure S3**). After 28 h, glucose consumption in ATCC 824 was 66.5 g/L and was maintained at 39.5 g/L (**Figure 3**). 824-2866KD showed a similar decrease in glucose consumption rate, which reached 70.5 g/L at 28 h and was maintained at 34.5 g/L (**Figure 3**). Thus, these results show no significant changes in glucose consumption in *atpG*-knockdown *C. acetobutylicum* mutant comparing with the parent ATCC 824 strain.

The effects of *atpG* knockdown were further investigated by analyzing the production of metabolites (**Figure 3**; **Supplementary Figure S3**). The highest concentrations of acetate and butyrate in 824-2866KD culture were 3.9 g/L and 4.0 g/L, respectively, representing 91.6 and 88.9% of concentrations in ATCC 824 fermentation (**Figure 3**). During the solventogenic phase, the final concentrations of acetate and acetone in 824-2866KD were also similar to those in ATCC 824 (**Figure 3**). However, residual butyrate in the fermentation using 824-2866KD was slightly lower than that of the ATCC 824, with a difference of exactly 0.98 g/L at the endpoint (**Figure 3**). The lack of change (or minor change) in acid and acetone concentrations indicates that acid re-assimilation is also not majorly affected by ATPase knockdown. The production of ethanol and butanol in 824-2866KD culture were 1.4 g/L and 12.4 g/L, respectively, which were also similar to the corresponding concentrations of 1.0 g/L and 11.3 g/L in ATCC 824 fermentation (**Figure 3**). Previous studies have reported that disruption of ATPase shifts metabolic flux toward byproducts because ATPase-disrupted mutants produce ATP through substrate-level phosphorylation, not by oxidative phosphorylation (Koebmann et al., 2002a; Koebmann et al., 2002b). It seems that as most ATP in *C. acetobutylicum* is produced through substrate-level phosphorylation, the ATPase-knockdown mutant showed no significant changes in acidogenic or and solventogenic phases.

Effect of *atpG* Knockdown on Extracellular pH

The effect of *atpG* knockdown was also analyzed by comparing extracellular pH between ATCC 824 and 824-2866KD (**Figure 3**; **Supplementary Figure S3**). Throughout the entire fermentation period, the bioreactor controller adjusted the external pH to maintain it above 5.0. During the acidogenic phase, ATCC 824 and 824-2866KD reached pH 5.0 and maintained it by adding ammonia solution to avoid decreasing pH values by the production of organic acids. During the subsequent solventogenic phase, pH rose as a result of acid re-assimilation in both ATCC 824 and 824-2866KD cultures (**Figure 3**). The pH rose steadily after 20 h, reaching pH 5.74 in ATCC 824 culture (**Figure 3**). On the other hand, pH rose steadily for more than 40 h in 824-2866KD culture, reaching a value of 6.12 at the late stage of the solventogenic phase, a value significantly higher than that in ATCC 824 fermentation (**Figure 3**). These results show that ATPase activity is affected to the extracellular pH in *C. acetobutylicum* fermentation.

Effect of *atpG* Knockdown on Physiological Characteristics of *C. acetobutylicum* BEKW

Our previous work (Jang et al., 2012) showed that *C. acetobutylicum* BEKW exhibited higher butanol production (16.0 g/L) than *C. acetobutylicum* ATCC 824 (11.8 g/L). Two enzymes including phosphotransacetylase and butyrate kinase encoded by the *pta* and *buk*, respectively, operate primarily in the acidogenic phase to synthesize the organic acids, acetate and butyrate, respectively, in addition to producing ATP through substrate-level phosphorylation (Lütke-Eversloh, 2014). To determine the effects of *atpG* knockdown in BEKW, we cultured the mutant, BEKW-2866KD in 2-L bioreactor (**Figure 4A**; **Supplementary Figure S4**).

First, we compared cell growth and glucose consumption of BEKW-2866KD with that in BEKW. Glucose concentration decreased steadily during exponential and stationary phases in BEKW-2866KD (**Figure 4A**). Glucose consumption ceased by 38 h and was maintained at 39.91 g/L (**Figure 4A**). Ultimately, total glucose consumption was 56.60 g, which was not significantly different from that in BEKW (Jang et al., 2012). Consistent with the similar glucose consumption in BEKW and mutant strains, cell growth was also unaffected by *atpG* knockdown (**Figure 4A**; Jang et al., 2012). Production of the metabolites, acetate, butyrate, acetone, ethanol, and butanol, by BEKW-2866KD, was also analyzed and compared with that of BEKW (Jang et al., 2012). This analysis could be not confirmed significant changes in physiological characteristics (**Figure 4**). Furthermore, we found that the identified difference in residual butyrate between ATCC 824 and 824-2866KD was not repeated in the comparison between BEKW and BEKW-2866KD (**Figure 4D**).

The extracellular pH of BEKW and BEKW-2866KD, cultured while maintaining the pH above 5.0, was comparatively analyzed. During the solventogenic phase, pH steadily rose because of acid re-assimilation in both BEKW and BEKW-2866KD fermentations. The extracellular pH in BEKW cultures reached 5.9, a value that was

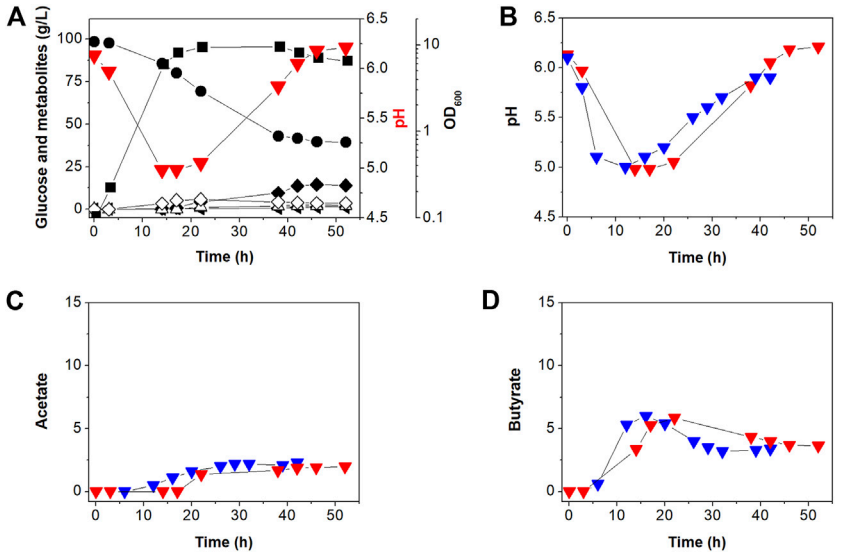

FIGURE 4 | Batch fermentation profiles of *C. acetobutylicum* BEKW-2866KD in bioreactor containing 2-L CGM (A). **(A)** Symbols are: ●, glucose; ■, cell density (OD_{600}); ▼, extracellular pH; △, acetate; ◇, butyrate; ▲, acetone; ◀, ethanol; and ◆, butanol. Other reproduced bioreactor cultivation profiles are shown in **Supplementary Figure S4**. **(B–D)** Comparison of the external pH change **(B)**, acetate **(C)**, and butyrate **(D)** in batch fermentations between *C. acetobutylicum* BEKW (blue) and its mutant BEKW-2866KD (red). For this comparison, pH, acetate, and butyrate values in the parent BEKW fermentation were obtained from our previous work (Jang et al., 2012).

maintained after 39 h (Jang et al., 2012). BEKW-2866KD reach a higher pH value of pH 6.54, which was maintained after 46 h (**Figure 4B**). In other reproduced bioreactor cultivation, pH 6.89 was observed at 46 h (**Supplementary Figure S4**). These results are similar to those obtained in comparisons between ATCC 824 and 824-2866KD, described above. The finding that *atpG* knockdown caused no significant differences in cell growth, glucose consumption, or metabolites production indicates that ATPase is relatively minor than acid-forming pathway in ATP metabolism in *C. acetobutylicum*. However, the fact that ATPase knockdown similarly affected extracellular pH in *atpG* knockdown strains indicates that ATPase is affected to extracellular pH at the late stationary phase in *C. acetobutylicum* fermentation. Taken together, it seems that the external pH was affected by not only the residual acids but also other effectors, such as inhibition of proton pumping by ATPase. Depending on the situation, F-ATPase can reversibly synthesize or degrade ATP (Löbau et al., 1998; Bowler et al., 2006; Hayashi et al., 2012). ATP is hydrolyzed to create a proton gradient through the plasma membrane, while PMF is used for ATP synthesis (Costa et al., 2021). The increase in extracellular pH shown in this study is presumed to be due to inhibition of proton pumping across the membrane by knockdown of the *atpG* gene. This seems to be closely related to the recent report that ATPase is inhibited by butanol, which resulted in a low intracellular pH and reduction of PMF (Costa et al., 2021).

In this study, we first constructed the *atpG* knockdown strains using the mobile group II intron system to investigate the role of the ATPase in *C. acetobutylicum*. Although other ATPase-disrupted non-clostridia organisms show prominent differences in ATP synthesis and cell growth, the *atpG* knockdown mutants of *C. acetobutylicum* ATCC 824 and BEKW, 824-2866KD and BEKW-2866KD, respectively, showed no significant changes in physiological characteristics except extracellular pH. The inference is that most ATP is produced through substrate-level phosphorylation in glycolysis and the acid-forming pathways in *C. acetobutylicum*. Detection of the ATP level may help to explain the phenomenon found in this work. As ATP and redox metabolism is complexly combined to biphasic fermentation in *C. acetobutylicum*, however, it is needed to approach it with a more elaborate strategy.

DATA AVAILABILITY STATEMENT

The original contributions presented in the study are included in the article/**Supplementary Material**, further inquiries can be directed to the corresponding authors.

AUTHOR CONTRIBUTIONS

SL and Y-SJ conceived the project. JI, HS, HL, and Y-SJ performed experiments. SK, Y-SL, HS, HL, YY, and Y-SJ were involved in analysis and interpretation of experimental data. SK, Y-SL, HS, HL, YY, SL and Y-SJ wrote the manuscript. All authors read and approved the final manuscript.

FUNDING

This work was supported by a grant from the Ministry of Science and ICT (MSIT) through the National Research Foundation

(NRF) of Korea (NRF-2019R1A4A1029125). SL was supported by the Technology Development Program to Solve Climate Changes on Systems Metabolic Engineering for Biorefineries from the MSIT through the NRF of Korea (NRF-2012M1A2A2026556 and NRF-2012M1A2A2026557).

SUPPLEMENTARY MATERIAL

The Supplementary Material for this article can be found online at: https://www.frontiersin.org/articles/10.3389/fbioe.2021.754250/full#supplementary-material

REFERENCES

An, S. H., Choi, G.-S., and Ahn, J.-H. (2020). Biosynthesis of Fraxetin from Three Different Substrates Using Engineered *Escherichia coli*. *Appl. Biol. Chem.* 63, 55. doi:10.1186/s13765-020-00543-9

Baek, S.-A., Ahn, S. K., Kim, K. W., Choi, J., Kim, J., Ahn, J., et al. (2019). Metabolic Profiling Reveals Glucose and Fructose Accumulation in *Gcr1* Knock-Out Mutant of *Arabidopsis*. *Appl. Biol. Chem.* 62, 23. doi:10.1186/s13765-019-0427-3

Borghese, R., Turina, P., Lambertini, L., and Melandri, B. A. (1998). The *atpIBEXF* Operon Coding for the F_0 Sector of the ATP Synthase from the Purple Nonsulfur Photosynthetic Bacterium Rhodobacter Capsulatus. *Arch. Microbiol.* 170, 385–388. doi:10.1007/s002030050657

Bowler, M. W., Montgomery, M. G., Leslie, A. G. W., and Walker, J. E. (2006). How Azide Inhibits ATP Hydrolysis by the F-ATPases. *Proc. Natl. Acad. Sci.* 103, 8646–8649. doi:10.1073/pnas.0602915103

Burger, M., Rein, S., Weber, S., Gräber, P., and Kacprzak, S. (2020). Distance Measurements in the F_0F_1-ATP Synthase from *E. coli* Using smFRET and PELDOR Spectroscopy. *Eur. Biophys. J.* 49, 1–10. doi:10.1007/s00249-019-01408-w

Causey, T. B., Zhou, S., Shanmugam, K. T., and Ingram, L. O. (2003). Engineering the Metabolism of *Escherichia coli* W3110 for the Conversion of Sugar to Redox-Neutral and Oxidized Products: Homoacetate Production. *Proc. Natl. Acad. Sci.* 100, 825–832. doi:10.1073/pnas.0337684100

Cho, C., Choe, D., Jang, Y.-S., Kim, K.-J., Kim, W. J., Cho, B.-K., et al. (2017). Genome Analysis of a Hyper Acetone-Butanol-Ethanol (ABE) Producing *Clostridium acetobutylicum* BKM19. *Biotechnol. J.* 12, 1600457. doi:10.1002/biot.201600457

Chun, J., and Sang, B.-I. (2020). Enzymatic Esterification under High-Pressure CO2 Conditions for *In Situ* Recovery of Butyric Acid from Anaerobic Fermenters. *Biotechnol. Bioproc. E* 25, 616–622. doi:10.1007/s12257-020-0158-7

Cipriano, D. J., Wood, K. S., Bi, Y., and Dunn, S. D. (2006). Mutations in the Dimerization Domain of the B Subunit from the *Escherichia coli* ATP Synthase. *J. Biol. Chem.* 281, 12408–12413. doi:10.1074/jbc.m513368200

Costa, P., Usai, G., Re, A., Manfredi, M., Mannino, G., Bertea, C. M., et al. (2021). *Clostridium Cellulovorans* Proteomic Responses to Butanol Stress. *Front. Microbiol.* 12, 674639. doi:10.3389/fmicb.2021.674639

Dai, Z., Zhu, Y., Dong, H., Zhao, C., Zhang, Y., and Li, Y. (2020). Enforcing ATP Hydrolysis Enhanced Glycolysis and Promoted Solvent Production under Anaerobic Conditions. *Microb. Cel Fact.* 20, 149. doi:10.21203/rs.3.rs-20422/v1

Du, G., Che, J., Wu, Y., Wang, Z., Jiang, Z., Ji, F., et al. (2021). Disruption of Hydrogenase Gene for Enhancing Butanol Selectivity and Production in *Clostridium acetobutylicum*. *Biochem. Eng. J.* 171, 108014. doi:10.1016/j.bej.2021.108014

Externbrink, T., Hujer, S., Winzer, K., and Dürre, P. (2000). Sequence Analysis of the *atp* Operon of *Clostridium acetobutylicum* DSM 792 Encoding the F_0F_1 ATP Synthase. *DNA Seq.* 11, 109–118. doi:10.3109/10425170009033977

Fast, A. G., and Papoutsakis, E. T. (2018). Functional Expression of the *Clostridium Ljungdahlii* Acetyl-Coenzyme A Synthase in *Clostridium acetobutylicum* as Demonstrated by a Novel *In Vivo* CO Exchange Activity En Route to Heterologous Installation of a Functional Wood-Ljungdahl Pathway. *Appl. Environ. Microbiol.* 84, e02307–02317. doi:10.1128/AEM.02307-17

Ferrándiz, M., and De La Campa, A. G. (2002). The Membrane-Associated F_0F_1 ATPase Is Essential for the Viability of *Streptococcus pneumoniae*. *FEMS Microbiol. Lett.* 212, 133–138. doi:10.1016/s0378-1097(02)00717-6

Hayashi, S., Ueno, H., Shaikh, A. R., Umemura, M., Kamiya, M., Ito, Y., et al. (2012). Molecular Mechanism of ATP Hydrolysis in F1-ATPase Revealed by Molecular Simulations and Single-Molecule Observations. *J. Am. Chem. Soc.* 134, 8447–8454. doi:10.1021/ja211027m

Heap, J. T., Pennington, O. J., Cartman, S. T., Carter, G. P., and Minton, N. P. (2007). The ClosTron: a Universal Gene Knock-Out System for the Genus *Clostridium*. *J. Microbiol. Methods* 70, 452–464. doi:10.1016/j.mimet.2007.05.021

Im, H. S., Kim, C., Song, Y. E., Baek, J., Im, C. H., and Kim, J. R. (2019). Isolation of Novel CO Converting Microorganism Using Zero Valent Iron for a Bioelectrochemical System (BES). *Biotechnol. Bioproc. E* 24, 232–239. doi:10.1007/s12257-018-0373-7

Im, H., An, T., Kwon, R., Park, S., and Kim, Y.-K. (2021). Effect of Organic Nitrogen Supplements on Syngas Fermentation Using *Clostridium Autoethanogenum*. *Biotechnol. Bioproc. Eng.* 26, 476–482. doi:10.1007/s12257-020-0221-4

Iwamoto, A., Miki, J., Maeda, M., and Futai, M. (1990). H(+)-ATPase Gamma Subunit of *Escherichia coli*. Role of the Conserved Carboxyl-Terminal Region. *J. Biol. Chem.* 265, 5043–5048. doi:10.1016/s0021-9258(19)34081-5

Jang, Y. S., Lee, J. Y., Lee, J., Park, J. H., Im, J. A., Eom, M. H., et al. (2012). Enhanced Butanol Production Obtained by Reinforcing the Direct Butanol-Forming Route in *Clostridium acetobutylicum*. *mBio* 3, e00314–00312. doi:10.1128/mBio.00314-12

Jang, Y.-S., Han, M.-J., Lee, J., Im, J. A., Lee, Y. H., Papoutsakis, E. T., et al. (2014a). Proteomic Analyses of the Phase Transition from Acidogenesis to Solventogenesis Using Solventogenic and Non-solventogenic *Clostridium acetobutylicum* Strains. *Appl. Microbiol. Biotechnol.* 98, 5105–5115. doi:10.1007/s00253-014-5738-z

Jang, Y.-S., Im, J. A., Choi, S. Y., Lee, J. I., and Lee, S. Y. (2014b). Metabolic Engineering of *Clostridium acetobutylicum* for Butyric Acid Production with High Butyric Acid Selectivity. *Metab. Eng.* 23, 165–174. doi:10.1016/j.ymben.2014.03.004

Jensen, P. R., and Michelsen, O. (1992). Carbon and Energy Metabolism of *atp* Mutants of *Escherichia coli*. *J. Bacteriol.* 174, 7635–7641. doi:10.1128/jb.174.23.7635-7641.1992

Jiang, Y., Wu, R., Lu, J., Dong, W., Zhou, J., Zhang, W., et al. (2021). Quantitative Proteomic Analysis to Reveal Expression Differences for Butanol Production from Glycerol and Glucose by *Clostridium* Sp. Strain CT7. *Microb. Cell Fact.* 20, 12. doi:10.1186/s12934-021-01508-3

Kang, C., Sun, F., Yan, L., Li, R., Bai, J., and Caetano-Anollés, G. (2019). Genome-Wide Identification and Characterization of the Vacuolar H^+-ATPase Subunit H Gene Family in Crop Plants. *Ijms* 20, 5125. doi:10.3390/ijms20205125

Kim, S., Jang, Y.-S., Ha, S.-C., Ahn, J.-W., Kim, E.-J., Hong Lim, J., et al. (2015). Redox-switch Regulatory Mechanism of Thiolase from *Clostridium acetobutylicum*. *Nat. Commun.* 6, 8410. doi:10.1038/ncomms9410

Kim, J.-T., Yi, G., Kim, M.-J., Son, B.-Y., Bae, H.-H., Go, Y. S., et al. (2020). Glycolysis Stimulation and Storage Protein Accumulation Are Hallmarks of maize (*Zea mays* L.) Grain Filling. *Appl. Biol. Chem.* 63, 54. doi:10.1186/s13765-020-00538-6

Koch-Koerfges, A., Kabus, A., Ochrombel, I., Marin, K., and Bott, M. (2012). Physiology and Global Gene Expression of a *Corynebacterium glutamicum* ΔF_1F_O-ATP Synthase Mutant Devoid of Oxidative Phosphorylation. *Biochim. Biophys. Acta (BBA) - Bioenerg.* 1817, 370–380. doi:10.1016/j.bbabio.2011.10.006

Koebmann, B. J., Nilsson, D., Kuipers, O. P., and Jensen, P. R. (2000). The Membrane-Bound H^+-ATPase Complex Is Essential for Growth of *Lactococcus lactis*. *J. Bacteriol.* 182, 4738–4743. doi:10.1128/jb.182.17.4738-4743.2000

Koebmann, B. J., Solem, C., Pedersen, M. B., Nilsson, D., and Jensen, P. R. (2002a). Expression of Genes Encoding F_1 -ATPase Results in Uncoupling of Glycolysis from Biomass Production in *Lactococcus lactis*. *Appl. Environ. Microbiol.* 68, 4274–4282. doi:10.1128/aem.68.9.4274-4282.2002

Koebmann, B. J., Westerhoff, H. V., Snoep, J. L., Nilsson, D., and Jensen, P. R. (2002b). The Glycolytic Flux in *Escherichia coli* Is Controlled by the Demand for ATP. *J. Bacteriol.* 184, 3909–3916. doi:10.1128/jb.184.14.3909-3916.2002

Kwon, S. W., Paari, K. A., Malaviya, A., and Jang, Y.-S. (2020). Synthetic Biology Tools for Genome and Transcriptome Engineering of Solventogenic *Clostridium*. *Front. Bioeng. Biotechnol.* 8, 282. doi:10.3389/fbioe.2020.00282

Lai-Zhang, J., Xiao, Y., and Mueller, D. M. (1999). Epistatic Interactions of Deletion Mutants in the Genes Encoding the F_1-ATPase in Yeast *Saccharomyces cerevisiae*. *EMBO J.* 18, 58–64. doi:10.1093/emboj/18.1.58

Lee, J. S., Paje, L. A., Choi, W.-H., Cho, E. J., Kim, H. Y., Jacinto, S. D., et al. (2020). Validation of an Optimized HPLC/UV Method for the Quantification of Flavonoids in Lotus. *Appl. Biol. Chem.* 63, 84. doi:10.1186/s13765-020-00568-0

Li, S., Huang, L., Ke, C., Pang, Z., and Liu, L. (2020). Pathway Dissection, Regulation, Engineering and Application: Lessons Learned from Biobutanol Production by Solventogenic Clostridia. *Biotechnol. Biofuels* 13, 39. doi:10.1186/s13068-020-01674-3

Löbau, S., Weber, J., and Senior, A. E. (1998). Catalytic Site Nucleotide Binding and Hydrolysis in F_1Fo-ATP Synthase. *Biochemistry* 37, 10846–10853. doi:10.1021/bi9807153

Lone, S. R., Kumar, V., Seay, J. R., Englert, D. L., and Hwang, H. T. (2020). Mass Transfer and Rheological Characteristics in a Stirred Tank Bioreactor for Cultivation of *Escherichia coli* BL21. *Biotechnol. Bioproc. Eng.* 25, 766–776. doi:10.1007/s12257-020-0028-3

Lütke-Eversloh, T. (2014). Application of New Metabolic Engineering Tools for *Clostridium acetobutylicum*. *Appl. Microbiol. Biotechnol.* 98, 5823–5837. doi:10.1007/s00253-014-5785-5

Mermelstein, L. D., and Papoutsakis, E. T. (1993). *In Vivo* Methylation in *Escherichia coli* by the *Bacillus Subtilis* Phage Phi 3T I Methyltransferase to Protect Plasmids from Restriction upon Transformation of *Clostridium acetobutylicum* ATCC 824. *Appl. Environ. Microbiol.* 59, 1077–1081. doi:10.1128/aem.59.4.1077-1081.1993

Mukherjee, S., and Warshel, A. (2015). Dissecting the Role of the γ-subunit in the Rotary-Chemical Coupling and Torque Generation of F_1-ATPase. *Proc. Natl. Acad. Sci. U.S.A* 112, 2746–2751. doi:10.1073/pnas.1500979112

Nölling, J., Breton, G., Omelchenko, M. V., Makarova, K. S., Zeng, Q., Gibson, R., et al. (2001). Genome Sequence and Comparative Analysis of the Solvent-Producing Bacterium *Clostridium acetobutylicum*. *J. Bacteriol.* 183, 4823–4838. doi:10.1128/JB.183.16.4823-4838.2001

Poehlein, A., Solano, J. D. M., Flitsch, S. K., Krabben, P., Winzer, K., Reid, S. J., et al. (2017). Microbial Solvent Formation Revisited by Comparative Genome Analysis. *Biotechnol. Biofuels* 10, 58. doi:10.1186/s13068-017-0742-z

Santana, M., Ionescu, M. S., Vertes, A., Longin, R., Kunst, F., Danchin, A., et al. (1994). *Bacillus subtilis* F_0F_1 ATPase: DNA Sequence of the *atp* Operon and Characterization of *atp* Mutants. *J. Bacteriol.* 176, 6802–6811. doi:10.1128/jb.176.22.6802-6811.1994

Sekine, H., Shimada, T., Hayashi, C., Ishiguro, A., Tomita, F., and Yokota, A. (2001). H^+-ATPase Defect in *Corynebacterium glutamicum* Abolishes Glutamic Acid Production with Enhancement of Glucose Consumption Rate. *Appl. Microbiol. Biotechnol.* 57, 534–540. doi:10.1007/s002530100778

Shah, N. B., and Duncan, T. M. (2015). Aerobic Growth of *Escherichia coli* Is Reduced, and ATP Synthesis Is Selectively Inhibited when Five C-terminal Residues Are Deleted from the ϵ Subunit of ATP Synthase. *J. Biol. Chem.* 290, 21032–21041. doi:10.1074/jbc.m115.665059

Shao, L., Hu, S., Yang, Y., Gu, Y., Chen, J., Yang, Y., et al. (2007). Targeted Gene Disruption by Use of A Group II Intron (Targetron) Vector in *Clostridium acetobutylicum*. *Cell Res.* 17, 963–965. doi:10.1038/cr.2007.91

Shin, K., Nakamoto, R. K., Maeda, M., and Futai, M. (1992). F_0F_1-ATPase Gamma Subunit Mutations Perturb the Coupling between Catalysis and Transport. *J. Biol. Chem.* 267, 20835–20839. doi:10.1016/s0021-9258(19)36763-8

Shin, Y.-A., Choi, S., and Han, M. (2021). Simultaneous Fermentation of Mixed Sugar by a Newly Isolated *Clostridium beijerinckii* GSC1. *Biotechnol. Bioproc. Eng.* 26, 137–144. doi:10.1007/s12257-020-0183-6

Thi, H. N., Park, S., Li, H., and Kim, Y.-K. (2020). Medium Compositions for the Improvement of Productivity in Syngas Fermentation with *Clostridium autoethanogenum*. *Biotechnol. Bioproc. E.* 25, 493–501. doi:10.1007/s12257-019-0428-4

Tremblay, P. L., Zhang, T., Dar, S. A., Leang, C., and Lovley, D. R. (2012). The Rnf Complex of *Clostridium ljungdahlii* Is a Proton-Translocating ferredoxin: NAD^+ Oxidoreductase Essential for Autotrophic Growth. *mBio* 4, e00406–12. doi:10.1128/mBio.00406-12

Weber, E. R., Rooks, R. S., Shafer, K. S., Chase, J. W., and Thorsness, P. E. (1995). Mutations in the Mitochondrial ATP Synthase Gamma Subunit Suppress A Slow-Growth Phenotype of *yme1* Yeast Lacking Mitochondrial DNA. *Genetics* 140, 435–442. doi:10.1093/genetics/140.2.435

Zhang, X. C., and Zhang, H. (2019). P-type ATPases Use a Domain-Association Mechanism to Couple ATP Hydrolysis to Conformational Change. *Biophys. Rep.* 5, 167–175. doi:10.1007/s41048-019-0087-1

Zharova, T. V., and Vinogradov, A. D. (2017). Functional Heterogeneity of Fo·F_1H^+-ATPase/synthase in Coupled *Paracoccus denitrificans* Plasma Membranes. *Biochim. Biophys. Acta (BBA) - Bioenerg.* 1858, 939–944. doi:10.1016/j.bbabio.2017.08.006

Conflict of Interest: The authors declare that the research was conducted in the absence of any commercial or financial relationships that could be construed as a potential conflict of interest.

Publisher's Note: All claims expressed in this article are solely those of the authors and do not necessarily represent those of their affiliated organizations, or those of the publisher, the editors and the reviewers. Any product that may be evaluated in this article, or claim that may be made by its manufacturer, is not guaranteed or endorsed by the publisher.

frontiers in Bioengineering and Biotechnology

ORIGINAL RESEARCH
published: 10 January 2022
doi: 10.3389/fbioe.2021.760500

Enhanced L-Malic Acid Production by *Aspergillus oryzae* DSM 1863 Using Repeated-Batch Cultivation

*Vanessa Schmitt, Laura Derenbach and Katrin Ochsenreither**

Institute of Process Engineering in Life Sciences 2: Technical Biology, Karlsruhe Institute of Technology (KIT), Karlsruhe, Germany

L-Malic acid is a C4-dicarboxylic acid and a potential key building block for a bio-based economy. At present, malic acid is synthesized petrochemically and its major market is the food and beverages industry. In future, malic acid might also serve as a building block for biopolymers or even replace the commodity chemical maleic anhydride. For a sustainable production of L-malic acid from renewable resources, the microbial synthesis by the mold *Aspergillus oryzae* is one possible route. As CO_2 fixation is involved in the biosynthesis, high yields are possible, and at the same time greenhouse gases can be reduced. In order to enhance the production potential of the wild-type strain *Aspergillus oryzae* DSM 1863, process characteristics were studied in shake flasks, comparing batch, fed-batch, and repeated-batch cultivations. In the batch process, a prolonged cultivation time led to malic acid consumption. Keeping carbon source concentration on a high level by pulsed feeding could prolong cell viability and cultivation time, however, did not result in significant higher product levels. In contrast, continuous malic acid production could be achieved over six exchange cycles and a total fermentation time of 19 days in repeated-batch cultivations. Up to 178 g/L L-malic acid was produced. The maximum productivity (0.90 ± 0.05 g/L/h) achieved in the repeated-batch cultivation had more than doubled than that achieved in the batch process and also the average productivity (0.42 ± 0.03 g/L/h for five exchange cycles and 16 days) was increased considerably. Further repeated-batch experiments confirmed a positive effect of regular calcium carbonate additions on pH stability and malic acid synthesis. Besides calcium carbonate, nitrogen supplementation proved to be essential for the prolonged malic acid production in repeated-batch. As prolonged malic acid production was only observed in cultivations with product removal, product inhibition seems to be the major limiting factor for malic acid production by the wild-type strain. This study provides a systematic comparison of different process strategies under consideration of major influencing factors and thereby delivers important insights into natural L-malic acid production.

Keywords: organic acids, malic acid, *Aspergillus oryzae*, fungi, batch, repeated-batch, fed-batch, productivity

OPEN ACCESS

Edited by:
Fengjie Cui,
Jiangsu University, China

Reviewed by:
Chi Cheng,
Dalian University of Technology, China
Xue Cai,
Zhejiang University of Technology, China

****Correspondence:***
Katrin Ochsenreither
katrin.ochsenreither@kit.edu

Specialty section:
This article was submitted to Industrial Biotechnology, a section of the journal Frontiers in Bioengineering and Biotechnology

Received: *18 August 2021*
Accepted: *11 November 2021*
Published: *10 January 2022*

Citation:
Schmitt V, Derenbach L and Ochsenreither K (2022) Enhanced L-Malic Acid Production by Aspergillus oryzae *DSM 1863 Using Repeated-Batch Cultivation. Front. Bioeng. Biotechnol. 9:760500. doi: 10.3389/fbioe.2021.760500*

INTRODUCTION

Over the past decades, concerns about climate change and oil depletion led to a growing interest in the idea of a bio-based economy, in which fuels, chemicals, and pharmaceuticals are produced from renewable resources *via* eco-friendly synthesis routes. In 2004, malic acid was identified as one potential key building block for the bio-economy (Werpy et al., 2004). As a dicarboxylic acid with an additional hydroxy group, malic acid has several established applications in the food and beverages industry, as a buffer and chelating agent, and in the pharmaceutical industry. Furthermore, it might be applied as a building block for homo- and heteropolymers, for biomedical applications, such as drug carriers, and as a component in low transition temperature mixtures for eco-friendly extraction purposes. Moreover, it has the potential to replace the established platform chemical maleic anhydride (Koevilein et al., 2020).

Malic acid is mainly produced chemically as a racemic mixture from fossil resources with an estimated global market volume of 80,000–100,000 ton per year (Koevilein et al., 2020). In contrast, enantiopure L-malic acid (physiological form) can be exclusively produced enzymatically or by microbial synthesis. Advantageous in this case is the classification as "nature identical" (NATRUE lable, https://www.natrue.org/), which results in a higher sales value and is needed for pharmaceutical applications. The polymer of L-malic acid is also adsorbed differently than a polymer of the racemate when used as a carrier material for pharmaceuticals (Lee et al., 2011). In addition, homo- and heteropolymers derived from L-, D-, or DL-malic acid might have different characteristics since the racemate and both enantiomers vary in melting and boiling point (Fiume, 2001).

A sustainable route for the L-malic acid production is the microbial fermentation. Although L-malic acid is part of the TCA cycle, its accumulation and secretion into culture broth was only observed under certain stress conditions in a few filamentous fungi and yeasts, such as *Aspergillus* and *Ustilago* species (Koevilein et al., 2020). These fungi accumulate L-malic acid *via* a reductive branch of the TCA cycle located in the cytosol, under nitrogen limitation and simultaneous excess of the carbon source. The biosynthesis is ATP neutral and includes a CO_2 fixation step, resulting in a theoretical yield of 2 mol L-malic acid per mol glucose (Zelle et al., 2008).

Among the genus *Aspergillus*, *A. oryzae* is a very promising natural L-malic acid producer for industrial scale fermentations, due to the combination of strain safety, robustness, wide substrate range, and a high production capacity (Koevilein et al., 2020). However, L-malic acid production from renewable resources is still missing the economic competitiveness to substitute petrochemical synthesis routes. The key aspects for increasing productivities and yields and therefore economic viability of biotechnological processes are optimization of media and process conditions as well as genetical engineering.

In terms of media optimization, the nitrogen source and the C:N ratio have been identified as important aspects for the L-malic acid production with *A. oryzae*. According to Ding et al. much higher malic acid titers can be achieved by using complex nitrogen sources such as tryptone instead of ammonium sulfate. Furthermore, malic acid production can be increased by optimization and control of the C:N ratio (Ochsenreither et al., 2014; Liu et al., 2017; Ding et al., 2018; Ji et al., 2021). Another study proved the importance of calcium carbonate supply for pH stability and malic acid production (Geyer et al., 2018).

Concerning genetical engineering, L-malic acid production was improved considerably by strengthening the malic acid export due to the overexpression of a C4-dicarboxylate transporter gene from *A. oryzae* and the L-malate permease gene from *Schizosaccharomyces pombe* (Brown et al., 2013; Liu et al., 2017; Liu et al., 2018). The genetical modifications introduced by Brown et al. (2013) resulted in the highest reported yields, so far. In 2 L bioreactor batch cultivations on 100 g glucose and 6 g peptone, a yield of 1.00 g/g or 1.38 mol/mol was reached after 164 h, corresponding to 69% of the theoretical maximum. The best results for malic acid production using ammonium sulfate as a nitrogen source were achieved by Ding et al. in 7.5 L fed-batch with a mutant strain of *A. oryzae*. On 176 g/L glucose and 5.5 g/L $(NH_4)_2SO_4$, a titer of 95.2 g/L L-malic acid was achieved, corresponding to productivity of 0.57 g/L/h and a yield of 0.54 g/g or 0.73 mol/mol.

It is noticeable that for the L-malic acid production with natural producers, mostly batch processes and only occasionally fed-batch processes are applied. To our knowledge, there is only one study, in which batch and fed-batch cultivations of *A. oryzae* are directly compared regarding the malic acid synthesis. Liu et al. (2017) tested an automated fed-batch process for a genetically modified *A. oryzae* high-performance strain and compared it to batch fermentation. In this 3 L fed-batch cultivation, the L-malic acid concentration reached a maximum of 165 g/L after 120 h, resulting in a productivity of 1.38 g/L/h. This is the highest malic acid titer achieved with *A. oryzae*. In contrast, only 73 g/L L-malic acid was produced in the batch process until glucose depletion after 60 h. A fed-batch process was also applied for the L-malic acid production with *U. trichophora* using large quantities of glycerol (Zambanini et al., 2016), probably due to the high viscosity of the substrate.

In contrast, data for repeated-batch processes are only available for fungal production of other organic acids. Advantages, such as prolonged product synthesis and increased productivities, were observed in fungal repeated-batch cultivations for the production of organic acids, such as kojic acid (Wan et al., 2005), fumaric acid (Petruccioli et al., 1996), itaconic acid (Park et al., 1994; Hosseinpour Tehrani et al., 2019), citric acid (Roukas, 1991; Sakurai and Imai, 1992; Yu et al., 2018), lactic acid (Yang et al., 1995; Yin et al., 1998), and isocitric acid (Morgunov et al., 2019). As a reason for the improved acid synthesis, a reduction of product inhibition is assumed. Accordingly, repeated-batch cultivation should also be beneficial for L-malic acid production with *A. oryzae*.

This study aims to compare systematically different cultivation strategies for the L-malic acid synthesis by the wild-type *A. oryzae* DSM 1863. For this purpose, process characteristics of batch, fed-batch, and repeated-batch cultivations were determined in parallel shake flask experiments. Thereby, the study

TABLE 1 | Overview of the experimental conditions.

Experiment no. and general conditions	Cultivation name/process mode	Addition of $CaCO_3$[a]	Feed/exchange medium
No. 1 Feeding and exchange rate[b]: every 3 days; temperature: 35°C	Batch A	—	—
	FB A	—	Glucose
	FB B	—	Glucose and N-source
	FB C	—	Complete medium[c]
	RB A	6 g after every exchange	Complete medium[c]
	RB B	3 g after every exchange	Complete medium[c]
No. 2 Feeding and exchange rate[b]: every 2 days; temperature: 32°C	Batch B	—	—
	RB C	Regular additions of 2.5 g as needed[d]	Complete medium[c]
	RB D	t = 336 h: 9 g and t > 336 h: Regular additions of 2.5 g as needed[d]	Complete medium[c]
	RB E	Regular additions of 2.5 g as needed[d]	Complete medium[c] and without N-source

[a]*Starting concentration of calcium carbonate of all cultivations was 90 g/L.*
[b]*Feeding and exchange rates after the initial growth phase of 4 days.*
[c]*The "complete medium" comprises all components of the batch medium as listed in the Materials and Methods section, except for sodium chloride.*
[d]*"As needed" means that calcium carbonate was only added in case the medium has cleared up.*

illuminates the question whether the high productivities, observed in genetically modified organisms (GMOs) with overexpressed transporter genes, can also be achieved with a wild-type strain by changing the process mode. Hence, different feeding regimes for fed-batch and repeated-batch cultivations were tested, and the overall produced malic acid amount, productivities, and yields were compared to batch fermentations. Additionally, the study provides new insights into the role of nitrogen and calcium carbonate for prolonged L-malic acid production processes.

MATERIALS AND METHODS

Chemicals

All chemicals were either purchased from Sigma-Aldrich (Munich, Germany) or Roth (Karlsruhe, Germany).

General Cultivation Aspects: Fungi, Media, and Cultivation Conditions

The fungal strain *A. oryzae* DSM 1863 was obtained from the DSMZ strain collection (Deutsche Sammlung von Mikroorganismen und Zellkulturen GmbH, Braunschweig, Germany). The strain was treated as described by Dörsam et al. (Dörsam et al., 2016), and the generated conidia aliquots in glycerin were stored at −80°C until further usage.

The L-malic acid production was performed in a two-step process, including a pre-culture and a main culture medium. The pre-culture medium consists of 40 g/L glucose monohydrate, 4 g/L $(NH_4)_2SO_4$, 0.75 g/L KH_2PO_4, 0.98 g/L K_2HPO_4 $3H_2O$, 0.1 g/L $MgSO_4$ $7H_2O$, 0.1 g/L $CaCl_2$ $2H_2O$, 0.005 g/L NaCl, and 0.005 g/L $FeSO_4$ $7H_2O$. The main culture medium comprises 120 g/L glucose monohydrate, 1.2 g/L $(NH_4)_2SO_4$, 0.1 g/L KH_2PO_4, 0.17 g/L K_2HPO_4 $3H_2O$, 0.1 g/L $MgSO_4$ $7H_2O$, 0.1 g/L $CaCl_2$ $2H_2O$, 0.005 g/L NaCl, and 0.060 g/L $FeSO_4$ $7H_2O$. The media were sterilized by autoclaving. For pH regulation, sterile 90 g/L $CaCO_3$ was added to the autoclaved main culture medium.

The fermentation process for L-malic acid production with *A. oryzae* was carried out in 500-ml baffled Erlenmeyer shake flasks with a working volume of 100 ml. The pre-culture was inoculated with 2×10^7 conidia and incubated at 100 rpm and 30°C for 24 h in a rotary shaker with a shaking diameter of 25 mm. Next, the pre-culture medium was removed; the fungal pellets were washed twice and resuspended in 100 ml water before being transferred to the main culture medium. The shake flasks were inoculated with 10% (v/v) washed pre-culture and incubated at 120 rpm and 32 or 35°C (**Table 1**).

L-Malic Acid Production

In the first experiment, five shake flask cultivations were carried out in parallel: one batch (Batch A), two repeated-batch (RB A/B), and three fed-batch fermentations (FB A/B/C). In the repeated-batch approach, the addition of different amounts of calcium carbonate with every media exchange was compared (6 g $CaCO_3$ in RB A vs. 3 g in RB B). In the fed-batch process, three different feed compositions were tested. Feeding or medium replacement in the first parallel cultivation experiment was performed every third day. For further evaluation of the repeated-batch process, another set of experiments was conducted, including a batch process (Batch B) as a control and three different repeated-batch scenarios (RB C/D/E) with a 2-day medium exchange regime. This second set of fermentations (RB C/D/E) was run at 32°C. Besides the more frequent medium replacements, the role of calcium carbonate and ammonium was evaluated by omitting the addition of one of the two chemicals during the cultivation in RB D and E, respectively.

All experiments (**Table 1**) were performed as triplicate with three individual shake flasks for each tested condition. The cultivations were run for a minimum of at least 2 weeks (Batch A) to a maximum of 23 days (RB C). For sampling, 5 ml from the fermentation broth was transferred to a sampling vessel, excluding fungal pellets. After pH measurement, the samples were stored at −20°C until HPLC analysis. After initial sampling prior incubation, no samples were taken in the first 72 h of the fermentation. Afterward, regular

sampling was performed, depending on the needs of the cultivation process. In batch fermentations, samples were taken every 24–48 h. In the fed-batch and repeated-batch cultivations, samples were also taken prior and directly after each feeding or medium replacement.

In the fed-batch approach, feed volume was chosen to be 20 ml to compensate the volume loss due to sampling. The glucose concentration of all feed solutions was 250 g/L, except for the first feed with only 200 g/L, assuming lower glucose consumption during the growth phase at the beginning of the cultivation. While in FB A, the feed solely includes glucose, all main culture medium components, except for NaCl, were incorporated in FB C. The feeds of FB C comprised 6 g/L $(NH_4)_2SO_4$, 0.5 g/L KH_2PO_4, 0.75 g/L $K_2HPO_4{\cdot}3H_2O$, 0.5 g/L$MgSO_4$ $7H_2O$, 0.5 g/L $CaCl_2$ $2H_2O$, 0.3 mg/L $FeSO_4$ $7H_2O$, and glucose with the aforementioned variable concentration. FB B combines a carbon and nitrogen feed, adding 6 g/L $(NH_4)_2SO_4$ to the glucose solution.

In repeated-batch cultivations, the medium was removed by decanting, and shake flasks were refilled with the 100 ml fresh medium. In RB A, B, C, and D, the fresh medium had the same composition as the initial main culture medium, whereas in RB E ammonium sulfate was omitted from the exchange medium. The medium of the first batch included in all cultivations contained 9 g $CaCO_3$. Additional calcium carbonate was regularly added in all repeated-batch cultivations, except for RB D, to supplement the loss of calcium carbonate caused by the exchange procedure. While calcium carbonate was added after each medium replacement in RB A (6 g) and RB B (3 g), in RB C and E, 2.5 g $CaCO_3$ was only added to the fresh medium in case the medium has become quite clear. In RB E, the regular calcium carbonate additions were omitted, and 9 g $CaCO_3$ was added twice; at the beginning of the experiment and after the L-malic acid production had virtually stopped. Afterward, calcium carbonate (2.5 g) was added only in case the medium has become quite clear.

L-Malic Acid and Glucose Analytics

The quantification of L-malic acid and glucose was carried out with a high-performance liquid chromatography (HPLC) using an Agilent 1100 Series LC system (Agilent, Germany).

The glucose concentration was determined in the supernatant of the fermentation broth samples after centrifugation for 5 min at 20,000 × g in a benchtop device. HPLC was equipped with a Rezex™ ROA-Organic Acid H+ (8%) LC Column (300 x 7.8, Phenomenex, Aschaffenburg, Germany) and a pre-connected Rezex™ ROA-Organic Acid H+ Guard Column (50 × 7.8 mm, Phenomenex). Glucose was detected *via* a refractive index detector (Agilent 1200 Series, Agilent, Germany). The analysis was performed under isocratic conditions at a column temperature of 50°C for 20 min with 5 mM H_2SO_4 as the mobile phase and at a constant flow rate of 0.5 ml/min. The injection volume was 10 µl.

For malic acid quantification, 1 ml culture broth was mixed with 1 ml 3 M H_2SO_4 and 3 ml water and heated to 80°C for 20 min to resolve the precipitated calcium malate. After centrifugation of the mixture for 5 min at 20,000 × g, the supernatant was analyzed *via* HPLC. The device was equipped with a Synergi™ 4 µm Fusion-RP 80Å LC Column (150 × 4.6 mm, Phenomenex, Aschaffenburg, Germany). The analysis was performed at a column temperature of 30°C and a flow rate of 1 ml/min. The following gradient was applied using 100% methanol (eluant A) and 20 mM KH_2PO_4 with a pH of 2.5 (eluant B): 0–0.5 min 100% eluant B, 0.5–10 min increase of eluant A from 0–10%, 10–12 min decrease of eluant A from 10% back to 0%, and 12–14 min again 100% eluant B. Malic acid was detected *via* UV at a wavelength of 220 nm. The injection volume was 10 µl.

RESULTS

Previously, we reported that *A. oryzae* DSM 1863 is a promising natural L-malic acid producer with a wide substrate range (Ochsenreither et al., 2014; Dörsam et al., 2017; Kövilein et al., 2021). For further process understanding and optimization of malic acid production, we compared the three fermentation strategies, batch, fed-batch, and repeated-batch, in parallel shake flask cultivations. A variety of different experimental setups was tested in triplicate.

Characterization of L-Malic Acid Production in Batch Cultivations

The L-malic acid production in batch cultivations can be divided into three phases (Batch A1-3 in **Figures 1A–C**): the fungal growth phase, the major production phase, and a final malic acid reduction phase. In the first 72 h of cultivation, when fungal pellets grow, glucose and ammonium are consumed and malic acid synthesis starts; a steep decrease of the pH value from 7.84 ± 0.08 to 6.75 ± 0.01 occurred (**Figure 1C**). From further experiments with daily sampling between 0 and 72 h, it is known that the pH drop has happened already in the first 48 h until ammonium is depleted (data not shown). After the initial growth phase, a slow but continuous decline of the pH value over time could be observed, when the malic acid production accelerated. The triplicate showed significant deviations with regard to the maximum malic acid titers and the time points, at which the maximum product concentration was measured (**Figure 1B**). However, in each individual batch cultivation, malic acid concentration clearly peaked, followed by a steep decline afterward, presumably due to product metabolization. For the glucose concentration, the triplicate data were much more consistent. In all cultivations, glucose was fully consumed after 263 h of incubation (**Figure 1A**). Starting with an initial concentration of 88.3 ± 2.1 g/L, glucose was consumed continuously with an average glucose consumption rate of 0.40 ± 0.05 g/L/h in the first 191 h of cultivation. Accordingly, the estimated time of glucose depletion was 222 h. The highest L-malic acid titer was measured in Batch A1 with 50.7 g/L after 191 h. But the maximum might have been even higher, as no sample was taken at the calculated glucose depletion time. In contrast, malic acid production in Batch A2 and Batch A3 stopped

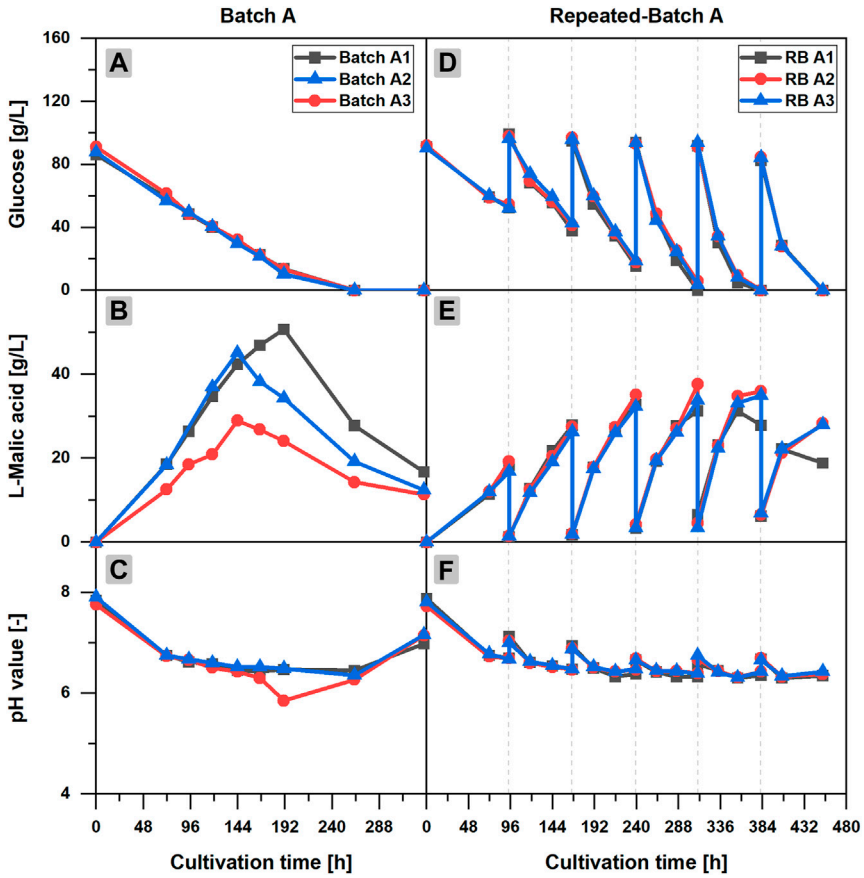

FIGURE 1 | L-Malic acid production in batch and repeated-batch cultivations of *Aspergillus oryzae* DSM 1863. Course of the glucose concentration **(A,D)**, the L-malic acid concentration **(B,E)**, the pH value **(C,F)** of Batch A **(A–C),** and repeated-batch A **(D–F)** over the cultivation time. The triplicate data A1–3 of the batch and repeated-batch cultivations are distinguishable by color and symbol. The gray vertical, dotted lines indicate the times of medium exchange for the repeated-batch cultivation.

before glucose was totally consumed, reaching maximum product concentrations of 45.1 g/L and 29.0 g/L, respectively, after 144 h and leaving about 30 g/L of residual glucose. Despite different time points for the maxima, a similar increase of the malic acid concentration could be observed in Batch A1 and Batch A2 until 144 h of cultivation. In contrast, the malic acid synthesis in Batch A3 was slower, right from the start of the cultivation, although the glucose consumption was comparable in all batches. Batch A3 also showed deviations with regard to the pH value, in particular the pH drops from 6.30 after 166 h to a minimum of 5.85 after 191 h (**Figures 1C**). Nevertheless, the course of the pH value was similar for all batches. The slow decline of the pH value during the major malic acid production phase continued after the malic acid concentration peaked, reaching a minimum of 6.36 ± 0.09 after 263 h, disregarding the pH drop of Batch A3 at 191 h. The end of the fermentation was characterized by a steep increase of the pH to 7.10 ± 0.10 after 336 h and an increasing number of fragmented fungal pellets.

For a later comparison to the other process mode experiments, yields, productivities, and glucose consumption rates were calculated based on glucose and L-malic acid concentrations after 144 h (**Table 2**).

Longer Productive Phase in Repeated-Batch Cultivations

Two repeated-batch cultivations were performed with regular additions of either 6 g (RB A) or 3 g (RB B) $CaCO_3$ to the fermentation broth after each medium replacement. In both fermentations, L-malic acid was continuously synthesized in considerable amounts throughout the 453 h (19 days) of cultivation. However, with 178.0 ± 4.2 g/L, the total L-malic acid production was the highest for the cultivation with regular additions of 6 g $CaCO_3$ (RB A). Accordingly, the overall glucose consumption in cultivations with the larger calcium carbonate dosage also exceeded (**Table 2**) the substrate consumption in the fermentations with only 3 g $CaCO_3$ (RB B). Regarding pH, the reduced calcium carbonate supplementation resulted in lower values, especially in the second half of the cultivation, and with 6.09 in a lower pH minimum (**Table 2**). However, increasing the calcium carbonate additions

TABLE 2 | Comparison of process modes for L-malic acid production with *A. oryzae* DSM 1863 in 100-ml shake flasks.

Process mode[a]	Time[b] (h)	$CaCO_3$ addition[c] (g)	MA productivity[d] (g)	SD (g)	Glucose consumption rate[d] (g)	SD (g)	Yield (g/g)	SD (g)	pH min (-)	SD (-)
Batch A	144	—	3.88	0.70	5.74	0.17	0.68	0.13	6.36[e]	0.09
RB A	453	6	17.80	0.42	44.05	0.54	0.40	0.01	6.31	0.01
RB B	453	3	15.02	0.81	43.24	0.73	0.35	0.02	6.09	0.01
FB C	453	—	4.67	0.29	41.90	0.33	0.11	0.01	5.19	0.05

[a]*Best performing experiments for the individual process modes batch, repeated-batch (RB), and fed-batch (FB) were selected for comparison of the process modes based on specific process characteristics.*
[b]*For Batch A, the cultivation time until the maximum product titer is given (total cultivation time 333 h). For RB A/B and FB C, the overall cultivation time is given.*
[c]*Regular additions of calcium carbonate during cultivation. Starting concentration of calcium carbonate of all cultivations was 90 g/L and is not included.*
[d]*Overall L-malic acid/glucose amount produced/consumed as sum of all repeated-batch or fed-batch cycles. For Batch A, the amount of L-malic acid/glucose produced/consumed until 144 h is given.*
[e]*Average pH value minimum (after 263 h), disregarding the pH drop of Batch A3 at 191 h.*

also had a drawback: More solid particles result in a higher viscosity of the culture broth, thus complicating medium exchange. Despite these differences, the similarities prevailed, which is why only RB A is described in detail in the following sections.

Time courses of pH value, and L-malic acid and glucose concentration of RB A are characterized by the typical zigzag pattern of repeated-batch cultivations (**Figures 1D–F**). A closer look at the product curve reveals an acceleration of the malic acid production after each medium replacement from repeated-batch phase one to five. Due to the medium exchange procedure *via* decantation, the medium was not removed entirely, and the initial L-malic acid concentration of the repeated batches was increased from 1.6 ± 0.1 g/L after the first medium exchange to 7.2 ± 0.3 g/L after the last medium replacement. However, malic acid production clearly exceeded the rise of the initial concentrations. The L-malic acid titers at the end of each repeated-batch phase increased from 21.2 ± 1.2 g/L in the first phase to a maximum of 36.8 ± 1.4 g/L in phase three.

The high consistency of the triplicate data is remarkable. Only after glucose became a limiting factor in phase four, malic acid titers started to differ considerably. Although the initial glucose concentrations of each repeated-batch phase remained almost constant, a decline of the residual glucose at the end of each batch phase was observed over time due to an acceleration of the glucose consumption. Thus, glucose was completely consumed for the first time in phase three. Varying times for glucose depletion led to different malic acid maxima. While the maximum titer of repeated-batch A1 was measured alongside with glucose depletion at the end of the third phase, small amounts of residual glucose could still be detected in the other two cultivations. In phase four, glucose was completely consumed in each flask of the triplicate set. Accordingly, repeated-batch A2 reached the maximum titer in the fourth phase, whereas in repeated-batch A3 malic acid concentration was marginally higher in phase five instead of phase four. In the last repeated-batch phase, malic acid concentration was considerably reduced in all three fermentations.

With regard to the pH value, the triplicate data were highly consistent throughout the fermentation. The pH increased with every medium exchange and calcium carbonate addition. Within the individual phases of the repeated-batch cultivation, the course of the pH value was characterized by a pH drop in the first 24 h after medium replacement, followed by a slower decline of the pH value afterward. With 6.31 ± 0.01, the pH minimum of the repeated-batch cultivation was similar to the pH minimum of the batch process. Regarding the biomass, a considerable increase of the pellet sizes was observed over time, indicating continuous cell growth in the repeated-batch cultivations, fueled by the steady nitrogen supply.

Comparison of Fed-Batch Cultivations With Different Feed Compositions

Three different feed compositions were tested in fed-batch cultivations, but L-malic acid production could not be enhanced compared to the batch fermentation. However, a better process understanding can be obtained by looking at the results of the individual feeding experiments.

In fed-batch scenario A (FB A) (**Figures 2A–C**), glucose depletion could be avoided by regular additions of concentrated glucose solution to the cultivation broth. More than 40 g/L glucose was available at any time of the cultivation in each flask of the triplicate set, but the L-malic acid concentration already reached a maximum of 26.5 g/L (FB A2) after 166 h, (3 days) after the first feeding. A longer cultivation with additional feedings did not increase the malic acid titer, although glucose was continuously consumed until the end of the fermentation. On the contrary, malic acid concentration was reduced in the further course of the fermentation, due to the dilution effect of the feedings and a net zero production of malic acid in several fed-batch phases. In phase 3–6, malic acid concentration increased slightly for 24 or 48 h after each feeding, staying constant or even decreasing afterward. The only exception was a slight increase of the malic acid concentration at the very end of the cultivation, probably caused by cell fragmentation and liberation of intracellular malic acid.

Regarding the glucose concentration, an accumulation of the substrate could be observed over time. Obviously, the feeding exceeded the glucose consumption. The pH value showed a similar course as in the batch cultivation. However, after 216 h, a steeper decrease of the pH value occurred in the fed-batch fermentation, reaching a minimum pH of 5.74 ± 0.11 after

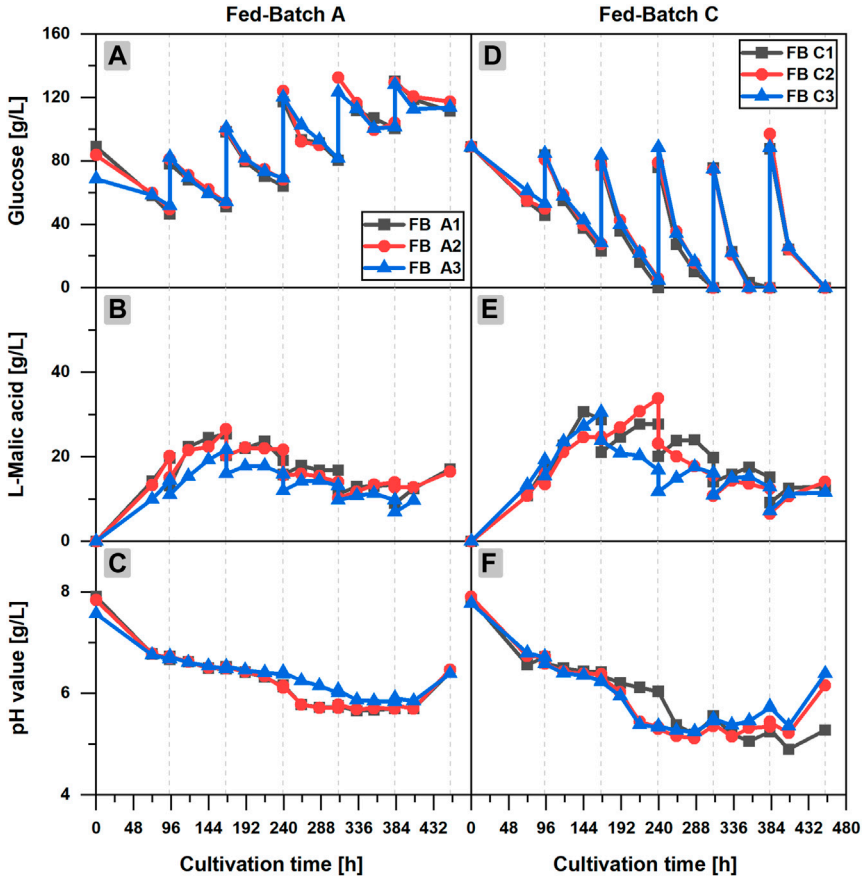

FIGURE 2 | L-Malic acid production in fed-batch cultivations of *Aspergillus oryzae* DSM 1863. Comparison of fed-batch A with a glucose feed **(A–C)** and fed-batch C with a complete medium feed **(D–F)**.Course of the glucose concentration **(A,D)**, the L-malic acid concentration **(B,E)** and the pH value **(C,F)** over the cultivation time. The triplicate data A1–3 and C 1–3 of the fed-batch cultivations are distinguishable by color and symbol. The gray vertical, dotted lines indicate the feeding times.

333 h. The final increase of the pH value in the fed-batch cultivations happened after 406 h, considerably later as in the batch process. On the whole, it can be stated that feeding with only glucose increased the long-term viability of the fungal cells but exerted no positive effect on malic acid production.

In fed-batch cultivations with additional ammonium sulfate in the feed solution (FB B/C), much higher glucose consumption and larger fungal pellets could be observed (data shown only for FB C in **Figure 2**). Furthermore, a considerably lower pH minimum close to 5.0 was recognized in the late phase of the cultivation. However, malic acid production did not benefit from the additional nitrogen feeds in FB B (data not shown). In fed-batch scenario C (**Figures 2D–F**), in which the feeds also comprised mineral salts, the highest glucose consumption and malic acid synthesis of all fed-batch cultivations occurred. However, with a maximum titer of 33.6–39.4 g/L L-malic acid, FB C did not outperform the malic acid production in batch cultivations. The highest malic acid concentrations of FB C were measured after the first or second feeding. In the further course of the fermentation, malic acid synthesis declined, although the glucose consumption was accelerated with each feeding, resulting in glucose depletion in feed phase two to five. The minimum pH of 5.19 ± 0.05 after 288 h was considerably lower as in the batch and repeated-batch cultivations. With regard to the triplicate quality, the observations made in the batch process also applied for the fed-batch cultivation: The high consistency of the glucose concentrations did not reflect in congruent malic acid titers. Additionally, the data point to a strong effect of a deviant initial glucose concentration on malic acid production (FB A3).

Process Mode Comparison: Highest Productivity in the Repeated-Batch Process

As previously stated, an acceleration of L-malic acid production and glucose consumption after each medium exchange could be recognized in repeated-batch cultivations upon closer examination of the product and substrate concentrations. This observation becomes more obvious by looking at the productivities and glucose consumption rates of RB A, determined for each time interval between two sample points (**Figures 3A,B**). Regarding the productivities calculated for the first 24 h after each medium exchange, an increase from repeated-batch phase two to five was observed, reaching a maximum of

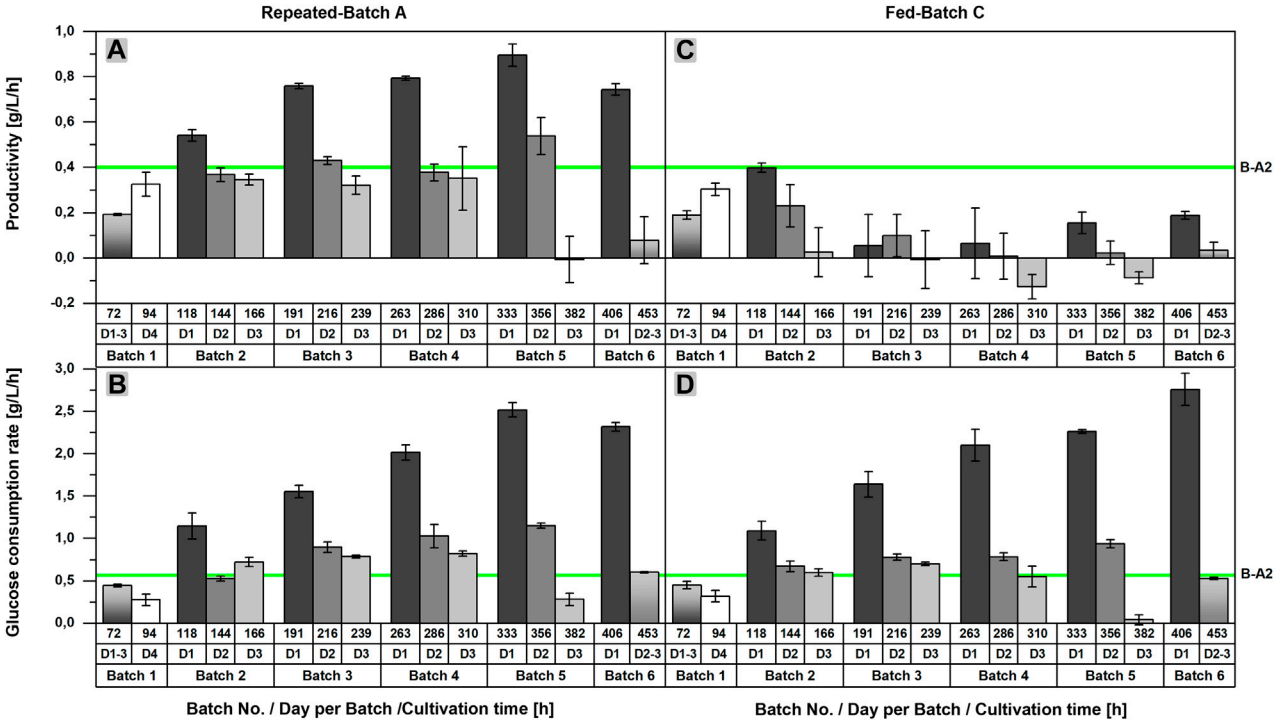

FIGURE 3 | Comparison of the productivities and glucose consumption rates of batch, repeated-batch, and fed-batch cultivations for the L-malic acid production with *Aspergillus oryzae* DSM 1863. Productivities **(A,C)** and glucose consumption rates **(B,D)** between two sample points are displayed for repeated batch A **(A–B)** and fed-batch C **(C–D)**. The error bar gives the standard deviation of the mean of each triplicate. The green line indicates the maximum productivity and glucose consumption rate between two sample points determined for Batch A2.

0.90 ± 0.05 g/L/h, which was more than twice as high as the maximum productivity of the batch process (0.40 g/L/h in Batch A2). Likewise, the glucose consumption rate achieved a maximum of 2.52 ± 0.09 g/L/h in the fifth phase, thereby exceeding the maximum glucose consumption rate of the batch process (0.57 g/L/h in Batch A2) by a multiple. Within each repeated-batch phase, the productivities and glucose consumption rates decreased over time. In phase five, the glucose consumption rate on day three was, especially low, as glucose became limiting. Hence, the malic acid productivity on the third day was close to zero. In the subsequent phase six, the overall productivity and glucose consumption rate decreased further.

In the fed-batch approaches with nitrogen supply (FB B,C), the glucose consumption rate showed a similar profile as observed in the repeated-batch process (**Figures 3B,D**). A maximum of 2.76 ± 0.19 g/L/h was achieved in the sixth fed-batch phase of FB C, which was the highest maximum glucose consumption rate of all fermentations. Differences between the initial glucose concentration of the single fed-batch and repeated-batch phases provide an explanation for the varying time points of the consumption maxima. As glucose was entirely consumed in phase five and six, the maxima were directly depending on the initial glucose concentrations and the time interval of each phase. In contrast to the glucose consumption rate, the difference between the productivites of the fed-batch and repeated-batch fermentations could not have been clearer (**Figure 3A, C**). The productivity of the fed-batch cultivation increased only until 118 h. With a maximum of 0.40 ± 0.02 g/L/h on day one after the first feeding, the overall productivity of the batch process was never exceeded. In the further course of the fermentation, the productivity of the fed-batch process decreased to zero and even negative productivities were calculated, presumably due to malic acid metabolization.

In sum, the parallel shake flask experiment revealed a clear advantage of the repeated-batch process over the batch cultivation with regard to the maximum productivity and a prolonged cultivation time, whereas L-malic acid synthesis could not be improved by fed-batch fermentation. The result was conclusive despite the low reproducibility of the batch process. Regarding the comparability of the fermentations, the malic acid concentrations after 72 and 94 h can give a hint on whether the starting conditions of the batch, fed-batch, and repeated-batch processes were similar. Under ideal conditions, the malic acid concentration after 94 h should be similar in all parallel fermentations, but the inoculation procedure, without biomass measurement, leaves some room for inaccuracies. The differences between the L-malic acid concentrations of the individual batch cultivations previously described already occurred after 72 h and became even more apparent after 94 h with 18.5 g/L in Batch A3 and 26.4 g/L in Batch A1. In contrast, malic acid concentrations after 94 h were much more consistent in fed-batch and repeated-batch fermentations. With an L-malic acid concentration of 20.5 ± 1.5 g/L

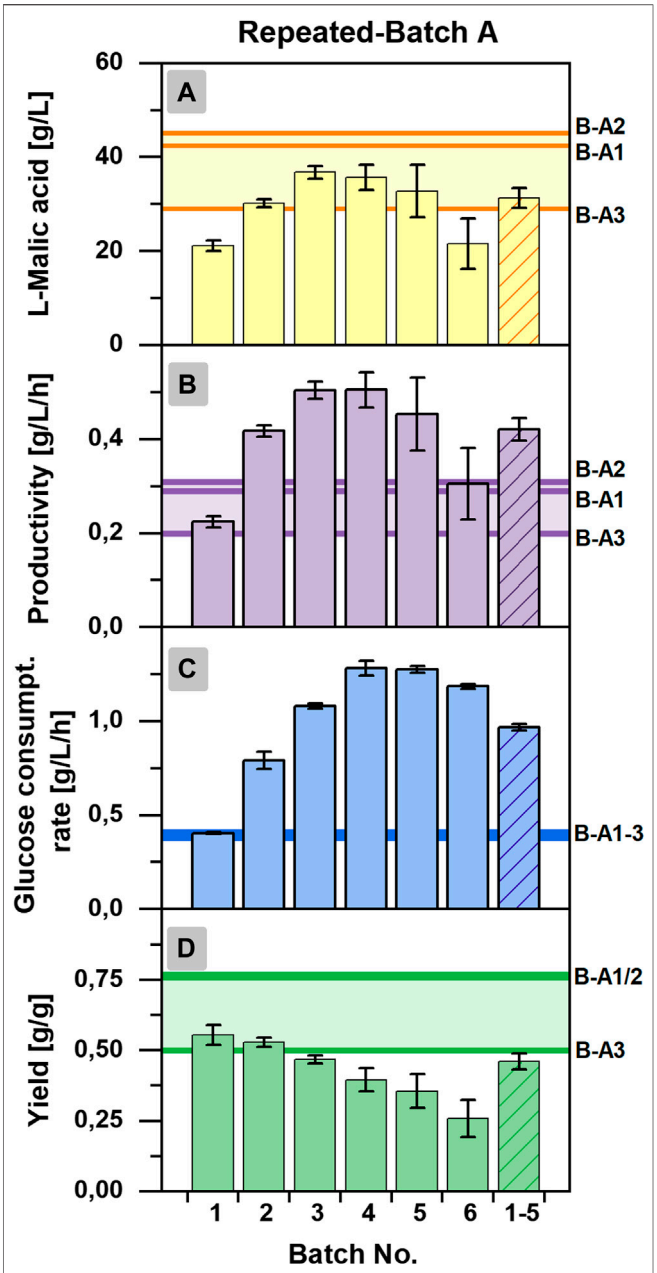

FIGURE 4 | Batch-wise calculated process characteristics for the repeated-batch cultivation A with *Aspergillus oryzae* DSM 1863. **(A)** L-Malic acid concentration, **(B)** productivity, **(C)** glucose consumption rate, and **(D)** yield. The vertical lines indicate the process characteristics of each individual cultivation of Batch A (indicated as B-A1/A2/A3), calculated for a process time of 144 h.

in the fed-batch and 21.2 ± 1.2 g/L in the repeated-batch cultivation, the initial malic acid production was only slightly higher as in Batch A3 but lower as in Batch A1 and A2.

For further analysis of the repeated-batch cultivation, performance indicators were calculated for the individual repeated-batch phase and compared to the overall titers, yields, productivities, and consumption rates determined for each individual cultivation of the batch process (Batch A1-A3) and a cultivation time of 144 h (**Figures 4A–D**). The L-malic acid concentration of repeated-batch phase two to five surpassed the maximum titer achieved in Batch A3 but was lower than that of Batch A1 and A2. In the context of glucose limitation, the malic acid concentration of the final repeated-batch phase fell below the titer of Batch A3. Hence, only phases one to five were considered for the mean value to obtain reasonable performance indicators for the overall assessment of the repeated-batch process. Regarding these five phases, performed within 16 days, the average L-malic acid concentration of the repeated-batch fermentation was with 31.3 ± 2.0 g/L in the lower range of the batch cultivations, whereas the average productivity of 0.42 ± 0.03 g/L/h clearly exceeded the overall productivity of all batch fermentations. The mean glucose consumption rate of the repeated-batch process was with 0.97 ± 0.02 g/L/h more than twice as high as in the batch cultivation. In the course of the repeated-batch fermentation, a steeper and longer increase of glucose consumption than the malic acid production could be observed. Accordingly, the highest yield was determined in the first repeated-batch phase and decreased over time with each new phase. With 0.46 ± 0.03 g/g, the average yield was lower as in all batch cultivations but nearly reached Batch A3.

The Role of Nitrogen and Calcium Carbonate in Repeated-Batch Cultivations

Another experiment was performed to investigate the role of nitrogen and calcium carbonate for the L-malic acid production in repeated-batch cultivations. Due to some deviations in the experimental conditions (**Table 1**), RB C, D and E are not directly comparable to RB A and B. One major difference was that a faster medium exchange rate applied in RB C/D/E. The medium was replaced every 2 days, after an initial phase of 4 days, thereby the glucose concentration was kept above 0 g/L throughout the entire cultivation. RB C revealed no obvious advantage of the faster exchange rhythm and the better glucose supply on the malic acid production (data not shown), but a 3°C lower temperature in the second experiment (including RB C/D/E) might have reduced the L-malic acid production and thereby concealed a positive effect of the better glucose supply. Ochsenreither et al. reported that in bioreactor experiments, malic acid production could be considerably increased by elevating the cultivation temperature from 30 to 35°C (Ochsenreither et al., 2014). Hence, a direct comparison under identical conditions would be needed to identify the optimal exchange rhythm.

In contrast, the important role of the calcium carbonate addition for pH stabilization and L-malic acid production could be clearly demonstrated in RB D, in which calcium carbonate was provided at the beginning of the cultivation, but was not added after the medium exchanges. Without a regular calcium carbonate supply, the pH dropped to a very low minimum of 3.59 ± 0.06 after 313 h (**Figure 5B**). In the first 192 h of the cultivation, the L-malic acid production increased with each repeated-batch phase, but a maximum product concentration of only 23.7 ± 1.1 g/L was already reached in phase three (**Figure 5A**). Afterward, the malic acid concentration decreased until 336 h and only 3.7 ± 0.4 g/L

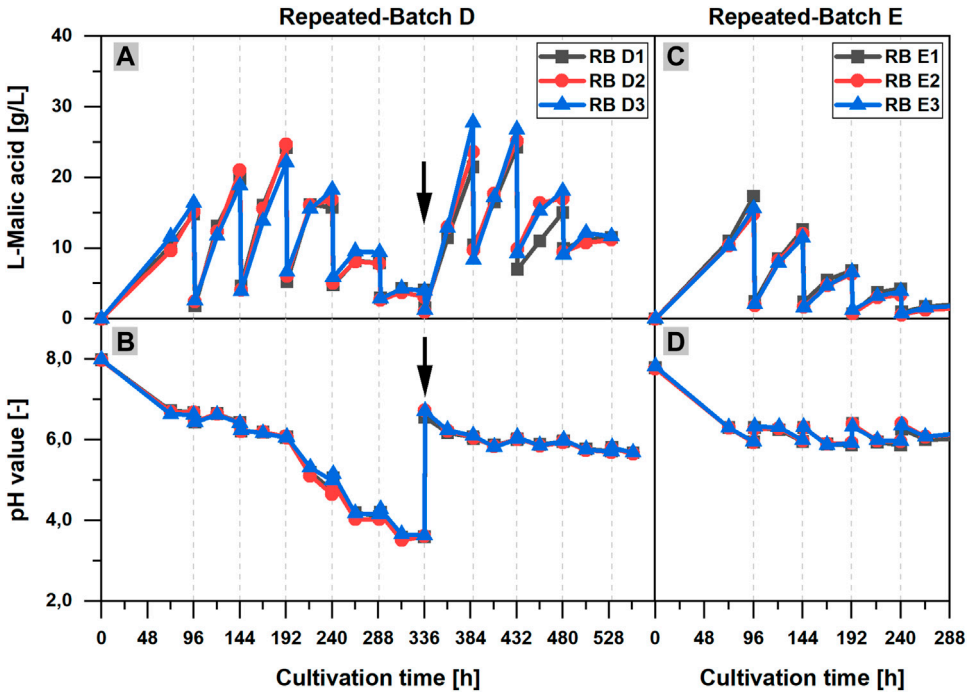

FIGURE 5 | Influence of calcium carbonate and ammonium on the L-malic acid production in repeated-batch cultivations of *Aspergillus oryzae* DSM 1863. **(A,C)** L-Malic acid concentration and **(B,D)** pH value over the cultivation time for repeated-batch D **(A,B)** with ammonium in the exchange medium and calcium carbonate additions at the beginning of the cultivation and after 336 h (black arrow) and repeated-batch E **(C,D)** without ammonium in the exchange medium and regular additions of calcium carbonate. The gray vertical, dotted lines indicate the times of medium exchange for the repeated-batch cultivations.

L-malic acid was measured at the end of repeated-batch phase six. Although less malic acid was produced after 192 h, the course of the pH value showed a particular steep decrease after 192 h. After the sixth medium replacement (336 h), 9 g/L $CaCO_3$ was added to the shake flasks. As a consequence, the pH value was raised to 6.21 ± 0.03. Subsequently, a strong acceleration of the malic acid production could be observed, reaching 24.3 ± 2.6 g/L L-malic acid in phase seven after 387 h. In the further course of the fermentation, the pH decreased to 5.67 ± 0.01, and the malic acid production declined again with each repeated-batch phase, despite further calcium carbonate additions.

In another parallel repeated-batch fermentation (RB E), the necessity of a steady nitrogen supply for the L-malic acid production was proved. Needless to say, without ammonium sulfate in the exchange medium, the pellet growth was limited by nitrogen depletion in the initial repeated-batch phase. Moreover, the experiment clearly demonstrates that the absence of nitrogen has a significant effect on the malic acid production. The maximum product titer of 15.9 ± 1.3 g/L was already measured after 96 h, at the end of the initial repeated-batch phase (**Figure 5C**). Afterward, the malic acid production declined with each subsequent repeated-batch phase, whereas in the reference cultivation with full ammonium supply (RB C, data not shown) the maximum L-malic acid concentration was 21.5 g/L (RB C2) to 39.1 g/L (RB C1) after 288 h, which was significantly higher. Regarding the pH curve (**Figure 5D**), only a slight decrease of the pH value over time could be observed after the initial pH drop in the cultivations without ammonium in the exchange medium (RB E). The pH minimum was 6.33 ± 0.01 after 168 h, which was comparably high.

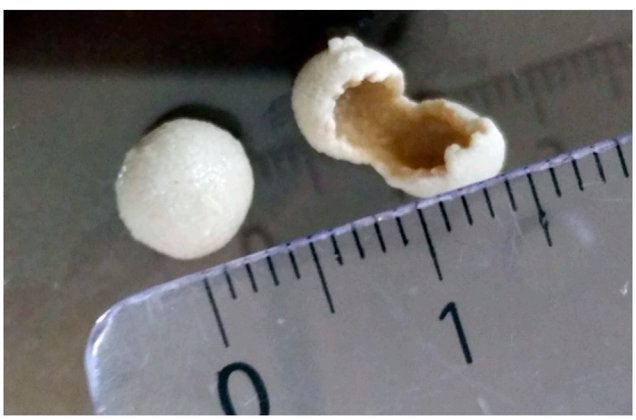

FIGURE 6 | Fungal pellets of *Aspergillus oryzae* DSM 1863 with a hollow core. The picture was taken at the end of the repeated-batch cultivation RB C.

Regarding the fungal biomass, it could be observed that a steady nitrogen supply leads to a continuous pellet growth in the repeated-batch experiments (RB A/B/C), as already seen in the fed-batch cultivations (FB B/C). While the pellets reached a size of up to 8 mm, they were hollow in the inside (**Figure 6**), probably

caused by cell degradation as a consequence of transport limitations.

DISCUSSION

In general, biotechnological processes can be operated as batch, fed-batch, repeated-batch, or continuously. Batch processes are the easiest to implement and therefore widely used, but in some cases alternative process modes are economically preferable. Fed-batch processes can be used to prolong the productive phase of a cultivation, especially if the carbon source cannot or should not be presented in high concentrations. Furthermore, the substrate concentration can be kept in the optimal range for product synthesis, avoiding both substrate inhibition and carbon limitation. If, on the other hand, product inhibition is present, a repeated-batch process can be advantageous, since the product concentration can be kept at a low level by replacing the medium while the biomass remains active. In this way, the production phase can be greatly extended.

In the last years, more studies dealing with L-malic acid production have been published; however, its regulation is still not well understood which renders a rationale choice of process modes and operation conditions. The present study compares the three process modes for the first time systematically in parallel shake flask cultivations and provides new insights into L-malic acid production by the natural production host *Aspergillus oryzae* DSM 1863.

Batch Cultivation

To determine what happens during the late phase of L-malic acid production in the batch mode, the cultivation time was prolonged to ensure that the substrate will be exhausted at the end of the experiment. It has been recognized before that a high C:N ratio is mandatory for organic acid production in general and also for malic acid production in batch processes (Peleg et al., 1988; Ochsenreither et al., 2014; Ding et al., 2018), meaning that the carbon source should be provided in high excess during the process. However, to the best of our knowledge, it was not clear whether malic acid production would simply stop upon carbon source depletion, that is, malic acid concentration would stay constant, or whether it would be reassimilated, that is, malic acid concentration would decrease. In this study, malic acid was reassimilated in all batch cultivations. However, in only one of the three shake flasks, a timely correlation between glucose depletion and malic acid maximum occurred. In the other two shake flasks, the malic acid titer peaked when still more than 30 g/L of glucose was left. According to these observations, glucose depletion might be one but not the only reason for malic acid reassimilation in batch cultivations. This aspect is further illuminated by the results of the fed-batch and repeated-batch cultivations conducted in parallel, which will be discussed in the subsequent sections.

The reason for the high variances in product formation cannot be explained comprehensively by the obtained data. While being fairly comparable after the first 72 h, differences became more prominent thereafter. Given the similar consumption of glucose, the question arises, if other products are formed, which could explain the findings. Biomass formation as carbon sink is unlikely since same amounts of nitrogen were provided for each culture and were regularly depleted after about 48 h. Hence, other explanations are needed. *A. oryzae* has a complex morphology, which is not well understood (Papagianni, 2004). Under our culture conditions, *A. oryzae* grows in the form of large pellets with a size of several millimeters. Accordingly, mass transfer limitations, cell differentiation, or aging processes, and therefore changes in cell metabolism are likely. For L-malic acid production with *A. oryzae*, Chen et al. proved the general importance of cell morphology (Chen et al., 2019).

In terms of pH, batch culture A3 is particularly interesting. The pH value declined further after malic acid reassimilation started, thereby differing from the other two cultures. Since we applied the same amount of calcium carbonate in all cultures and did not observe any differences in glucose consumption, lower malic acid production, and different pH minima might also indicate changes in by-product formation. This aspect should be investigated in more detail for *A. oryzae* in subsequent studies.

Fed-Batch Cultivations

Fed-batch scenario A proved that glucose limitation is not the decisive limiting factor in L-malic acid production with the *A. oryzae* wild-type strain. Although glucose was fed regularly, keeping the substrate concentration above 40 g/L at all times, malic acid concentration was consistently lower as the maximum titer achieved in the batch cultivations. While malic acid was continuously synthesized after each feeding, the low level of production could not compensate for the dilution effect of the feeding, resulting in decreasing malic acid concentrations in the course of fermentation. However, it is noteworthy that the viability of the cells was prolonged in the fed-batch mode. The characteristic pH increase indicated cell degradation only after 17 days (408 h).

In prolonged fed-batch fermentations, the viability and productivity of the cells might profit from additional nutrient supply. This was investigated in fed-batch scenario B, in which carbon and nitrogen was fed, and scenario C, in which the complete medium was supplemented. In both cases, accelerated glucose consumption and lower pH values were observed, both probably due to biomass growth after nitrogen uptake (data of FB C in **Figure 2**). Biomass was not determined; however, pellet growth was noticed. A prolonged viability could not be recognized; the pH rise occurred in FB C after 17 days and was comparable to FB A. The much higher overall glucose consumption did not reflect in a comparable increase of the malic acid production in FB B and C. In this case, biomass as carbon sink is likely, as continuous pellet growth could be observed. The slight increase of the overall product titer was, therefore, achieved on the cost of a strong reduction of the yield (**Table 2**). Hence, the fed-batch process seems not to be beneficial for L-malic acid production with the wild-type *A. oryzae* strain.

Our results seem to be in conflict with the study of Liu et al. (2017), in which only glucose was supplied during fed-batch and much higher malic acid concentrations were reached than those in the batch fermentation. However, Liu et al. (2017) used a genetically modified strain instead of the wild-type. By

overexpression of C4-carboxylic acid transporters, Liu et al. (2017) achieved a significant increase of the malic acid titers compared to the wild-type, confirming the results of a previous study by Brown et al. (2013). Accordingly, product inhibition could be a decisive limiting factor for malic acid production in *A. oryzae* wild-type strains. This might explain why the maximum malic acid concentration of the batch process in our study with the wild-type strain could not be improved by fed-batch cultivation, regardless which feeding scenario was applied.

Product inhibition depends on not only the acid concentration but also the ratio of the undissociated form, which could re-enter the cell *via* diffusion and disturb pH homeostasis and cause a loss of energy (Zambanini et al., 2016). For malic acid with pK_a values of 3.40 and 5.20, the ratio of the undissociated form increases below pH 7. Therefore, it is noteworthy that another difference to our study was the constant pH value of 6.0 as in the work of Liu et al. (2017), since both batch and fed-batch cultivations were conducted in a bioreactor with pH regulation with sodium carbonate in addition to the buffering with 90 g/L $CaCO_3$. However, in calcium carbonate buffered FB A (glucose only feed), the pH decreased only slightly below six in the later feeding phases. In contrast, in FB B and FB C, a stronger decrease of the ambient pH down to a minimum of 5.0–5.2 could be observed in consequence of the steady nitrogen consumption. The low pH values and glucose limitation in the later fed-batch phases could have impeded malic acid production. Hence, additional fed-batch experiments with better pH control and sufficient glucose supply would be interesting to complete our findings. Further studies should also include quantification of possible acidic by-products and nitrogen consumption, as deviations between the pH curves of the individual fed-batch cultivations were observed that did not reflect in increased malic acid synthesis.

In general, the complex interplay between organic acid accumulation in the cell, internal and external pH values, transport processes, and the regulation of the metabolism in filamentous fungi are not sufficiently understood (Vrabl et al., 2012). However, avoiding (malic) acid accumulation in the cytosol and the control of the ambient pH are known key factors for prevention of product inhibition. Genetic manipulation (Liu et al., 2017) is not the only option to improve malic acid production by *A. oryzae*. Lowering the malic acid concentration in the medium can also prevent product inhibition, as a concentration gradient could facilitate the malic acid export. Although the role of calcium carbonate in organic acid production is not completely clear, product removal by precipitation of the acids as calcium salts is supposed to contribute to improved organic acid production with increased calcium carbonate concentrations, ensuring a pH above 6 (Geyer et al., 2018). In our study, we investigated the impact of calcium carbonate only in repeated-batch cultivation, which is discussed in the following section. The repeated-batch process itself can also reduce product inhibition by lowering the malic acid concentration in the medium. Our results for the repeated-batch cultivation of *A. oryzae* are discussed in the next section.

Repeated-Batch Cultivations

In the literature, the advantages of the repeated-batch process for microbial organic acid production were already described for different acids and production strains. For example, Park et al. reported an extended itaconic acid production in shake flask cultivations with *A. terreus* for 45 days in nine repeated-batch cycles. The productivity (0.47 g/L/h) was 1.5 times increased compared to the 7-day batch process (Park et al., 1994). In another study, *A. niger* cells immobilized in Ca-alginate gel beads retained the ability to produce citric acid for up to 84 days in repeated-batch shake flask fermentations (Roukas, 1991). However, studies on the repeated-batch cultivation for L-malic acid production are missing.

This study closes the literature gap with results from several repeated-batch cultivations of *A. oryzae*, carried out in shake flasks under different conditions with cell recycling by decantation. The results for L-malic acid production are comparable to the observations of Park et al. regarding itaconic acid. The average productivity of the repeated-batch cultivation (0.42 ± 0.03 g/L/h) with a runtime of 16 days (5 cycles) was 1.5-fold higher than that of the batch process (6 days), while malic acid concentration and yield was more or less similar. The repeated-batch process was stopped after six cycles and 19 days, due to decreasing productivities, most likely caused by a temporary glucose limitation in later repeated-batch phases. However, malic acid production could be restored with the next medium exchange, proving the robustness of the process. As longer runtimes at high productivities could reduce operation costs, it would be interesting to see if a sufficient glucose supply would enable a further prolongation of the malic acid production or if other factors would become limiting in extended repeated-batch experiments. Additionally, the usage of immobilized cells in repeated-batch cultivations could be an interesting topic for further studies, as there are promising results for kojic acid production with immobilized *A. oryzae* (Kwak and Rhee, 1992).

Although the repeated-batch cultivation proved to be advantageous for L-malic acid production of the wild-type strain compared to the batch and fed-batch processes, higher productivities, titers, and yields were reported for batch and fed-batch cultivations with metabolic engineered or mutant strains of *A. oryzae*. So far, the highest productivity was reported by Liu et al. (2017) in 3 L fed-batch cultivation (1.38 g/L/h) with a multiple engineered strain. However, a direct comparison with the results of Liu et al. could be misleading due to the usage of peptone and the fact that complex nitrogen sources are known to increase malic acid production significantly compared to cultivations on ammonium sulfate (Knuf et al., 2013; Ding et al., 2018). This also applies for most of the other studies regarding malic acid production with *A. oryzae*. Only in the studies of Knuf et al. and Ding et al., ammonium sulfate was used as a nitrogen source (Knuf et al., 2014; Ding et al., 2018). Knuf et al. achieved a productivity of 0.34 ± 0.06 g/L/h with the wild-type strain *A. oryzae* NRRL 3488 in 2.7-L bioreactor batch cultivations and a productivity of 1.05 ± 0.13 g/L/h under the same conditions with the engineered strain *A. oryzae* NRRL 3488 2103a-68. Ding et al. (2018) reported a productivity of 0.57 g/L/h in 7.5 L fed-batch cultivation with a mutant *A. oryzae* strain. The studies of Liu et al. and Knuf et al., demonstrate the power of metabolic engineering and the impact of product inhibition as in both studies the overexpression of

transporter genes resulted in a strong improvement of the malic acid synthesis. A closer look at our results reveals that the repeated-batch process might not reduce the product inhibition sufficiently, as the productivity was the highest directly after each medium exchange with an overall maximum of 0.97 ± 0.02 g/L/h but decreased significantly with increasing product concentration in the course of each repeated-batch phase (**Figure 3**). However, the maximum productivity clearly shows the potential of the wild-type strain. In further studies with the wild-type strain, the inhibitory concentration of malic acid under typical cultivation conditions should be determined.

The observed decreasing productivities within each repeated-batch phase were accompanied by a slight decrease of the pH value, as a result from nitrogen consumption and acid production, but the pH value was above six at all times due to regular calcium carbonate additions with each medium exchange. The buffering agent stabilizes the pH value and should reduce product inhibition by keeping the malic acid concentration in the media low *via* precipitation of the acid as calcium salts. Moreover, the additional calcium and CO_2 supply *via* calcium carbonate might also have a positive effect on the malic acid production. In a study that investigated the role of calcium carbonate in the L-malic acid production with *A. oryzae* from acetate, the authors concluded that the formation of Ca-malate might have been the main function of calcium carbonate (Kövilein et al., 2021), whereas its role as a CO_2 donor and buffering agent was assumed to be less important. However, for malic acid production on glucose, all functions of calcium carbonate could be beneficial. While the individual impact of the different calcium carbonate functions on the malic acid synthesis is still not sufficiently understood and should be investigated further, the positive impact of calcium carbonate on L-malic acid production is undoubted. Geyer et al. (2018) previously reported a correlation between malic acid production and the calcium carbonate amount, and the comparison of the overall malic acid production in repeated-batch scenario A and B (**Table 2**) seems to confirm this. Furthermore, repeated-batch scenario D clearly proved the necessity of regular calcium carbonate additions during repeated-batch cultivations. Without regular calcium carbonate supply, the productivity and pH value decreased with each phase, but malic acid synthesis could be fully restored by adding calcium carbonate in a later stage of the cultivation, while the pH was increased to more than six. All in all, repeated-batch scenario D demonstrates the pH tolerance of *A. oryzae*, while the productivity clearly depends on calcium carbonate. However, the usage of calcium carbonate has several drawbacks, such as an increased viscosity of the cultivation broth and issues in downstream processing (Li and Xing, 2017; Koevilein et al., 2020). Therefore, *in situ* product recovery combined with a regular nutrient feeding would be interesting for prolonged malic acid production with the wild-type strain. Processes with *in situ* product recovery already proved to be beneficial for itaconic acid (Kreyenschulte et al., 2018) and fumaric acid production (Cao et al., 1996; Xu et al., 2017). Malic acid can be separated by reactive extraction with, for example, tri-octylamine (Uslu and Kirbaslar, 2009; Uslu and Kırbaşlar, 2010), which was already successfully tested for *in situ* recovery of itaconic acid from a fermentation broth with *A. terreus* (Kreyenschulte et al., 2018). Accordingly, it would be interesting to test this option also for the malic acid production with an *A. oryzae* wild-type strain. Separation *via* adsorption columns or electrodialysis could be further options for *in situ* product recovery of malic acid (Lameloise and Lewandowski, 2012; Liu et al., 2014; López-Garzón and Straathof, 2014; Pandurić et al., 2017). To get a clearer picture of the optimal pH value for the malic acid production and its impact on the spectrum of acidic by-products, bioreactor cultivations with pH statization by a liquid titration agent should be evaluated in a subsequent study.

Besides the influence of calcium carbonate and pH value, the nitrogen–carbon ratio is known to have a strong impact on growth and L-malic acid production in batch and fed-batch cultivations (Ochsenreither et al., 2014; Liu et al., 2017; Ding et al., 2018; Ji et al., 2021). In our study, repeated-batch scenario E proves that a steady supply of nitrogen in the production phase is necessary for a prolonged malic acid synthesis with high productivities. The improved nutrient supply in the repeated-batch cultivations (A–D) in combination with reduced product inhibition resulted in higher productivities, than the (fed-) batch cultivations. The addition of nitrogen and other nutrients enables biomass formation, keeping the outer cells of fungal pellets juvenile and might therefore prevent metabolic differences due to differences in aging processes. Although the relationship between productivity and fungal morphology is not entirely understood (Papagianni, 2004; Krull et al., 2013), small sized pellets are supposed to be optimal for malic acid production, due to a limited mass transfer into the core of larger pellets (Chen et al., 2019). For larger pellets with a hollow core (**Figure 6**), our study indicates that an increase of pellet size obtained by a steady nitrogen supply reflects in higher productivities. This might be caused by the larger pellet surface with an increased number of active cells that do not face any transport limitation.

A drawback of the steady pellet growth is the corresponding reduction of the yields over time, as more and more glucose was used for biomass formation. The average yield for five repeated-batch phases (0.46 ± 0.03 g/g) was already lower as in the batch process and would decrease further in prolonged cultivations. Hence, a further increase of cultivation runtime and productivity would be on the expense of lower yields. To compensate the reduction, the formation of by-products needs to be determined and reduced. Key parameters that impact the side-product formation are the pH value (Vrabl et al., 2012) and the C/N ratio (Ochsenreither et al., 2014; Ding et al., 2018; Ji et al., 2021). While Ochsenreither et al. tested the C/N ratio for the batch cultivation of the wild-type strain, which was also used in this study, Ding et al. and Ji et al. evaluated the C/N ratio and nitrogen supply strategy for fed-batch cultivations of different mutant strains. These literature insights are not directly transferable to the repeated-batch process with the wild-type strain but should be considered for the optimization of the nitrogen and glucose supply of the repeated-batch cultivation. For a deeper understanding and further optimization of the repeated-batch process, a comprehensive analysis would be required, including by-product detection and biomass measurement. Furthermore,

the ratio between living and dead biomass could be an important parameter, worth investigation.

In conclusion, our systematic comparison of different process modes for the L-malic acid production with the wild-type strain *A. oryzae* DSM 1863 showed that the repeated-batch process was clearly advantageous compared to batch and fed-batch processes with regard to the productivity and a prolonged cultivation time. Furthermore, the study demonstrates that sufficient glucose, nitrogen, and calcium carbonate supply during the repeated-batch process is required to achieve high productivities in prolonged cultivations. In a next step, pH control, calcium carbonate supply, and the C/N ratio should be optimized. To achieve higher yields, by-products should be reduced, and the biomass-related productivity should be increased.

To our knowledge, this study is the first evaluation of a repeated-batch process for the L-malic acid production with *A. oryzae*. Next, repeated-batch cultivations could be tested for the malic acid production with genetically modified high-performance strains to enable prolonged cultivations with high productivities, titers, and yields. Due to the drawbacks of the calcium carbonate for downstream processing, *in situ* product recovery, for example, *via* reactive extraction or electrodialysis, should also be considered an alternative process strategy to overcome product inhibition.

All in all, the study underlines the potential of *A. oryzae* for the L-malic acid production and gives valuable insights and new starting points for further process development toward an economic viable fungal malic acid production process.

DATA AVAILABILITY STATEMENT

The raw data supporting the conclusion of this article will be made available by the authors, without undue reservation.

AUTHOR CONTRIBUTIONS

VS substantially contributed to the conception of the experiments and data evaluation and also performed the experiments and wrote the manuscript as the first author. LD substantially performed the experiments RB C–E. KO substantially contributed to the conception of the experiments and critically revised the final manuscript version.

FUNDING

The work of VS was funded by the Bioeconomy International Program of Federal Ministry of Education and Research (BMBF), Germany (Grant number Az: 031B0178).

ACKNOWLEDGMENTS

We acknowledge the support provided by the Ministry of Education and Research of Germany and Open Access Publishing Fund of Karlsruhe Institute of Technology.

REFERENCES

Brown, S. H., Bashkirova, L., Berka, R., Chandler, T., Doty, T., McCall, K., et al. (2013). Metabolic Engineering of *Aspergillus oryzae* NRRL 3488 for Increased Production of L-Malic Acid. *Appl. Microbiol. Biotechnol.* 97, 8903–8912. doi:10.1007/s00253-013-5132-2

Cao, N., Du, J., Gong, C. S., and Tsao, G. T. (1996). Simultaneous Production and Recovery of Fumaric Acid from Immobilized Rhizopus Oryzae with a Rotary Biofilm Contactor and an Adsorption Column. *Appl. Environ. Microbiol.* 62, 2926–2931. doi:10.1128/aem.62.8.2926-2931.1996

Chen, X., Zhou, J., Ding, Q., Luo, Q., and Liu, L. (2019). Morphology Engineering ofAspergillus Oryzaeforl-malate Production. *Biotechnol. Bioeng.* 116, 2662–2673. doi:10.1002/bit.27089

Dörsam, S., Kirchhoff, J., Bigalke, M., Dahmen, N., Syldatk, C., and Ochsenreither, K. (2016). Evaluation of Pyrolysis Oil as Carbon Source for Fungal Fermentation. *Front. Microbiol.* 7, 2059. doi:10.3389/fmicb.2016.02059

Ding, Q., Luo, Q., Zhou, J., Chen, X., and Liu, L. (2018). Enhancing L-Malate Production of Aspergillus oryzae FMME218-37 by Improving Inorganic Nitrogen Utilization. *Appl. Microbiol. Biotechnol.* 102, 8739–8751. doi:10.1007/s00253-018-9272-2

Dörsam, S., Fesseler, J., Gorte, O., Hahn, T., Zibek, S., Syldatk, C., et al. (2017). Sustainable Carbon Sources for Microbial Organic Acid Production with Filamentous Fungi. *Biotechnol. Biofuels* 10, 242. doi:10.1186/s13068-017-0930-x

Fiume, Z. (2001). Final Report on the Safety Assessment of Malic Acid and Sodium Malate. *Int. J. Toxicol.* 20, 47–55. doi:10.1080/109158101750300946

Geyer, M., Onyancha, F. M., Nicol, W., and Brink, H. G. (2018). Malic Acid Production by Aspergillus Oryzae: The Role of CaCO3. *Chem. Eng. Trans.* 70, 1801–1806. doi:10.3303/CET1870301

Hosseinpour Tehrani, H., Saur, K., Tharmasothirajan, A., Blank, L. M., and Wierckx, N. (2019). Process Engineering of pH Tolerant Ustilago Cynodontis for Efficient Itaconic Acid Production. *Microb. Cel. Fact.* 18, 213. doi:10.1186/s12934-019-1266-y

Ji, L., Wang, J., Luo, Q., Ding, Q., Tang, W., Chen, X., et al. (2021). Enhancing L-Malate Production of Aspergillus oryzae by Nitrogen Regulation Strategy. *Appl. Microbiol. Biotechnol.* 105, 3101–3113. doi:10.1007/s00253-021-11149-6

Knuf, C., Nookaew, I., Brown, S. H., McCulloch, M., Berry, A., and Nielsen, J. (2013). Investigation of Malic Acid Production in *Aspergillus oryzae* under Nitrogen Starvation Conditions. *Appl. Environ. Microbiol.* 79, 6050–6058. doi:10.1128/AEM.01445-13

Knuf, C., Nookaew, I., Remmers, I., Khoomrung, S., Brown, S., Berry, A., et al. (2014). Physiological Characterization of the High Malic Acid-Producing *Aspergillus oryzae* Strain 2103a-68. *Appl. Microbiol. Biotechnol.* 98, 3517–3527. doi:10.1007/s00253-013-5465-x

Kövilein, A., Kubisch, C., Cai, L., and Ochsenreither, K. (2020). Malic Acid Production from Renewables: A Review. *J. Chem. Technol. Biotechnol.* 95, 513–526. doi:10.1002/jctb.6269

Kövilein, A., Umpfenbach, J., and Ochsenreither, K. (2021). Acetate as Substrate for L-Malic Acid Production with Aspergillus oryzae DSM 1863. *Biotechnol. Biofuels* 14, 48. doi:10.1186/s13068-021-01901-5

Kreyenschulte, D., Heyman, B., Eggert, A., Maßmann, T., Kalvelage, C., Kossack, R., et al. (2018). *In Situ* reactive Extraction of Itaconic Acid during Fermentation of Aspergillus terreus. *Biochem. Eng. J.* 135, 133–141. doi:10.1016/j.bej.2018.04.014

Krull, R., Wucherpfennig, T., Esfandabadi, M. E., Walisko, R., Melzer, G., Hempel, D. C., et al. (2013). Characterization and Control of Fungal Morphology for Improved Production Performance in Biotechnology. *J. Biotechnol.* 163, 112–123. doi:10.1016/j.jbiotec.2012.06.024

Kwak, M. Y., and Rhee, J. S. (1992). Cultivation Characteristics of immobilizedAspergillus Oryzae for Kojic Acid Production. *Biotechnol. Bioeng.* 39, 903–906. doi:10.1002/bit.260390904

Lameloise, M.-L., and Lewandowski, R. (2012). Recovering L-Malic Acid from a Beverage Industry Waste Water: Experimental Study of the Conversion Stage Using Bipolar Membrane Electrodialysis. *J. Membr. Sci.* 403-404, 196–202. doi:10.1016/j.memsci.2012.02.053

Lee, J. W., Han, M.-S., Choi, S., Yi, J., Lee, T. W., and Lee, S. Y. (2011). "Organic Acids," in *Comprehensive Biotechnology*. Editor M. Moo-Young. Second Edition (Burlington: Academic Press), 149–161. doi:10.1016/b978-0-08-088504-9.00183-5

Li, Q., and Xing, J. (2017). "Production of 1,4-Diacids (Succinic, Fumaric, and Malic) from Biomass," in *Production of Platform Chemicals from Sustainable Resources*. Editors Z. Fang, J. R. L. Smith, and X. Qi (Singapore: Springer Singapore), 231–262. doi:10.1007/978-981-10-4172-3_8

Liu, G., Luo, H., Wang, H., Wang, B., Zhang, R., and Chen, S. (2014). Malic Acid Production Using a Biological Electrodialysis with Bipolar Membrane. *J. Membr. Sci.* 471, 179–184. doi:10.1016/j.memsci.2014.08.014

Liu, J., Li, J., Liu, Y., Shin, H.-d., Ledesma-Amaro, R., Du, G., et al. (2018). Synergistic Rewiring of Carbon Metabolism and Redox Metabolism in Cytoplasm and Mitochondria of Aspergillus oryzae for Increased L-Malate Production. *ACS Synth. Biol.* 7, 2139–2147. doi:10.1021/acssynbio.8b00130

Liu, J., Xie, Z., Shin, H.-d., Li, J., Du, G., Chen, J., et al. (2017). Rewiring the Reductive Tricarboxylic Acid Pathway and L-Malate Transport Pathway of *Aspergillus oryzae* for Overproduction of L-Malate. *J. Biotechnol.* 253, 1–9. doi:10.1016/j.jbiotec.2017.05.011

López-Garzón, C. S., and Straathof, A. J. J. (2014). Recovery of Carboxylic Acids Produced by Fermentation. *Biotechnol. Adv.* 32, 873–904. doi:10.1016/j.biotechadv.2014.04.002

Morgunov, I. G., Kamzolova, S. V., Karpukhina, O. V., Bokieva, S. B., and Inozemtsev, A. N. (2019). Biosynthesis of Isocitric Acid in Repeated-Batch Culture and Testing of its Stress-Protective Activity. *Appl. Microbiol. Biotechnol.* 103, 3549–3558. doi:10.1007/s00253-019-09729-8

Ochsenreither, K., Fischer, C., Neumann, A., and Syldatk, C. (2014). Process Characterization and Influence of Alternative Carbon Sources and Carbon-To-Nitrogen Ratio on Organic Acid Production by *Aspergillus oryzae* DSM1863. *Appl. Microbiol. Biotechnol.* 98, 5449–5460. doi:10.1007/s00253-014-5614-x

Pandurić, N., Šalić, A., and Zelić, B. (2017). Fully Integrated Biotransformation of Fumaric Acid by Permeabilized baker's Yeast Cells with *In Situ* Separation of L-Malic Acid Using Ultrafiltration, Acidification and Electrodialysis. *Biochem. Eng. J.* 125, 221–229. doi:10.1016/j.bej.2017.06.005

Papagianni, M. (2004). Fungal Morphology and Metabolite Production in Submerged Mycelial Processes. *Biotechnol. Adv.* 22, 189–259. doi:10.1016/j.biotechadv.2003.09.005

Park, Y. S., Itida, M., Ohta, N., and Okabe, M. (1994). Itaconic Acid Production Using an Air-Lift Bioreactor in Repeated Batch Culture of Aspergillus terreus. *J. Ferment. Bioeng.* 77, 329–331. doi:10.1016/0922-338X(94)90245-3

Peleg, Y., Stieglitz, B., and Goldberg, I. (1988). Malic Acid Accumulation by Aspergillus flavus. *Appl. Microbiol. Biotechnol.* 28, 69–75. doi:10.1007/bf00250501

Petruccioli, M., Angiani, E., and Federici, F. (1996). Semi-continuous Fumaric Acid Production by Rhizopus Arrhizus Immobilized in Polyurethane Sponge. *Process Biochem.* 31, 463–469. doi:10.1016/0032-9592(95)00089-5

Roukas, T. (1991). Production of Citric Acid from Beet Molasses by Immobilized Cells of Aspergillus niger. *J. Food Sci.* 56, 878–880. doi:10.1111/j.1365-2621.1991.tb05409.x

Sakurai, A., and Imai, H. (1992). Effect of Operational Conditions on the Rate of Citric Acid Production by Rotating Disk Contactor Using Aspergillus niger. *J. Ferment. Bioeng.* 73, 251–254. doi:10.1016/0922-338X(92)90175-T

Uslu, H., and Kırbaşlar, Ş. İ. (2010). Extraction of Aqueous of Malic Acid by Trioctylamine Extractant in Various Diluents. *Fluid Phase Equilibria* 287, 134–140. doi:10.1016/j.fluid.2009.09.022

Uslu, H., and Kırbaşlar, S. I. (2009). Purification Ofl-Malic Acid from Aqueous Solution by a Method of Reactive Extraction. *J. Chem. Eng. Data* 54, 2819–2826. doi:10.1021/je800750q

Vrabl, P., Fuchs, V., Pichler, B., Schinagl, C. W., and Burgstaller, W. (2012). Organic Acid Excretion in Penicillium ochrochloron Increases with Ambient pH. *Front. Microbio.* 3, 121. doi:10.3389/fmicb.2012.00121

Wan, H. M., Chen, C. C., Giridhar, R., Chang, T. S., and Wu, W. T. (2005). Repeated-batch Production of Kojic Acid in a Cell-Retention Fermenter Using Aspergillus oryzae M3B9. *J. Ind. Microbiol. Biotechnol.* 32, 227–233. doi:10.1007/s10295-005-0230-5

Werpy, T., Petersen, G., Bozell, J., Aden, A., Holladay, J., White, J., et al. (2004). *Top Value Added Chemicals from Biomass: Volume I – Results of Screening for Potential Candidates from Sugars and Synthesis Gas*. Washington, DC, United States: U.S. Department of Energy.

Xu, Q., He, S., Jiang, L., Li, S., Wen, J., Guan, R., et al. (2017). Extractive Fermentation for Fumaric Acid Production by Rhizopus Oryzae. *Separat. Sci. Techn.* 52, 1–9. doi:10.1080/01496395.2017.1282962

Yang, C. W., Lu, Z., and Tsao, G. T. (1995). Lactic Acid Production by Pellet-formRhizopus Oryzae in a Submerged System. *Appl. Biochem. Biotechnol.* 51-52, 57–71. doi:10.1007/Bf02933411

Yin, P., Yahiro, K., Ishigaki, T., Park, Y., and Okabe, M. (1998). L(+)-lactic Acid Production by Repeated Batch Culture of *Rhizopus Oryzae* in Air-Lift Bioreactor. *J. Ferment. Bioeng.* 85, 96–100. doi:10.1016/S0922-338x(97)80361-3

Yu, B., Zhang, X., Sun, W., Xi, X., Zhao, N., Huang, Z., et al. (2018). Continuous Citric Acid Production in Repeated-Fed Batch Fermentation by Aspergillus niger Immobilized on a New Porous Foam. *J. Biotechnol.* 276-277, 1–9. doi:10.1016/j.jbiotec.2018.03.015

Zambanini, T., Kleineberg, W., Sarikaya, E., Buescher, J. M., Meurer, G., Wierckx, N., et al. (2016). Enhanced Malic Acid Production from Glycerol with High-Cell Density Ustilago Trichophora TZ1 Cultivations. *Biotechnol. Biofuels* 9, 135. doi:10.1186/s13068-016-0553-7

Zelle, R. M., de Hulster, E., van Winden, W. A., de Waard, P., Dijkema, C., Winkler, A. A., et al. (2008). Malic Acid Production by *Saccharomyces cerevisiae* : Engineering of Pyruvate Carboxylation, Oxaloacetate Reduction, and Malate Export. *Appl. Environ. Microbiol.* 74, 2766–2777. doi:10.1128/Aem.02591-07

Conflict of Interest: The authors declare that the research was conducted in the absence of any commercial or financial relationships that could be construed as a potential conflict of interest.

Publisher's Note: All claims expressed in this article are solely those of the authors and do not necessarily represent those of their affiliated organizations, or those of the publisher, the editors, and the reviewers. Any product that may be evaluated in this article, or claim that may be made by its manufacturer, is not guaranteed or endorsed by the publisher.

frontiers in Bioengineering and Biotechnology

ORIGINAL RESEARCH
published: 11 January 2022
doi: 10.3389/fbioe.2021.799756

Meiosis-Based Laboratory Evolution of the Thermal Tolerance in *Kluyveromyces marxianus*

Li Wu[1,2], *Yilin Lyu*[1,2], *Pingping Wu*[1,2], *Tongyu Luo*[1,2], *Junyuan Zeng*[1,2], *Tianfang Shi*[1,2], *Jungang Zhou*[1,2], *Yao Yu*[1,2]* *and Hong Lu*[1,2,3]*

[1]State Key Laboratory of Genetic Engineering, School of Life Sciences, Fudan University, Shanghai, China, [2]Shanghai Engineering Research Center of Industrial Microorganisms, Shanghai, China, [3]Shanghai Collaborative Innovation Center for Biomanufacturing Technology, Shanghai, China

Kluyveromyces marxianus is the fastest-growing eukaryote and a promising host for producing bioethanol and heterologous proteins. To perform a laboratory evolution of thermal tolerance in *K. marxianus*, diploid, triploid and tetraploid strains were constructed, respectively. Considering the genetic diversity caused by genetic recombination in meiosis, we established an iterative cycle of "diploid/polyploid - meiosis - selection of spores at high temperature" to screen thermotolerant strains. Results showed that the evolution of thermal tolerance in diploid strain was more efficient than that in triploid and tetraploid strains. The thermal tolerance of the progenies of diploid and triploid strains after a two-round screen was significantly improved than that after a one-round screen, while the thermal tolerance of the progenies after the one-round screen was better than that of the initial strain. After a two-round screen, the maximum tolerable temperature of Dip2-8, a progeny of diploid strain, was 3°C higher than that of the original strain. Whole-genome sequencing revealed nonsense mutations of *PSR1* and *PDE2* in the thermotolerant progenies. Deletion of either *PSR1* or *PDE2* in the original strain improved thermotolerance and two deletions displayed additive effects, suggesting *PSR1* and *PDE2* negatively regulated the thermotolerance of *K. marxianus* in parallel pathways. Therefore, the iterative cycle of "meiosis - spore screening" developed in this study provides an efficient way to perform the laboratory evolution of heat resistance in yeast.

Keywords: Kluyveromyces marxianus, thermal tolerance, laboratory evolution, meiosis, iterative cycle, PSR1, PDE2

OPEN ACCESS

Edited by:
Panagiotis Madesis, University of Thessaly, Greece

Reviewed by:
David T. Stuart, University of Alberta, Canada
Dae-Hee Lee, Korea Research Institute of Bioscience and Biotechnology (KRIBB), South Korea
Mamoru Yamada, Yamaguchi University, Japan

***Correspondence:**
Yao Yu
yaoyu@fudan.edu.cn
Hong Lu
honglv@fudan.edu.cn

Specialty section:
This article was submitted to Industrial Biotechnology, a section of the journal Frontiers in Bioengineering and Biotechnology

Received: *22 October 2021*
Accepted: *20 December 2021*
Published: *11 January 2022*

Citation:
Wu L, Lyu Y, Wu P, Luo T, Zeng J, Shi T, Zhou J, Yu Y and Lu H (2022) Meiosis-Based Laboratory Evolution of the Thermal Tolerance in Kluyveromyces marxianus. *Front. Bioeng. Biotechnol. 9:799756. doi: 10.3389/fbioe.2021.799756*

INTRODUCTION

The mutation is the major driving force of the adaptive evolution, leading to traits in coping with various environmental stress, including heat, salinity, alkalinity, acidity and so on (Wright, 2004). Heat resistance, also called thermal tolerance, is well-recognized as a quantitative trait controlled by a range of genes and pathways (Gao et al., 2016). For example, mutations of Rho1-Pkc1 pathway increase the thermal tolerance by affecting the integrity of the cell wall (Huang et al., 2018). Glutathione directly reduces the hydroxyl radical to form H_2O, thereby removing oxygen free radicals in cells, to increase the heat resistance of cells (Grant et al., 1996). Trehalose mainly protects cells from high-temperature damage by stabilizing the cell membrane structure and maintaining the conformation of intracellular proteins (Martinez-Esparza et al., 2011).

TABLE 1 | Strains used in this study.

Names	Genotypes	Sources
FIM1		Zhou et al. (2018)
FIM1Δ*u*	*ura3*Δ	Zhou et al. (2018)
a-FIM1Δ*u*Δ*w*	*MAT*a *ura3*Δ *hml*Δ *trp1*Δ	This study
α-FIM1Δ*u*Δ*h*	*MAT*α *ura3*Δ *hmr*Δ *his3*Δ	This study
KM-Diploid-S	*MAT*a/α *ura3*Δ	This study
KM-Diploid	*MAT*a/α *ura3*Δ *hml*Δ *hmr*Δ	This study
KM-Diploid-*MAT*a/a	*MAT*a/a *ura3*Δ *hml*Δ *hmr*Δ	This study
KM-Diploid-*MAT*α/α	*MAT*α/α *ura3*Δ *hml*Δ *hmr*Δ	This study
KM-Triploid	*MAT*a/a/α *ura3*Δ *hml*Δ *hmr*Δ	This study
KM-Tetraploid	*MAT*a/a/α/α *ura3*Δ *hml*Δ *hmr*Δ	This study
FIM1-*psr1*Δ	*ura3*Δ *psr1*Δ	This study
FIM1-*pde2*Δ	*ura3*Δ *pde2*Δ	This study
FIM1-*psr1*Δ*pde2*Δ	*ura3*Δ *psr1*Δ *ped2*Δ	This study

Kluyveromyces marxianus is a food-grade yeast commonly isolated in dairy environments. *K. marxianus* is the fastest-growing eukaryote reported so far, with a specific growth rate of 0.7–0.99 h^{-1} (Groeneveld et al., 2009). *K. marxianus* displays superior thermotolerance, as it can grow at 45°C and tolerate temperatures over 50°C, making it a promising platform for the production of bioethanol and chemicals (Lane and Morrissey, 2010; Gombert et al., 2016). Same as *Saccharomyces cerevisiae*, *K. marxianus* is a homothallic yeast with two mating types, *MAT*a and *MAT*α. Haploid cells switch the mating type spontaneously and haploid cells are capable of mating with other haploid cells of the opposite mating type to produce *MAT*a/α diploids (Cernak et al., 2018). When encountering adversities unsuitable for growth, diploid cells tend to undergo meiosis to produce tetrad. During meiosis, chromosomal crossover occurs, generating novel allele combinations, and some of which may help cells through harsh environments and subsequently promote the evolution of stress resistance (Owens et al., 2018). By combining meiosis and screen, the researcher successfully increased the ethanol production of *S. cerevisiae* by 10.96% (Hou, 2010). In our previous study, a 5-fold increase in the production of ferulic acid lipase was achieved by performing meiosis of *K. marxianus* diploids and subsequent screening of high-yield spores (Wu et al., 2020a). To our knowledge, there is no report of meiosis-mediated evolution of thermal tolerance in yeast yet.

Besides diploid, triploid and tetraploid can also undergo meiosis. In the meiosis of the triploids, homologous chromosomes cannot be distributed equally, resulting in aneuploidy (Charles et al., 2010). In the meiosis of tetraploids, there was an increased chance of asymmetric separation of homologous chromosomes, resulting in progeny cells of multiple ploidies (Loidl, 1995). Therefore, the genetic diversity of spores generated by triploids and tetraploids was expected to be different from that of spores generated by diploids, which might provide a valuable source for the screen of desired phenotypes. However, the triploid and tetraploid strain of *K. marxianus* has not been built in the laboratory yet.

In this study, triploid and tetraploid cells were constructed from diploid *K. marxianus* cells. Cells were screened by an iterative cycle of "diploid/polyploid - meiosis - selection of spores at high temperature". After a two-round screen, progenies displaying significantly enhanced thermal tolerance were obtained. Whole-genome sequencing suggested *PSR1* and *PDE2* were negative regulators of the thermotolerance. This study provides the first meiosis-based iterative cycle for the evolution of thermal tolerance in yeast. The method can be applied in the laboratory evolution of resistance to other stresses.

MATERIALS AND METHODS

Strains and Plasmids

Strains used in this study were listed in **Table 1**. Wild-type *K. marxianus* strain FIM1 was deposited in China General Microbiological Culture Collection Center (CGMCC No.10621). *URA3* was deleted in FIM1 to obtain FIM1Δ*u* as described before (Zhou et al., 2018). In FIM1Δ*u*, the *HML* locus and *TRP1* locus were deleted to obtain a-FIM1Δ*u*Δ*w*, the *HMR* locus and *HIS3* were deleted to obtain α-FIM1Δ*u*Δ*h*, *PSR1* and *PED2* were deleted to obtain FIM1-*psr1*Δ and FIM1-*pde2*Δ, respectively. *PED2* was deleted in FIM1-*psr1*Δ to obtain FIM1-*psr1*Δ*pde2*Δ. Genes were deleted by CRISPR/Cas9 as described before (Liu et al., 2018). Primers and plasmids used in the construction were shown in **Supplementary Tables S1 and S2**.

a-FIM1Δ*u*Δ*w* mated with α-FIM1Δ*u*Δ*h* to form KM-Diploid-S (*MAT*a/α, *ura3*Δ) as described before (Wu et al., 2020b). The *HML* and *HMR* locus of KM-Diploid-S were deleted by CRISPR/Cas9 to obtain KM-Diploid. The primer pairs W29F/W29R and W30F/W30R were used to identify the deletion of *HMR* or *HML* locus. The mating type of KM-Diploid (*MAT*a/α) was switched to *MAT*a/a by replacing *MAT*α locus with *MAT*a using CRISPR/Cas9, and the resultant strain was KM-Diploid-*MAT*a/a. Similarly, the mating type of KM-Diploid was switched to *MAT*α/α by replacing *MAT*a locus with *MAT*α, and the resultant strain was KM-Diploid-*MAT*α/α.

To construct the tetraploid strain, a pKD1-based plasmid carrying *KanMX6* (pUKDN127-Kan) was transformed into KM-Diploid-*MAT*a/a strain, and a pKD1-based plasmid carrying *hphMX4* (pUKDN127-Hyg) was transformed into KM-Diploid-*MAT*α/α strain. Transformants were cultured separately in YPD plates (10 g/L yeast extract, 20 g/L hipolypepton, 20 g/L glucose, 20 g/L agar) overnight. Cells were mixed and spread onto ME medium (50 g/L maltose extract, 30 g/L agar) to mate. Cells were then cultured at 30°C for 2 days and selected on YPD + G418 (0.2 mg/ml) +Hygromycin (0.25 mg/ml) plates to obtain tetraploid strain KM-tetraploid. The triploid strain was constructed similarly. KM-Diploid-*MAT*a/a cells transformed with pUKDN127-Kan were mated with α-FIM1Δ*u*Δ*h* cells transformed with pUKDN127-Hyg. Triploid strain KM-triploid was selected on the YPD + G418 + Hygromycin plate.

Meiosis and Selection of Spores at High Temperature

Diploid, triploid or tetraploid cells were cultured in 3 ml YPD liquid medium (10 g/L yeast extract, 20 g/L hipolypepton, 20 g/L

glucose) at 30°C for 12 h. Then cultures were inoculated into 50 ml YPA liquid medium (10 g/L potassium acetate, 20 g/L hipolypepton, 10 g/L yeast extract) at an initial optical density at 600 nm (OD_{600}) of 0.1, and cultured at 30°C for 6–8 h till OD_{600} reached 1.0–1.2. Cells were centrifuged and washed twice with sterile water. Cells were resuspended in 50 ml 2% potassium acetate (KAc) and cultured at 30°C for 24 h to initiate meiosis and sporulation. 1 ml sample was centrifuged and washed twice with sterile water. The cells were resuspended in 500 µl sterile water and then treated with 25 µl zymolyase (5 U/µl, E1004, Zymoresearch, United States) and 5 µl β-mercaptoethanol at 4°C for 24 h. The sample was supplemented with 200 µl 1.5% NP-40 and incubated at 30°C for 30 min to lyse vegetative cells. Cells were sonicated for 30 s times (Bioruptor UCD-300, Diagenode, Belgium), and then spread to YPD plates. For the first round of screen, spores generated by KM-Diploid, KM-Triploid and KM-tetraploid cells were grown at 43°C for 2 days. A total of 392 clones formed on the plates were selected and grown at 43°C in 3 ml YPD liquid medium for 4 h. Then, 3 µl culture was spotted onto YPD plates and grown at 43, 43, 45, and 46°C for 2 days. For the second-round screen, spores generated by diploid 2–2 and triploid 3–2 were grown at 46°C for 2 days. A total of 580 clones from 2–2 and 680 clones from 3–2 formed on the plates were selected and grown at 46°C in 3 ml liquid YPD for 4 h. Then, 3 µl culture was spotted onto YPD plates and grown at 45, 46, 47, and 48 for 2 days. Substantial growth on the plates indicated thermal tolerance to the temperature.

Determination of Mating Type and Auxotrophic Markers

The mating types were determined by PCR using three primers (YY270F, YY271F, YY272F). *MAT*a locus produced a band of 1,062 bp and *MAT*α locus produced a band of 1,515 bp. Cells failing to grow on the SC-his (20 g/L glucose, 6.7 g/L yeast nitrogen base, 40 mg/L uracil, 40 mg/L leucine, 40 mg/L tryptophan, 20 g/L agar) and SC-trp plate (20 g/L glucose, 6.7 g/L yeast nitrogen base, 40 mg/L histidine, 40 mg/L leucine, 40 mg/L uracil, 20 g/L agar) carried *his3*Δ and *trp1*Δ auxotrophic markers, respectively. Primers were listed in **Supplementary Table S1**.

Flow Cytometry

Cells were grown in YPD overnight. Cells of 800 µl cultures were pelleted and washed twice by 1 ml phosphate buffer (0.2 M Na_2HPO_4, pH adjusted to 7.0 by 0.1 M citric acid). Cells were resuspended gently in 1 ml of cold 75% ethanol and stored at 4°C for 5 h. Cells were washed by the phosphate buffer once and then resuspended in 800 µl phosphate buffer. The sample was supplemented with 10 µL RNase (50 mg/ml) and incubated at 37°C for 24 h. Cells were pelleted and resuspended in 1 ml phosphate buffer. Cells were supplemented with 5 µl propidium iodide solution (10 µg/ml propidium iodide in phosphate buffer) and stained for 30 min in dark. Cells were sonicated for 30 s 3 times. 10,000 cells were measured by a FACS Calibur flow cytometer (Becton Dickinson, United States) and data were analyzed by Flowjo 2.0.

Spot Assay

For spot assays of FIM1, KM-Diploid, KM-Triploid, KM-tetraploid, FIM1-*psr1*Δ, FIM1-*pde2*Δ and FIM1-*psr1*Δ*pder2*Δ, cells were grown in 3 ml YPD liquid medium at 30°C for 12 h. For the spot assay of spores, individual spore was grown in 3 ml YPD liquid medium and grown at 43°C or 46°C for 12 h. The culture was adjusted to an OD_{600} of 0.6 and then diluted fivefold five times. 3 µl dilutions were spotted on YPD plates. Plates were incubated at 30–48°C.

Growth Curves

Cells were grown in 3 ml YPD liquid medium at 30°C for 12 h and then diluted into 50 ml fresh YPD liquid medium to start at an OD_{600} of 0.01. Cells were grown at 47°C for 120 h. The OD_{600} of the culture was measured every 6 or 12 h. The experiment was performed with three parallel cultures.

Whole-Genome Sequencing

Cells were grown in 3 ml YPD liquid medium at 30°C for 12 h. Genomic DNA was extracted by a Yeast Genomic DNA Extraction kit (D1900, Solarbio, China). Whole-genome sequencing was performed by Illumina Hiseq (Mingma technologies, Shanghai, China). Significant SNPs and InDELs were identified by sequence alignment using the genome of FIM1 as a reference (Yu et al., 2021).

RESULTS

Improving the Thermal Tolerance of *Kluyveromyces marxianus* by Meiosis-Based Iterative Screen

The mating type of *K. marxianus* cells is determined by genes located in the *MAT* locus. The mating-type switches in *K. marxianus* are expected to occur spontaneously in the same way as reported in *Kluyveromyces lactis*, during which sequence of *MAT* locus was replaced by that of *HML* locus carrying silent *MAT*α information or by that of *HMR* locus carrying silent *MAT*a information, in a manner independent of homothallic switching (HO) endonuclease (Barsoum et al., 2010; Lee et al., 2018) (**Figure 1A**). To prevent the switch of mating type in this study, *HML* locus was deleted in *MAT*a cells and *HMR* locus was deleted in *MAT*α cells to obtain stable *MAT*a (a-FIM1Δ*u*Δ*w*) and *MAT*α (α-FIM1Δ*u*Δ*h*) haploid cells, respectively (**Figure 1B**).

a-FIM1Δ*u*Δ*w* mated with α-FIM1Δ*u*Δ*h* to form diploid (KM-Diploid-S), in which *HML* and *HMR* loci were deleted subsequently to form stable diploid strain (KM-Diploid). The mating type of KM-Diploid (*MAT*a/α) was switched to *MAT*a/a and *MAT*α/α, respectively. *MAT*a/a cells mated with *MAT*α and *MAT*α/α cells, to obtain triploid *MAT*a/a/α and tetraploid *MAT*a/a/α/α cells, respectively (**Figure 1C**). Details of the strain construction were described in methods. Ploidies were determined by flow cytometry. DNA contents of haploid, diploid, triploid and tetraploid strains were consistent with theoretical values (**Supplementary Figure S1A**).

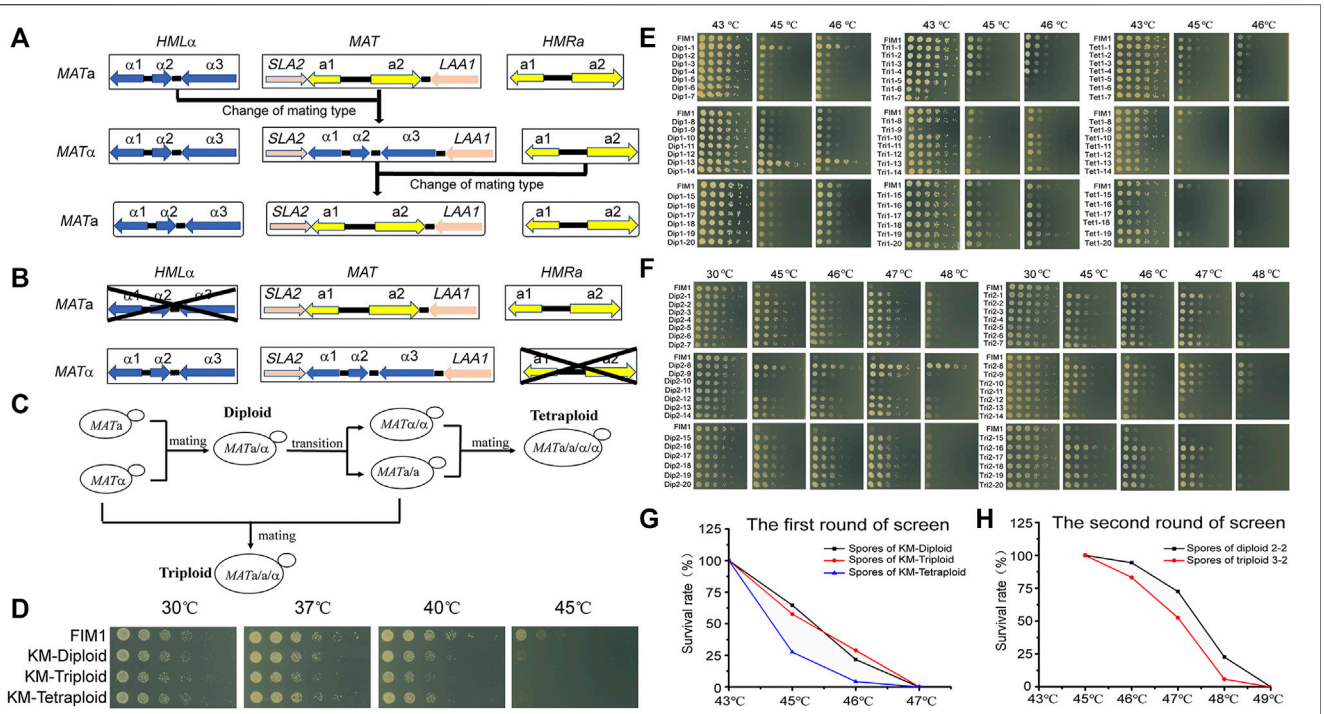

FIGURE 1 | The meiosis-based evolution of the thermotolerance in *K. marxianus*. **(A)** Switches of mating type in *K. marxianus*. **(B)** Constructions of stable *MAT*a and *MAT*α cells. **(C)** Constructions of diploid, triploid and tetraploid cells. **(D)** Spot assay of FIM1, KM-Diploid, KM-Triploid and KM-Tetraploid strains at different temperatures. **(E)** Spot assay of spores generated by KM-Diploid, KM-Triploid and KM-Tetraploid at different temperatures. **(F)** Spot assay of spores generated by 2–2 and 3–2 at different temperatures. **(G, H)** Survival rates of spores generated in the first **(G)** and second **(H)** rounds of the screen at different temperatures.

The effect of the ploidy on the thermal tolerance was investigated by a spot assay in the first place. The result showed that ploidy has little effect on cell growth under 30 and 37°C. The growth of diploid, triploid and tetraploid cells was poorer than that of haploid cells at 40°C. Haploid cells displayed limited growth at 45°C, while diploid, triploid and tetraploid cells could not grow at this temperature (**Figure 1D**). The result suggested, in *K. marxianus*, cells of higher ploidy levels, including diploid, triploid and tetraploid cells, displayed reduced thermotolerance than haploid cells. A similar result was reported in *S. cerevisiae*, as the thermotolerance of diploid and tetraploid cells at 50°C declined compared to that of haploid cells after a pre-heat shock (Piper et al., 1987).

Diploid, triploid and tetraploid cells underwent meiosis and produced spores in 2% KAc (**Supplementary Figure S1B**). Spores were grown at 43°C for 2 days till thermotolerant spores formed clones on the plates. A total of 392 clones generated by diploid, triploid or tetraploid were selected and grown at 43, 45, and 46°C for 2 days. Less than half of the clones sporulated from diploid, triploid and tetraploid strains could grow at 46°C (**Supplementary Figure S2**). Twenty spores displaying the best thermotolerance in the progenies of diploid, triploid and tetraploid strains were named Dip1-1~20, Tri1-1~20 and Tet1-1~20, respectively. The thermotolerance of these spores was investigated by a spot assay (**Figure 1E**). Among the spores generated by KM-Diploid, Dip1-1 and Dip1-13 displayed better growth than wild-type FIM1 strain, while the thermal tolerance of the rest 18 spores was similar to that of the FIM1 strain. In the spores generated by KM-Triploid, Tri1-19 displayed better thermal tolerance than FIM1. Five spores, including Tri1-5, 6, 7, 9, 15 displayed worse thermal tolerance than FIM1, while the rest spores were similar to FIM1. In the spores generated by KM-Tetraploid, only Tet1-1 and Tet1-19 displayed similar thermal tolerance as FIM1, while the thermal tolerance of the rest clones was worse than that of FIM1. Results suggested that in the first round of "meiosis - selection of spores at high temperature", the frequency of producing thermotolerant spores from the diploid strain was higher than that from triploid and tetraploid strains.

To find compatible pairs to construct diploid and polyploid strains in the second round of screen, the auxotrophic markers (Δ*trp*1 and Δ*his*3), the mating types and ploidies of spores were investigated (**Supplementary Figure S3**). To evaluate the effect of ploidy on the efficiency of evolution, spores generated by the diploid in the first round of screen were selected to construct the initial diploid strain for the second round of screen. Similarly, spores generated by the triploid were selected to construct triploid, and those by tetraploid were used to construct tetraploid. Based on the above considerations, Dip1-1(*MAT*α, *ura3*Δ) was selected to mate with Dip1-13 (*MAT*a, *ura3*Δ*his3*Δ) to form diploid 2-2 (*MAT*a/α, *ura3*Δ). Tri1-19 (*MAT*α, *ura3*Δ) mated with Tri1-5 (*MAT*a/a, *ura3*Δ) to form triploid 3-2 (*MAT*a/a/α, *ura3*Δ). Tet1-1 (*MAT*a/a, *ura3*Δ) mated with Tet1-15 (*MAT*α/α, *ura3*Δ*his3*Δ) to form tetraploid 4-2 (*MAT*a/a/α/α,

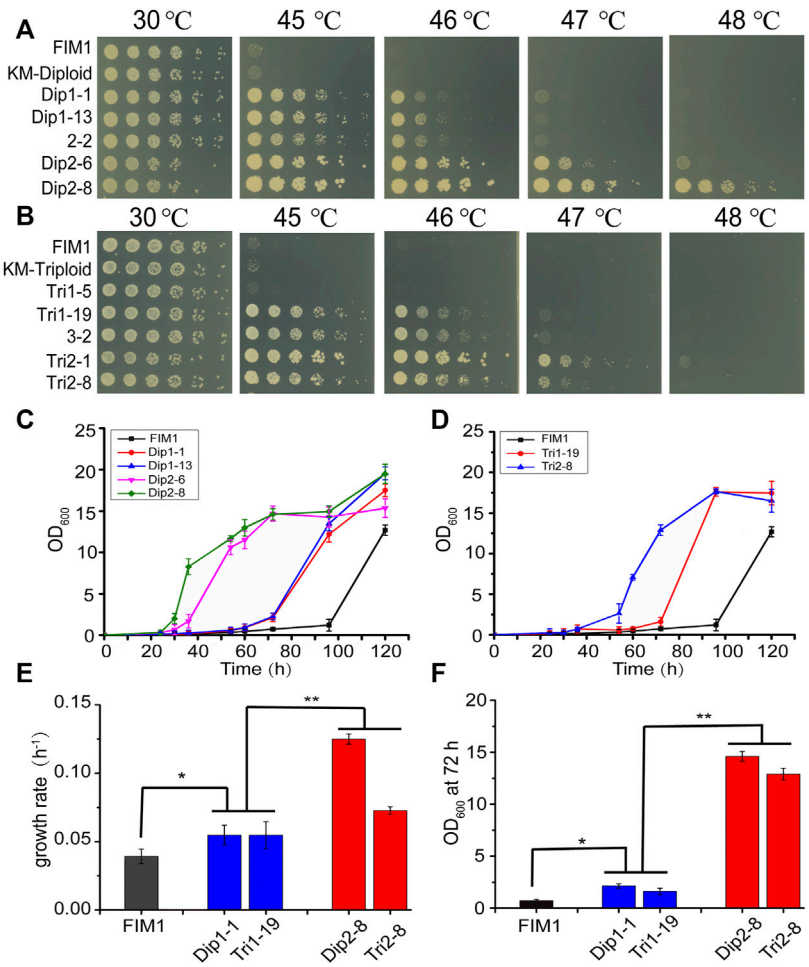

FIGURE 2 | Comparison of the thermotolerant spores generated by diploid and triploid strains. **(A, B)** Spot assays of the thermotolerant spores generated by diploid strains **(A)** and triploid strains **(B)**. **(C, D)** The growth curves of the thermotolerant spores generated by diploid **(C)** and triploid strains **(D)** at 47°C. Values here and below represented mean ± SD (n = 3). **(E)** The maximum growth rate of representative spores generated by diploid and triploid strains at 47°C. **(F)** OD_{600} of representative spores at 72 h. The significant difference was measured by a Student's *t*-test. $^{*}p < 0.05$, $^{**}p < 0.01$.

*ura3*Δ). The flow cytometry analysis results showed that the DNA contents of 2–2, 3–2 and 4–2 were consistent with their expected ploidies (**Supplementary Figure S4A**).

In the second round of screen, 2–2, 3–2 and 4–2 were cultured in 2% KAc to produce spores (**Supplementary Figure S4B**). First, a portion of spores was grown at 43, 45, 46, and 47°C for 2 days. Spores of 2–2 and 3–2 could grow at 46°C, but no spore of 4–2 could grow at 43°C. Therefore, 46°C was chosen as the temperature for selection in the second round, which was 3°C higher than that of the first round. Then, more spores of 2–2 and 3–2 were grown at 46°C for 2 days till thermotolerant spores formed clones on the plates. A total of 580 clones generated by 2–2 and 680 clones generated by 3–2 were selected. Clones were grown at 30, 45, 46, 47, and 48°C. The number of highly thermotolerant spores generated by diploid 2–2, which were able to grow at 47°C or above, was much higher than by triploid 3–2 (**Supplementary Figure S5**). Twenty spores of 2-2 displaying the best thermotolerance at 48°C were named Dip2-1~20 and those of 3–2 were named Tri2-1~20. The thermal tolerance of these spores was investigated by a spot assay (**Figure 1F**). Dip2-1~20 and Tri2-1~20 exhibited the same growth as FIM1 at 30°C, while displaying better thermotolerance than FIM1 at higher temperatures. Results indicated that the frequency to obtain thermotolerant spores in the second round of screen was higher than that in the first round of screen. Meanwhile, the highest temperature allowed for growth in the second round of screen, as shown by Dip2-8, was 2°C higher than that in the first round of screen. The results suggested that an iterative screen based on the meiosis of diploid and triploid efficiently promoted the evolution of thermal tolerance.

The survival rates of spores growing at different temperatures were compared. In the first round of screen, the survival rates of spores produced by KM-Diploid, KM-Triploid and KM-Tetraploid at 45°C were 64.6, 57.5, and 27.6%, respectively, while those at 46°C were 21.8, 28.9, and 4.2%, respectively (**Figure 1G**). In the second round of screen, the survival rates of spores produced by diploid 2-2 and triploid 3-2 at 46°C were

TABLE 2 | SNPs and InDels in thermotolerant spores.

Posi-tion[a]	Chromo-some	Mutation sites	ORFs	Change in nucleotide(s)	Change of amino acid	Strain	Origin of the mutation[b]
CDS	2	872630	*MUC1*	T1942G	Ser648 > Ala	Dip1-1	Dip1-1
	3	487709	*PSR1*	G256T	Glu86 > *Stop*	Dip2-6	Dip2-6
	3	1272805	*PDE2*	C1019A	Ser340 > *Stop*	Dip2-6	Dip2-6
	3	487709	*PSR1*	G256T	Glu86 > *Stop*	Dip2-8	Dip2-8
	3	1273144	*PDE2*	G680A	Trp227 > *Stop*	Dip2-8	Dip2-8
	3	487943	*PSR1*	+TAAAGAGG	*Frameshift*	Tri1-19	Tri1-19
	3	487943	*PSR1*	+TAAAGAGG	*Frameshift*	Tri2-8	***Tri1-19***
NCDS	7	357288	—	+C	—	Dip1-1	***KM-Diploid***
	3	1572771	—	+T	—	Dip1-13	Dip1-13
	7	357288	—	+C	—	Dip1-13	***KM-Diploid***
	1	1240060	—	C- > A	—	Dip2-6	Dip2-6
	8	620828	—	T- > G	—	Dip2-6	Dip2-6
	3	1572771	—	+T	—	Dip2-6	***Dip1-13***
	7	357288	—	+C	—	Dip2-6	***KM-Diploid***
	1	483871	—	G- > A	—	Dip2-8	Dip2-8
	1	541343	—	G- > A	—	Dip2-8	Dip2-8
	1	1182783	—	A- > T	—	Dip2-8	Dip2-8
	1	1240060	—	C- > A	—	Dip2-8	Dip2-8
	3	631197	—	G- > A	—	Dip2-8	Dip2-8
	7	357288	—	+C	—	Dip2-8	***KM-Diploid***
	1	204786	—	+A	—	Tri1-19	Tri1-19
	3	1572771	—	+T	—	Tri1-19	Tri1-19
	7	357288	—	+C	—	Tri1-19	***KM-Diploid***
	7	357288	—	+C	—	Tri2-8	***KM-Diploid***

[a]*CDS, was short for coding sequence and NCDS, was for non-coding sequence.*
[b]*Name of the ancestor strain from which the mutation was inherited was in bold.*

94.3 and 83.3% respectively, those at 47°C were 72.4 and 52.7%, respectively, and those at 48°C were 22.6 and 5.9%, respectively (**Figure 1H**). In general, spores of diploid strain were more thermotolerant than those of triploid and tetraploid strains. The result suggested that the thermotolerance evolved faster in the meiosis of diploid strain than of triploid or tetraploid strain.

The Thermal Tolerance of Spores Generated by a Two-Round Screen was Better Than by a One-Round Screen.

In the first round of screen, Dip1-1/Dip1-13 and Tri1-19 were the most thermotolerant spores generated by KM-Diploid and KM-Triploid, respectively. In the second round of screen, Dip2-8 and Tri2-1/Tri2-8 were the most thermotolerant spores produced by diploid 2–2 and triploid 3–2, respectively. The thermal tolerance of these spores was compared in spot assays (**Figures 2A,B**). Compared with the wild-type strain FIM1, the highest temperatures allowed for the growth of Dip1-13 and Tri1-19 were 46°C, that of Dip2-8 was 48°C, and those of Tri2-1 and Tri2-8 were 47°C. The results showed that Dip2-8 was the most thermotolerant spore, which was obtained in the two-round screen.

The growth curves of thermotolerant spores at 47°C were investigated. The lag phases of FIM1, Dip1-1, Dip1-13, Dip2-6 and Dip2-8 were 96, 60, 60, 34, 26 h, respectively (**Figure 2C**). The lag phases of Tri1-19 and Tri2-8 were 70 and 40 h, respectively (**Figure 2D**). The results suggested spores obtained in the second round of screen displayed shorter lag phases than in the first round screen. The maximum growth rates of spores from the second round of screen (Dip2-8 and Tri2-8) were significantly higher than those of spores from the first round of screen (Dip1-1 and Tri1-19), while maximum growth rates of first-round spores were significantly higher than that of FIM1 (**Figure 2E**). Similarly, values of OD_{600}, which were indicators of the biomass, of the second-round spores at 72 h were significantly higher than those of the first-round spores, while values of OD_{600} of the first-round spores at 72 h were significantly higher than that of FIM1 (**Figure 2F**). The shorter the lag phase, the higher the growth rate and the higher biomass at the high temperature indicated the better thermal tolerance. Therefore, through the iterative cycle of "diploid/polyploid -meiosis -selection of spores at high temperature", the thermal tolerance of spores generated by the two-round screen was significantly better than by the one-round screen, while the thermal tolerance of spores generated by the one-round screen was better than that of the original strain.

PSR1 and *PDE2* Negatively Regulated the Thermotolerance of *K. marxianus*

To investigate the mutations underlying the thermal tolerance, Dip1-1, Dip1-13, Dip2-6, Dip2-8, Tri1-19 and Tri2-8 were subjected to the whole-genome sequencing. Seven mutations inside coding sequences, ten single-nucleotide polymorphisms (SNPs) and three insertion-deletions (InDels) inside non-coding sequences (NCDS) were identified in the spores (**Table 2**). Origins of some mutations could be traced back to ancestor strains (**Table 2**). For example, a frameshift in *PSR1* in Tri2-8 was

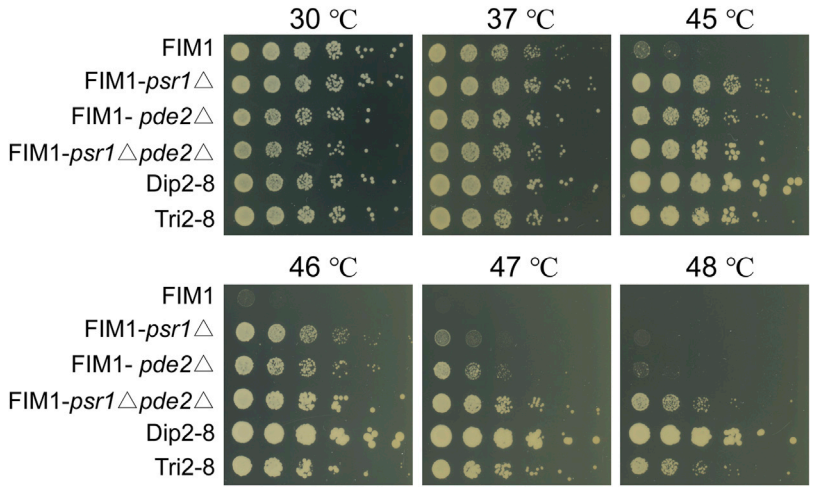

FIGURE 3 | Spot assays of FIM1 carrying the deletion of *PSR1*, *PDE2* or a combination of both deletions. FIM1, Dip2-8 and Tri2-8 were spotted as controls.

inherited from Tri1-19. An insertion of "C" at 357288bp of chromosome 7 in all six spores was presumably inherited from KM-Diploid. Other SNPs and InDels might be caused by replication and repair errors during the meiosis or the vegetative growth afterwards. Notably, compared with the wild-type strain FIM1, Dip2-6 and Dip2-8 contained nonsense mutations of *PSR1* and *PDE2* genes, while Tri1-19 and Tri2-8 contained frameshift of *PSR1*. The result suggested mutations of *PSR1* and *PDE2* were the major contributors to the improved thermotolerance. To validate this idea, *PSR1* and *PDE2* were deleted individually or together in FIM1 to construct FIM1-*psr1*Δ, FIM1-*pde2*Δ and FIM1-*psr1*Δ*pde2*Δ strains, respectively (**Supplementary Figure S6**). These strains, along with Dip2-8, Tri2-8 and FIM1, were grown at 30°C, 37°C, 45°C, 46°C, 47°C, and 48°C. No significant growth difference was found between strains at 30°C and 37°C. The growth of FIM1-*psr1*Δ and FIM1-*pde2*Δ was significantly better than that of FIM1 at 45°C, 46°C and 47°C. The growth of FIM1-*psr1*Δ*pde2*Δ was better than that of FIM1-*psr1*Δ and FIM1-*pde2*Δ at 45, 46, and 47°C (**Figure 3**). These results suggested that *PSR1* and *PDE2* were key genes that negatively regulated the thermotolerance in *K. marxianus* and that two genes functioned in parallel pathways. However, the growth of FIM1-*psr1*Δ*pde2*Δ at 47°C and 48°C was poorer than that of Dip2-8, which contained five SNP and one InDel inside NCDS, besides the mutation of *PSR1* and *PDE2* (**Table 2**). The growth FIM1-*psr1*Δ at 47°C and 48°C was poorer than that of Tri2-8, which contained one InDel inside NCDS, besides the mutation of *PSR1* (**Table 2**). The result suggested that mutations inside NCDS, other than the mutations of *PSR1* and *PDE2*, also contributed to the thermotolerance.

DISCUSSION

High yielding of heterologous proteins, including β-glucosidase (Su et al., 2021), feruloyl esterase (Liu et al., 2018), and virus-like particles (Duan et al., 2019), has been successfully achieved in *K. marxianus*. Meanwhile, superior features of fast growth, thermotolerance and the capacity to assimilate pentose facilitate the production of bioethanol and chemicals in *K. marxianus* (Suzuki et al., 2019). Collectively, *K. marxianus* is a microbial cell factory with great potentials.

Improving the thermal tolerance of *K. marxianus* is a necessity to promote its industrial applications, especially in the production of ethanol. Based on the genetic diversity produced by the recombination of meiosis, we established an iterative cycle of "diploid/polyploid - meiosis - selection of spores at high temperature" to improve the thermal tolerance of *K. marxianus*. During the vegetative growth of yeast cells, the genome-wide single-nucleotide mutation rate was at 2–3 × 10^{-10} per base per generation (Lynch et al., 2008; Zhu et al., 2014), and continuous culturing yeast cells at high temperature were expected to enrich mutations that improved thermal tolerance of cells. Consistent with this idea, the growth rate of *S. cerevisiae* at 40°C was increased by 1.57 times, through the continuous passage of the culture at 39.5°C for more than 90 days (Caspeta et al., 2014). During meiosis, DNA repair associated recombination was mutagenic, providing extra genetic diversity that can contribute to adaptive evolution (Rattray et al., 2015). In this study, we established an iterative cycle of "diploid/polyploid - meiosis - selection of spores at high temperature" in *K. marxianus*, and successfully improved the maximum temperature allowed for growth by 3°C after only two rounds of the screen. Furthermore, the average concentration of ethanol produced by second-round spores (Dip 2-8 and Tri2-8) at 45°C was significantly more than that by one-round spores (Dip1-1 and Tri1-19) (**Supplementary Figure S7**). The result suggested the ethanol productivity at high temperatures was also improved during the iterative cycle of evolution.

Compared with the evolution of vegetatively growing cells, one obstacle to the meiosis-based evolution was the requirement of constructing diploid/polyploid strains for each round of screen. In some cases, spores displaying better thermotolerance could not be selected to construct diploid/polyploid strains because mating types of spores were not compatible. For example, Tri1-4 (*MAT*α/

α) was more thermotolerant than Tri1-5 (*MAT*a/a), but the latter was selected to construct a triploid strain as it was compatible with Tri1-19 (*MAT*α) (**Figure 1E**, **Supplementary Figure S3**). Therefore, to construct diploid/triploid from the most thermotolerant spores, a convenient protocol to switch the mating type needed to be established in the following study. In some cases, the mating type was not consistent with the ploidy. For example, the mating type of Dip1-2 was identified as *MAT*a/α by PCR (**Supplementary Figure S3**). However, Dip1-2 was identified to be a haploid strain in the flow cytometry analysis. Meiosis might result in rearrangement at the *MAT* locus and lead to the production of multiple *MAT* loci in the genome.

In this study, diploid, triploid and tetraploid strains were selected for the iterative screen. The proportion of thermotolerant spores from the diploid was higher than that from the triploid, and that from the triploid was higher than that from the tetraploid (**Figures 1E,F**). This result might be related to the fact that the thermal tolerance of *K. marxianus* decreased with increased ploidies (**Figure 1D**). The same results were reported for *S. cerevisiae* (Zhang et al., 2017). In addition, aneuploidy spores generated by the triploid strain might lead to an imbalance of cellular energy metabolism, which was detrimental to stress resistance (Torres et al., 2007). The growth of aneuploid cells at high temperatures imposed an extra burden on the chromosome segregation and might cause a higher frequency of chromosome rearrangements and loss, which reduced the viability of progenies and efficiency of adaptive evolution (Yona et al., 2012).

Thermotolerant spores obtained in this screen, including Dip1-1, Dip1-13, Dip2-6, Dip2-8, Tri1-19 and Tri2-8, grew as well as wild-type FIM1 at 30°C. Whole-genome sequencing of these spores obtained in our screen did not reveal any rearrangement or loss of chromosome fragments, suggesting the natural chromosome structures of *K. marxianus* were required for the balance of normal growth at the regular temperature and improved growth at high temperatures. Four out of six thermotolerant spores contained mutations of *PSR1*, while two spores contained mutations of *PDE2*. FIM1 cells carrying an individual deletion of *PSR1* or *PDE2* exhibited increased thermotolerance, while deletion of both genes displayed additive effects on the thermotolerance. The result indicated that *PSR1* and *PDE2* negatively regulated the growth of *K. marxianus* at high temperatures (up to 48°C) through parallel pathways. In *S. cerevisiae*, *PDE2* encodes a high-affinity cAMP phosphodiesterase that catalyzes the degradation of cAMP, and thus negatively regulates numerous cAMP-dependent pathways (Sass et al., 1986). Psr1 is a membrane-associated phosphatase. Psr1 and its partner Psr2 form a complex with Whi2 to negative regulate TORC1, which is a signalling complex regulating the response to nutrients (Kaida et al., 2002; Chen et al., 2018). Notably, deletion of *PDE2* and *PSR1* reduced the viability of the cells after a transient heat shock, probably through constitutively activated cAMP-dependent pathways and TORC1 pathways, respectively (Jones et al., 2004; Teng et al., 2011). The results indicated *PSR1* and *PDE2* were positive regulators of the response to heat shock in *S. cerevisiae*, which looks like contradicting the results in *K. marxianus*. However, the mechanism supporting the survival of short exposure to extremely high temperatures differs that regulating growth at high temperatures. For example, Hsp104 plays a vital role in helping cells survive short-term heat shock, but is not required for the growth at high temperatures (Lindquist and Kim, 1996). Besides, there was no direct proof indicating that *PSR1* and *PDE2* were required for continuous growth at high temperatures in *S. cerevisiae*. *K. marxianus* is more thermotolerant than *S. cerevisiae* (Fonseca et al., 2008). It is possible that complex networks regulated by *PSR1* and *PDE2* in *K. marxianus*, such as PKA and TORC1 pathways, are rewired during the evolution to negatively regulate the growth at high temperatures. The detailed mechanism is worthwhile to be investigated in the following study.

DATA AVAILABILITY STATEMENT

The original contributions presented in the study are publicly available. This data can be found here: https://www.ncbi.nlm.nih.gov/bioproject/PRJNA732519.

AUTHOR CONTRIBUTIONS

HL and YY designed the study and supervised the project. LW performed the screen, analyzed the data, and wrote the manuscript. YL and WP assisted the screen. TL and JZe analyzed the sequencing data. TS constructed strains for mating. JZh assisted mating and screen. All authors have revised the manuscript and approved the final version.

FUNDING

This work was supported by the National Key Research and Development Program of China 2021YFC2100203, Tianjin Synthetic Biotechnology Innovation Capacity Improvement Project TSBICIP-KJGG-006, Science and Technology Research Program of Shanghai 19DZ2282100, and National Natural Science Foundation of China 31770094.

ACKNOWLEDGMENTS

We thank Qin Lan, Haiyan Ren for their assistance in the experiment of ethanol productivity.

SUPPLEMENTARY MATERIAL

The Supplementary Material for this article can be found online at: https://www.frontiersin.org/articles/10.3389/fbioe.2021.799756/full#supplementary-material

REFERENCES

Barsoum, E., Martinez, P., and Åström, S. U. (2010). α3, a Transposable Element that Promotes Host Sexual Reproduction. *Genes Dev.* 24 (1), 33–44. doi:10.1101/gad.557310

Caspeta, L., Chen, Y., Ghiaci, P., Feizi, A., Buskov, S., Hallström, B. M., et al. (2014). Altered Sterol Composition Renders Yeast Thermotolerant. *Science* 346 (6205), 75–78. doi:10.1126/science.1258137

Cernak, P., Estrela, R., Poddar, S., Skerker, J. M., Cheng, Y.-F., Carlson, A. K., et al. (2018). Engineering Kluyveromyces Marxianus as a Robust Synthetic Biology Platform Host. *mBio* 9 (5), e01410-18. doi:10.1128/mBio.01410-18

Charles, J. S., Hamilton, M. L., and Petes, T. D. (2010). Meiotic Chromosome Segregation in Triploid Strains of *Saccharomyces cerevisiae*. *Genetics* 186 (2), 537–550. doi:10.1534/genetics.110.121533

Chen, X., Wang, G., Zhang, Y., Dayhoff-Brannigan, M., Diny, N. L., Zhao, M., et al. (2018). Whi2 Is a Conserved Negative Regulator of TORC1 in Response to Low Amino Acids. *Plos Genet.* 14 (8), e1007592. doi:10.1371/journal.pgen.1007592

Duan, J., Yang, D., Chen, L., Yu, Y., Zhou, J., and Lu, H. (2019). Efficient Production of Porcine Circovirus Virus-like Particles Using the Nonconventional Yeast Kluyveromyces Marxianus. *Appl. Microbiol. Biotechnol.* 103 (2), 833–842. doi:10.1007/s00253-018-9487-2

Fonseca, G. G., Heinzle, E., Wittmann, C., and Gombert, A. K. (2008). The Yeast Kluyveromyces Marxianus and its Biotechnological Potential. *Appl. Microbiol. Biotechnol.* 79 (3), 339–354. doi:10.1007/s00253-008-1458-6

Gao, L., Liu, Y., Sun, H., Li, C., Zhao, Z., and Liu, G. (2016). Advances in Mechanisms and Modifications for Rendering Yeast Thermotolerance. *J. Biosci. Bioeng.* 121 (6), 599–606. doi:10.1016/j.jbiosc.2015.11.002

Gombert, A. K., Madeira, J. V., Jr., Cerdán, M.-E., and González-Siso, M.-I. (2016). Kluyveromyces Marxianus as a Host for Heterologous Protein Synthesis. *Appl. Microbiol. Biotechnol.* 100 (14), 6193–6208. doi:10.1007/s00253-016-7645-y

Grant, C. M., MacIver, F. H., and Dawes, I. W. (1996). Glutathione Is an Essential Metabolite Required for Resistance to Oxidative Stress in the yeastSaccharomyces Cerevisiae. *Curr. Genet.* 29 (6), 511–515. doi:10.1007/BF02426954

Groeneveld, P., Stouthamer, A. H., and Westerhoff, H. V. (2009). Super Life - How and Why 'cell Selection' Leads to the Fastest-Growing Eukaryote. *FEBS J.* 276 (1), 254–270. doi:10.1111/j.1742-4658.2008.06778.x

Hou, L. (2010). Improved Production of Ethanol by Novel Genome Shuffling in *Saccharomyces cerevisiae*. *Appl. Biochem. Biotechnol.* 160 (4), 1084–1093. doi:10.1007/s12010-009-8552-9

Huang, C.-J., Lu, M.-Y., Chang, Y.-W., and Li, W.-H. (2018). Experimental Evolution of Yeast for High-Temperature Tolerance. *Mol. Biol. Evol.* 35 (8), 1823–1839. doi:10.1093/molbev/msy077

Jones, D. L., Petty, J., Hoyle, D. C., Hayes, A., Oliver, S. G., Riba-Garcia, I., et al. (2004). Genome-Wide Analysis of the Effects of Heat Shock on aSaccharomyces cerevisiaeMutant with a Constitutively Activated cAMP-dependent Pathway. *Comp. Funct. Genomics* 5 (5), 419–431. doi:10.1002/cfg.415

Kaida, D., Yashiroda, H., Toh-e, A., and Kikuchi, Y. (2002). Yeast Whi2 and Psr1-Phosphatase Form a Complex and Regulate STRE-Mediated Gene Expression. *Genes Cells* 7 (6), 543–552. doi:10.1046/j.1365-2443.2002.00538.x

Lane, M. M., and Morrissey, J. P. (2010). Kluyveromyces Marxianus: A Yeast Emerging from its Sister's Shadow. *Fungal Biol. Rev.* 24 (1), 17–26. doi:10.1016/j.fbr.2010.01.001

Lee, M.-H., Lin, J.-J., Lin, Y.-J., Chang, J.-J., Ke, H.-M., Fan, W.-L., et al. (2018). Genome-wide Prediction of CRISPR/Cas9 Targets in Kluyveromyces Marxianus and its Application to Obtain a Stable Haploid Strain. *Sci. Rep.* 8 (1), 7305. doi:10.1038/s41598-018-25366-z

Lindquist, S., and Kim, G. (1996). Heat-shock Protein 104 Expression Is Sufficient for Thermotolerance in Yeast. *Proc. Natl. Acad. Sci.* 93 (11), 5301–5306. doi:10.1073/pnas.93.11.5301

Liu, Y., Mo, W.-J., Shi, T.-F., Wang, M.-Z., Zhou, J.-G., Yu, Y., et al. (2018). Mutational Mtc6p Attenuates Autophagy and Improves Secretory Expression of Heterologous Proteins in Kluyveromyces Marxianus. *Microb. Cel Fact* 17 (1), 144. doi:10.1186/s12934-018-0993-9

Loidl, J. (1995). Meiotic Chromosome Pairing in Triploid and Tetraploid *Saccharomyces cerevisiae*. *Genetics* 139 (4), 1511–1520. doi:10.1093/genetics/139.4.1511

Lynch, M., Sung, W., Morris, K., Coffey, N., Landry, C. R., Dopman, E. B., et al. (2008). A Genome-wide View of the Spectrum of Spontaneous Mutations in Yeast. *Proc. Natl. Acad. Sci.* 105 (27), 9272–9277. doi:10.1073/pnas.0803466105

Martinez-Esparza, M., Tapia-Abellan, A., Vitse-Standaert, A., Garcia-Penarrubia, P., Arguelles, J. C., Poulain, D., et al. (2011). Glycoconjugate Expression on the Cell wall of Tps1/tps1 Trehalose-Deficient Candida Albicans Strain and Implications for its Interaction with Macrophages. *Glycobiology* 21 (6), 796–805. doi:10.1093/glycob/cwr007

Owens, S., Tang, S., and Hunter, N. (2018). Monitoring Recombination during Meiosis in Budding Yeast. *Methods Enzymol.* 601, 275–307. doi:10.1016/bs.mie.2017.12.005

Piper, P. W., Davies, M. W., Curran, B., Lockheart, A., Spalding, A., and Tuite, M. F. (1987). The Influence of Cell Ploidy on the Thermotolerance of *Saccharomyces cerevisiae*. *Curr. Genet.* 11 (8), 595–598. doi:10.1007/BF00393921

Rattray, A., Santoyo, G., Shafer, B., and Strathern, J. N. (2015). Elevated Mutation Rate during Meiosis in *Saccharomyces cerevisiae*. *Plos Genet.* 11 (1), e1004910. doi:10.1371/journal.pgen.1004910

Sass, P., Field, J., Nikawa, J., Toda, T., and Wigler, M. (1986). Cloning and Characterization of the High-Affinity cAMP Phosphodiesterase of *Saccharomyces cerevisiae*. *Proc. Natl. Acad. Sci.* 83 (24), 9303–9307. doi:10.1073/pnas.83.24.9303

Su, M., Hu, Y., Cui, Y., Wang, Y., Yu, H., Liu, J., et al. (2021). Production of β-glucosidase from Okara Fermentation Using Kluyveromyces Marxianus. *J. Food Sci. Technol.* 58 (1), 366–376. doi:10.1007/s13197-020-04550-y

Suzuki, T., Hoshino, T., and Matsushika, A. (2019). High-temperature Ethanol Production by a Series of Recombinant Xylose-Fermenting Kluyveromyces Marxianus Strains. *Enzyme Microb. Technol.* 129, 109359. doi:10.1016/j.enzmictec.2019.109359

Teng, X., Cheng, W.-C., Qi, B., Yu, T.-X., Ramachandran, K., Boersma, M. D., et al. (2011). Gene-dependent Cell Death in Yeast. *Cell Death Dis* 2, e188. doi:10.1038/cddis.2011.72

Torres, E. M., Sokolsky, T., Tucker, C. M., Chan, L. Y., Boselli, M., Dunham, M. J., et al. (2007). Effects of Aneuploidy on Cellular Physiology and Cell Division in Haploid Yeast. *Science* 317 (5840), 916–924. doi:10.1126/science.1142210

Wright, B. E. (2004). Stress-directed Adaptive Mutations and Evolution. *Mol. Microbiol.* 52 (3), 643–650. doi:10.1111/j.1365-2958.2004.04012.x

Wu, L., Wang, M., Zha, G., Zhou, J., Yu, Y., and Lu, H. (2020b). A Protocol of Rapid Laboratory Evolution by Genome Shuffling in Kluyveromyces Marxianus. *MethodsX* 7, 101138. doi:10.1016/j.mex.2020.101138

Wu, L., Wang, M., Zha, G., Zhou, J., Yu, Y., and Lu, H. (2020a). Improving the Expression of a Heterologous Protein by Genome Shuffling in Kluyveromyces Marxianus. *J. Biotechnol.* 320, 11–16. doi:10.1016/j.jbiotec.2020.06.007

Yona, A. H., Manor, Y. S., Herbst, R. H., Romano, G. H., Mitchell, A., Kupiec, M., et al. (2012). Chromosomal Duplication Is a Transient Evolutionary Solution to Stress. *Proc. Natl. Acad. Sci.* 109 (51), 21010–21015. doi:10.1073/pnas.1211150109

Yu, Y., Mo, W., Ren, H., Yang, X., Lu, W., Luo, T., et al. (2021). Comparative Genomic and Transcriptomic Analysis Reveals Specific Features of Gene Regulation in Kluyveromyces Marxianus. *Front. Microbiol.* 12, 598060. doi:10.3389/fmicb.2021.598060

Zhang, K., Fang, Y.-H., Gao, K.-H., Sui, Y., Zheng, D.-Q., and Wu, X.-C. (2017). Effects of Genome Duplication on Phenotypes and Industrial Applications of *Saccharomyces cerevisiae* Strains. *Appl. Microbiol. Biotechnol.* 101 (13), 5405–5414. doi:10.1007/s00253-017-8284-7

Zhou, J., Zhu, P., Hu, X., Lu, H., and Yu, Y. (2018). Improved Secretory Expression of Lignocellulolytic Enzymes in Kluyveromyces Marxianus by Promoter and Signal Sequence Engineering. *Biotechnol. Biofuels* 11, 235. doi:10.1186/s13068-018-1232-7

Zhu, Y. O., Siegal, M. L., Hall, D. W., and Petrov, D. A. (2014). Precise Estimates of Mutation Rate and Spectrum in Yeast. *Proc. Natl. Acad. Sci.* 111 (22), E2310–E2318. doi:10.1073/pnas.1323011111

Conflict of Interest: The authors declare that the research was conducted in the absence of any commercial or financial relationships that could be construed as a potential conflict of interest.

frontiers in Bioengineering and Biotechnology

REVIEW
published: 14 February 2022
doi: 10.3389/fbioe.2021.802031

Biotechnological Innovations and Therapeutic Application of Pediococcus and Lactic Acid Bacteria: The Next-Generation Microorganism

*Sunday Bulus Peter, Zhina Qiao, Hero Nmeri Godspower, Samaila Boyi Ajeje, Meijuan Xu, Xian Zhang, Taowei Yang and Zhiming Rao**

The Key Laboratory of Industrial Biotechnology, Ministry of Education, School of Biotechnology, Jiangnan University, Wuxi, China

Lactic acid bacteria represent a worthwhile organism within the microbial consortium for the food sector, health, and biotechnological applications. They tend to offer high stability to environmental conditions, with an indicated increase in product yield, alongside their moderate antimicrobial activity. Lack of endotoxins and inclusion bodies, extracellular secretion, and surface display with other unique properties, are all winning attributes of these Gram-positive lactic acid bacteria, of which, *Pediococcus* is progressively becoming an attractive and promising host, as the next-generation probiotic comparable with other well-known model systems. Here, we presented the biotechnological developments in *Pediococcal* bacteriocin expression system, contemporary variegated models of *Pediococcus* and lactic acid bacteria strains as microbial cell factory, most recent applications as possible live delivery vector for use as therapeutics, as well as upsurging challenges and future perspective. With the radical introduction of artificial intelligence and neural network in Synthetic Biology, the microbial usage of lactic acid bacteria as an alternative eco-friendly strain, with safe use properties compared with the already known conventional strains is expected to see an increase in various food and biotechnological applications in years to come as it offers better hope of safety, accuracy, and higher efficiency.

Keywords: probiotics, *Pediococcus*, biotherapeutics, bacteriocin, genome editing, deep neural network

OPEN ACCESS

Edited by:
Fengjie Cui,
Jiangsu University, China

Reviewed by:
Xuetuan Wei,
Huazhong Agricultural University, China
Zaiwei Man,
Changzhou University, China

****Correspondence:***
Zhiming Rao
raozhm@jiangnan.edu.cn

Specialty section:
This article was submitted to Industrial Biotechnology, a section of the journal Frontiers in Bioengineering and Biotechnology

Received: *26 October 2021*
Accepted: *08 December 2021*
Published: *14 February 2022*

Citation:
Peter SB, Qiao Z, Godspower HN, Ajeje SB, Xu M, Zhang X, Yang T and Rao Z (2022) Biotechnological Innovations and Therapeutic Application of Pediococcus and Lactic Acid Bacteria: The Next-Generation Microorganism. Front. Bioeng. Biotechnol. 9:802031. doi: 10.3389/fbioe.2021.802031

INTRODUCTION

The idea that bacteria are useful can be difficult to understand. Today, however, some are known as friendly, good, or healthy bacteria that are widely used in foods, beverages, and supplements that help promote a healthy digestive tract and immune system. Currently, research continued to support these findings and suggest even more benefits.

Among these bacteria, is lactic acid bacteria (LAB), made up of different sets of Gram-positive, non-pathogenic bacteria that are diverse and taxonomically heterogeneous (George et al., 2018). Generally, they are catalase negative and occur as cocci or rod shaped, although pseudocatalase can be seen in rare cases. The genera *Pediococcus*, *Streptococcus*, and certain species of *Lactobacillus* carry out homolactic fermentation. As observed in *Lactobacillus* species, *Pediococcus* can also create a number of enzymes that releases unique food flavor compounds. Heterolactic fermentation on the other hand is performed by bacteria of the genus *Leuconostoc* and some *Lactobacillus* species

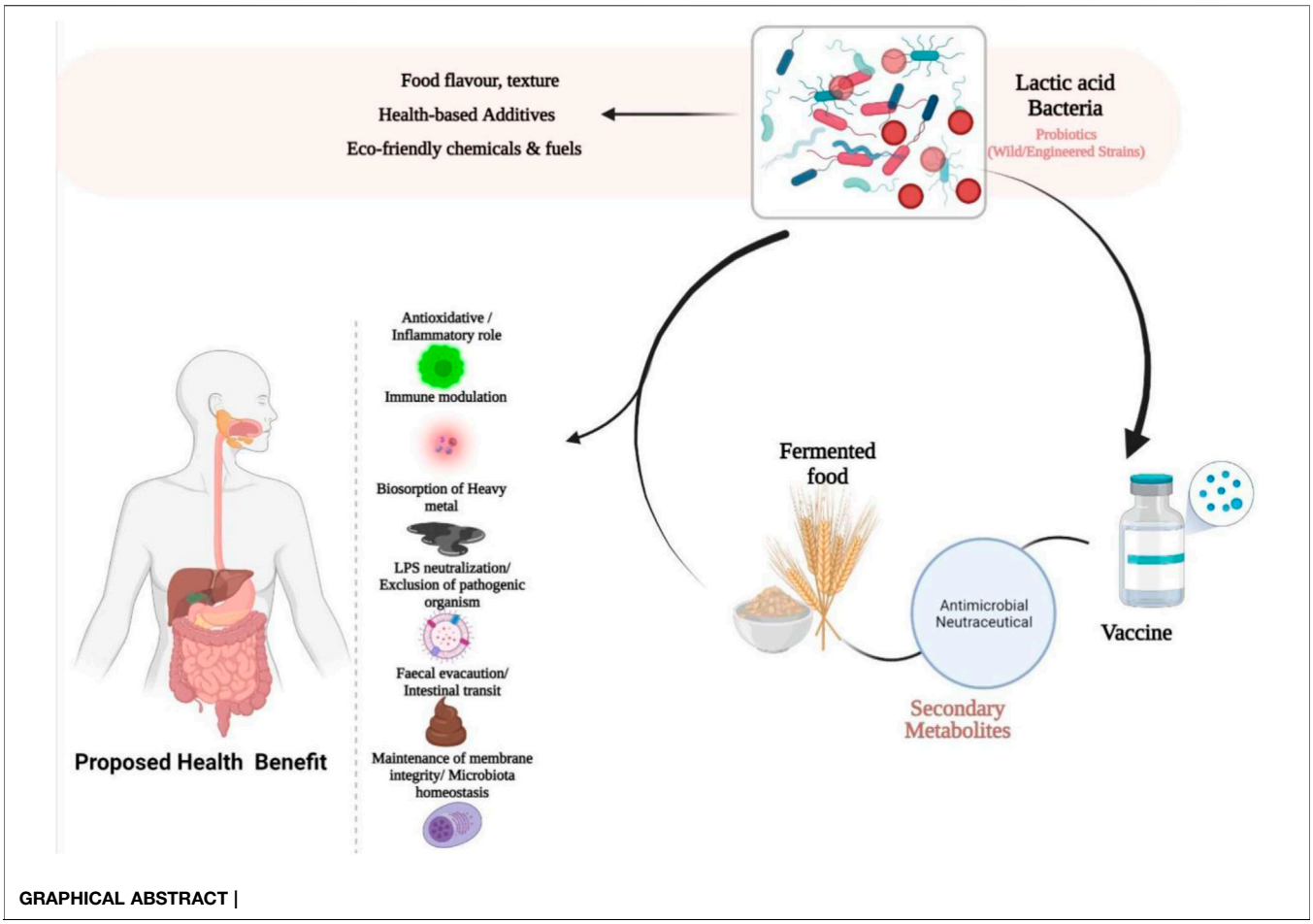

GRAPHICAL ABSTRACT |

(González-Centeno et al., 2017). The *Lactobacillus* and *Pediococcus* genera are found within the family *Lactobacillaceae*, made up of 80 identified species and 15 subspecies that are uniquely different on the basis of the outcome of genotyping. So far, the current classification is based on 16S rRNA (ribosomal RNA) and 23S rRNA sequence comparative analysis, for phylogenetic relationships. This catalogs and sequences reveal that the evolutionary lineage is within the clostridial class for *Pediococcus*, with a low G + C ratio less than 50% compared with other related *Lactobacillus* species, ranging from 84% to 87%. Their cell wall is made up of the amino acid sequence Lys-d-Asp, a peptidoglycan or diaminopimelic acid in some cases (Raccach, 2014). The common sources of these genera are plants, cheese, and processed meats, with industrial relevance as starter culture.

The health-promoting and disease-preventing function of LAB in immune modulation, gut epithelial barrier integrity maintenance, antioxidative capacity, with their important safe record of application in food processing, has warranted the generally recognized as safe (GRAS) status for consumption. In accordance with the Qualified Presumption of Safety (QPS) recommendation, *Lactobacillus*, *Leuconostoc*, *Bifidobacterium*, *Streptococcus*, and *Pediococcus* genera have been considered safe based on taxonomy and appropriate identification at species level (Ricci et al., 2018). In order to properly convey the expected health benefits, the incorporation of beneficial organisms, prebiotics, or symbiotics into food products is important for the gastrointestinal tract (GIT) microbiota and of great technological concern. The right dosage of probiotic, therefore, is required during transit, as it passes through the GIT. In protecting probiotics, enteric coating, microencapsulation, and prebiotic usage are directed toward stimulating the proliferation and activity of the required bacteria, by initiating low-redox potential environment and other factors that address their sensitivity to metabolites formed in the course of growth or as co-adjuvant with other starter culture (Davani-Davari et al., 2019). The generation of off-flavors in food are posed by some metabolites; however, mixed culture with inducer strains, might result in growth-enhancing metabolite production or oxygen content reduction by adjuvant starter culture (Kongo and Malcata, 2016). Withal, the molecular processes attributed to these probiotic bacteria in exerting their health-enhancing benefits is relatively unknown; therefore, precise molecular processes of probiotics action are required.

As the gastrointestinal tract remains the pathway that allows the passage of food and removal of solid waste from the body, it is also understood that the gut microflora that occupies it plays a unique function in various facet of preserving human health,

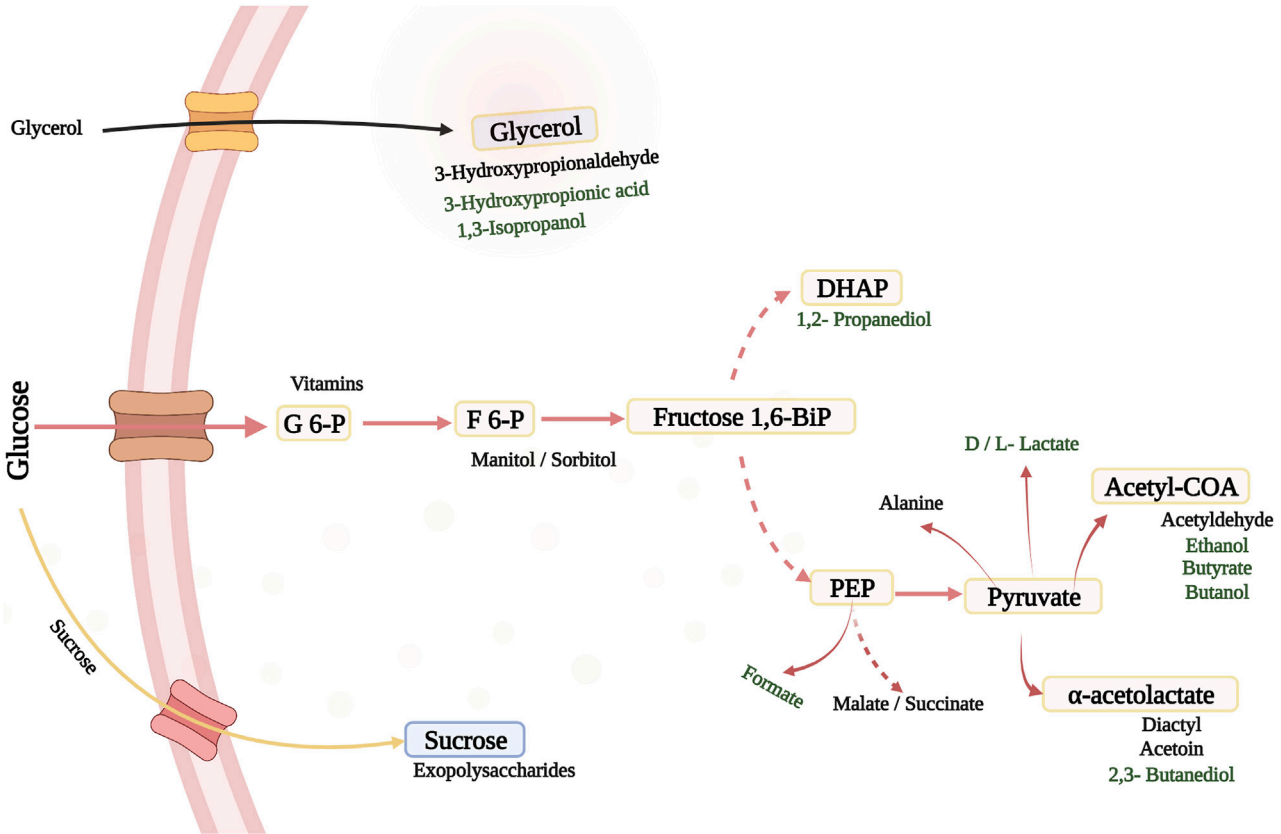

FIGURE 1 | Possible Products in the Natural Metabolic Pathways of LAB and Pediococci under Various Conditions. The dashed arrows indicate different enzymatic steps. Black: taste, texture, medicinal ingredients and health uses; Green: chemicals and fuels. F 6-P, fructose 6-phosphate; DHAP, dihydroxyacetone phosphate; Fructose 1,6BiP, fructose 1,6 bisphosphate; PEP, phosphoenolpyruvate; G 6-P, Glucose-6-Phosphate.

including promoting nutrient digestion and absorption, defending against pathogens, and modulating the immune system. A variety of disorders, like inflammatory bowel disease, asthma, obesity, cardiovascular and autoimmune conditions, are associated with gut microbiota imbalance (Bull and Plummer, 2014). Recently, with the growing understanding of the human microbiome, to prevent and cure some health conditions, probiotics have received considerable attention in bioengineering to support human health. Helped by the extended creation of tools and methods, probiotics are engineered as live biotherapeutics for studying and prevention of many diseases (Mazhar et al., 2020). By stabilizing the gastrointestinal tract, it might offer health-promoting benefits.

Genomic proves for adaptations to the GIT *via* cell-surface anchoring proteins associated with the intestinal barrier causes these bacteria to induce an increase in polysaccharides diversity that are directed toward degradation and the expression of host genes innate immunity. Analogy with completely sequenced LAB genomes shows that the primary impetus of evolution within these genomes is lateral gene transfer. Genomic analysis to a great extent has unravel the core mechanisms by which "Probiogenome" encodes key functions that regulates the growth, survival, signaling, fermentative mechanism, and relatively, the ultimate potential of probiotic activities within multifaceted microbial and host biota (Goh and Klaenhammer, 2015). The evolutionary distance between distant phyla might have an effect on the array of gene availability or its absence in a given set of genomes. Therefore, engineering, in order to maintain a favorable balance in the intestinal microbiota, is essential for a better health status.

Despite LAB therapeutic prowess, these microbes could also be employed to manufacture substances that are currently unavailable, owing to a number of favorable characteristics (Bosma et al., 2017), resulting in the introduction of novel products and microbially produced compounds with the capability of replacing existing products. This might allow for an alternative and cost-effective manufacturing methods in sustainable bulk biochemical production (Bosma et al., 2013; Budzianowski and Postawa, 2016; Budzianowski, 2017), with applications in food, medicine, and pharmaceutical industries. LAB has been utilized in the production of low-calorie polyols including high value products like mannitol and sorbitol produced naturally by several heterofermentative and homofermentative LAB as well (Bozell and Petersen, 2010). Fructose is employed as a carbon source as well as an electron acceptor in certain LAB, where it is transformed to mannitol by

TABLE 1 | Plasmid and genome-based protein expression system in LAB.

Organism	Vector expression system	Description	References
Plasmid-encoded System			
Lactococcus lactis	P_{zn} zitR and Zirex	*P_{Zn}zitR* built on *P_{Zn}* promoter and *zitR* repressor of *zit* operon. Zirex based on pneumococcal repressor *SczA* and *PczcD*. Both requires Zn^{2+} utilization and regulation	(D. and I., 2004; Mu et al., 2013)
	P170	At low pH, the *P170* promoter is upregulated during the transition to stationary phase	Madsen et al. (1999)
	PxylT	Xylose induced; promoter, *PxylT*	Miyoshi et al. (2004)
	SICE	Stress induced	Benbouziane et al. (2013)
	ACE	Agmatine induced; having *AguR* and *P_{aguB} as* the target promoter	Linares et al. (2015)
	NICE	Nisin induced; based on a two-component signal transduction	Mierau and Kleerebezem, (2005)
Genome-encoded System			
Lactobacillus jonsonii	pSA3-based suicide vector (pTRK327)	A non-repetitive vector with sequences homologous to the insertion site	Walker and Klaenhammer, (1994)
Lactobacillus gasseri	pTNI with thermosensitive replicon	Site-specific replacement of chromosomal DNA sequence	Neu and Henrich, (2003)
Lactococcus lactis	pSEUDO vector	Stable genetic insertion in a pre-set transcriptionally inert part of genome	Pinto et al. (2011)

Application: Use for over-expression of genes required for functional evaluation, metabolic engineering, membrane proteins expression, secretion of protein and cell surface anchoring. ACE, agmatine-controlled expression system; SICE, stress-inducible controlled expression system; NICE, nisin-controlled gene expression system.

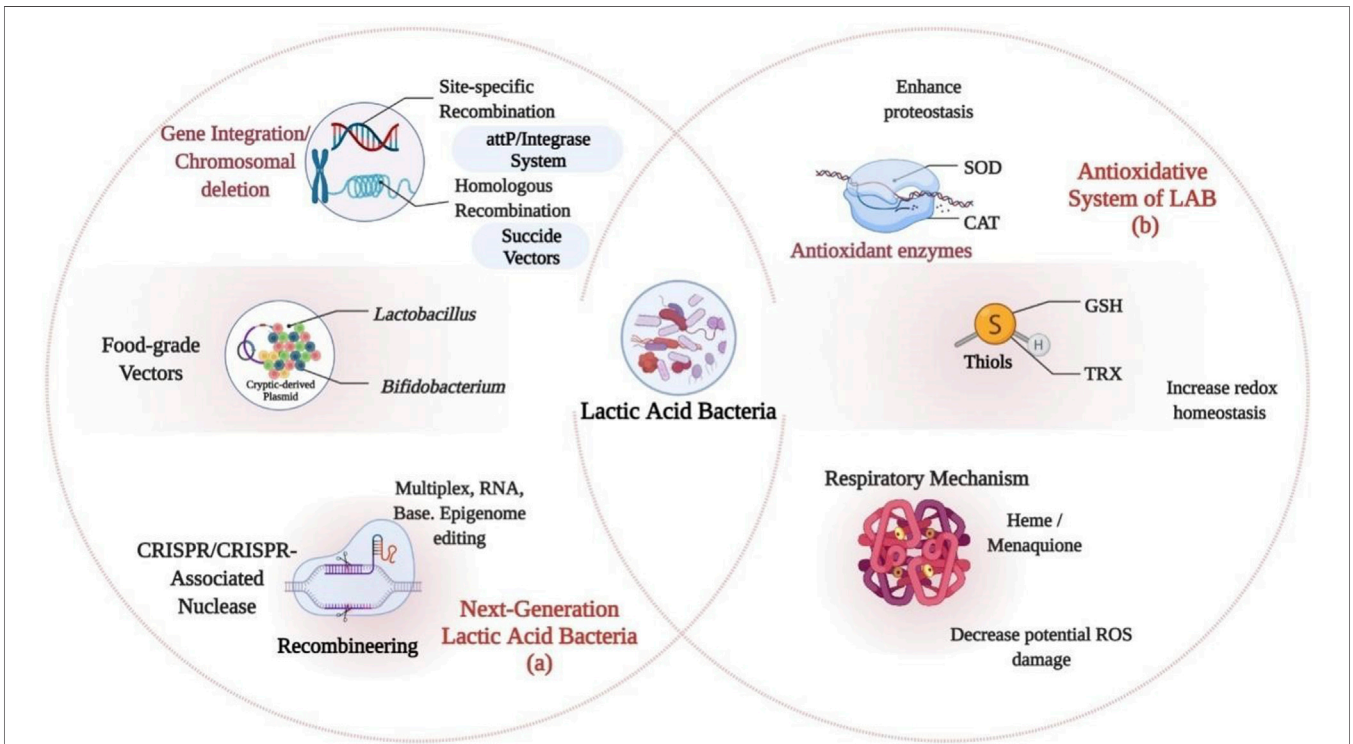

FIGURE 2 | Genomic Approaches and Antioxidative System of Lactic Acid Bacteria (LAB): **(A)** Genome-based approaches to the characterization of promising probiotic strains. **(B)** Antioxidative system of LAB; Thiols, Antioxidant enzymes and Respiratory repertoire which allows them to withstand various environmental stresses that generates highly reactive species or through the NOX (NADH oxidase) like H_2O_2. ROS, Reactive oxygen species; SOD, Superoxide dismutase; GSH, Glutathione; TRX, Thioredoxin-thioredoxin reductase system; CAT, catalase.

mannitol dehydrogenase (Saha and Racine, 2011). Mannitol phosphate dehydrogenase and lactate dehydrogenase (LDH) enzymes were inactivated in *Lactobacillus plantarum* for sorbitol synthesis, and a sorbitol dehydrogenase gene was overexpressed, allowing more fructose 6-phosphate to be converted to sorbitol 6-phosphate (Nissen et al., 2005; Ladero et al., 2007). In addition, there has also been interest in producing xylitol from LAB, a low-calorie sugar alcohol with five carbons that is not formed naturally by LAB. In a *Lactococcus lactis* strain modified with xylose reductase from *Pichia stiptis* and a xylose

TABLE 2 | New genome engineering possibility with recombineering and CRISPR–Cas system in LAB.

Organism	Vector/system	Characteristics	References
Lactococcus lactis	pLABTarget	For introducing sgRNA sequence to target specific genetic loci	Simon et al. (2021)
Lactococcus lactis	pNZCRISPR (a single plasmid inducible CRISPR-Cas 9 system)	To drive Cas9 expression and transcription of two nisin promoters, respectively	Berlec et al. (2018)
Lactobacillus reuteri	CRISPR-Cas system + (ss)DNA recombineering (RecT-assisted CRISPR–Cas9 system)	Enhances performance in bacteria with low recombineering efficiency; Cas 9 directed toward eliminating unmodified bacterial strains (codon saturation mutagenesis and gene deletions) (100% efficiency)	Oh and van Pijkeren, (2014)
Lactobacillus casei	pLCNICK A CRISPR–Cas9^{D10A}-based plasmid	Replaces wild-type Cas 9 with Cas 9^{N10A} (nickase), increasing efficiency (25%–65%)	Song et al. (2017)
Lactococcus lactis NZ9000	a RecT-assisted CRISPR–Cas9 approach	Easy insertion or deletion of genomic DNA within less time	Guo et al. (2019)
Lactobacillus plantarum WJL	CRISPR-Cas system + ssDNA recombineering	A plasmid-encoded template, oligonucleotide donor and an inducible DNA recombinase	Leenay et al. (2019)
Lactococcus lactis MG1363	*Streptococcus* pyogenes CRISPR-Cas9	Genome modification of *L. lactis* virulent phage P2 with exact mutations without heterologous recombinases	Lemay et al. (2017)
Lactobacillus plantarum	CRISPR interference (CRISPRi) systems	CRISPRi with catalytically dormant form of Cas9 (dCas9) for gene expression. Marker free	(Berlec et al., 2018; Storaker et al., 2021)
Lactobacillus reuteri and Lactococcus lactis,	Single-strand (ss) DNA recombineering	Mediates chromosomal incorporation of mutation. Antibiotic selection free (0.4%–16% efficiency)	(Yu et al., 2003; van Pijkeren and Britton, 2012)
Lactobacillus plantarum WCFS1	λ-Red-like recombinase system, a (Ds) DNA recombineering	A site-specific recombinase system for precise deletion and replacement with high efficiency	Yang et al. (2015a)
Lactobacillus casei BL23	λ-Red-like recombinase system, a (Ds) DNA recombineering	For deletion and insertion of Gfp gene. marker free	Xin et al. (2017)

transporter from *Lactobacillus brevis,* and cultured in a glucose-limited fed-batch cultivation method with high xylose concentrations, xylitol synthesis was observed (Nyyssölä et al., 2005). Lactate may be converted to 1,2-propanediol (1,2-PDO) by *Lactobacillus buchneri*, *Lactobacillus brevis*, and *Lactobacillus fermentum*, a polyol commonly utilized in anti-freeze fluids, polyester resins, non-ionic detergents, coolants, and as an addition in cosmetics, nutritional goods, medicines, and colors (Bennett and San, 2001; Oude Elferink et al., 2001; Bosma et al., 2017).

EXPLOITING POWERFUL TOOLS IN *PEDIOCOCCUS* AND LACTIC ACID BACTERIA

Plasmid and Genome-Based Protein Expression System in Lactic Acid Bacteria

Lactic acid as a globally integrated bio-product, in the manufacture of biodegradable polymers, replacement of oil-based plastics and building-block molecule in the chemical industry (Singhvi et al., 2019), is of great importance, especially in the usage of LAB as new field of application in medicine. New possibilities are posed by genetically modified LAB (**Figure 1**), which could establish a strong trend in few years.

Plasmids are broadly found in many LAB sources, as a self-replicating material and have gained much attention due to their proximity with a lot of essential functions and industrial importance (O'Connor et al., 2007). *Pediococcus pentosaceus* and *Pediococcus acidilactici* of *Pediococcus species* harbor various plasmids, from 1.82 to 190 kb size that encodes a variety of traits. Some plasmids from *Pediococcus* includes pEOC01, pMD136, pRS4 (A cryptic plasmid), pUCL287 (A cryptic plasmid), and pSMB 74. All plasmids mentioned, with the exception of pRS4, exhibit theta replicating mechanism.

Plasmids enable direct distribution of multiple copies of recombinant genes and the degree of expression is decided by promoter properties. Inducible promoters are more preferred as they allow efficient control over the expression of recombinant protein than constitutive promoters (**Table 1**). In the expression of genome-encoded proteins, integration of genome offers lower copy number of gene. However, genome integration brings various support-like stability, acceptability for various species, and void of surrounding effects (Zhu et al., 2015). Introducing classical methods are not often correlated with probiotic effectiveness and safe use. Nevertheless, the use of genome-based approaches for characterization of promising probiotic strains like LAB will help validate the role of these species and might stand as a useful instrument in the regulatory scenario for LAB, allowing them to acquire new attributes and increase in their beneficial characteristics. For human applications, genetic modifications may be used, if antibiotic resistance is eliminated and these bacteria are altered in their genetic code. This could be accomplished by genetic integration or chromosomal deletion, use of food-grade vectors, and clustered regularly interspaced short palindromic repeats (CRISPR) technology (Bravo and Landete, 2017; Castro-López et al., 2021) (**Figure 2A**).

These will provide a broad range of opportunities for commercially important *Lactobacillus* and *Bifidobacteria* to be engineered by genetically modifying and improving their therapeutic potential for vaccination or host immune response

modulation. Gene editing tools such as transcription activator-like effector nucleases (TALEN), zinc-finger nucleases (ZFNs), CRISPR, and various approaches to omics, and systems biology could allow better comprehension and restructuring of metabolic pathways. These methods will strengthen the awareness of researchers toward the gut microbiome and provide novel routes for probiotic bacteria to be studied (Yadav et al., 2018). CRISPR, as a revolutionary genome editing technology has provided a key bioengineering tool for investigating different diseases with great sensitivity, speed, precision, and a comprehension of biological processes (Yadav et al., 2021). However, an extensive strategy to diversifying the genome engineering toolbox is to discover new CRISPR systems. Recently, developments in detection of specific CRISPR systems and the restructuring of the Cas9 protein for extended functionalities have been made possible. This could improve and expand the efficiency of the Cas9 nuclease.

Recombineering and CRISPR–Cas System in Lactic Acid Bacteria

Novel techniques have been introduced recently that seems to overcome the time-consuming and relatively inefficient procedures of insertion by classical chromosomal integration techniques. Recombineering allows precision genome engineering, while CRISPR Cas-based engineering helps in putrefying selection for both recombineering and homologous recombination (**Table 2**; **Figure 2**) (Doudna and Charpentier, 2014; Ortiz-Velez and Britton, 2017), which help circumvent the need for mutation screening.

In LAB and starter cultures of industrial concern, this technology grasps a better assurance for application. Its DNA-encoded, RNA-mediated, and DNA-targeting protective roles offer sequence-specific targeting of DNA (Rath et al., 2015), by producing alteration at the excision site using different pathways, that results in the initiation of double-stranded DNA breaks. These technologies will continue to remodel total bacterial exploitation and the editing of eukaryotic genomes. In CRISPR-based technologies for probiotic organisms. Application of (ss)DNA recombineering merged with CRISPR-Cas selection for gene editing of bacteria has an immense value in the production of industrial bacteria of the next century (Barrangou and van Pijkeren, 2016). CRISPR–Cas systems are extensively found in most LAB with eight subtypes and can be present in bacterial genomes alone or in multiple occurrences. These helps enhance the efficacy of fermentation, allows phage resistance or provide basic perception into starter cultures. Problems, particularly discharge and the release of antibiotic resistance markers, can arise from their engineering. Nevertheless, this may be alleviated by biocontainment of genetically modified LAB in a closed system, use of other selection markers and homologous DNA (Plavec and Berlec, 2020). However, unlike (Ds)DNA recombineering, in which the selection of positive mutants is marker dependent, which allows excision of the selection marker, leaving a scar on the loxP site of the modification locus, in (ss)DNA recombineering, it is uniformly avoided.

Cell metabolism rewiring occurs progressively and often at low throughput, but for efficient microbial cell factories, a combinatorial metabolic engineering method based on an orthogonal trifunctional CRISPR system (CRISPRAID) with three CRISPR proteins, a nuclease-deficient CRISPR protein fused to an activation domain (CRISPRa), nuclease-deficient mutant fused to a repression domain (CRISPRi), and finally a catalytically active CRISPR protein (CRISPRd) have been proposed for an effective metabolic and regulatory network with high performance permitting the examination of all possible gRNA combinations to build optimal cell factories (Lian et al., 2017). This has contributed to a 2.5-fold increase in β-carotene and an improved presence of endoglucanase on yeast surface. The ideal genome editing method for achieving any desired modification with minimal adverse effects is still a work in progress. Nevertheless, unlike previous methods, prime editing has implemented exogenous reverse transcriptase action to "write" DNA modifications directly to genomic DNA using a programmable RNA nickase linked to a reverse transcriptase and prime editing guide RNA (Anzalone et al., 2019). Both the genomic target and the sequence may be edited using approaches. By creating a powerful, inducible, broad-spectrum vector-based mutagenesis system that amplifies mutations above baseline and exceeds the mutation efficiencies and range of commonly used *in vivo* and *in vitro* approach, a mechanism-driven approach could have advantages over current methods as it offers improved random mutagenesis in cells with control, genomic stability, improved efficiency, and wider mutation spectra. The introduction of a system for the detection of antibiotic resistance that overcome chemical mutagens, ultraviolet light, and the mutant strain XL1Red subjected to the same conditions in *E. coli* could allow for the progressive evolution of T7 RNA polymerase variants with the potential to initiate transcription using the T3 promoter on both bacterial and bacteriophage-mediated laboratory evolution procedures (Badran and Liu, 2015).

ANTIMICROBIAL PEPTIDES OF *PEDIOCOCCUS*

Biopreservation systems have gained growing attention in recent years, causing consumers to be more conscious of the danger to health triggered by chemical preservatives in foods. Interestingly, most producers of bacteriocin are part of LAB, a category found in food with a historic record of safe utilization in the dairy industry. Since bacteriocins, either refined or released by its producing strains show no health risk issues, they offer an alternative to the use of deleterious preservatives (Silva et al., 2018). The possibility of engineering and improving their biological activity could be realized when the alteration systems in bacterial cell use in processing these proteins are known. In LAB, this is a current frontier and one with a lot of possible rewards.

A proposed universal scheme for bacteriocin alongside the original scheme of classification for lactic acid bacteria bacteriocins by Klaenhammer has been put forward, by

integrating the revised scheme of Cotter and establishing linear, globular, and multi-component into the lantibiotics subgroups. Antimicrobial peptides (AMPs) with its broad multifunctional tools to fight microbial infections and modulate immune response of the host enhance or restrict the entrance of cells and harmful chemicals to the infection site, henceforth, protecting cells from serious tissue damage. *Pediococcus pentosaceus* zy-B, produced by bacteriocin PE-ZYB1, shows heat resistance and a wide variety of antimicrobial action with increased electrical extracellular conductivity and bactericidal degradation of *L. monocytogenes* cell membrane integrity (Heng and Tagg 2006; Zhang Y. et al., 2020). For pediocin usage as food additive, the most desired feature is its stability in heterogenous food system. Various bacteriocins from *Pediococcus* contain residues of methionine, the sulfur particle of which might be oxidized, leading to bacteriocin instability. With an emphasis on Pediocin PA-1 methionine residue, substituted Met13 residue with *Ala*, *Leu*, or *Ile* has proven to shield peptide from the effect of oxidation with moderate influence on the action of antimicrobials, while the replacement of *Asp* results in obvious fall in efficiency against indicator strains. Therefore, a relevant point in transforming Pediocin PA-1 into a valuable food additive is to increase its stability by substituting methionine with a different hydrophobic residue to conserve its function (Brumfitt et al., 2002). Continuous research can bring about pediocins with enhanced stability and improved functions. However, acetic acid, which is indirectly associated with the cell center metabolism, influencing and controlling bacteriocin production, in its undissociated state was found to freely disperse and dissociate through the hydrophobic layer of the membrane (Ge et al., 2019), influencing the development, yield, and activity of bacteriocin production.

Cloning and Expression of Bacteriocin in *Pediococcus*

Pediocins (Bacteriocin Class II) are made by *Pediococcus acidilactic* and *Pediococcus pentosaceus* strains with GRAS status in certain food applications, characterized by exceptional antimicrobial potency, good thermostability, wide pH range, and efficacy against spoilage and pathogenic organisms. In targeting members of the same species, bacteriocins can exhibit a narrow range of activity; meanwhile, others can show a wider activity for targeting other species and genus. Variants of bacteriocins have proven more significant activity than their native counterpart. This is made possible through DNA shuffling techniques by creating chimeric gene sequences having desirable traits. Bacteriocin like Pediocin PA-1 applies its role by disrupting the cytoplasmic membrane, causing outflow of ions and small molecules (Villalobos-Delgado et al., 2019). Nisin was, until recently, the only bacteriocin to be sold as a food biopreservative. However, a bacteriocin produced by *Pediococcus* species has also been commercially sold under the name Alta 2341™ with an effectiveness relatively as that of Nisin against *L. monocytogenes*, *Staphylococcus aureus*, *Pseudomonas*, and *E. coli* (Deegan et al., 2006). Pediocin A, Pediocin N5p, Pediocin L, Pediocin S, Pediocin ACCEL, Pediocin ST18, Pediocin SM-1, Pediocin pK23-2, Pediocin 05–10, Bacteriocin ST44AM, and Pediocin P are among the examples of pediocins (Papagianni and Anastasiadou, 2009). Single or co-adjuvant cultures of lactic acid bacteria producing bacteriocin help regulate adventitious flora and induce cell lysis, which improves food quality and sensory attributes. Recently, the incorporation into bioactive films and coatings of bacteriocins into food surfaces and packaging of bacteriocin-producing LAB has been made possible (Silva et al., 2018). Research findings on the efficacy of bacteriocins as bio-preservatives is remarkable, but the industry is a bit reluctant to commit itself financially to the production of commercial preparations of bacteriocins due to low production rates, costly downstream processing, and the legal problems that could occur from their production.

Strategies for Production of Other Metabolites from *Pediococcus*

Effect of temperature, acid, osmotic pressure, and oxidative effects are some of the environmental conditions encountered by LAB in the gastrointestinal tract and during food processing that possess a significant effect on their biological functionalities. However, LAB is empowered with adaptation mechanisms that protectively saves them from harsh environmental stresses and gene alteration (**Figure 2B**) (Aakko et al., 2014). Some LAB like *Lactobacillus fermentum* (KGPMF28, KGPMF2) can survive at 45°C for 24 h. At high temperatures, cellular activities are disrupted with increase membrane fluidity due to degradation and loss of function of proteins and nucleic acids. Condition optimization for γ-aminobutyric acid (GABA) production by *P. pentosaceus* MN12 has provided the basis for the formulation of a GABA-rich fermented product. The use of heat shock proteins and enzymes has recently been applied to reduce biomolecule denaturation and degradation (Chen et al., 2017; Thuy et al., 2021). Understanding LAB adaptation mechanisms at extreme temperatures is crucial for sorting out LAB species as starter cultures and probiotics.

In single-strain fermentation, the development of most products is typically poor. However, improving bacterial cocultures suited for high yield, diversification, and sustainability for fermented products might be required. Fermentation of products made from selected species has shown increased productivity, reduced volatile hexanal off-flavor-generating compounds, and created several attractive flavor compounds (Sharma et al., 2020). In assessing the complex growth of *P. pentosaceus* and *S. cerevisiae* during fermentation, the forms and contents of esters showed an increase in co-culture with *P. pentosaceus*. Also, the concentration of bacteriocins yield by P. pentosaceus 147 increased from 1.92×10^4 AU/ml to 5.12×10^4 AU/ml as coadjuvant with *Lactobacillus plantarum* LE27 (Gong and Qi, 2020). Interestingly, in our laboratory, *C. glutamicum* G01 in coculture with a multimutagenized *L. plantarum* GB01-21 yielded a high concentration of 80.5 g/L, 2.68 g/L/h productivity of γ-aminobutyric acid (GABA) from glutamic

TABLE 3 | Application of *Pediococcus* in health-related conditions.

Disorder/disease	Organism/strain	Characteristics	References
Oxidative stress	*P. pentosaceus* ZJUAF-4	ZJUAF-4 administration improved Nrf2 expression and its downstream genes, preserved activity of the intestinal. Exerts antioxidant potential	Hao et al. (2021)
Colitis	*P. pentosaceus* LI05	Incredibly preserved intestinal membrane integrity, modulates the immunological profiles, gut microbiota, and metabolite content	Bian et al. (2020)
Biosorption of heavy metal	*P. pentosaceus* FB145 *and* FB181, *P. acidilactici* BT36	Good human gastrointestinal system tolerance properties, reduced Cd bioaccessibility, and protection against Cr toxicity	(Le and Yang, 2019; Feng et al., 2020)
Shields brush border membrane effect	*P. pentosaceus* GS4	Improved fecal evacuation of cadmium with a reduced tissue deposition effect, decreased hyperplasia, reduced invasion of lymphocytes, and enhancement of BBM-based disaccharidases	Dubey et al. (2019)
Aging	*P. pentosaceus* DK1	Improved collagen in UVB-irradiated human skin fibroblasts	(Ji Hoon et al., 2019)
Melanogenesis	*P. acidilactici* PMC48	Reduced overproduction and accumulation of melanin that induces skin darkening and abnormalities	(Sukyung et al., 2020)
Intestinal inflammation	*P. pentosaceus* AK-23, ON89A, *P. parvulus* 2.6	*P. pentosaceus* AK-23; ability to bind LPS, neutralizes LPS *P. Parvulus* 2.6 excretes a ropy EPS with probiotic potential	Asami et al. (2017)

TABLE 4 | Summaries of available therapeutics from various recombinant LAB.

Strains	Therapeutic products	Health-related condition	References
Lactococcus lactis	Interleukin-10, proinsulin	Diabetes mellitus (Type I)	Steidler et al. (2000)
Lactococcus lactis NZ9000	Interleukin-12	Asthma	Bermúdez-Humarán et al. (2003)
Lactococcus lactis NZ9000	HSP65–6P277	Diabetes mellitus (Type I)	Ma et al. (2014)
Lactococcus lactis NZ9000	Kisspeptin	Colorectal cancer	Zhang et al. (2016)
Lactococcus lactis NZ9000, *Lactobacillus casei*	HPV-16-E7	Human papillomavirus 16-induced cancers	(Bermúdez-Humarán et al., 2005)—
Lactococcus lactis IL1403	Interleukin-6	Adjuvant	Li et al. (2015)
Lactococcus lactis CHW9	Peanut allergen Ara2	Hypersensitivity intolerance (Type I)	Glenting et al. (2007)
Lactococcus lactis NZ9800	Birch allergen Betv1	Hypersensitivity intolerance (Type I)	Daniel et al. (2006)
Lactococcus lactis MG1363	Glycosylated tyrosinase-related protein-2	Skin cancer	Kalyanasundram et al. (2015)
Lactobacillus plantarum NCL21	Japanese cedar pollen allergen Cry j1	Hypersensitivity intolerance (Type I)	Ohkouchi et al. (2012)
Lactobacillus pentosus SS6	γ-Amino butyric acid	Anxiety, hypertension	Zhong et al. (2019)
Lactobacillus acidophilus PTCC1643	Hyaluronic acid	Dermatitis, wound healing	Chahuki et al. (2019)

acid using glucose from cassava via a two-stage fermentation strategy (Yang T. et al., 2015). These present exceptional strains required for microbial co-adjuvant in increasing desired product yield from a glucose-based substrate for health and food.

Lactic acid bacteria can form protective biofilms that allows its survival in harsh environment. Nevertheless, surrounding factors, like additives, can serve a major function in biofilm formation (BF), pH and addition of sugar supplements, with effect on LAB metabolism, growth, lactate output, and bacteriocin production. Research using *P. pentosaceus* ATCC 43200 grown at pH 5.0–6.0 in MRS medium (control) or in the same amounts after inclusion of 0.5, 1.0, and 1.5% (w/w) of sucrose and inulin. A variation in these parameters existed at pH 6.0 between the control medium and the supplemented media. At exponential level, both sucrose and inulin accelerated *P. pentosaceus* growth (de Souza de Azevedo et al., 2017). Recently reported as a potential threonine producer, *P. pentosaceus* TL-3 showed a boost in threonine output via optimized medium (Lim et al., 2019). These can help ensure a more economical growth medium for prospective large-scale application. However, the addition of certain substances (e.g., honey phenolic extract) might decrease LAB biofilm formation.

THERAPEUTIC APPLICATION OF PROBIOTIC LACTIC ACID BACTERIA

Undoubtedly, probiotics is currently becoming a great deal of focus in scientific probing and application in prevention or treatment of health conditions (**Tables 3** and **4**). In the pathology and development of chronic inflammation of digestive tract, the gastrointestinal microbiota is considered a critical factor, through the preservation of gut membrane integrity and regulation of the host immune system. Reduced colitis, decreased weight loss and disease activity index, and short-chain fatty acid formation are but a few unique observed features (Bian et al., 2020).

The resultant effect of exposure to highly reactive intermediates is oxidative damage to proteins, lipids, and nucleic acids. This is due to instability in the production of these intermediates and the antioxidant activity of the organism (Tan et al., 2018). Interestingly, the amount of oxidative damage increase and NAD^+ decline has been linked to aging symptoms and can be at the root of a number of age-associated diseases. According to recent proof, increasing NAD^+ levels might help reduce or even reverse the effects of aging, as well as retard the progression of age-related diseases. At the

moment, a great deal of research has been centered on foodstuff sources, nutritional ingredients, and components that confers antioxidant result in humans and other life forms (Amaretti et al., 2013). However, the principal mechanism by which LAB relieves oxidative stress and intestinal damage is not fully comprehended. Another increasing health-related concern is the enormous increase level in heavy metal toxicants in human body. *P. pentosaceus* (FB145, FB181) reduced cadmium bioaccessibility by 46%, serving as an effective biosorbent to prevent cadmium harmful effect and reduce its assimilation into the human body (Le and Yang, 2019), thereby reducing toxicity to essential organs.

The capacity to degrade histamine, reduce bile salts from cholesterol, strain susceptibility to gastrointestinal diseases, adhesion to $CaCO_3$ cells, antibiotic tolerance, and the removal of virulence genes are of importance as a unique attribute of a good probiotic strain. *Lactobacillus paracasei* L3C21M6 offers an increase in cholesterol and histamine-lowering potentials, absence of virulence genes, and good susceptibility to relevant antibiotics (Amaral et al., 2017; Domingos-Lopes et al., 2020). *Pediococcus parvulus* shows no ability to produce tyramine, histamine, or putrescine (Garai et al., 2007), suggesting that this ability may be strain specific instead of being associated to certain bacteria species. The main cause of sepsis is by lipopolysaccharide (LPS), which is linked to an increased death toll in patients. There are currently no effective therapeutic agents available to prevent patients from sepsis, which is depicted by LPS-mediated tissue damage and organ breakdown (Hu et al., 2013). Among intestinal bacteria, *Escherichia coli* or *Salmonella* spp. possesses lipopolysaccharide, which could cause inflammation of the intestines of humans. LPS, particularly its lipid A portion, is actually toxic. Using *Pediococcus pentosaceus* AK-23, with the capacity to bind LPS (Asami et al., 2017; Kawahara, 2021), these harmful bacteria might be managed effectively. Additionally, melanocytes, a specialized pigment-generating cell, houses pigmented particles called melanosomes, responsible for the production of melanin. Previously, a melanin synthase of melanocytes that can suppress tyrosinase, from kimchi-derived *Pediococcus acidilactici* PMC48, was developed and used as a medicinal component to actively fight the overproduction and accumulation of melanin that induces skin darkening and abnormalities (Sukyung et al., 2020). In anticipation, this could be of great importance as a basic material for melanin degradation in pharmaceutical products.

CHALLENGES AND FUTURE OUTLOOKS

Probiotic candidates like *Pediococcus* and other well-known LAB are chosen to assess their sufficient tolerance to physiological barriers. Further research is required, however, to explain the awareness of their metabolic capacities, main adaptation characteristics, health and physiological functions. Bioengineering techniques can create characteristics that may be very rewarding, yet, they can also be detrimental, if not properly handled. Nevertheless, as the consumption pattern of minimally processed and preserved foods is growing, the use of pediocins of the food industry, as moderate antimicrobials, may provide solutions and alternatives to traditional means of preservation. Pediocin is projected to see more uses in medicinal application in the future (Bron and Kleerebezem, 2011). Understanding the mechanisms in *Pediococcus* and certainly other probiotic species will result to the creation of a molecular toolbox for applications in various sectors.

Nanotechnology and Microencapsulation

Probiotics are primarily delivered to humans by dairy-based products. The next likely food category appearance of this bacteria would be in non-dairy products. Methods that will provide probiotics with the requisite safety allow them to step beyond medicinal and supplemental uses into the field of food ingredients. Probiotics can be protected from environmental stresses using microcapsules and released in a regulated manner. Its absorption in the intestinal tract can also be aided by mucoadhesive polymers (Razavi et al., 2021). Nanocomposite, nano-emulsification, and nano-structuration will help open up a whole new chapter of possibilities for probiotics applications. Food with nanostructures might possess the ability to enhance flavor, texture, consistency, and increase yield in other important metabolite production. By using alginate, these can be applicable in several probiotic strains, with high survival rate besides non-encapsulated cells at low pH and moderate heat treatment. Microencapsulation techniques with gelatin, to offer a protective coat to acid-sensitive *Lactobacillus* and *Bifidobacterium*, have also been tried. Encapsulation of food additives has the potential to prolong product shelf life, enhance interaction with specific receptors (Sekhon, 2010), and function as *de novo* vaccines (Ravi Sankar and Dastagiri Reddy, 2010) to modulate immune responses.

Bioinformatics and Biosensors

Current approaches in "Probiogenomics" study have incited much interests and provided means for studying probiotic mechanisms and the identification of new strains from broad microbial sources. PROBIO and other probiotics database were put in place for these efforts. With the continuous change in sequencing and bioinformatic techniques, genomic sequence data for the species of interest could allow for improved regulation, optimization, and recognition of novel genes necessary for survival during processing and technical versatility of probiotics by allowing gene expression profiles of the strain during fermenter growth and different production steps (Ahmed, 2003; Song et al., 2021). In the future, this might help to tailor the technical properties of probiotic strains. Also, detecting quorum-sensing signal of pathogenic bacteria in GIT by release of reporter enzymes (Mao et al., 2018), generation and secretion of anti-enterococcal peptides upon sensing *Enterococcus* peptide pheromone with precise suppression of *enterococcal* growth (Borrero et al., 2015), the use of nisin-producing strains and immunity proteins in combination, to express reporter proteins in a tractable spatial manner (Kong et al., 2017), and an independent inducible degradation of marked proteins with accurate control of the abundance of specific proteins (Cameron and Collins, 2014),

all these ushers probiotics and LAB to the world of synthetic engineering for therapeutic applications.

Artificial Intelligence, Neural Network, and "SynBio" Approaches

The anti-malarial medicine artemisinin took a very long time to develop; however, we could revolutionize what we can achieve with bioengineering if we can grow new cells to specification in a matter of weeks or months rather than years. Scientists are now working on a new tool that will adapt machine learning algorithms to the demands of synthetic biology in order to methodically steer progress and avoid a lengthy process (Zhang J. et al., 2020; Radivojević et al., 2020). The options are limitless. Scientists will no longer have to spend years learning about each part of a cell and what it does in order to manipulate it; instead, using a small set of training data, the algorithms will be able to predict how changes in the DNA of a cell or biochemistry will affect its behavior, then make recommendations for the next engineering phase, as well as probabilistic predictions for achieving the desired goal.

One of such development is Unified Representation (UniRep), a versatile summary of fundamental protein features that applies deep learning to unlabeled amino acid sequences, in order to distill the essential properties of a protein into a statistical representation. This tends to integrate unpredictable protein sequences into fixed-length vectors that resemble the capabilities, function, and configuration of critical proteins in the absence of structural or evolutionary histories. UniRep pushes protein computing to move straight from sequence to design by learning a novel base from scratch (Alley et al., 2019). Surprisingly, the UniRep might be used to rapidly generalize distant and invisible sections, revamp protein engineering roadmaps, or, at best, facilitate the detection of sequence variants that are not accessible to conventional procedures. Although it is limited by sampling bias in the length of the training sequence data, the size and coverage of the sequence databases and specific deep learning computer hardware has improved exponentially. UniRep-guided protein design pledges to boost the rate of manufacturing biosensors, DNA and protein binders, and develop genome-editing enzymes. Experts have also sought for decades to use handcoded heuristic algorithms to prescribe the rules of chemistry to computers. Discovering retrosynthetic routes using Monte Carlo tree search and symbolic artificial intelligence (AI) might assist in delivering high-quality findings. This scheme uses an expansion rule network to help choose the most efficient retrosynthetic steps more quickly than the usual computational search approach. Almost every published answer in organic chemistry has been trained into these deep neural networks (Segler et al., 2018). This makes the target molecules simpler precursors that facilitates the development of a suitable strategy for the synthesis of small organic compounds. This could be crucial in keeping the machine a useful chemical synthesis assistant capable of solving the most pressing problems in agriculture, health, and materials science.

Phage-Assisted Continuous Evolution

Soluble expression phage-assisted continuous evolution (SE PACE) is a scheme for swiftly developing proteins with high solubility in expression, applicable in many proteins to increase their soluble expression through the rapid generation of improved variants without library cloning, or to improve time-consuming methods that allows protein-driven evolutionary methods. By using a PACE compatible splitintein pIII that functions as an AND gate to join two orthogonal positive selections, SE-PACE is able to develop proteins in the presence or lack of concurrent selection for protein action and improve the expression of a wide range of proteins, along with bacterially derived proteins (MBP), genetically modified antibodies (scFv), and eukaryotic enzymes, as well as proteins with lower stability that have developed via protracted directed evolution. In conclusion, SE-PACE may provide a method for swiftly reversing the negative consequences of large-scale mutations in order to improve the usability of advanced or previously designed proteins (Wang et al., 2018).

The introduction of phage-assisted continuous evolution (PACE) of TEV protease was an early attempt at this, which involves protease generated from approximately 2,500 generations of PACE with 20 non-silent mutations that clears human IL23 at the target peptide bond and suppresses IL23-mediated immune activation when pre-mixed with IL23 in primary mouse splenocyte cultures. The specificity profile of mutation cleavage and an additional protease showed the molecular basis for some changes and supports the creation of custom-made proteases that catalytically change or terminate target proteins for biotechnological and therapeutic applications (Packer et al., 2017). This work establishes not only the ability to change the substrate specificity of a protease at various positions but also on a suitable time scale.

CONCLUSION

Lactic acid bacteria not only offer great potential as an established organic product, but as public interest in the importance of probiotic usage in food and health-related aspect rises, researchers of this millennium are increasingly introducing classical therapies into genomic approaches. While the results for recombinant bacteria and their metabolites are relatively mixed, they are anticipated in the near future. The importance of recombinant probiotics has been reported in mouse models, but some few human clinical studies is also encouraging. However, the main problem with the development and usage of probiotics and other well-established organisms lies in the selection of the strains, the appropriate dose, and the lateral transfer of genes from recombinants to other types of bacteria. The use of CRISPR Cas9 selection with LAB recombination tools, PACE, and the continuous introduction of AI-based protocols (machine learning and deep neural network) could be useful in the production of important compounds and the ability to restore health with high efficiency and precision. In summary, *Pediococcus* and other related LAB species remain an effective, safe, and innovative alternative for food, health, and biotechnology applications.

AUTHOR CONTRIBUTIONS

SP and ZR wrote the first draft of the manuscript. ZQ, HN, SA made all the necessary corrections and carried out the final editing of the manuscript. Visualization and Graphic design was by SP. MX, XZ and TY reviewed the manuscript. ZR gave the final approval for publication.

FUNDING

This research was funded by the National Key Research and Development Program of China (grant number 2021YFC2100900), the National Natural Science Foundation of China (grant number 32071470), and the Science and Technology Project of Xinjiang Production and Construction Corps (grant number 2019AB009).

REFERENCES

Aakko, J., Sánchez, B., Gueimonde, M., and Salminen, S. (2014). Assessment of Stress Tolerance Acquisition in the Heat-Tolerant Derivative Strains of Bifidobacterium Animalis Subsp. Lactis BB-12 and Lactobacillus Rhamnosus GG. *J. Appl. Microbiol.* 117, 239–248. doi:10.1111/jam.12520

Ahmed, F. E. (2003). Genetically Modified Probiotics in Foods. *Trends Biotechnol.* 21, 491–497. doi:10.1016/j.tibtech.2003.09.006

Alley, E. C., Khimulya, G., Biswas, S., AlQuraishi, M., and Church, G. M. (2019). Unified Rational Protein Engineering with Sequence-Only Deep Representation Learning. *Nat. Methods* 16, 589333. doi:10.1038/s41592-019-0598-1

Amaral, D. M. F., Silva, L. F., Casarotti, S. N., Nascimento, L. C. S., and Penna, A. L. B. (2017). Enterococcus Faecium and Enterococcus Durans Isolated from Cheese: Survival in the Presence of Medications under Simulated Gastrointestinal Conditions and Adhesion Properties. *J. Dairy Sci.* 100, 933–949. doi:10.3168/jds.2016-11513

Amaretti, A., di Nunzio, M., Pompei, A., Raimondi, S., Rossi, M., and Bordoni, A. (2013). Antioxidant Properties of Potentially Probiotic Bacteria: *In Vitro* and *In Vivo* Activities. *Appl. Microbiol. Biotechnol.* 97, 809–817. doi:10.1007/s00253-012-4241-7

Asami, K., Kondo, A., Suda, Y., Shimoyamada, M., and Kanauchi, M. (2017). Neutralization of Lipopolysaccharide by Heat Shock Protein inPediococcus pentosaceusAK-23. *J. Food Sci.* 82, 1657–1663. doi:10.1111/1750-3841.13679

Badran, A. H., and Liu, D. R. (2015). Development of Potent *In Vivo* Mutagenesis Plasmids with Broad Mutational Spectra. *Nat. Commun.* 6, 8425. doi:10.1038/ncomms9425

Barrangou, R., and van Pijkeren, J.-P. (2016). Exploiting CRISPR-Cas Immune Systems for Genome Editing in Bacteria. *Curr. Opin. Biotechnol.* 37, 61–68. doi:10.1016/j.copbio.2015.10.003

Benbouziane, B., Ribelles, P., Aubry, C., Martin, R., Kharrat, P., Riazi, A., et al. (2013). Development of a Stress-Inducible Controlled Expression (SICE) System in Lactococcus Lactis for the Production and Delivery of Therapeutic Molecules at Mucosal Surfaces. *J. Biotechnol.* 168, 120–129. doi:10.1016/j.jbiotec.2013.04.019

Bennett, G. N., and San, K.-Y. (2001). Microbial Formation, Biotechnological Production and Applications of 1,2-propanediol. *Appl. Microbiol. Biotechnol.* 55, 1–9. doi:10.1007/s002530000476

Berlec, A., Škrlec, K., Kocjan, J., Olenic, M., and Štrukelj, B. (2018). Single Plasmid Systems for Inducible Dual Protein Expression and for CRISPR-Cas9/CRISPRi Gene Regulation in Lactic Acid Bacterium Lactococcus Lactis. *Sci. Rep.* 8, 1009. doi:10.1038/s41598-018-19402-1

Bermúdez-Humarán, L. G., Cortes-Perez, N. G., Lefèvre, F., Guimarães, V., Rabot, S., Alcocer-Gonzalez, J. M., et al. (2005). A Novel Mucosal Vaccine Based on Live Lactococci Expressing E7 Antigen and IL-12 Induces Systemic and Mucosal Immune Responses and Protects Mice against Human Papillomavirus Type 16-induced Tumors. *J. Immunol.* 175, 7297–7302. doi:10.4049/jimmunol.175.11.7297

Bermúdez-Humarán, L. G., Langella, P., Cortes-Perez, N. G., Gruss, A., Tamez-Guerra, R. S., Oliveira, S. C., et al. (2003). Intranasal Immunization with Recombinant Lactococcus Lactis Secreting Murine Interleukin-12 Enhances Antigen-specific Th1 Cytokine Production. *Infect. Immun.* 71, 1887–1896. doi:10.1128/IAI.71.4.1887-1896.2003

Bian, X., Yang, L., Wu, W., Lv, L., Jiang, X., Wang, Q., et al. (2020). Pediococcus Pentosaceus LI05 Alleviates DSS-induced Colitis by Modulating Immunological Profiles, the Gut Microbiota and Short-chain Fatty Acid Levels in a Mouse Model. *Microb. Biotechnol.* 13, 1228–1244. doi:10.1111/1751-7915.13583

Borrero, J., Chen, Y., Dunny, G. M., and Kaznessis, Y. N. (2015). Modified Lactic Acid Bacteria Detect and Inhibit Multiresistant Enterococci. *ACS Synth. Biol.* 4, 299–306. doi:10.1021/sb500090b

Bosma, E. F., Forster, J., and Nielsen, A. T. (2017). Lactobacilli and Pediococci as Versatile Cell Factories - Evaluation of Strain Properties and Genetic Tools. *Biotechnol. Adv.* 35, 419–442. doi:10.1016/j.biotechadv.2017.04.002

Bozell, J. J., and Petersen, G. R. (2010). Technology Development for the Production of Biobased Products from Biorefinery Carbohydrates-The US Department of Energy's "Top 10" Revisited. *Green. Chem.* 12, 539–554. doi:10.1039/b922014c

Bravo, D., and Landete, J. M. (2017). Genetic Engineering as a Powerful Tool to Improve Probiotic Strains. *Biotechnol. Genet. Eng. Rev.* 33, 173–189. doi:10.1080/02648725.2017.1408257

Bron, P. A., and Kleerebezem, M. (2011). Engineering Lactic Acid Bacteria for Increased Industrial Functionality. *Bioengineered Bugs* 2, 80–87. doi:10.4161/bbug.2.2.13910

Brumfitt, W., Salton, M. R. J., and Hamilton-Miller, J. M. T. (2002). Nisin, Alone and Combined with Peptidoglycan-Modulating Antibiotics: Activity against Methicillin-Resistant *Staphylococcus aureus* and Vancomycin-Resistant Enterococci. *J. Antimicrob. Chemother.* 50, 731–734. doi:10.1093/jac/dkf190

Budzianowski, W. M. (2017). High-value Low-Volume Bioproducts Coupled to Bioenergies with Potential to Enhance Business Development of Sustainable Biorefineries. *Renew. Sustainable Energ. Rev.* 70, 793–804. doi:10.1016/j.rser.2016.11.260

Budzianowski, W. M., and Postawa, K. (2016). Total Chain Integration of Sustainable Biorefinery Systems. *Appl. Energ.* 184, 1432–1446. doi:10.1016/j.apenergy.2016.06.050

Bull, M. J., and Plummer, N. T. (2014). Part 1: The Human Gut Microbiome in Health and Disease. *Integr. Med. (Encinitas)* 13, 17–22. Available at: https://pubmed.ncbi.nlm.nih.gov/26770121.

Cameron, D. E., and Collins, J. J. (2014). Tunable Protein Degradation in Bacteria. *Nat. Biotechnol.* 32, 1276–1281. doi:10.1038/nbt.3053

Castro-López, C., García, H. S., Guadalupe Martínez-Ávila, G. C., González-Córdova, A. F., Vallejo-Cordoba, B., and Hernández-Mendoza, A. (2021). Genomics-based Approaches to Identify and Predict the Health-Promoting and Safety Activities of Promising Probiotic Strains - A Probiogenomics Review. *Trends Food Sci. Technology* 108, 148–163. doi:10.1016/j.tifs.2020.12.017

Chahuki, F. F., Aminzadeh, S., Jafarian, V., Tabandeh, F., and Khodabandeh, M. (2019). Hyaluronic Acid Production Enhancement via Genetically Modification and Culture Medium Optimization in Lactobacillus Acidophilus. *Int. J. Biol. Macromolecules* 121, 870–881. doi:10.1016/j.ijbiomac.2018.10.112

Chen, M.-J., Tang, H.-Y., and Chiang, M.-L. (2017). Effects of Heat, Cold, Acid and Bile Salt Adaptations on the Stress Tolerance and Protein Expression of Kefir-Isolated Probiotic Lactobacillus Kefiranofaciens M1. *Food Microbiol.* 66, 20–27. doi:10.1016/j.fm.2017.03.020

Daniel, C., Repa, A., Wild, C., Pollak, A., Pot, B., Breiteneder, H., et al. (2006). Modulation of Allergic Immune Responses by Mucosal Application of Recombinant Lactic Acid Bacteria Producing the Major Birch Pollen Allergen Bet V 1. *Allergy* 61, 812–819. doi:10.1111/j.1398-9995.2006.01071.x

Davani-Davari, D., Negahdaripour, M., Karimzadeh, I., Seifan, M., Mohkam, M., Masoumi, S., et al. (2019). Prebiotics: Definition, Types, Sources, Mechanisms, and Clinical Applications. *Foods* 8, 92. doi:10.3390/foods8030092

de Souza de Azevedo, P. O., Converti, A., Domínguez, J. M., and de Souza Oliveira, R. P. (2017). Stimulating Effects of Sucrose and Inulin on Growth, Lactate, and Bacteriocin Productions by Pediococcus Pentosaceus. *Probiotics Antimicro. Prot.* 9, 466–472. doi:10.1007/s12602-017-9292-8

Deegan, L. H., Cotter, P. D., Hill, C., and Ross, P. (2006). Bacteriocins: Biological Tools for Bio-Preservation and Shelf-Life Extension. *Int. Dairy J.* 16, 1058–1071. doi:10.1016/j.idairyj.2005.10.026

Domingos-Lopes, M. F. P., Stanton, C., Ross, R. P., and Silva, C. C. G. (2020). Histamine and Cholesterol Lowering Abilities of Lactic Acid Bacteria Isolated from Artisanal Pico Cheese. *J. Appl. Microbiol.* 129, 1428–1440. doi:10.1111/jam.14733

Doudna, J. A., and Charpentier, E. (2014). The New Frontier of Genome Engineering with CRISPR-Cas9. *Science* 346, 1258096. doi:10.1126/science.1258096

Dubey, V., Mishra, A. K., Ghosh, A. R., and Mandal, B. K. (2019). Probiotic Pediococcus Pentosaceus GS 4 Shields brush Border Membrane and Alleviates Liver Toxicity Imposed by Chronic Cadmium Exposure in Swiss Albino Mice. *J. Appl. Microbiol.* 126, 1233–1244. doi:10.1111/jam.14195

F. Bosma, E., van der Oost, J., M. de Vos, W., and van Kranenburg, R. (2013). Sustainable Production of Bio-Based Chemicals by Extremophiles. *Cbiot* 2, 360–379. doi:10.2174/18722083113076660028

Feng, P., Ye, Z., Han, H., Ling, Z., Zhou, T., Zhao, S., et al. (2020). Tibet Plateau Probiotic Mitigates Chromate Toxicity in Mice by Alleviating Oxidative Stress in Gut Microbiota. *Commun. Biol.* 3, 242. doi:10.1038/s42003-020-0968-3

Garai, G., Dueñas, M. T., Irastorza, A., and Moreno-Arribas, M. V. (2007). Biogenic Amine Production by Lactic Acid Bacteria Isolated from Cider. *Lett. Appl. Microbiol.* 45, 473–478. doi:10.1111/j.1472-765X.2007.02207.x

Ge, J., Kang, J., and Ping, W. (2019). Effect of Acetic Acid on Bacteriocin Production by Gram-Positive. *J. Microbiol. Biotechnol.* 29, 1341–1348. doi:10.4014/jmb.1905.05060

George, F., Daniel, C., Thomas, M., Singer, E., Guilbaud, A., Tessier, F. J., et al. (2018). Occurrence and Dynamism of Lactic Acid Bacteria in Distinct Ecological Niches: A Multifaceted Functional Health Perspective. *Front. Microbiol.* 9, 2899. doi:10.3389/fmicb.2018.02899

Glenting, J., Poulsen, L. K., Kato, K., Madsen, S. M., Frøkiær, H., Wendt, C., et al. (2007). Production of Recombinant Peanut Allergen Ara H 2 Using Lactococcus Lactis. *Microb. Cel Fact.* 6, 28. doi:10.1186/1475-2859-6-28

Goh, Y. J., and Klaenhammer, T. R. (2015). Genetic Mechanisms of Prebiotic Oligosaccharide Metabolism in Probiotic Microbes. *Annu. Rev. Food Sci. Technol.* 6, 137–156. doi:10.1146/annurev-food-022814-015706

Gong, Y., and Qi, X. (2020). A Study Revealing Volatile Aroma Produced by Pediococcus Pentosaceus in Dough Fermentation. *Food Sci. Nutr.* 8, 5077–5085. doi:10.1002/fsn3.1807

González-Centeno, M. R., Chira, K., and Teissedre, P.-L. (2017). Comparison between Malolactic Fermentation Container and Barrel Toasting Effects on Phenolic, Volatile, and Sensory Profiles of Red Wines. *J. Agric. Food Chem.* 65, 3320–3329. doi:10.1021/acs.jafc.6b05497

Guo, T., Xin, Y., Zhang, Y., Gu, X., and Kong, J. (2019). A Rapid and Versatile Tool for Genomic Engineering in Lactococcus Lactis. *Microb. Cel Fact.* 18, 22. doi:10.1186/s12934-019-1075-3

Hao, L., Cheng, Y., Su, W., Wang, C., Lu, Z., Jin, M., et al. (2021). Pediococcus Pentosaceus ZJUAF-4 Relieves Oxidative Stress and Restores the Gut Microbiota in Diquat-Induced Intestinal Injury. *Appl. Microbiol. Biotechnol.* 105, 1657–1668. doi:10.1007/s00253-021-11111-6

Heng, N. C. K., and Tagg, J. R. (2006). What's in a Name? Class Distinction for Bacteriocins. *Nat. Rev. Microbiol.* 4, 160. doi:10.1038/nrmicro1273-c1

Hu, L., Sun, C., Wang, S., Su, F., and Zhang, S. (2013). Lipopolysaccharide Neutralization by a Novel Peptide Derived from Phosvitin. *Int. J. Biochem. Cel Biol.* 45, 2622–2631. doi:10.1016/j.biocel.2013.09.002

Kalyanasundram, J., Chia, S. L., Song, A. A.-L., Raha, A. R., Young, H. A., and Yusoff, K. (2015). Surface Display of Glycosylated Tyrosinase Related Protein-2 (TRP-2) Tumour Antigen on Lactococcus Lactis. *BMC Biotechnol.* 15, 113. doi:10.1186/s12896-015-0231-z

Kawahara, K. (2021). Variation, Modification and Engineering of Lipid A in Endotoxin of Gram-Negative Bacteria. *Int. J. Mol. Sci.* 22, 2281. doi:10.3390/ijms22052281

Kong, W., Blanchard, A. E., Liao, C., and Lu, T. (2017). Engineering Robust and Tunable Spatial Structures with Synthetic Gene Circuits. *Nucleic Acids Res.* 45, 1005–1014. doi:10.1093/nar/gkw1045

Kongo, J. M., and Malcata, F. X. (2016). "*Acidophilus Milk*" in, eds. B. Caballero, P. M. Finglas, and H. Toldrá (Oxford: Academic Press), 6–14. doi:10.1016/B978-0-12-384947-2.00002-7

Ladero, V., Ramos, A., Wiersma, A., Goffin, P., Schanck, A., Kleerebezem, M., et al. (2007). High-level Production of the Low-Calorie Sugar Sorbitol by Lactobacillus Plantarum through Metabolic Engineering. *Appl. Environ. Microbiol.* 73, 1864–1872. doi:10.1128/AEM.02304-06

Le, B., and Yang, S. H. (2019). Biosorption of Cadmium by Potential Probiotic Pediococcus Pentosaceus Using *In Vitro* Digestion Model. *Biotechnol. Appl. Biochem.* 66, 673–680. doi:10.1002/bab.1783

Leenay, R. T., Vento, J. M., Shah, M., Martino, M. E., Leulier, F., and Beisel, C. L. (2019). Genome Editing with CRISPR-Cas9 in Lactobacillus Plantarum Revealed that Editing Outcomes Can Vary across Strains and between Methods. *Biotechnol. J.* 14, 1700583. doi:10.1002/biot.201700583

Lemay, M.-L., Tremblay, D. M., and Moineau, S. (2017). Genome Engineering of Virulent Lactococcal Phages Using CRISPR-Cas9. *ACS Synth. Biol.* 6, 1351–1358. doi:10.1021/acssynbio.6b00388

Li, H.-S., Piao, D.-C., Jiang, T., Bok, J.-D., Cho, C.-S., Lee, Y.-S., et al. (2015). Recombinant Interleukin 6 with M Cell-Targeting Moiety Produced in Lactococcus Lactis IL1403 as a Potent Mucosal Adjuvant for Peroral Immunization. *Vaccine* 33, 1959–1967. doi:10.1016/j.vaccine.2015.02.061

Lian, J., HamediRad, M., Hu, S., and Zhao, H. (2017). Combinatorial Metabolic Engineering Using an Orthogonal Tri-functional CRISPR System. *Nat. Commun.* 8, 1688. doi:10.1038/s41467-017-01695-x

Lim, Y. H., Foo, H. L., Loh, T. C., Mohamad, R., Abdul Rahim, R., and Idrus, Z. (2019). Optimized Medium via Statistical Approach Enhanced Threonine Production by Pediococcus Pentosaceus TL-3 Isolated from Malaysian Food. *Microb. Cel Fact.* 18, 125. doi:10.1186/s12934-019-1173-2

Linares, D. M., Alvarez-Sieiro, P., del Rio, B., Ladero, V., Redruello, B., Martin, M. C., et al. (2015). Implementation of the Agmatine-Controlled Expression System for Inducible Gene Expression in Lactococcus Lactis. *Microb. Cel Fact.* 14, 208. doi:10.1186/s12934-015-0399-x

Ma, Y., Liu, J., Hou, J., Dong, Y., Lu, Y., Jin, L., et al. (2014). Oral Administration of Recombinant Lactococcus Lactis Expressing HSP65 and Tandemly Repeated P277 Reduces the Incidence of Type I Diabetes in Non-obese Diabetic Mice. *PLoS One* 9, e105701. doi:10.1371/journal.pone.0105701

Madsen, S. M., Arnau, J., Vrang, A., Givskov, M., and Israelsen, H. (1999). Molecular Characterization of the pH-Inducible and Growth Phase-dependent Promoter P170 of Lactococcus Lactis. *Mol. Microbiol.* 32, 75–87. doi:10.1046/j.1365-2958.1999.01326.x

Mao, N., Cubillos-Ruiz, A., Cameron, D. E., and Collins, J. J. (2018). Probiotic Strains Detect and Suppress Cholera in Mice. *Sci. Transl. Med.* 10, eaao2586. doi:10.1126/scitranslmed.aao2586

Mazhar, S. F., Afzal, M., Almatroudi, A., Munir, S., Ashfaq, U. A., Rasool, M., et al. (2020). The Prospects for the Therapeutic Implications of Genetically Engineered Probiotics. *J. Food Qual.* 2020, 9676452. doi:10.1155/2020/9676452

Mierau, I., and Kleerebezem, M. (2005). 10 Years of the Nisin-Controlled Gene Expression System (NICE) in Lactococcus Lactis. *Appl. Microbiol. Biotechnol.* 68, 705–717. doi:10.1007/s00253-005-0107-6

Miyoshi, A., Jamet, E., Commissaire, J., Renault, P., Langella, P., and Azevedo, V. (2004). A Xylose-Inducible Expression System for Lactococcus Lactis. *FEMS Microbiol. Lett.* 239, 205–212. doi:10.1016/j.femsle.2004.08.018

Mu, D., Montalbán-López, M., Masuda, Y., and Kuipers, O. P. (2013). Zirex: a Novel Zinc-Regulated Expression System for Lactococcus Lactis. *Appl. Environ. Microbiol.* 79, 4503–4508. doi:10.1128/AEM.00866-13

Neu, T., and Henrich, B. (2003). New Thermosensitive Delivery Vector and its Use to Enable Nisin-Controlled Gene Expression in Lactobacillus Gasseri. *Appl. Environ. Microbiol.* 69, 1377–1382. doi:10.1128/AEM.69.3.1377-1382.2003

Nissen, L., Pérez-Martínez, G., and Yebra, M. J. (2005). Sorbitol Synthesis by an Engineered Lactobacillus Casei Strain Expressing a Sorbitol-6-Phosphate Dehydrogenase Gene within the Lactose Operon. *FEMS Microbiol. Lett.* 249, 177–183. doi:10.1016/j.femsle.2005.06.010

Nyyssölä, A., Pihlajaniemi, A., Palva, A., von Weymarn, N., and Leisola, M. (2005). Production of Xylitol from D-Xylose by Recombinant Lactococcus Lactis. *J. Biotechnol.* 118, 55–66. doi:10.1016/j.jbiotec.2005.03.014

O'Connor, E. B., O'Sullivan, O., Stanton, C., Danielsen, M., Simpson, P. J., Callanan, M. J., et al. (2007). pEOC01: A Plasmid from Pediococcus Acidilactici Which Encodes an Identical Streptomycin Resistance (aadE) Gene to that Found in Campylobacter Jejuni. *Plasmid* 58, 115–126. doi:10.1016/j.plasmid.2007.02.002

Oh, J.-H., and van Pijkeren, J.-P. (2014). CRISPR-Cas9-assisted Recombineering in Lactobacillus Reuteri. *Nucleic Acids Res.* 42, e131. doi:10.1093/nar/gku623

Ohkouchi, K., Kawamoto, S., Tatsugawa, K., Yoshikawa, N., Takaoka, Y., Miyauchi, S., et al. (2012). Prophylactic Effect of Lactobacillus Oral Vaccine Expressing a Japanese Cedar Pollen Allergen. *J. Biosci. Bioeng.* 113, 536–541. doi:10.1016/j.jbiosc.2011.11.025

Ortiz-Velez, L., and Britton, R. (2017). Genetic Tools for the Enhancement of Probiotic Properties. *Microbiol. Spectr.* 5, 1. doi:10.1128/microbiolspec.BAD-0018-2016

Oude Elferink, S. J., Krooneman, J., Gottschal, J. C., Spoelstra, S. F., Faber, F., and Driehuis, F. (2001). Anaerobic Conversion of Lactic Acid to Acetic Acid and 1, 2-propanediol by Lactobacillus Buchneri. *Appl. Environ. Microbiol.* 67, 125–132. doi:10.1128/AEM.67.1.125-132.2001

Packer, M. S., Rees, H. A., and Liu, D. R. (2017). Phage-assisted Continuous Evolution of Proteases with Altered Substrate Specificity. *Nat. Commun.* 8, 956. doi:10.1038/s41467-017-01055-9

Papagianni, M., and Anastasiadou, S. (2009). Pediocins: The Bacteriocins of Pediococci. Sources, Production, Properties and Applications. *Microb. Cel Fact* 8, 3. doi:10.1186/1475-2859-8-3

Pinto, J. P. C., Zeyniyev, A., Karsens, H., Trip, H., Lolkema, J. S., Kuipers, O. P., et al. (2011). pSEUDO, a Genetic Integration Standard for Lactococcus Lactis. *Appl. Environ. Microbiol.* 77, 6687–6690. doi:10.1128/AEM.05196-11

Plavec, T. V., and Berlec, A. (2020). Safety Aspects of Genetically Modified Lactic Acid Bacteria. *Microorganisms* 8, 297. doi:10.3390/microorganisms8020297

Raccach, M. (2014). "*Pediococcus*" in, eds. C. A. Batt and S. E. Tortorello. (Oxford: Academic Press), 1–5. doi:10.1016/B978-0-12-384730-0.00247-0

Radivojević, T., Costello, Z., Workman, K., and Garcia Martin, H. (2020). A Machine Learning Automated Recommendation Tool for Synthetic Biology. *Nat. Commun.* 11, 4879. doi:10.1038/s41467-020-18008-4

Rath, D., Amlinger, L., Rath, A., and Lundgren, M. (2015). The CRISPR-Cas Immune System: Biology, Mechanisms and Applications. *Biochimie* 117, 119–128. doi:10.1016/j.biochi.2015.03.025

Ravi Sankar, V., and Dastagiri Reddy, Y. (2010). Nanocochleate - a New Approch in Lipid Drug Delivery. *Int. J. Pharm. Pharm. Sci.* 2, 220–223.

Razavi, S., Janfaza, S., Tasnim, N., Gibson, D. L., and Hoorfar, M. (2021). *Microencapsulating Polymers for Probiotics Delivery Systems: Preparation, Characterization, and Applications*, 120, 106882. doi:10.1016/j.foodhyd.2021.106882*Food Hydrocolloids*

Ricci, A., Ricci, A., Allende, A., Bolton, D., Chemaly, M., Davies, R., et al. (2018). Update of the List of QPS-recommended Biological Agents Intentionally Added to Food or Feed as Notified to EFSA 7: Suitability of Taxonomic Units Notified to EFSA until September 2017. *Efs2* 16, e05131. doi:10.2903/j.efsa.2018.5131

Saha, B. C., and Racine, F. M. (2011). Biotechnological Production of Mannitol and its Applications. *Appl. Microbiol. Biotechnol.* 89, 879–891. doi:10.1007/s00253-010-2979-3

Segler, M. H. S., Preuss, M., and Waller, M. P. (2018). Planning Chemical Syntheses with Deep Neural Networks and Symbolic AI. *Nature* 555, 604–610. doi:10.1038/nature25978

Sekhon, B. S. (2010). Food Nanotechnology - an Overview. *Nanotechnol. Sci. Appl.* 3, 1–15. doi:10.2147/NSA.S8677

Sharma, R., Garg, P., Kumar, P., Bhatia, S. K., and Kulshrestha, S. (2020). Microbial Fermentation and its Role in Quality Improvement of Fermented Foods. *Ferment* 6. doi:10.3390/fermentation6040106

Silva, C. C. G., Silva, S. P. M., and Ribeiro, S. C. (2018). Application of Bacteriocins and Protective Cultures in Dairy Food Preservation. *Front. Microbiol.* 9, 594. doi:10.3389/fmicb.2018.00594

Singhvi, M. S., Zinjarde, S. S., and Gokhale, D. V ((2019). Polylactic Acid: Synthesis and Biomedical Applications. *J. Appl. Microbiol.* 127, 1612–1626. doi:10.1111/jam.14290

Song, D., Ibrahim, S., and Hayek, S. (2021). *Recent Application of Probiotics in Food and Agricultural Science*. doi:10.5772/50121

Song, X., Huang, H., Xiong, Z., Ai, L., and Yang, S. (2017). CRISPR-Cas9(D10A) Nickase-Assisted Genome Editing in Lactobacillus Casei. *Appl. Environ. Microbiol.* 83, e01259. doi:10.1128/AEM.01259-17

Steidler, L., Hans, W., Schotte, L., Neirynck, S., Obermeier, F., Falk, W., et al. (2000). Treatment of Murine Colitis by Lactococcus Lactis Secreting Interleukin-10. *Science* 289, 1352–1355. doi:10.1126/science.289.5483.1352

Storaker, M. I., Kamilla, W., Zhian, S., Sigve, H. L., Daniel, S., Geir, M., et al. (2021). CRISPR Interference for Rapid Knockdown of Essential Cell Cycle Genes in Lactobacillus Plantarum. *mSphere* 4, e00007–19. doi:10.1128/mSphere.00007-19

Tan, B. L., Norhaizan, M. E., Liew, W.-P.-P., and Sulaiman Rahman, H. (2018). Antioxidant and Oxidative Stress: A Mutual Interplay in Age-Related Diseases. *Front. Pharmacol.* 9, 1162. doi:10.3389/fphar.2018.01162

Thuy, D. T. B., Nguyen, A., Khoo, K. S., Chew, K. W., Cnockaert, M., Vandamme, P., et al. (2021). Optimization of Culture Conditions for Gamma-Aminobutyric Acid Production by Newly Identified Pediococcus Pentosaceus MN12 Isolated from "Mam Nem". *A Fermented Fish Sauce. Bioengineered* 12, 54–62. doi:10.1080/21655979.2020.1857626

van der Els, S., James, J. K., Kleerebezem, M., and Bron, P. A. (2021). Versatile Cas9-Driven Subpopulation Selection Toolbox for Lactococcus Lactis. *Appl. Environ. Microbiol.* 84, e02752–17. doi:10.1128/AEM.02752-17

van Pijkeren, J.-P., and Britton, R. A. (2012). High Efficiency Recombineering in Lactic Acid Bacteria. *Nucleic Acids Res.* 40, e76. doi:10.1093/nar/gks147

Villalobos-Delgado, L. H., Nevárez-Moorillon, G. V., Caro, I., Quinto, E. J., and Mateo, J. (2019). 4 - Natural Antimicrobial Agents to Improve Foods Shelf Life. *Food Qual. Shelf Life* 2019, 125–157. doi:10.1016/B978-0-12-817190-5.00004-5

Walker, D. C., and Klaenhammer, T. R. (1994). Isolation of a Novel IS3 Group Insertion Element and Construction of an Integration Vector for Lactobacillus Spp. *J. Bacteriol.* 176, 5330–5340. doi:10.1128/jb.176.17.5330-5340.1994

Wang, T., Badran, A. H., Huang, T. P., and Liu, D. R. (2018). Continuous Directed Evolution of Proteins with Improved Soluble Expression. *Nat. Chem. Biol.* 14, 972–980. doi:10.1038/s41589-018-0121-5

Xin, Y., Guo, T., Mu, Y., and Kong, J. (2017). Identification and Functional Analysis of Potential Prophage-Derived Recombinases for Genome Editing in Lactobacillus Casei. *FEMS Microbiol. Lett.* 364, 364. doi:10.1093/femsle/fnx243

Yadav, N., Narang, J., Chhillar, A. K., and Rana, J. S. (2021). CRISPR: A New Paradigm of Theranostics. *Nanomedicine Nanotechnology, Biol. Med.* 33, 102350. doi:10.1016/j.nano.2020.102350

Yadav, R., Kumar, V., Baweja, M., and Shukla, P. (2018). Gene Editing and Genetic Engineering Approaches for Advanced Probiotics: A Review. *Crit. Rev. Food Sci. Nutr.* 58, 1735–1746. doi:10.1080/10408398.2016.1274877

Yang, P., Wang, J., and Qi, Q. (2015a). Prophage Recombinases-Mediated Genome Engineering in Lactobacillus Plantarum. *Microb. Cel Fact.* 14, 154. doi:10.1186/s12934-015-0344-z

Yang, T., Rao, Z., Kimani, B. G., Xu, M., Zhang, X., and Yang, S.-T. (2015b). Two-step Production of Gamma-Aminobutyric Acid from Cassava Powder Using Corynebacterium Glutamicum and Lactobacillus Plantarum. *J. Ind. Microbiol. Biotechnol.* 42, 1157–1165. doi:10.1007/s10295-015-1645-2

Yu, D., Sawitzke, J. A., Ellis, H., and Court, D. L. (2003). Recombineering with Overlapping Single-Stranded DNA Oligonucleotides: Testing a Recombination Intermediate. *Proc. Natl. Acad. Sci. U. S. A.* 100, 7207–7212. doi:10.1073/pnas.1232375100

Zhang, B., Li, A., Zuo, F., Yu, R., Zeng, Z., Ma, H., et al. (2016). Recombinant Lactococcus Lactis NZ9000 Secretes a Bioactive Kisspeptin that Inhibits Proliferation and Migration of Human colon Carcinoma HT-29 Cells. *Microb. Cel Fact.* 15, 102. doi:10.1186/s12934-016-0506-7

Zhang, J., Petersen, S. D., Radivojevic, T., Ramirez, A., Pérez-Manríquez, A., Abeliuk, E., et al. (2020a). Combining Mechanistic and Machine Learning Models for Predictive Engineering and Optimization of Tryptophan Metabolism. *Nat. Commun.* 11, 4880. doi:10.1038/s41467-020-17910-1

Zhang, Y., Yang, J., Liu, Y., Wu, Y., Fang, Z., Wang, Y., et al. (2020b). A Novel Bacteriocin PE-ZYB1 Produced by Pediococcus Pentosaceus Zy-B Isolated from Intestine of Mimachlamys Nobilis: Purification, Identification and its Anti-listerial Action. *LWT* 118, 108760. doi:10.1016/j.lwt.2019.108760

Zhong, Y., Wu, S., Chen, F., He, M., and Lin, J. (2019). Isolation of High γ-aminobutyric Acid-Producing Lactic Acid Bacteria and Fermentation in mulberry Leaf Powders. *Exp. Ther. Med.* 18, 147–153. doi:10.3892/etm.2019.7557

Zhu, D., Liu, F., Xu, H., Bai, Y., Zhang, X., Saris, P. E. J., et al. (2015). Isolation of strong Constitutive Promoters from Lactococcus Lactis Subsp. Lactis N8. *FEMS Microbiol. Lett.* 362, fnv107. doi:10.1093/femsle/fnv107

Conflict of Interest: The authors declare that the research was conducted in the absence of any commercial or financial relationships that could be construed as a potential conflict of interest.

Publisher's Note: All claims expressed in this article are solely those of the authors and do not necessarily represent those of their affiliated organizations, or those of the publisher, the editors, and the reviewers. Any product that may be evaluated in this article, or claim that may be made by its manufacturer, is not guaranteed or endorsed by the publisher.

frontiers in Bioengineering and Biotechnology

DATA REPORT
published: 17 February 2022
doi: 10.3389/fbioe.2021.810571

The Complete Genome Sequence and Structure of the Oleaginous *Rhodococcus opacus* Strain PD630 Through Nanopore Technology

Andrea Firrincieli[1†], *Beatrice Grigoriev*[1†], *Hana Dostálová*[2] *and Martina Cappelletti*[1*]

[1]*Department of Pharmacy and Biotechnology, University of Bologna, Bologna, Italy,* [2]*Institute of Microbiology of the CAS, Prague, Czechia*

Keywords: ***Rhodococcus opacus*** **PD630, nanopore sequencing, oleaginous bacteria, complete genome,** ***Rhodococcus*** **genomics,** ***Rhodococcus opacus*** **plasmids, xenobiotic degradation genes, lipid metabolism genes**

OPEN ACCESS

Edited by:
Panagiotis Madesis,
University of Thessaly, Greece

Reviewed by:
Iain Sutcliffe,
Northumbria University,
United Kingdom
Artem Kasianov,
Vavilov Institute of General Genetics (RAS), Russia

***Correspondence:**
Martina Cappelletti
martina.cappelletti2@unibo.it

†These authors have contributed equally to this work

Specialty section:
This article was submitted to Industrial Biotechnology, a section of the journal Frontiers in Bioengineering and Biotechnology

Received: *07 November 2021*
Accepted: *27 December 2021*
Published: *17 February 2022*

Citation:
Firrincieli A, Grigoriev B, Dostálová H and Cappelletti M (2022) The Complete Genome Sequence and Structure of the Oleaginous Rhodococcus opacus *Strain PD630 Through Nanopore Technology. Front. Bioeng. Biotechnol. 9:810571. doi: 10.3389/fbioe.2021.810571*

INTRODUCTION

Rhodococcus bacterial strains are characterized by wide metabolic versatility and extraordinary resistance to environmental stresses (de Carvalho et al., 2014; Orro et al., 2015; Cappelletti et al., 2016, 2019; Pátek et al., 2021). The high versatility and adaptability of *Rhodococcus* strains is partly related with large and complex genomes (up to 10.1 Mbp) including high genetic redundancy and the presence of several circular and linear (mega)plasmids, which harbour peculiar catabolic and biosynthetic genes (Cappelletti et al., 2019). Within *Rhodococcus* genus, *R. opacus* strain PD630 is considered a model oleaginous strain for its ability to produce and accumulate lipids (mostly triacyglycerols, TAGs) using different carbon sources, including low-cost and renewable resources such as lignocellulose (Alvarez et al., 1996; Anthony et al., 2019; Cappelletti et al., 2020; Alvarez et al., 2021; Donini et al., 2021). Notably, under specific growth conditions, this strain is capable of accumulating up to 80% of its cellular dry weight in TAGs (Alvarez and Steinbüchel, 2002); that is a rare feature in the prokaryotic and eukaryotic kingdoms. Multi-omic approaches have been applied to obtain system-level information about metabolic and regulatory pathways involved in these biosynthetic processes. Novel molecular tools for genome editing (CRISPR/Cas9 and recombineering) have been recently developed highlighting the possible utilization of *R. opacus* PD630 as synthetic biology platform for lipids production (Donini et al., 2021; Liang and Yu, 2021).

A first assembly of the *R. opacus* PD630 genome was submitted by the Broad Institute in 2011 (Holder et al., 2011) and included 491 contigs. Later in 2014, a "complete" version of the PD630 genome was submitted by the Institute of Biophysics of the Chinese Academy of Sciences (hereafter IBP_PD630) (Chen et al., 2013) that was recently indicated as "Anomalous assembly" and "contaminated" and therefore deleted from NCBI RefSeq. IBP_PD630 reported the PD630 genome to be composed by one chromosome and nine plasmids (two circular and seven linear plasmids). This result was divergent from the typical number of extrachromosomal elements reported for genomes of this genus, five being the maximum number of extrachromosomal elements described in a single *Rhodococcus* strain (Cappelletti et al., 2019). Despite the assembly-related issues, IBP_PD630 has been used as reference genome in many works involving -omics analyses for the detection of genetic determinants involved in aromatics tolerance and conversion into lipids (DeLorenzo et al., 2018; Kim et al., 2019; Chen et al., 2013; Yoneda et al., 2016; Henson et al., 2018).

In this study, we combined Oxford Nanopore sequencing with Illumina high quality data to solve the architecture of the *R. opacus* PD630 genome and to obtain its whole sequence. Here, in addition to the high-quality complete genome sequence, we demonstrate that this strain does not possess nine

plasmids as previously stated, but instead harbours one chromosome and three (one linear and two circular) plasmids. Further, by solving the final structure of *R. opacus* PD630, we found that the large linear plasmid included extrachromosomal genes involved in lipid and xenobiotics' metabolism. This work provides the correct PD630 genomic framework for the development of genetic engineering strategies to boost the application of this strain as microbial cell factory for lipid production.

MATERIALS AND METHODS

Bacterial Growth and Genomic DNA Extraction

R. opacus PD630 (DSM 44 193) was purchased from the Leibniz Institute DSMZ-German Collection of Microorganisms and Cell Cultures (Braunschweig, Germany). For genomic DNA extraction, PD630 was cultivated in 50 ml Luria Bertani (LB) broth at 30°C for 24 h under shaking conditions at 150 rpm. The culture was centrifuged at 4°C for 10 min at 5,000 rpm and the whole cell pellet was subjected to the procedure indicated by Cappelletti et al. (Cappelletti et al., 2011) with slight modifications that involved the utilization of a 10% sodium dodecyl sulfate (SDS)-based lysis buffer to disrupt the cells instead of the mechanical treatment (mediated by bead beater). The genomic DNA was quantified via Qubit dsDNA BR assay kit with the Qubit 4.0 fluorometer (Life Technologies).

Oxford Nanopore Whole Genome Sequencing

The genomic DNA was fragmented for 10 s via sonication and the integrity of the DNA after fragmentation was checked via electrophoresis gel. The sequencing library was performed with the Oxford Nanopore Ligation Sequencing Kit (SQK-LSK110), according to manufacturer's instructions. The genomic library was loaded on a FLO-MIN106D (chemistry R9.4.1) flow cell and sequenced with the MinION Mk1C device (Oxford Nanopore Technology, ONT). The sequencing run was performed until 3.5 Gb of bases were obtained that corresponded to a total of 694,680 reads. Base calling of the FAST5 data from MinION was carried out with Guppy GPU 5.0 in high-accuracy mode and with default parameters (chunks per runner 256; chunk size 2000; minimum qscore 7). Evaluation of sequencing quality of the basecalled FAST5 data was performed using PycoQC v2.5.2. Sequencing reads were deposited in the Sequence Read Archive (SRA) SRX12606194.

Sequencing Data Assembly and Annotation

The genome was assembled using Canu assembler v1.2 (Koren et al., 2017) and the draft assembly was corrected using Illumina short reads [SRX875494 (Janet, 2014)] (Illumina HiSeq 2500) with a single round of Pilon v. 1.24 (Walker et al., 2014). The draft assembly was finally circularized using Circlator (Hunt et al., 2015) indicating the *dnaA* gene of *R. opacus* PD630 (OPAG_07542) as the chromosomal sequence start. A final round of polishing was performed with Berokka to trim overhanging ends from plasmids. Finally, genome completeness was assessed via BUSCO (Manni et al., 2021) and annotated *de novo* using the standalone version of Prokaryotic Genome Annotation Pipeline (PGAP) (Li et al., 2020).

Comparative Analysis With Other PD630 Genome Assembly Versions

The synteny analysis between the overall organization of PD630 Chen's assembly (Chen et al., 2013) and the genome presented in this work was performed by Sibelia (Minkin et al., 2013). Liftoff was used to identify the PD630 genes from Chen's assembly that did not map against our genome due to the presence of miscalled nucleotides, insertion/deletions (indels), and structural variants. A gene was considered to successfully map when the alignment coverage and sequence identity was equal to 100%.

Functional Annotation of Protein Coding Genes in Plasmids of *R. opacus* Strains

Proteins harbored by plasmids of *R. opacus* strains and *R. jostii* RHA1 were downloaded from RefSeq and annotated using the functional database KEGG with KofamKOALA (Aramaki et al., 2019) (**Supplementary Table S1**). According to the Genome Taxonomy Database (Chaumeil et al., 2019), we included in the analysis the only *R. opacus* strains with a complete genome currently available in RefSeq (Accessed: December 10th, 2021), i.e., *R. opacus* B4, *R. opacus* DSM 44 186, *R. opacus* 1CP, and *R. opacus* KT112-7.

INTERPRETATION OF DATA SET

Genome Assembly and Annotation

After base calling a total of 667,679 reads with a median Phred score of 13.43, and a median length of 3.1 Kb were generated (**Supplementary Figures S1A,B**). The draft assembly generated by Canu consisted of four contigs with a total length of 9.16 Mbp. After one polishing round in Pilon using Illumina HiSeq paired-end reads, the size of the Canu-assembled contig slightly increased mostly because of single and/or di-nucleotide insertions (**Supplementary File 1**). Large variants (>100 bp) were manually checked via blastn. As a result, all of them perfectly matched with sequences of *R. opacus* PD630 (**Supplementary File 1**). A change in the final size (>10 Kb) of the contigs RoPD630, pRoPD630_2, and pRoPD630_3 was observed after the circularization and trimming steps (Circlator + Berokka) (**Table 1**), due to the removal of duplicated sequences at their ends. The presence of start-end overlaps in contigs is a well-known behaviour of Canu assembler which tends to generate contigs with a contiguity above 100% (Wick and Holt, 2021).

The final assembly (obtained after circularization and trimming) provided a genome with an overall size of 9.16 Mb, including one circular chromosome (RoPD630) of 8.37 Mb and three plasmids, one linear (pRoPD630_1) and two circular (pRoPD630_2 and pRoPD630_3). The average G + C content

TABLE 1 | Length (bp) of chromosome and plasmids throughout the correction and circularization steps.

Predicted topology	RoPD630 (CP080954)	pRoPD630_1 (CP080955)	pRoPD630_2 (CP080956)	pRoPD630_3 (CP080957)
	Circular	Linear	Circular	Circular
Canu	8,411,399	538,757	210,131	121,266
Pilon	8,412,872	538,909	210,169	121,283
Circlator	8,374,353	538,909	210,169	85,051
Berokka	8,374,353	538,909	67,985	85,051
Final bp - Canu bp[a]	−37,046	+152	−42,145	−36,215

[a]*Difference in the number of bp after all the steps with respect to the initial Canu output.*

of the circular chromosome was 67.38% whereas plasmids pRoPD630_1, pRoPD630_2, and pRoPD630_3 showed lower G + C values, i.e., 65.27, 65.06, and 63.91%, respectively (**Table 1**). The genome completeness was checked via BUSCO, resulting in 100% completeness and 1.4% duplication. According to the PGAP, FABIT_PD630 genome contained 8,280 genes, of which 7,972 protein coding genes, 66 RNA genes, and 242 pseudo-genes.

Genome Assembly Comparison Between the IBP_PD630 and FABIT_PD630 Genomes

We specifically performed comparative analysis between the IBP_PD630 and FABIT_PD630 genomes to analyse their differences at structural and genetic levels. As a result, FABIT_PD630 possesses a lower number of genes as compared with IBP_PD630, i.e., 8,280 against the 9,005 genes detected in IBP_PD630 assembly. The different number of genes can be attributed to the distinct annotation pipelines that were used in the two works and/or to actual differences in the genome sequence (i.e., sequence variants). To get deep into the reason on this discrepancy, we investigated the possibility that missing genes were due to structural and nucleotide variants. Therefore, we only focused on the identification of the IBP_PD630 genes that did not map with a perfect alignment (i.e., alignment coverage and sequence identity of 100%) with FABIT_PD630 assembly. As a result, only 238 IBP_PD630 genes (around 30% of the number of genes missing in FABIT_PD630 as compared to IBP_PD630) did not align with a perfect match. Furthermore, the number of genes not mapping to our genome was reduced to 84 (<1% of all the genes of Chen's assembly) when a coverage and sequence identity of 90% was imposed (**Supplementary File 2**). These results indicate that the differences observed between FABIT_PD630 and IBP_PD630 in terms of identified gene number were mainly due to the annotation pipeline. Annotation pipelines are known to have different sensitivity to misannotations and therefore to the detection of open reading frames (Monnahan et al., 2020).

Syntenic analysis of IBP_PD630 plasmids showed near-perfect match between the seven linear plasmids (CP03952-CP03958) of IBP_PD630 and the linear plasmid pRoPD630_1 of FABIT_PD630. This indicates that the sequences CP03952-CP03958 do not correspond to distinct plasmids but represent the fragments of a single linear megaplasmid present in *R. opacus* PD630. Similarly, a nearly-perfect match was observed between each of the circular plasmids CP03950 and CP03951 and the circular plasmids pRoPD630_2 and pRoPD630_3, respectively (**Figure 1**). Therefore, these results demonstrate that *R. opacus* PD630 possesses only three plasmids instead of nine. The difference between the genetic structure of the two genomes can be attributed to the distinct sequencing and library preparation technologies used in the two works to assemble BIP_PD630 and FABIT_PD630. Indeed, Chen et al. (Chen et al., 2013) carried out a primary assembly using 454 pyrosequencing reads, followed by scaffolding step using Illumina mate-pair library with insert size of 3,000 bp. Although Illumina mate-pair libraries can be successfully used to improve contiguity and therefore close gaps between contigs (Wetzel et al., 2011), the utilization of a single mate-pair library could have been not able to correctly solve repetitive regions of different sizes. Indeed, the capacity of finding links between contigs is limited by the length of the gap itself (Wetzel et al., 2011). An additional downside of Illumina mate-pair reads that might have hampered a correct assembly is the uneven sequencing depth introduced during PCR amplification step which is prone to GC content related bias (Sohn and Nam, 2016). Conversely, long-read sequencing technologies, including the ONT sequencing used in our work, are not typically affected by these issues as they apply library preparation strategies that are PCR-free and therefore less biased towards regions with high AT/GC content. On the other hand, in order to cope with the error rate limits of the ONT technology (Laver et al., 2015), we used high quality Illumina sequencing data (available online under the accession number SRX875494) to correct the possible sequencing errors introduced during long-reads sequence generation.

Our work provides the definitive structure of the plasmids of PD630 that have drawn attention in relation with the aromatics bioconversion capacity of this strain. In this regard, Henson et al. (Henson et al., 2018) showed that Adaptive Laboratory Evolution (ALE) of PD630 strain that was sequentially cultured on different aromatics led to multiple plasmid loss events. The selective loss of extrachromosomal elements seemed to benefit the PD630 growth under specific conditions by leading to the deletion of superfluous genes and saving in large plasmid replication costs (DeLorenzo et al., 2018). Furthermore, the PD630 plasmids were found to harbour several genes encoding enzymes involved in the catabolism of hetero- and poly-cyclic aromatic compounds as well as multiple uncharacterized mono and dioxygenases. This observation pointed out the interest of these plasmids as potential targets for genetic engineering strategies and bacterial strain

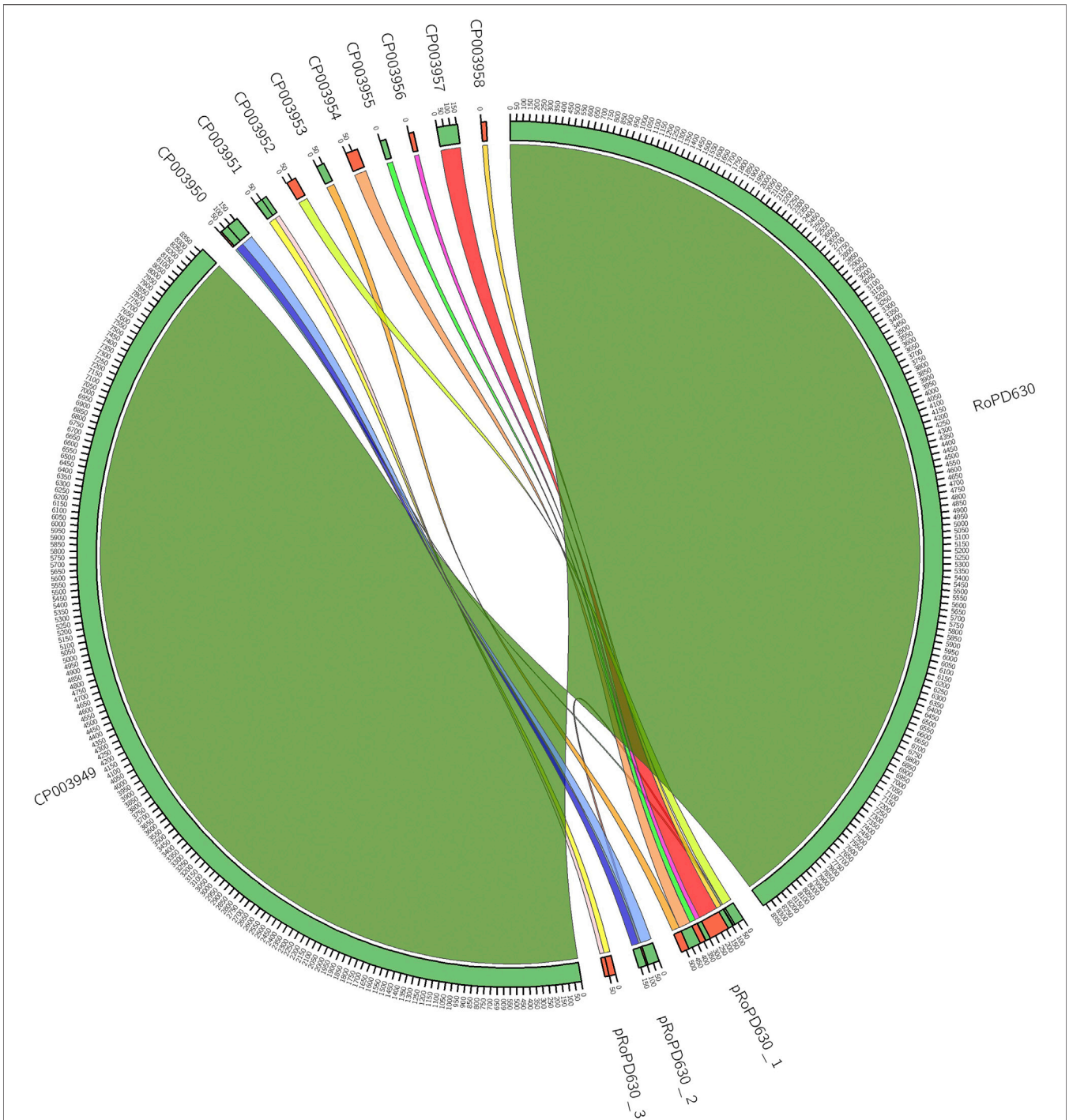

FIGURE 1 | Inferred synteny between IBP_PD630 and FABIT_PD630 assemblies. A minimum synteny block of 10 Kb was selected.

improvement (Cappelletti et al., 2019; Anthony et al., 2019; DeLorenzo et al., 2018). The knowledge of the correct PD630 genome structure and plasmid organization provided by our work is therefore crucial to assess the molecular and genetic bases of the PD630 peculiar metabolic capacities and to correctly design strain improvement strategies.

Functional Profiles of the *R. opacus* Species Plasmids

To gain a better understanding on the repertoire of catabolic potential harbored by each of the three *R. opacus* PD630 plasmids defined in this study, their KEGG functional annotation was performed. Additionally, a comparative analysis of all the

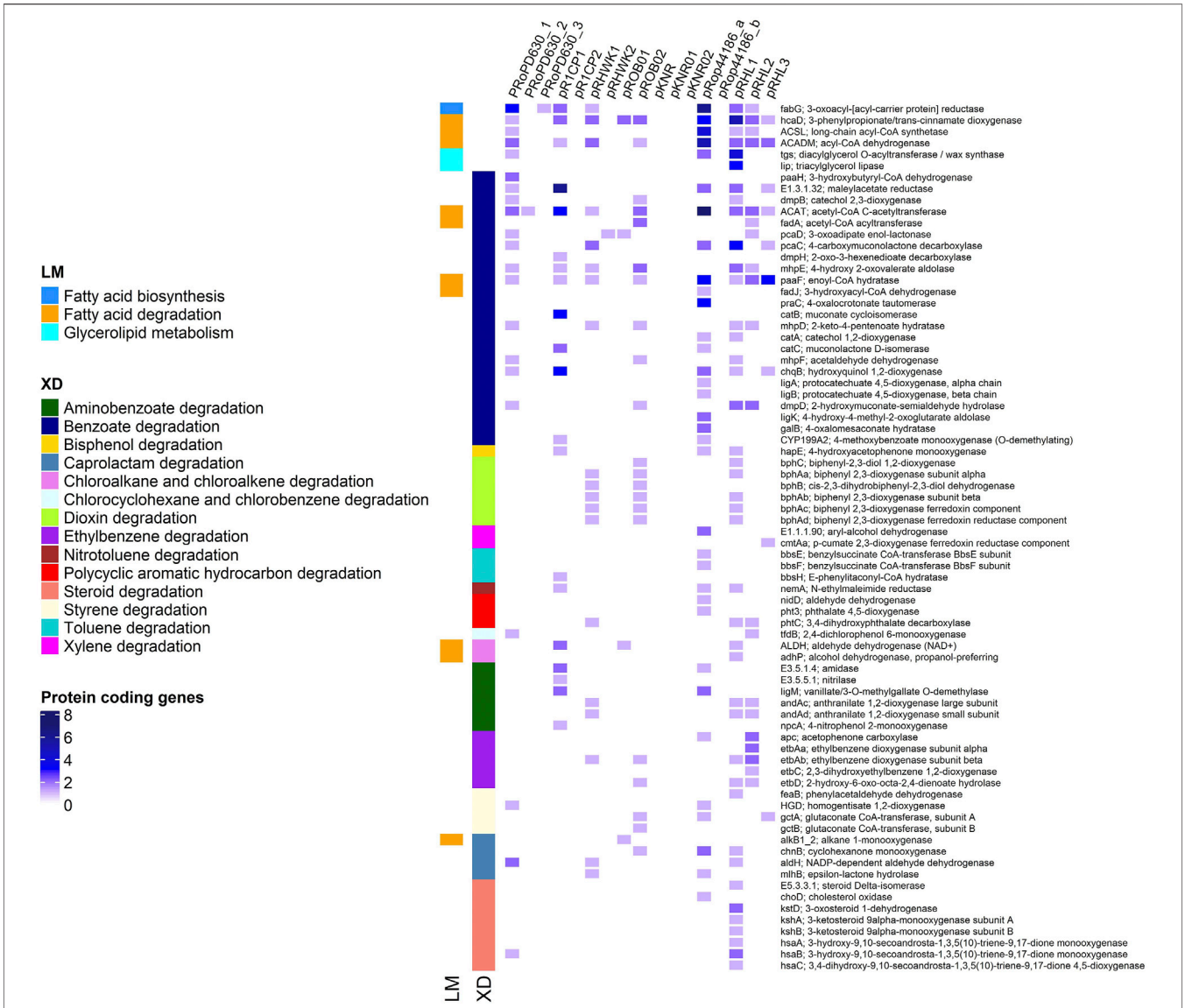

FIGURE 2 | Functional profiling of the protein coding genes involved in xenobiotic degradation (XD) and lipid metabolism (LM) in plasmids of *R. opacus* species and *R. jostii* RHA1 (pRHL). The *Rhodococcus* opacus strains analyzed in this study were *R. opacus* PD630 (pRoPD630), *R. opacus* 1CP (pR1CP), *R. opacus* KT112-7 (pRHWK), *R. opacus* B4 (pROB and pKNR), and *R. opacus* DSM 44 186 (pRop44186).

plasmids of *R. opacus* strains available in the database (with a complete genome and unanimously identified as belonging to this species) was conducted. *R. jostii* RHA1 was also included in the analysis as the model strain of *Rhodococcus* genus. As a result, the percentage of KEGG orthologues detected in PD630 was 30.8% in pRoPD630_1, 18.7% in pRoPD630_2, and 11.8% in pRoPD630_3. All the three PD630 plasmids harbored genes associated with lipid metabolism, biosynthesis of vitamin, and secondary metabolites, whereas only pRoPD630_1 and pRoPD630_2 included also genes related to carbon, energy, amino acid, and nucleotide metabolism and xenobiotic degradation (**Supplementary Table S1**). However, pRoPD630_1 included a significantly higher number of genes associated to all of these metabolisms as compared to pRoPD630_2 and pRoPD630_3. In particular, pRoPD630_1 showed a high number of genes associated with xenobiotics degradation and fatty acid catabolism/anabolism that are the metabolic capacities mostly studied for this strain and in general for *R. opacus* species (Anthony et al., 2019; Donini et al., 2021). Conversely, in the PD630 genome version of (Chen et al., 2013), these genes were distributed over the seven scaffolds that were erroneously identified as separate plasmids. These gene functions were also found to be mostly co-localized on one of the several plasmids carried by the other *R. opacus* strains under analysis, while in *R. jostii* RHA1 they were scattered (**Figure 2**). By resolving the final structure of all the PD630 replicons, we have now the full comprehension of the organization of biotechnologically relevant genes also associated with its plasmids.

DATA AVAILABILITY STATEMENT

The original contributions presented in the study are publicly available. This data can be found here: https://doi.org/10.6084/m9.figshare.16944811 for the supplementary file 1 and 2; https://www.ncbi.nlm.nih.gov/assembly/GCF_020542785.1 for the genome assembly; https://www.ncbi.nlm.nih.gov/sra/SRX12606194 for the Nanopore sequencing reads.

AUTHOR CONTRIBUTIONS

AF conceived the bioinformatic analysis and together with BG conducted the in silico analyses and wrote the first draft of the manuscript. HD carried out the PD630 culture preparation, DNA extraction, and together with MC prepared the library and carried out the experiment on the MinION Mk1C. MC conceived and supervised the study, acquired the funding, edited the manuscript and shaped the last version of it.

FUNDING

The experiments were funded by Fondazione Carisbo and the Bachelor Degree in Genomics Alma Mater Studiorum University of Bologna (Italy).

ACKNOWLEDGMENTS

The authors gratefully acknowledge Prof. Janet R. Donaldson for granting the utilization of the Illumina sequencing reads used in this study (SRX875494) that were sequenced (Project ID: 1031 315) and submitted by the Department of Energy Joint Genome Institute (JGI) on the public repository. The work conducted by the U.S. Department of Energy Joint Genome Institute, a DOE Office of Science User Facility, is supported by the Office of Science of the U.S. Department of Energy under Contract No. DE-AC02-05CH11231.

SUPPLEMENTARY MATERIAL

The Supplementary Material for this article can be found online at: https://www.frontiersin.org/articles/10.3389/fbioe.2021.810571/full#supplementary-material

Supplementary File 1 | Pilon polishing round results.

Supplementary File 2 | Liftoff analysis results of IBP_PD630 genes mapped over FABIT_PD630 assembly using increasing coverage and identity thresholds: (i) 100% coverage and identity, (ii) 95% coverage and identity, and (iii) 90% coverage and identity. Each folder includes two files, "mapped" and "unmapped." The "mapped" file is a GFF (General Feature Format) file including all IBP_PD630 genes successfully mapped against FABIT_PD630 and their coordinates. Conversely, the "unmapped" file is a text file reporting the IBP_PD630 genes that do not satisfy the minimum coverage and identity values specified in the Liftoff analysis. GFF files provide the framework to identify the IBP_PD630 genes in the FABIT_PD630 assembly Finally, a Sequence Alignment Map (SAM) file is provided to inspect the alignment of IBP_PD630 genes over FABIT_PD630 genome.

REFERENCES

Alvarez, H. M., and Steinbüchel, A. (2002). Triacylglycerols in Prokaryotic Microorganisms. *Appl. Microbiol. Biot.* 60, 367–376. doi:10.1007/s00253-002-1135-0

Alvarez, H. M., Hernández, M. A., Lanfranconi, M. P., Silva, R. A., and Villalba, M. S. (2021). Rhodococcus as Biofactories for Microbial Oil Production. *Molecules* 26, 4871. doi:10.3390/molecules26164871

Alvarez, H. M., Mayer, F., Fabritius, D., and Steinbüchel, A. (1996). Formation of Intracytoplasmic Lipid Inclusions by Rhodococcus opacus Strain PD630. *Arch. Microbiol.* 165, 377–386. doi:10.1007/s002030050341

Anthony, W. E., Carr, R. R., DeLorenzo, D. M., Campbell, T. P., Shang, Z., Foston, M., et al. (2019). Development of Rhodococcus opacus as a Chassis for Lignin Valorization and Bioproduction of High-Value Compounds. *Biotechnol. Biofuels* 12, 1–14. doi:10.1186/s13068-019-1535-3

Aramaki, T., Blanc-Mathieu, R., Endo, H., Ohkubo, K., Kanehisa, M., Goto, S., et al. (2019). KofamKOALA: Kegg Ortholog Assignment Based on Profile HMM and Adaptive Score Threshold. *Method. Biochem. Anal.* 36, 2251–2252. doi:10.1093/bioinformatics/btz859

Cappelletti, M., Fedi, S., Frascari, D., Ohtake, H., Turner, R. J., and Zannoni, D. (2011). Analyses of Both the alkB Gene Transcriptional Start Site and alkB Promoter-Inducing Properties of Rhodococcus sp. Strain BCP1 Grown on N -alkanes. *Appl. Environ. Microbiol.* 77, 1619–1627. doi:10.1128/aem.01987-10

Cappelletti, M., Fedi, S., Zampolli, J., Di Canito, A., D'Ursi, P., Orro, A., et al. (2016). Phenotype Microarray Analysis May Unravel Genetic Determinants of the Stress Response by Rhodococcus aetherivorans BCP1 and Rhodococcus opacus R7. *Res. Microbiol.* 167, 766–773. doi:10.1016/j.resmic.2016.06.008

Cappelletti, M., Presentato, A., Piacenza, E., Firrincieli, A., Turner, R. J., and Zannoni, D. (2020). Biotechnology of Rhodococcus for the Production of Valuable Compounds. *Appl. Microbiol. Biotechnol.* 104, 8567–8594. doi:10.1007/s00253-020-10861-z

Cappelletti, M., Zampolli, J., Di Gennaro, P., and Zannoni, D. (2019). "Genomics of Rhodococcus," in *Biology of Rhodococcus* (Springer International Publishing), 23–60. doi:10.1007/978-3-030-11461-9_2

Chaumeil, P.-A., Mussig, A. J., Hugenholtz, P., and Parks, D. H. (2019). GTDB-tk: A Toolkit to Classify Genomes with the Genome Taxonomy Database. *Method. Biochem. Anal.* 36, 1925–1927. doi:10.1093/bioinformatics/btz848

Chen, Y., Ding, Y., Yang, L., Yu, J., Liu, G., Wang, X., et al. (2013). Integrated Omics Study Delineates the Dynamics of Lipid Droplets in Rhodococcus opacus PD630. *Nucleic Acids Res.* 42, 1052–1064. doi:10.1093/nar/gkt932

de Carvalho, C. C. C. R., Marques, M. P. C., Hachicho, N., and Heipieper, H. J. (2014). Rapid Adaptation of Rhodococcus erythropolis Cells to Salt Stress by Synthesizing Polyunsaturated Fatty Acids. *Appl. Microbiol. Biotechnol.* 98, 5599–5606. doi:10.1007/s00253-014-5549-2

DeLorenzo, D. M., Rottinghaus, A. G., Henson, W. R., and Moon, T. S. (2018). Molecular Toolkit for Gene Expression Control and Genome Modification in Rhodococcus opacus PD630. *ACS Synth. Biol.* 7, 727–738. doi:10.1021/acssynbio.7b00416

Donini, E., Firrincieli, A., and Cappelletti, M. (2021). Systems Biology and Metabolic Engineering of Rhodococcus for Bioconversion and Biosynthesis Processes. *Folia Microbiol.* 66, 701–713. doi:10.1007/s12223-021-00892-y

Henson, W. R., Campbell, T., DeLorenzo, D. M., Gao, Y., Berla, B., Kim, S. J., et al. (2018). Multi-omic Elucidation of Aromatic Catabolism in Adaptively Evolved Rhodococcus opacus. *Metab. Eng.* 49, 69–83. doi:10.1016/j.ymben.2018.06.009

Holder, J. W., Ulrich, J. C., DeBono, A. C., Godfrey, P. A., Desjardins, C. A., Zucker, J., et al. (2011). Comparative and Functional Genomics of Rhodococcus opacus PD630 for Biofuels Development. *Plos Genet.* 7, e1002219. doi:10.1371/journal.pgen.1002219

Hunt, M., Silva, N. D., Otto, T. D., Parkhill, J., Keane, J. A., and Harris, S. R. (2015). Circlator: Automated Circularization of Genome Assemblies Using Long Sequencing Reads. *Genome Biol.* 16, 1–10. doi:10.1186/s13059-015-0849-0

Janet, D. (2014). Whole Genome Sequencing of *Rhodococcus opacus* PD630. Short Read Archive Available at: https://www.ncbi.nlm.nih.gov/sra/SRX875494.

Kim, H. M., Chae, T. U., Choi, S. Y., Kim, W. J., and Lee, S. Y. (2019). Engineering of an Oleaginous Bacterium for the Production of Fatty Acids and Fuels. *Nat. Chem. Biol.* 15, 721–729. doi:10.1038/s41589-019-0295-5

Koren, S., Walenz, B. P., Berlin, K., Miller, J. R., Bergman, N. H., and Phillippy, A. M. (2017). Canu: Scalable and Accurate Long-Read Assembly via Adaptive K-Mer Weighting and Repeat Separation. *Genome Res.* 27, 722–736. doi:10.1101/gr.215087.116

Laver, T., Harrison, J., O'Neill, P. A., Moore, K., Farbos, A., Paszkiewicz, K., et al. (2015). Assessing the Performance of the Oxford Nanopore Technologies MinION. *Biomol. Detect. Quantification* 3, 1–8. doi:10.1016/j.bdq.2015.02.001

Li, W., O'Neill, K. R., Haft, D. H., DiCuccio, M., Chetvernin, V., Badretdin, A., et al. (2020). RefSeq: Expanding the Prokaryotic Genome Annotation Pipeline Reach with Protein Family Model Curation. *Nucleic Acids Res.* 49, D1020–D1028. doi:10.1093/nar/gkaa1105

Liang, Y., and Yu, H. (2021). Genetic Toolkits for Engineering Rhodococcus Species with Versatile Applications. *Biotechnol. Adv.* 49, 107748. doi:10.1016/j.biotechadv.2021.107748

Manni, M., Berkeley, M. R., Seppey, M., Simão, F. A., and Zdobnov, E. M. (2021). BUSCO Update: Novel and Streamlined Workflows along with Broader and Deeper Phylogenetic Coverage for Scoring of Eukaryotic, Prokaryotic, and Viral Genomes. *Mol. Biol. Evol.* 38, 4647–4654. doi:10.1093/molbev/msab199

Minkin, I., Patel, A., Kolmogorov, M., Vyahhi, N., and Pham, S. (2013). Sibelia: A Scalable and Comprehensive Synteny Block Generation Tool for Closely Related Microbial Genomes. *Lecture Notes in Computer Science (including subseries Lecture Notes in Artificial Intelligence and Lecture Notes in Bioinformatics)* 8126 LNBI, 215–229. doi:10.1007/978-3-642-40453-5_17

Monnahan, P. J., Michno, J. M., O'Connor, C., Brohammer, A. B., Springer, N. M., McGaugh, S. E., et al. (2020). Using Multiple Reference Genomes to Identify and Resolve Annotation Inconsistencies. *BMC* 21. doi:10.1186/s12864-020-6696-8

Orro, A., Cappelletti, M., D'Ursi, P., Milanesi, L., Di Canito, A., Zampolli, J., et al. (2015). Genome and Phenotype Microarray Analyses of Rhodococcus sp. BCP1 and Rhodococcus opacus R7: Genetic Determinants and Metabolic Abilities with Environmental Relevance. *PLoS ONE* 10, e0139467. doi:10.1371/journal.pone.0139467

Pátek, M., Grulich, M., and Nešvera, J. (2021). Stress Response in Rhodococcus Strains. *Biotechnol. Adv.* 53, 107698. doi:10.1016/j.biotechadv.2021.107698

Sohn, J.-i., and Nam, J.-W. (2016). The Present and Future of de Novo Whole-Genome. *Brief Bioinform* 19, bbw096. doi:10.1093/bib/bbw096

Walker, B. J., Abeel, T., Shea, T., Priest, M., Abouelliel, A., Sakthikumar, S., et al. (2014). Pilon: An Integrated Tool for Comprehensive Microbial Variant Detection and Genome Assembly Improvement. *PLoS ONE* 9, e112963. doi:10.1371/journal.pone.0112963

Wetzel, J., Kingsford, C., and Pop, M. (2011). Assessing the Benefits of Using Mate-Pairs to Resolve Repeats in De Novo Short-Read Prokaryotic Assemblies. *BMC Bioinformatics* 12, 1–14. doi:10.1186/1471-2105-12-95

Wick, R. R., and Holt, K. E. (2021). Benchmarking of Long-Read Assemblers for Prokaryote Whole Genome Sequencing. *F1000Res* 8, 2138. doi:10.12688/f1000research.21782.4

Yoneda, A., Henson, W. R., Goldner, N. K., Park, K. J., Forsberg, K. J., Kim, S. J., et al. (2016). Comparative Transcriptomics Elucidates Adaptive Phenol Tolerance and Utilization in Lipid-accumulating Rhodococcus opacus PD630. *Nucleic Acids Res.* 44, 2240–2254. doi:10.1093/nar/gkw055

Conflict of Interest: The authors declare that the research was conducted in the absence of any commercial or financial relationships that could be construed as a potential conflict of interest.

Publisher's Note: All claims expressed in this article are solely those of the authors and do not necessarily represent those of their affiliated organizations, or those of the publisher, the editors, and the reviewers. Any product that may be evaluated in this article, or claim that may be made by its manufacturer, is not guaranteed or endorsed by the publisher.

frontiers | Frontiers in Bioengineering and Biotechnology

TYPE Original Research
PUBLISHED 02 September 2022
DOI 10.3389/fbioe.2022.998800

OPEN ACCESS

EDITED BY
Panagiotis Madesis,
University of Thessaly, Greece

REVIEWED BY
Richa Arora,
Punjab Agricultural University, India
Huaiwei Liu,
Shandong University, China

*CORRESPONDENCE
Yao Yu,
yaoyu@fudan.edu.cn
Hong Lu,
honglv@fudan.edu.cn

SPECIALTY SECTION
This article was submitted to Industrial Biotechnology,
a section of the journal
Frontiers in Bioengineering and Biotechnology

RECEIVED 20 July 2022
ACCEPTED 12 August 2022
PUBLISHED 02 September 2022

CITATION
Ai Y, Luo R, Yang D, Ma J, Yu Y and Lu H (2022), Fluorescence lifetime imaging of NAD(P)H upon oxidative stress in Kluyveromyces marxianus.
Front. Bioeng. Biotechnol. 10:998800.
doi: 10.3389/fbioe.2022.998800

Fluorescence lifetime imaging of NAD(P)H upon oxidative stress in *Kluyveromyces marxianus*

Yi Ai[1,2], Ruoyu Luo[1], Deqiang Yang[1,2], Jiong Ma[3], Yao Yu[1,2]* and Hong Lu[1,2]*

[1]State Key Laboratory of Genetic Engineering, School of Life Sciences, Fudan University, Shanghai, China, [2]Shanghai Engineering Research Center of Industrial Microorganisms, Fudan University, Shanghai, China, [3]Key Laboratory of Micro and Nano Photonic Structures (Ministry of Education), Shanghai Engineering Research Center of Ultra-precision Optical Manufacturing, Department of Optical Science and Engineering, School of Information Science and Technology, Fudan University, Shanghai, China

K. marxianus is a promising cell factory for producing heterologous proteins. Oxidative stresses were raised during overexpression of heterologous proteins, leading to the shift of the redox state. How to measure the redox state of live *K. marxianus* cells without perturbing their growth remains a big challenge. Here, a fluorescence lifetime imaging (FLIM)-based method was developed in live *K. marxianus* cells. During the early exponential growth, *K. marxianus* cells exhibited an increased mean fluorescence lifetime (τ-mean) of NAD(P)H compared with *Saccharomyces cerevisiae* cells, which was consistent with the preference for respiration in *K. marxianus* cells and that for fermentation in *S. cerevisiae* cells. Upon oxidative stresses induced by high temperature or H_2O_2, *K. marxianus* cells exhibited an increased τ-mean in company with decreased intracellular NAD(P)H/NAD(P)$^+$, suggesting a correlation between an increased τ-mean and a more oxidized redox state. The relationship between τ-mean and the expression level of a heterologous protein was investigated. There was no difference between the τ-means of *K. marxianus* strains which were not producing a heterologous protein. The τ-mean of a strain yielding a high level of a heterologous protein was higher than that of a low-yielding strain. The results suggested the potential application of FLIM in the non-invasive screen of high-yielding cells.

KEYWORDS

***Kluyveromyces marxianus*, oxidative stress, NAD(P)H autofluorescence, FLIM, heterologous protein**

Introduction

K. marxianus is a promising microbial cell factory for producing heterologous proteins, bioethanol and bulk chemicals (Karim et al., 2020; Leonel et al., 2021). During the production of heterologous proteins, yeast faces various extracellular disturbances, including high temperature, high salt and abnormal pH, which imbalance the redox state of yeast cells (Qiu et al., 2019). For example, high

temperature increases the production of intracellular reactive oxygen species (ROS), causing oxidative stress to the yeast (Fu et al., 2019). A high concentration of salt disturbs redox homeostasis, leading to oxidative damage (Ramos-Moreno et al., 2019). Meanwhile, oxidative stresses are invoked endogenously during the overexpression of heterologous proteins, because the increased demand for NAD(P)H is raised in different steps of protein production, including amino acid biosynthesis (Zhu et al., 2021), disulfide bond formation (Miller et al., 2018), and protein secretion (Tomàs-Gamisans et al., 2020). Therefore, measuring the redox state of live *K. marxianus* cells might be applied to monitor the production of heterologous proteins upon various disturbances.

Chemical and optical methods have been developed to assess the redox state of cells. Chemical methods indirectly infer the redox state of the cell mainly by measuring the concentration of redox pairs such as NAD(P)H/NAD(P)$^+$ (Wang et al., 2017). Optical methods include fluorescent biosensors and autofluorescence methods. Fluorescent biosensors assess redox status at the single-cell level by transferring fluorescent protein-encoding genes (Liao et al., 2020). Using NAD(P)H autofluorescence to assess cellular redox status emerges as a promising method in recent years, as it enables endogenous noninvasive indication of the redox status. NAD(P)H displays a maximum autofluorescence emission wavelength at 450–535 nm when using the single-photon excitation at 340 nm (Cannon et al., 2021). Fluorescence lifetime imaging (FLIM) measures the mean fluorescence lifetime (τ-mean) of NAD(P)H. The lifetime (τ) of free NAD(P)H (τ-free) is usually fixed at about 0.4 ns The τ of bound NAD(P)H (τ-bound) varies with different combined proteins and is usually around 1–4 ns (Schaefer et al., 2019). The ratio of free NAD(P)H and bound NAD(P)H to the total intracellular NAD(P)H is defined as a1 and a2, respectively (Kolenc and Quinn, 2019). a1/a2 is correlated with NAD(P)H/NAD(P)$^+$, which defines the redox state of cells (Sant'Anna-Silva et al., 2018). Usually, a more oxidized state increases both τ-mean and τ-bound, while reducing a1/a2 (Schaefer et al., 2017; Meleshina et al., 2018). However, there are few reports about the FILM analysis in living yeast cells, including *K. marxianus* cells (Kong et al., 2022).

In this study, the redox state of *K. marxianus* cells was assessed by FLIM of NAD(P)H. *K. marxianus* cells exhibited an increased τ-mean of NAD(P)H compared with *S. cerevisiae* cells during early exponential growth, which was consistent with different Crabtree-effect statuses of two yeasts. *K. marxianus* cells exhibited an increased τ-mean upon oxidative stresses induced by high temperature or H_2O_2, suggesting a correlation between an increased τ-mean and a more oxidized redox state. Notably, an increased τ-mean was correlated the high-level expression of a heterologous protein in *K. marxianus* cells, which suggested a potential application of FLIM in the non-invasive screen of high-yielding cells.

Materials and methods

Yeast strains and plasmids

The *K. marxianus* strain FIM-1 (Wu et al., 2020), and the *S. cerevisiae* strain S288C (Yu et al., 2021), were used in this study. *K. marxianus* strains KML and KMH were derived from KM-HPV2, which expressed IBDV-VP2 by pUKDN115 (Yang et al., 2021). Plasmid expressing IBDV-VP2 was replaced by the void pUKDN115 in KML and KMH to obtain KML_{void} and KMH_{void}, respectively.

Medium and culturing

To compare the redox states of *K. marxianus* and *S. cerevisiae* cells, FIM-1 and S288C cells were grown in a YPD medium (20 g/L tryptone, 10 g/L yeast extract, 20 g/L glucose) at 30°C overnight and the culture was diluted into a fresh YPD medium to start at an OD_{600} of 0.1. Cells were then grown at 30°C for 3 h. To compare redox states at different temperatures, overnight culture of FIM-1 was inoculated into a fresh YPD medium to start at an OD_{600} of 0.1 and then grown at 30°C or 45°C for 24 h. To perform the H_2O_2 treatment, FIM-1 cells were grown at 30°C for 24 h and then grown in the presence of 20 mM H_2O_2 for 1 h. Untreated culture served as a control. To compare redox states during expressing IBDV-VP2, KML and KMH cells were grown in the YD medium (20 g/L yeast extract, 40 g/L glucose) for 3 days. Cells were collected after 1 or 3 days.

Measurement of dissolved oxygen, residual glucose and ethanol

The culture of FIM-1 and S288C was centrifuged and the supernatant was subjected to analysis. The amount of dissolved oxygen was measured by a dissolved oxygen analyzer (JPSJ-605F, Shanghai INESA Scientific Instrument, China) according to the manufacturer's manual. Residual glucose and ethanol was measured on high-performance liquid chromatography (1260, Agilent, United States) as described before (Ai et al., 2022).

Preparation of yeast cells for fluorescence lifetime imaging

To immobilize yeast cells, 20–25 μl of ConA (10 mg/ml, C2010, Sigma-Aldrich, United States) was spread onto the bottom of a glass-bottom petri dish (801001, NEST, China) and the dish was left to dry overnight at room temperature. Yeast cells were pelleted and resuspended in sterile water to an OD_{600} of 5. A total of 5 μl sample was transferred to the ConA-coated dish for analysis.

Fluorescence lifetime imaging imaging and data analysis

FLIM was performed by a Leica TCS SP8 DIVE FALCON microscope (Leica, Germany) equipped with a ×63 water immersion objective (N.A. = 1.2) excited by a femtosecond pulsed laser with ~3 mW power at 740 nm (InSight X3 Dual, Spectra-Physics, United States). The FLIM images were exported in lif format and ROIs were selected for processing in Leica Application Suite X software to obtain fluorescence lifetime data. The sizes of experimental ROIs samples ranged from 52 to 104. The data were fitted using a double exponential model as τ-mean = a1 τ-free + a2 τ-bound (Kong et al., 2022). Statistical analyses were performed by GraphPad-Prism version 8.0 software (GraphPad, United States). As to the significance test, data that did not follow a normal distribution was tested using the nonparametric Mann-Whitney test. Data that followed a normal distribution and satisfied the homogeneity of variances was tested using an unpaired *t*-test. Otherwise, Welch's modified unpaired *t*-test was used.

Measurement of intracellular concentrations of NAD(P)$^+$ and NAD(P)H

Concentrations of intracellular NAD$^+$, NADH, NADP$^+$ and NADPH were determined by a WST-8 based colorimetric assay using commercial kits (S0175 and S0179, Beyotimes, China). To collect cells grown at different temperatures and cells treated with H_2O_2, FIM-1 cells were cultured as described above in "Medium and culturing". Cells of 20 OD_{600} were collected, washed and then suspended in 200 µl extraction buffer provided by the kit. Cells were then mixed with 200 µl acid-washed glass beads (G8772, Sigma-Aldrich, United States) and processed by a bead-beater (FastPrep-24, MP, United States) at 6 m/s for 2 min. The lysate was centrifuged at 13,200 rpm for 10 min at 4°C. A total of 20 and 50 µl supernatant was collected for NAD$^+$/NADH and NADP$^+$/NADPH assay, respectively. Experiments were performed in triplicates and repeated three times. Ratios of NADH/NAD$^+$, NADPH/NADP$^+$ and NAD(P)H/NAD(P)$^+$ were calculated based on the concentrations.

Results

The redox states of *K. Marxianus* and *S. cerevisiae* cells could be differentiated by the τ-mean of NAD(P)H

In yeast, the metabolic flow of glucose between ethanol fermentation and aerobic respiration influences the redox state of cells. In ethanol fermentation, 1 molecule of glucose produces 2 molecules of NADH through glycolysis and NADH is subsequently oxidized by ethanol dehydrogenase to regenerate NAD$^+$ (Figure 1A). In comparison, 10 molecules of NADH are produced in aerobic respiration and oxidized by oxidative phosphorylation, which increases the chance to produce reactive oxygen species (ROS) and biases the cell toward a more oxidized state (Scialò et al., 2017) (Figure 1A).

Metabolic flows of glucose in *S. cerevisiae* cells (SC228C) and *K. marxianus* cells (FIM-1) during the early exponential growth were investigated in the first place. After 3 h of growth in the YPD medium (containing 20 g/L glucose), the OD_{600} of *K. marxianus* cells was 1.49 times that of *S. cerevisiae* cells (Figure 1B). Compared with the medium without inoculation, dissolved oxygen in the culture of *S. cerevisiae* cells decreased by 1.36%, while that of *K. marxianus* cells decreased by 36.5% (Figure 1C). The amount of glucose consumed by *K. marxianus* cells was 29% of that by *S. cerevisiae* cells (Figure 1D). The concentration of ethanol in the culture of *S. cerevisiae* cells was 0.71 g/L, while there was hardly any ethanol produced by *K. marxianus* cells (Figure 1E). The results suggested that *S. cerevisiae* cells preferred fermentation in the aerobic condition with excess glucose, which was consistent with the Crabtree-positive identity of *S. cerevisiae* (Dai et al., 2018). Meanwhile, results suggested that *K. marxianus* cells preferentially used respiration in the presence of oxygen and glucose, which was consistent with the Crabtree-negative identity of *K. marxianus* (Sakihama et al., 2019; Yu et al., 2021). Different ways to assimilate glucose suggested distinct redox states in *S. cerevisiae* and *K. marxianus* cells.

To compare the redox states of two yeasts, the fluorescence lifetime of NAD(P)H in cells was analyzed by FLIM. In the pseudocolor mapping of NAD(P)H lifetime, *K. marxianus* cells displayed yellow-green and *S. cerevisiae* cells displayed light blue (Figure 1F), suggesting NAD(P)H lifetime of *K. marxianus* cells was longer. Consistently, τ-means of NAD(P)H *in K. marxianus and S. cerevisiae* cells were quantified as 1.21 ± 0.27 ns and 0.94 ± 0.19 ns, respectively (Figure 1G, left). The a1/a2 of *K. marxianus* cells (2.23) was significantly lower than that in *S. cerevisiae* cells (3.40) (Figure 1G, middle), suggesting the redox state of *K. marxianus* cells was relatively more oxidized. The lower a1/a2 of *K. marxianus* cells was mainly due to significantly increased τ-bound of NAD(P)H (Figure 1G, right), as more NAD(P)H might bind with enzymes during aerobic respiration in *K. marxianus* cells. In general, the redox state of *K. marxianus* and *S. cerevisiae* cells could be differentiated by the τ-mean of NAD(P)H, as a longer τ-mean of *K. marxianus cells* suggested a more oxidized state.

K. marxianus cells exhibited an increased τ-mean of NAD(P)H upon oxidative stress induced by high temperature or H_2O_2 treatment

High temperature and H_2O_2 induced oxidative stress in *K. marxianus* (Arellano-Plaza et al., 2017; Fu et al., 2019). Increased

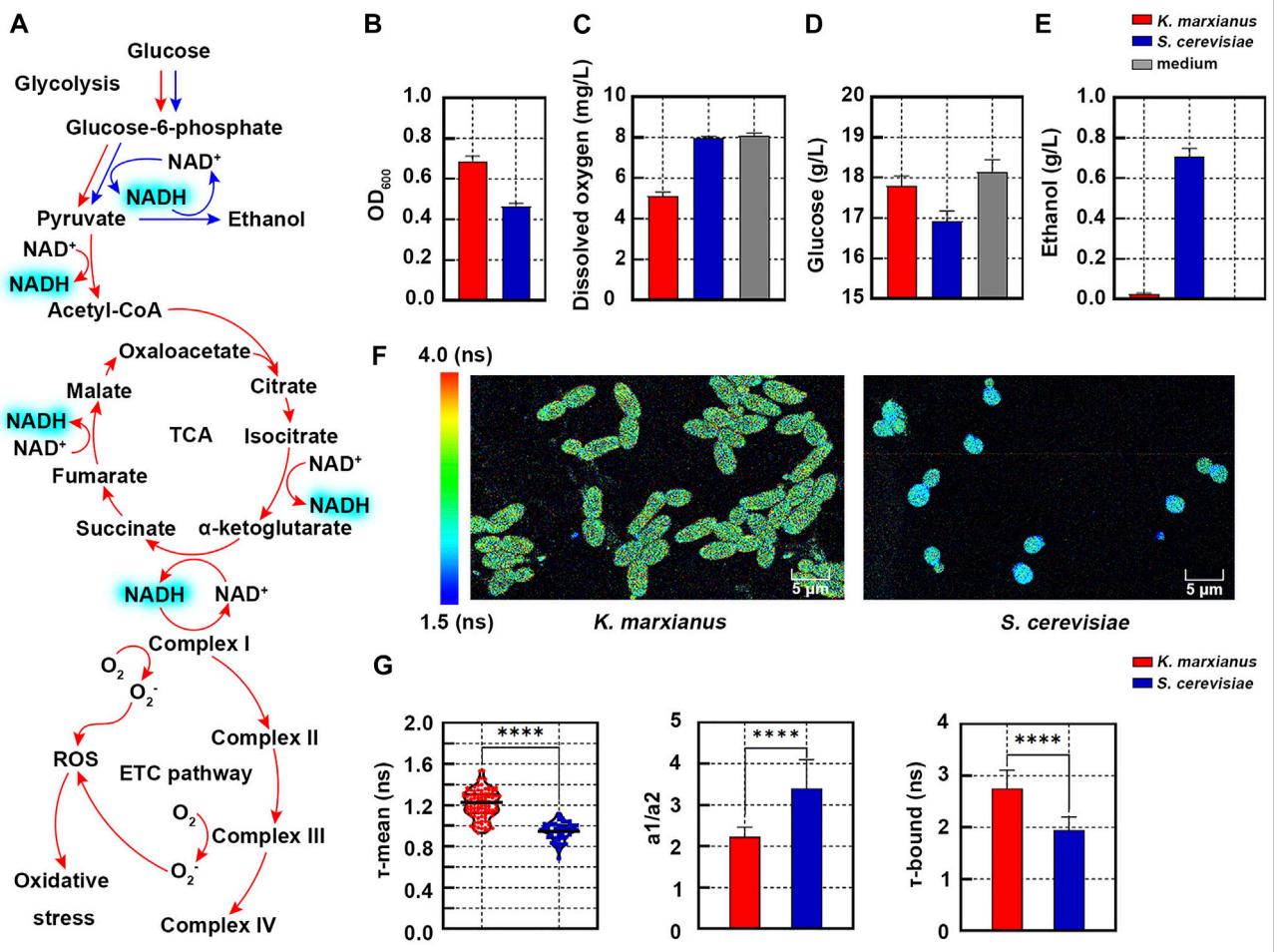

FIGURE 1
Redox states of *K. marxianus* and *S. cerevisiae* cells characterized by FLIM. **(A)** Aerobic respiration (red) and ethanol fermentation (blue) pathways in yeast. **(B–E)** OD_{600} **(B)**, dissolved oxygen **(C)**, residual glucose **(D)** and ethanol **(E)** in the culture of *K. marxianus* (FIM-1) and *S. cerevisiae* (S288C) cells after 3 h of growth. Medium without inoculation served as a control. Values represented mean ± SD (n = 3). **(F)** FLIM of NAD(P)H in *K. marxianus* and *S. cerevisiae* cells after 3 h of growth. Pseudocolor mapping of NAD(P)H fluorescence lifetimes was shown. The lifetime of NAD(P)H from 1.5 to 4.0 ns was assigned different colors. **(G)** Quantitative analysis of NAD(P)H fluorescence in cells from **(F)**. A violin plot showed the distribution of τ-mean of cells and the mean value was indicated by a black line. Histograms showed a1/a2 and τ-bound, in which values represented mean ± SD. A total of 101 *K. marxianus* cells and 52 *S. cerevisiae* cells were counted. ****$p < 0.0001$.

consumption of free NADPH is required to alleviate oxidative stress (Figure 2A), which is expected to shift the redox state (Mara et al., 2018).

To investigate the redox state at a high temperature, *K. marxianus* cells (FIM-1) were grown at 30°C or 45°C for 24 h. Pseudocolor mapping of NAD(P)H lifetime of cells at 30°C showed dark blue and faint cyan, indicating a shorter lifetime (Figure 2B). Most of the cells at 45°C displayed yellow-green, indicating a longer lifetime (Figure 2B). The τ-mean of NAD(P)H of cells grown at 30°C was 0.94 ± 0.09 ns and that of cells grown at 45°C was significantly increased to 1.10 ± 0.09 ns (Figure 2C, left), suggesting a relative oxidative state of cells at high temperature. The a1/a2 of cells grown at 45°C was significantly lower than that at 30°C (Figure 2C, middle). τ-bound of cells grown at 45°C was significantly longer than that at 30°C (Figure 2C, right).

Similar to the situation of cells grown at a high temperature, the τ-mean of NAD(P)H of cells treated with 20 mM H_2O_2 (1.12 ± 0.13 ns) was significantly longer than that in untreated cells (1.04 ± 0.07 ns) (Figure 2D, left). τ-bound of treated cells was significantly longer than that of control cells (Figure 2D, right). However, a1/a2 of treated cells did not change significantly (Figure 2D, middle), probably due to the increased fluctuation of cell statuses upon H_2O_2 treatment.

To confirm the relationship between NAD(P)H content and τ-mean, concentrations of intracellular NADH, NAD^+, NADPH and $NADP^+$ were determined by a colorimetric chemical assay. As shown in Figure 2E, NADH/NAD^+, NADPH/$NADP^+$ and

10.3389/fbioe.2022.998800

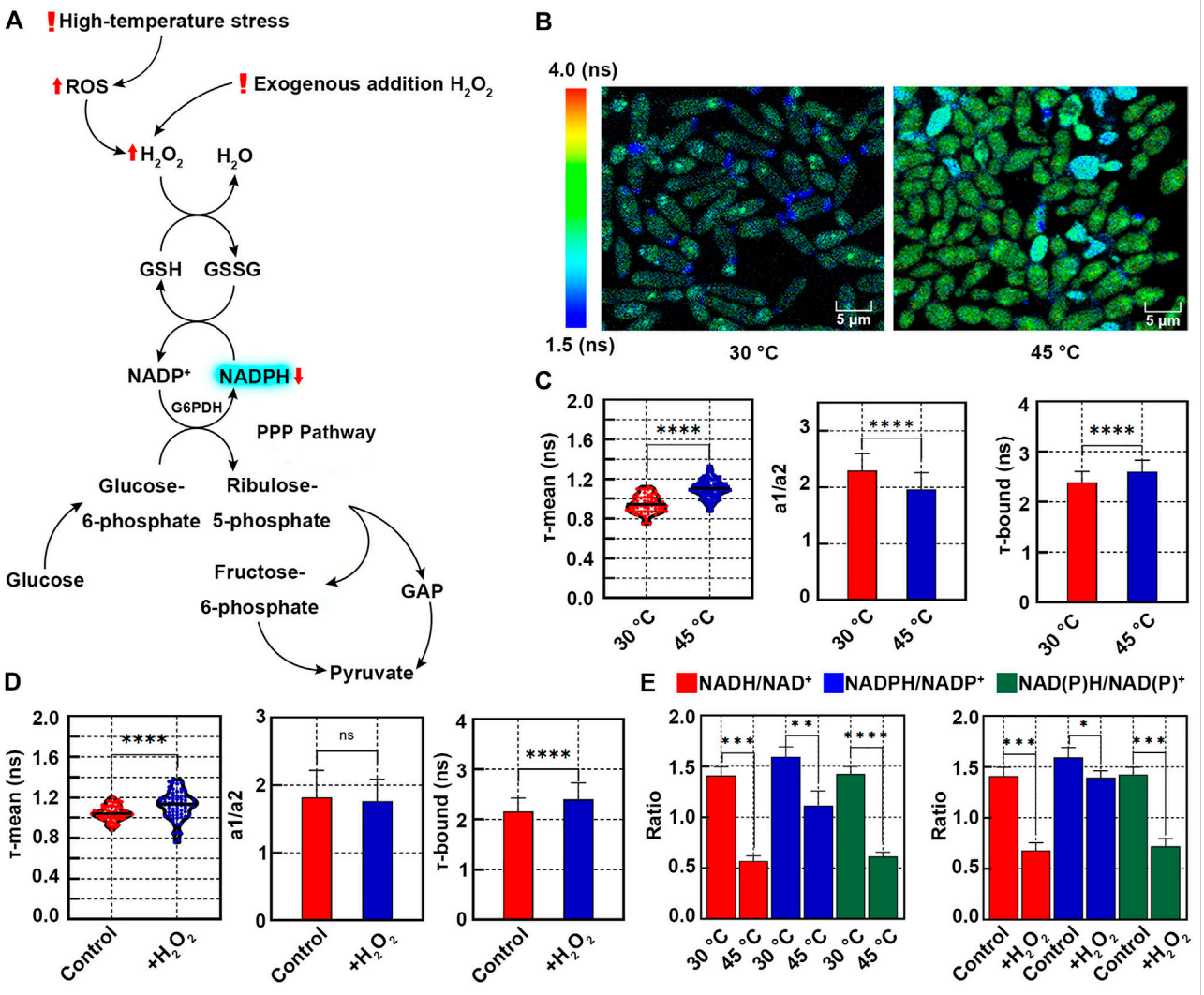

FIGURE 2
Redox states of *K. marxianus* cells upon oxidative stress induced by high-temperature or H_2O_2 treatment. **(A)** Oxidative stress induced by high temperature or H_2O_2 leads to the increased consumption of NADPH. **(B)** FLIM of NAD(P)H in cells grown at 30°C or 45°C. Pseudocolor mapping of NAD(P)H fluorescence lifetimes was shown. The lifetime from 1.5 to 4.0 ns was assigned different colors. **(C)** Quantitative analysis of NAD(P)H fluorescence lifetimes of cells in **(B)**. A violin plot showed the distribution of τ-mean of cells and the mean value was indicated by a black line. Histograms showed a1/a2 and τ-bound, in which values represented mean ± SD. A total of 68 cells grown at 30°C and 112 cells grown at 45°C were counted. ****$p < 0.0001$. **(D)** Quantitative analysis of NAD(P)H fluorescence lifetimes of cells treated with H_2O_2. A total of 66 control cells and 69 cells treated with H_2O_2 were counted. "ns" indicated $p > 0.05$. **(E)** Ratios of $NADH/NAD^+$, $NADPH/NADP^+$ and $NAD(P)H/NAD(P)^+$ of cells grown at high temperature or treated with H_2O_2. Concentrations of intracellular NAD^+, NADH, $NADP^+$ and NADPH were measured by a chemical assay. Ratios were calculated based on the concentrations. Values represented mean ± SD ($n = 3$). *$p < 0.05$; **$p < 0.01$; ***$p < 0.001$.

$NAD(P)H/NAD(P)^+$ of cells grown at 45°C were all significantly decreased, compared with their counterparts of cells grown at 30°C. Similarly, H_2O_2 treatment significantly decreased $NADH/NAD^+$, $NADPH/NADP^+$ and $NAD(P)H/NAD(P)^+$ of cells (Figure 2E, right). The results were consistent with increased consumption of free NADPH upon oxidative stress induced by high temperature or H_2O_2 (Figure 2A). Therefore, an increased τ-mean of NAD(P)H of *K. marxianus* cells could be applied to indicate a shift in redox state [defined by $NAD(P)H/NAD(P)^+$] toward a more oxidative status.

K. marxianus cells with a high yield of a heterologous protein exhibited an increased τ-mean of NAD(P)H

Overexpressing heterologous proteins raised oxidative stress in yeast (Huang et al., 2017). To compare redox states of cells displaying different expression levels of a heterologous protein, two *K. marxianus* strains, KML and KMH were selected. In our previous study, KM-HPV2 was constructed to express infectious

10.3389/fbioe.2022.998800

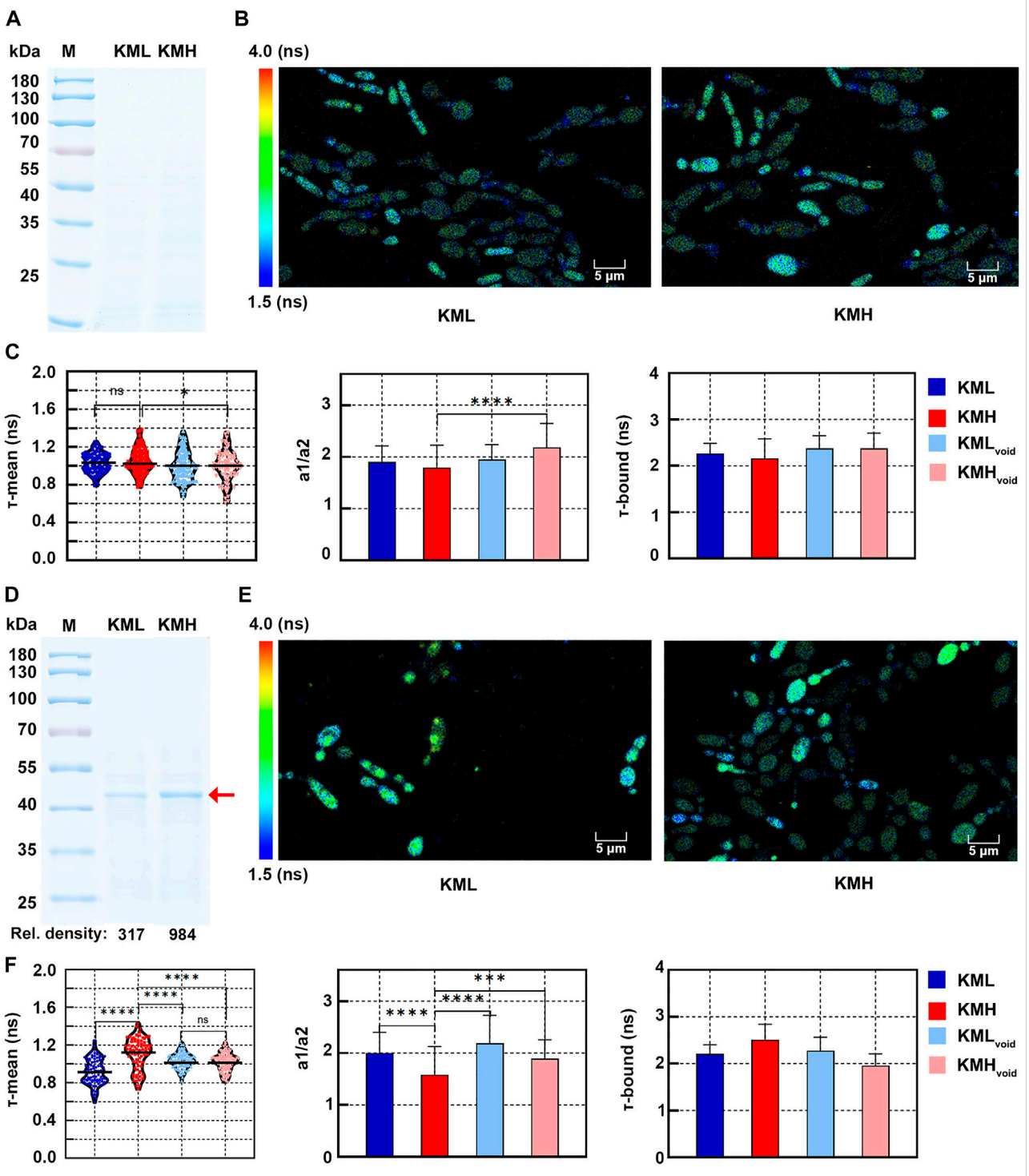

FIGURE 3
Redox states of *K. marxianus* cells displaying different expression levels of a heterologous protein. **(A)** SDS-PAGE of supernatant of KML and KMH culture after 1 day of growth. **(B)** FLIM of NAD(P)H in KML and KMH cells after 1 day of growth. Pseudocolor mapping of NAD(P)H fluorescence lifetimes was shown. The lifetime from 1.5 to 4.0 ns was assigned different colors. **(C)** Quantitative analysis of NAD(P)H fluorescence lifetimes of cells after 1 day of growth. A violin plot showed the distribution of τ-mean of cells and the mean value was indicated by a black line. Histograms showed a1/a2 and τ-bound, in which values represented mean ± SD. A total of 94 KML, 105 KMH, 104 KML$_{void}$ and 78 KMH$_{void}$ cells were counted. "ns" indicated $p > 0.05$. *$p < 0.05$; ****$p < 0.0001$. **(D)** SDS-PAGE of supernatant of KML and KMH culture after 3 days of growth. The position of IBDV-VP2 was indicated by a red arrow and the relative densities of bands were shown below. **(E)** Pseudocolor mapping of NAD(P)H fluorescence lifetimes of KML and KMH cells after 3 days of growth. **(F)** Quantitative analysis of NAD(P)H fluorescence lifetimes of cells after 1 day of growth. A total of 91 KML, 79 KMH, 96 KML$_{void}$ and 102 KML$_{void}$ cells were counted. ***$p < 0.001$.

bursal disease virus (IBDV) capsid VP2 by an episomal vector (Yang et al., 2021). KM-HPV2 was subjected to the H_2O_2 mutagenesis. Among the mutated strains, KML and KMH displayed low and high-level expressions of IBDV-VP2, respectively. As controls, VP2-expressing vectors in KML and KMH strains were replaced by void vectors to obtain KML_{void} and KMH_{void}, respectively.

After 1 day of growth, IBDV-VP2 could not be detected in the supernatant of KML or KMH culture in SDS-PAGE (Figure 3A), suggesting the expression of IBDV-VP2 in either strain was low. In the pseudocolor mapping of NAD(P)H lifetime, most KML and KMH cells displayed blue-green, indicating a short lifetime (Figure 3B). In the quantitative analysis (Figure 3C), there was no significant difference between the τ-mean of KMH (1.05 ± 0.13 ns) cells and that of KML (1.03 ± 0.10 ns) cells, suggesting both cells exhibited similar redox states while expressing low levels of IBDV-VP2. However, the τ-mean of KMH cells was significantly longer than that of KMH_{void} cells (1.00 ± 0.16 ns) (Figure 3C, left). Consistently, a1/a2 of KMH cells was significantly lower than that of KMH_{void} cells (Figure 3C, middle). It suggested the redox state of KMH cells was more oxidized than that of KMH_{void} cells, which might be related to IBDV-VP2 produced in KMH cells.

After 3 days of growth, bands corresponding to IBDV-VP2 were visible in the supernatant of KML and KMH culture in SDS-PAGE. The amount of IBDV-VP2 produced by KMH cells was 3 times that by KML cells, as deduced by the relative densities of bands (Figure 3D). A fraction of KML and KMH cells displayed yellow-green in the pseudocolor mapping of NAD(P)H lifetime (Figure 3E), suggesting a longer lifetime compared with that of cells after 1 day of growth. In the quantitative analysis (Figure 3F, left), the τ-mean of KMH cells (1.11 ± 0.17 ns) was significantly higher than that of KML (0.91 ± 0.13 ns), KMH_{void} (1.02 ± 0.09 ns) and KML_{void} cells (1.03 ± 0.08 ns). The distribution of τ-mean of KMH_{void} and KML_{void} cells was more concentrated. It suggested that, after entering the stationary phase, cells without expressing a heterologous protein exhibited a redox state with less fluctuation. Consistent with the highest τ-mean of KMH cells, a1/a2 of KMH cells was the lowest and τ-bound of KMH cells was the longest among their counterparts (Figure 3F, middle and right). The results suggested that, compared with cells with low or no expression of a heterologous protein, KMH cells with a high yield of a heterologous protein exhibited a more oxidized state, which could be indicated by an increased τ-mean of NAD(P)H.

Discussion

Since Britton Chance discovered the autofluorescence of NAD(P)H in the 1950s (Chance, 1952), methods to analyze the cellular redox state analysis based on NAD(P)H autofluorescence, such as FLIM, have been gradually developed (Tornmalm et al., 2019). FLIM is a non-invasive, label-free and *in situ* method, which is suitable for the long-term detection of living cells and therefore is widely applied in clinical research. For example, tumor cells tend to undergo glycolysis, the so-called Warburg effect, which leads to a low fluorescence lifetime of NAD(P)H (Kolenc and Quinn, 2019). Therefore, FLIM is used for early tumor detection (Alfonso-García et al., 2022). The redox states of stem cells change considerably during differentiation and FLIM was applied to track the metabolism changes of stem cells (Okkelman et al., 2020). Yeast is one of the most important microbial cell factories and the yielding of yeast cells was closely related to redox states (Chen et al., 2020). FLIM is well suited to measure the redox state of yeast, which might benefit strain engineering for improved yield. However, few applications of FLIM in yeast were reported so far.

In this study, FLIM was performed to assess the redox states of *K. marxianus* cells upon various oxidative stress. Among the current methods to analyze the redox states of cells, chemical analysis destroys cell integrity and does not allow for single-cell analysis (Kanamori et al., 2018). Although fluorescent biosensors can assess redox states at the single-cell level, they require a long preparation procedure and the introduction of exogenous genes (Liao et al., 2020). In comparison, FILM gives a more natural image of the cell state. For example, high-temperature stress resulted in some cells turning blue in the FLIM (Figure 2B), implying the presence of a large amount of short-lived NAD(P)H in these cells even τ-mean of NAD(P)H of all cells increased. Both high-temperature and H_2O_2 treatment led to an increase of τ-mean of NAD(P)H. But H_2O_2 caused more deviation of τ-mean than high temperature, suggesting more fluctuated redox states were raised among the cells treated by H_2O_2 (Figures 2C,D). There were also shortcomings of FLIM in assessing the redox states of cells. For example, the autofluorescence of NADH and NADPH is optically indistinguishable and therefore FLIM can not analyze individual redox pairs directly. In addition, the fluctuation of τ-mean among individual cells was considerable. Some fluctuation might be due to the genetic diversity among cells, as observed in the offspring of one mother cell (Maclean et al., 2017). Meanwhile, some fluctuation might be due to different phases in the cell cycle, different ages of cells, various epigenetic statuses and some technical issues, such as errors in detecting photorefractive rate. Therefore, synchronization of cells and a more accurate detection apparatus might help to reduce the fluctuation of τ-mean among the population.

Overproduction of heterologous proteins resulted in the reduction of NADPH and that led to an altered redox cofactor state (Tomàs-Gamisans et al., 2020). Consistent with this idea, *K. marxianus* cells with a high yield of a heterologous protein exhibited an increased τ-mean of NAD(P)H (Figure 3F). Therefore, τ-mean of NAD(P)H might be used as an intrinsic marker to screen high-yielding cells. Traditionally, cells expressing heterologous proteins are verified by SDS-PAGE, which was laborious and not suitable for high-throughput

screens. High-throughput screen techniques, such as microfluidics, were developing rapidly in recent years, in which fluorescent markers are usually required (Napiorkowska et al., 2021). For example, fluorescent groups released after enzymatic reactions are applied to the screen of enzymes. But this strategy is not applicable for the screen of non-enzymatic proteins, including antibodies, cytokines and vaccines. Fluorescent fusion proteins, such as GFP-fused proteins, are compatible with the high-throughput screen (Baumann et al., 2018). However, fluorescent fusion proteins sometimes inhibit the natural activity of target proteins (Wick et al., 2019). Since FLIM analysis of NAD(P)H does not require the fluorescent labelling of target proteins or their products, it might be applied to the screen of cells yielding the target protein in its natural form. With the aid of machine learning algorithms and robotic platforms, automatic FLIM analysis and screen are possible (Sagar et al., 2020). If a more general relationship between high-yielding cells and an increased τ-mean of NAD(P)H is confirmed in the future, a FLIM-based screen will boost the optimization of yeast cell factories.

Data availability statement

The original contributions presented in the study are included in the article/Supplementary Material, further inquiries can be directed to the corresponding authors.

Author contributions

HL and YY designed the study and supervised the project. YA performed most of the experiments and analyzed the data. RL and JM assisted data analysis. DY assisted the experiment involving KML and KMH. YA, HL, and YY wrote the manuscript. All authors have revised the manuscript and approved the final version.

Funding

This study was supported by Shanghai Municipal Education Commission (2021-03-52), Science and Technology Research Program of Shanghai (18391901800), Science and Technology Research Program of Shanghai (19DZ2282100), the National Key Research and Development Program of China (2021YFF0502900), National Natural Science Foundation of China (62175034, 62175036) and Shanghai Natural Science Foundation (20ZR1405100).

Conflict of interest

The authors declare that the research was conducted in the absence of any commercial or financial relationships that could be construed as a potential conflict of interest.

Publisher's note

All claims expressed in this article are solely those of the authors and do not necessarily represent those of their affiliated organizations, or those of the publisher, the editors and the reviewers. Any product that may be evaluated in this article, or claim that may be made by its manufacturer, is not guaranteed or endorsed by the publisher.

References

Ai, Y., Luo, T., Yu, Y., Zhou, J., and Lu, H. (2022). Downregulation of ammonium uptake improves the growth and tolerance of *Kluyveromyces marxianus* at high temperature. *MicrobiologyOpen* 11 (3), e1290. doi:10.1002/mbo3.1290

Alfonso-García, A., Zhou, X., Bec, J., Anbunesan, S. N., Fereidouni, F., Jin, L. W., et al. (2022). First in patient assessment of brain tumor infiltrative margins using simultaneous time-resolved measurements of 5-ALA-induced PpIX fluorescence and tissue autofluorescence. *J. Biomed. Opt.* 27 (2), 20501. doi:10.1117/1.Jbo.27.2.020501

Arellano-Plaza, M., Noriega-Cisneros, R., Clemente-Guerrero, M., Gonzalez-Hernandez, J. C., Robles-Herrera, P. D., Manzo-Avalos, S., et al. (2017). Fermentative capacity of *Kluyveromyces marxianus* and *Saccharomyces cerevisiae* after oxidative stress. *J. Inst. Brew.* 123, 519–526. doi:10.1002/jib.451

Baumann, L., Rajkumar, A. S., Morrissey, J. P., Boles, E., and Oreb, M. (2018). A yeast-based biosensor for screening of short- and medium-chain fatty acid production. *ACS Synth. Biol.* 7 (11), 2640–2646. doi:10.1021/acssynbio.8b00309

Cannon, T. M., Lagarto, J. L., Dyer, B. T., Garcia, E., Kelly, D. J., Peters, N. S., et al. (2021). Characterization of NADH fluorescence properties under one-photon excitation with respect to temperature, pH, and binding to lactate dehydrogenase. *OSA Contin.* 4 (5), 1610–1625. doi:10.1364/osac.423082

Chance, B. (1952). Spectra and reaction kinetics of respiratory pigments of homogenized and intact cells. *Nature* 169 (4293), 215–221. doi:10.1038/169215a0

Chen, R., Yang, S., Zhang, L., and Zhou, Y. J. (2020). Advanced strategies for production of natural products in yeast. *iScience* 23 (3), 100879. doi:10.1016/j.isci.2020.100879

Dai, Z., Huang, M., Chen, Y., Siewers, V., and Nielsen, J. (2018). Global rewiring of cellular metabolism renders *Saccharomyces cerevisiae* Crabtree negative. *Nat. Commun.* 9 (1), 3059. doi:10.1038/s41467-018-05409-9

Fu, X., Li, P., Zhang, L., and Li, S. (2019). Understanding the stress responses of *Kluyveromyces marxianus* after an arrest during high-temperature ethanol fermentation based on integration of RNA-Seq and metabolite data. *Appl. Microbiol. Biotechnol.* 103 (6), 2715–2729. doi:10.1007/s00253-019-09637-x

Huang, M., Bao, J., Hallström, B. M., Petranovic, D., and Nielsen, J. (2017). Efficient protein production by yeast requires global tuning of metabolism. *Nat. Commun.* 8 (1), 1131. doi:10.1038/s41467-017-00999-2

Kanamori, K. S., de Oliveira, G. C., Auxiliadora-Martins, M., Schoon, R. A., Reid, J. M., and Chini, E. N. (2018). Two different methods of quantification of oxidized nicotinamide adenine dinucleotide (NAD(+)) and reduced nicotinamide adenine dinucleotide (NADH) intracellular levels: Enzymatic coupled cycling assay and ultra-performance liquid chromatography (UPLC)-Mass spectrometry. *Bio. Protoc.* 8 (14), e2937. doi:10.21769/BioProtoc.2937

Karim, A., Gerliani, N., and Aïder, M. (2020). *Kluyveromyces marxianus*: An emerging yeast cell factory for applications in food and biotechnology. *Int. J. Food Microbiol.* 333, 108818. doi:10.1016/j.ijfoodmicro.2020.108818

Kolenc, O. I., and Quinn, K. P. (2019). Evaluating cell metabolism through autofluorescence imaging of NAD(P)H and FAD. *Antioxid. Redox Signal.* 30 (6), 875–889. doi:10.1089/ars.2017.7451

Kong, Y., Zhao, Y., Yu, Y., Su, W., Liu, Z., Fei, Y., et al. (2022). Single cell sorting of young yeast based on label-free fluorescence lifetime imaging microscopy. *J. Biophot.* 15 (4), e202100344. doi:10.1002/jbio.202100344

Leonel, L. V., Arruda, P. V., Chandel, A. K., Felipe, M. G. A., and Sene, L. (2021). *Kluyveromyces marxianus*: A potential biocatalyst of renewable chemicals and lignocellulosic ethanol production. *Crit. Rev. Biotechnol.* 41 (8), 1131–1152. doi:10.1080/07388551.2021.1917505

Liao, P. C., Yang, E. J., and Pon, L. A. (2020). Live-cell imaging of mitochondrial redox state in yeast cells. *Star. Protoc.* 1 (3), 100160. doi:10.1016/j.xpro.2020.100160

Maclean, C. J., Metzger, B. P. H., Yang, J. R., Ho, W. C., Moyers, B., and Zhang, J. (2017). Deciphering the genic basis of yeast fitness variation by simultaneous forward and reverse genetics. *Mol. Biol. Evol.* 34 (10), 2486–2502. doi:10.1093/molbev/msx151

Mara, P., Fragiadakis, G. S., Gkountromichos, F., and Alexandraki, D. (2018). The pleiotropic effects of the glutamate dehydrogenase (GDH) pathway in *Saccharomyces cerevisiae*. *Microb. Cell. Fact.* 17 (1), 170. doi:10.1186/s12934-018-1018-4

Meleshina, A. V., Rogovaya, O. S., Dudenkova, V. V., Sirotkina, M. A., Lukina, M. M., Bystrova, A. S., et al. (2018). Multimodal label-free imaging of living dermal equivalents including dermal papilla cells. *Stem Cell. Res. Ther.* 9 (1), 84. doi:10.1186/s13287-018-0838-9

Miller, C. G., Holmgren, A., Arnér, E. S. J., and Schmidt, E. E. (2018). NADPH-dependent and -independent disulfide reductase systems. *Free Radic. Biol. Med.* 127, 248–261. doi:10.1016/j.freeradbiomed.2018.03.051

Napiorkowska, M., Pestalozzi, L., Panke, S., Held, M., and Schmitt, S. (2021). High-throughput optimization of recombinant protein production in microfluidic gel beads. *Small* 17 (2), e2005523. doi:10.1002/smll.202005523

Okkelman, I. A., Puschhof, J., Papkovsky, D. B., and Dmitriev, R. I. (2020). Visualization of stem cell niche by fluorescence lifetime imaging microscopy. *Methods Mol. Biol.* 2171, 65–97. doi:10.1007/978-1-0716-0747-3_5

Qiu, X., Zhang, J., Zhou, J., Fang, Z., Zhu, Z., Li, J., et al. (2019). Stress tolerance phenotype of industrial yeast: Industrial cases, cellular changes, and improvement strategies. *Appl. Microbiol. Biotechnol.* 103 (16), 6449–6462. doi:10.1007/s00253-019-09993-8

Ramos-Moreno, L., Ramos, J., and Michán, C. (2019). Overlapping responses between salt and oxidative stress in *Debaryomyces hansenii*. *World J. Microbiol. Biotechnol.* 35 (11), 170. doi:10.1007/s11274-019-2753-3

Sagar, M. A. K., Cheng, K. P., Ouellette, J. N., Williams, J. C., Watters, J. J., and Eliceiri, K. W. (2020). Machine learning methods for fluorescence lifetime imaging (FLIM) based label-free detection of microglia. *Front. Neurosci.* 14, 931. doi:10.3389/fnins.2020.00931

Sakihama, Y., Hidese, R., Hasunuma, T., and Kondo, A. (2019). Increased flux in acetyl-CoA synthetic pathway and TCA cycle of *Kluyveromyces marxianus* under respiratory conditions. *Sci. Rep.* 9 (1), 5319. doi:10.1038/s41598-019-41863-1

Sant'Anna-Silva, A. C. B., Santos, G. C., Campos, S. P. C., Oliveira Gomes, A. M., Pérez-Valencia, J. A., and Rumjanek, F. D. (2018). Metabolic profile of oral squamous carcinoma cell lines relies on a higher demand of lipid metabolism in metastatic cells. *Front. Oncol.* 8, 13. doi:10.3389/fonc.2018.00013

Schaefer, P. M., Hilpert, D., Niederschweiberer, M., Neuhauser, L., Kalinina, S., Calzia, E., et al. (2017). Mitochondrial matrix pH as a decisive factor in neurometabolic imaging. *Neurophotonics* 4 (4), 1. doi:10.1117/1.NPh.4.4.045004

Schaefer, P. M., Kalinina, S., Rueck, A., von Arnim, C. A. F., and von Einem, B. (2019). NADH autofluorescence-A marker on its way to boost bioenergetic research. *Cytom. A* 95 (1), 34–46. doi:10.1002/cyto.a.23597

Scialò, F., Fernández-Ayala, D. J., and Sanz, A. (2017). Role of mitochondrial reverse electron transport in ROS signaling: Potential roles in health and disease. *Front. Physiol.* 8, 428. doi:10.3389/fphys.2017.00428

Tomàs-Gamisans, M., Andrade, C. C. P., Maresca, F., Monforte, S., Ferrer, P., and Albiol, J. (2020). Redox engineering by ectopic overexpression of NADH kinase in recombinant *Pichia pastoris (Komagataella phaffii)*: Impact on cell physiology and recombinant production of secreted proteins. *Appl. Environ. Microbiol.* 86 (6), e02038-19. doi:10.1128/aem.02038-19

Tornmalm, J., Sandberg, E., Rabasovic, M., and Widengren, J. (2019). Local redox conditions in cells imaged via non-fluorescent transient states of NAD(P)H. *Sci. Rep.* 9 (1), 15070. doi:10.1038/s41598-019-51526-w

Wang, M., Chen, B., Fang, Y., and Tan, T. (2017). Cofactor engineering for more efficient production of chemicals and biofuels. *Biotechnol. Adv.* 35 (8), 1032–1039. doi:10.1016/j.biotechadv.2017.09.008

Wick, S., Walsh, D. I., 3rd, Bobrow, J., Hamad-Schifferli, K., Kong, D. S., Thorsen, T., et al. (2019). PERSIA for direct fluorescence measurements of transcription, translation, and enzyme activity in cell-free systems. *ACS Synth. Biol.* 8 (5), 1010–1025. doi:10.1021/acssynbio.8b00450

Wu, L., Wang, M., Zha, G., Zhou, J., Yu, Y., and Lu, H. (2020). Improving the expression of a heterologous protein by genome shuffling in *Kluyveromyces marxianus*. *J. Biotechnol.* 320, 11–16. doi:10.1016/j.jbiotec.2020.06.007

Yang, D., Zhang, L., Duan, J., Huang, Q., Yu, Y., Zhou, J., et al. (2021). A single vaccination of IBDV subviral particles generated by *Kluyveromyces marxianus* efficiently protects chickens against novel variant and classical IBDV strains. *Vaccines (Basel)* 9 (12), 1443. doi:10.3390/vaccines9121443

Yu, Y., Mo, W., Ren, H., Yang, X., Lu, W., Luo, T., et al. (2021). Comparative genomic and transcriptomic analysis reveals specific features of gene regulation in *Kluyveromyces marxianus*. *Front. Microbiol.* 12, 598060. doi:10.3389/fmicb.2021.598060

Zhu, J., Schwörer, S., Berisa, M., Kyung, Y. J., Ryu, K. W., Yi, J., et al. (2021). Mitochondrial NADP(H) generation is essential for proline biosynthesis. *Science* 372 (6545), 968–972. doi:10.1126/science.abd5491

frontiers | Frontiers in Bioengineering and Biotechnology

TYPE Review
PUBLISHED 17 November 2022
DOI 10.3389/fbioe.2022.1067869

OPEN ACCESS

EDITED BY
Xiao-Jun Ji,
Nanjing Tech University, China

REVIEWED BY
Hu-Hu Liu,
Hunan Agricultural University, China
Yongqian Fu,
Taizhou University, China

*CORRESPONDENCE
Qing Xu,
xu_qing@njnu.edu.cn

†These authors have contributed equally to this work

SPECIALTY SECTION
This article was submitted to Industrial Biotechnology, a section of the journal Frontiers in Bioengineering and Biotechnology

RECEIVED 12 October 2022
ACCEPTED 03 November 2022
PUBLISHED 17 November 2022

CITATION
Li K, Jia J, Wu N and Xu Q (2022), Recent advances in the construction of biocomposites based on fungal mycelia. *Front. Bioeng. Biotechnol.* 10:1067869. doi: 10.3389/fbioe.2022.1067869

Recent advances in the construction of biocomposites based on fungal mycelia

Ke Li†, Jianyao Jia†, Na Wu and Qing Xu*

School of Food Science and Pharmaceutical Engineering, Nanjing Normal University, Nanjing, China

In recent years, environmental problems have become increasingly serious, significantly effecting the ecosystem and human health. To deal with the problem of environmental pollution in an eco-conscious way, sustainable composite biomaterials are being produced. Mycelium-based composite biomaterials combine biological systems with substrates such as nanomaterials or agricultural and industrial wastes, which can complement each other's advantages or turn waste into a useful resource. Such materials can solve practical wastewater problems as well as replace plastic products, thus reducing plastic pollution and contributing to the green transition of the environment. In this review, we summarized the recent findings of studies on these materials, indicating future research directions.

KEYWORDS

biocomposites, degradable, fungal mycelium, packing material, heavy metal adsorption

1 Introduction

With the rapid development of industrial technology and market economy, problems related to environmental pollution are becoming increasingly serious. This includes the "three wastes": pollution caused by industrial production, soil pollution caused by agricultural production, and plastic pollution caused by urban activities (Shah et al., 2008; Qiu et al., 2022). The problem of environmental pollution caused by industrial production and living activities is an urgent and persistent concern worldwide as it directly harms the ecosystem and indirectly affects the quality of human life.

As most plastic packaging materials are non-biodegradable and unsustainable, causing environmental pollution when they are landfilled, the development biodegradable or composite-stable materials is being increasingly researched (Su et al., 2022). The market demand for green environmental protection materials is increasing as well. To date, a series of degradable materials have been synthesized and developed based on different biomass feedstocks, such as cellulose (Huber et al., 2011), starch (Wang B. et al., 2022), and chitin (Duan et al., 2018).

The development of bio-based materials based on these substrates has slowed down the environmental pollution caused using traditional petroleum-based materials. However, the growth and development of these substrates requires water and land, which results in a waste of resources to a certain extent; thus, it is not recommended for

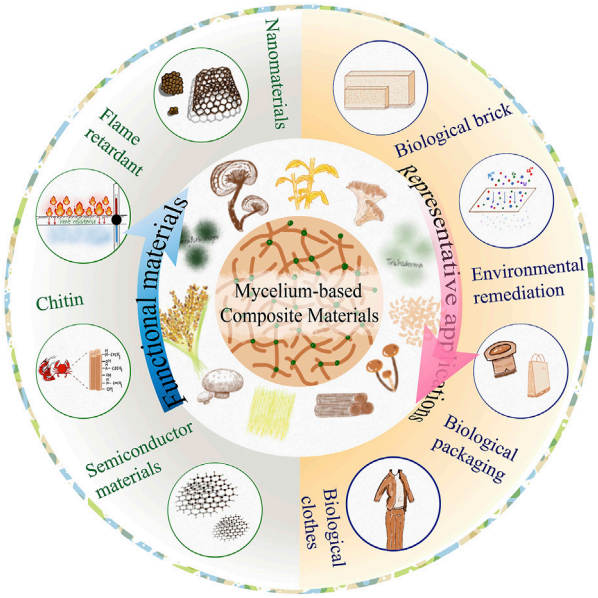

FIGURE 1
Comprehensive overview of mycelium-based composites (composite functional elements made with biomaterials to improve their biological properties and functionality).

frequent application (Liu et al., 2020). On the other hand, fungal mycelia, which are easy to culture, grow rapidly, and have low resource requirements (Tudryn et al., 2018), are a sustainable source of multifunctional and easily degradable biocomposites which can replace traditional petroleum-based materials or other bio-based materials (Antinori et al., 2020). Therefore, the demand for these sustainable materials with low environmental impact is increasing. Recently, researchers have begun to study and develop natural biodegradable materials based on fungal mycelia with the aim of using environmental resources for green environmental protection and progressive development (Hori et al., 2013; Hyde et al., 2019).

Fungal mycelia are natural and renewable valuable structural polymer materials (Gandia et al., 2021) mainly composed of glucan, proteins, chitin, and other natural polymers (Meyer et al., 2020). Unlike bacteria and yeast, fungi, as filamentous species, can produce single tubular hyphae and to form a large-area fibrous hyphal network structure in an appropriate medium. Their hyphae can spontaneously grow entwined and colonize the substrate, which is why they are called “bio adhesives” (Meyer et al., 2011). The term “mycelium-based composite material” refers to any new degradable material formed by combining and optimizing mycelium with materials of different properties through process design. This material can be used for packaging materials, building materials, environmental repair, wearable materials. etc. (Zhang et al., 2022). Mycelium composites have the advantages of being degradable, reusable, functionally diverse, safe, efficient, and environmentally friendly (Yang et al., 2021).

Previous reviews (Appels et al., 2019; Girometta et al., 2019; Sharma and Sumbria, 2022) on this topic have mainly described hyphal composites based on polymer-based materials, focusing on a single function of the material. However, most reviews have not provided comprehensive descriptions of existing materials. In this review, mycelium-based composite materials were divided into two categories according to the substrates: one category includes polymer-based composites, such as industrial and agricultural wastes, while the other includes inorganic-based composite materials, such as nano-metals and semiconductors. Biodegradable materials with different functions were reviewed to improve our understanding of these materials as well as to promote their research and development (Figure 1). Continuously degradable biocomposite materials have been the focus of research in recent years and are viewed as novel cutting-edge materials.

2 Synthetic materials for constructing biohybrids

2.1 Polymers

Polymers are a class of macromolecules that can be synthesized from a wide range of natural and synthetic monomers (such as wood chips, cottonseed husks, and flax). Polymeric materials can be designed with different tunable functionalities and physicochemical properties, including mechanical, thermal, acoustic, and water absorption properties, as well as termite resistance. This has attracted diverse interest in their applications in energy, environment, and biomedicine. So far, polymers have been the most exploited material for constructing biohybrids and manipulating the biological properties of the mycelium (Alemu et al., 2022).

2.1.1 Packaging materials

A varieties of researches suggest that switching to sustainable packaging could obtain a lot of benefits. Therefore the material uses the power of fungal mycelium to create an alternative to conventional packaging. Mechanical properties determine the durability of mycelium-based composite industrial products. For example, the degree of resistance depends on tensile strength, compressive strength, or elastic deformation, bending strength etc.G. A. Holt was the first to process and compound the mycelium of *Ganoderma lucidum* and cotton plant material (CPM) into cotton-based mycelium packaging materials (Holt et al., 2012). Cotton plant materials include starch and gypsum, as well as cotton cores and cottonseed hulls obtained from cotton mill waste. In this paper, six different blends with the same proportion of materials and different CPM particle sizes were tested. The fungal spores were inoculated on the mixture by two

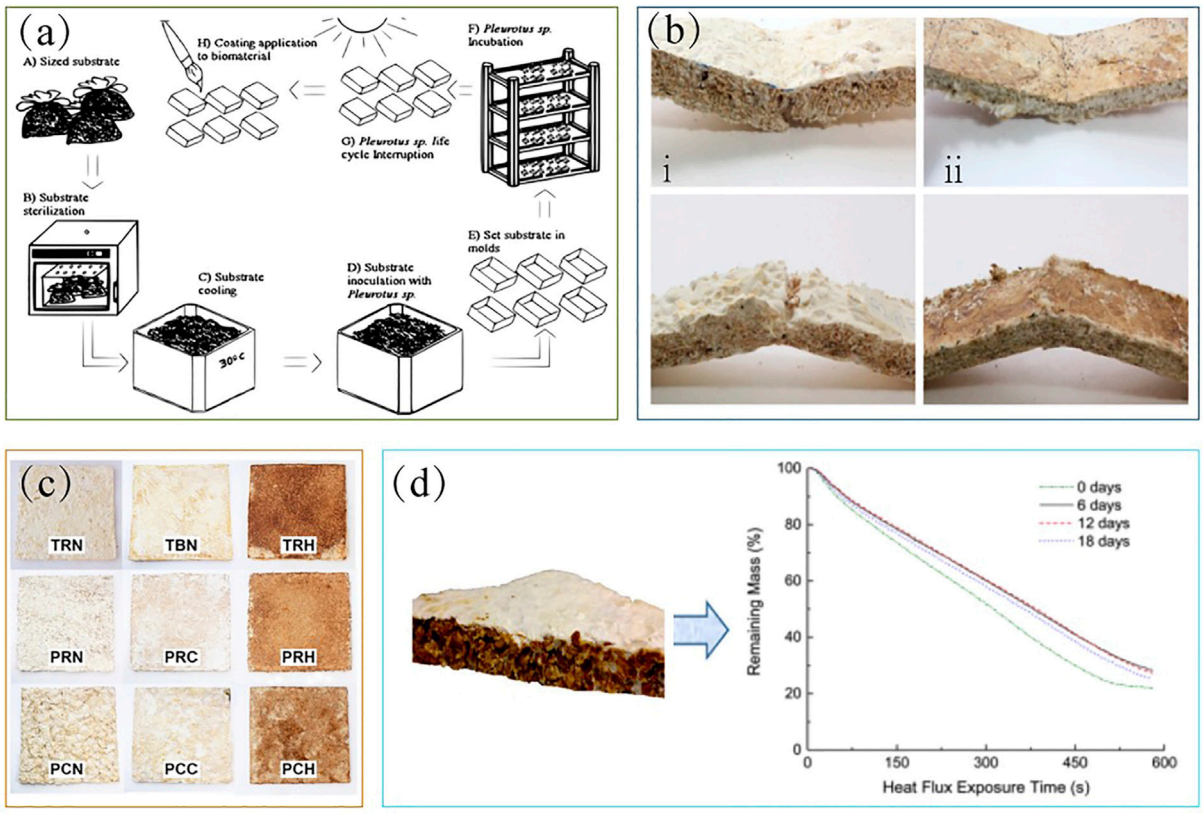

FIGURE 2
(A) EPS-like biodegradable composite biomaterial (López Nava et al., 2015) **(B)** comparison of different fungal materials (Elsacker et al., 2020) **(C)** comparison of different substrate matrix materials (Attias et al., 2020) **(D)** mycelium-based composite board and its thermal resistance test (Jones et al., 2018).

methods, namely grain and liquid culture, and the physical and mechanical properties of the products were evaluated after factory processing. The results showed that this material meets and exceeds the properties of polystyrene foam and can be used to make biodegradable packaging materials. This article was based on the research process of Bayer and McIntyre et al. J. A. López Nava et al. who modified a processing technique (López Nava et al., 2015) and composed bio-based materials using wheat crop residues and fungi oyster mushroom, *Pleurotus* sp. First, they used wheat residue particles as the matrix and oyster mushroom particles as the carrier, which were inoculated into a wooden mold for 1 month. The final product was taken out, dried, and coated with edible film (composed of carrageenan, chitosan, and xanthan gum) on the outer layer (Figure 2A). The physical and mechanical properties of the material were evaluated by applying different film types. Collectively, these results of tests showed that the composite had better tensile strength (42 kPa) than expanded polystyrene (EPS) (35 kPa), but the degree of bending (4.6–17.9 kPa)was not as good as the material created by Holt et al. (7–26.1 kPa). Therefore, the composite material developed in this study is suitable for purposes that do not require bending resistance, such as production of food packaging, small flowerpots, *etc.*

With the diversification of biomaterial mixtures and optimization of processing techniques, the mechanical and physical properties of these products can be further improved, making agricultural waste composites suitable for numerous applications using fossil fuel-based materials. The mechanical properties can be explored from three aspects: fungal type, culture substrate and processing technology.

First, the fungal type and its mycelial thickness affect the mechanical properties of mycelial composites. Lars De Laet et al. cultivated different fungi on different substrates (Elsacker et al., 2020) and showed that the compressive properties of *Trametes multicolor* (*T. multicolor*) were better than that of *Pleurotus ostreatus* (*P. ostreatus*) Han A.B.Wösten et al. used *P. ostreatus* and *T. multicolor* compounded with cotton, sawdust, and straw, and comprehensively characterized their properties after cold pressing, hot pressing, and no pressing (Appels et al., 2019). They concluded that hot pressing could change the tensile

strength of composites as well as their performance, increasing the uniformity and strength of mycelium-based material, which can make it similar in performance to natural materials. At the same time, they showed that the thickness of *T. multicolor* mycelium was thicker than that of *P. ostreatus* mycelium, as well as that straw-based material was harder and less moisture-resistant than cotton-based mycelium composite material (Figure 2B).

Second, the nutrient conditions of the substrate matrix have a certain influence on the growth of fungi. In 2017, Linda S. Schadler et al. used lignocellulosic agricultural waste as the substrate matrix to explore the effect of nutrition on the mechanical properties and modulus strength of materials using two methods: inoculation and after homogenization. They found that nutritional supplementation during inoculation had little effect on the overall strength of the material, but the addition of nutrients after homogenization and mixing could improve the overall uniformity and strength modulus of the substrate matrix, which was a consequence of the formation of a continuous network of hyphae. *Regina* Helena Marino used coconut flour combined with wheat bran to promote mycelial growth, and the mycelium-based composite biomaterials colonized by *Lentinula edodes* (*L. edodes*) strains exhibited better mechanical properties when colonized for 1 month than when colonized for half a month (Matos et al., 2019). Furthermore, Andrea Ehrmann investigated whether a modified PAN nanofiber mat can promote the growth of fungal hyphae (*P. ostreatus*), change their hyphal morphology, and increase their growth rate (Sabantina et al., 2019). Noam Attias selected five plant waste substrates and four fungal species to comprehensively evaluate which combination of substrates would be most suitable for future applications (Attias et al., 2020). By testing the fitness efficiency of each substrate and fungus, they found that the best performing combination was *P. ostreatus* mycelium grown on vine and apple substrates (Figure 2C).

Third, another important thing is the difference in processing technology used to control the mechanical properties of mycelial composites. Previous studies have shown that hot and cold pressing had different effects on the mechanical properties of biocomposites. During mycelium growth, some gaps can appear because of the differences in growing speed throughout the year, and compression can reduce the porosity and increase the density of the material. Cold pressing changes tensile and flexural strengths, while hot pressing achieves even greater improvements in the material's mechanical properties. The properties of the material change as water evaporates, temperature changes, and stress decreases. High-density materials are more widely used than low-density ones. Bajwa et al. (2017) and Pelletier et al. (2017) tried to increase the pressure during the growth and composite process, while others Liu et al. (2019), Sun et al. (2019)] tried to densify composite materials by hot pressing after the material was formed.

Other similar efforts include adding composite interlayers or compounding with materials such as cellulose nanofibers to enhance the mechanical properties of materials. For example, Mehdi Tajvidi (Sun et al., 2019) developed a new hybrid panel composite based on wood, fungal mycelium, and cellulose nanofibers (CNF) and optimized its performance at 5% CNF addition, showing its potential for packaging and furniture applications.

2.1.2 Insulation materials

The most basic thermal properties of polymers are thermal expansion, specific heat capacity, and thermal conductivity. Their values vary depending on polymer state and temperature, which are closely related to the processing of products and affect the application of materials. Polymers with low thermal conductivity can be used as insulation materials. The lower the thermal conductivity of the polymer, the better its thermal insulation performance. Therefore, mycelium-based polymer composites with low density and low thermal conductivity can be used as excellent thermal insulation materials. Marli Camassola et al. (Bruscato et al., 2019) developed bio-foams using *Pycnoporus sanguineus* (*P. sanguineus*) and *Lentinus velutinus* (*L. velutinus*) cultivated on wood chips and wheat bran. Comprehensive tests showed that the bio-based materials of *P. sanguineus* and *L. velutinus* have higher density and compressive strength than those of EPS, making them an appropriate substitute for sustainable insulation materials. Lars De Laet et al. processed white rot fungi and five lignocellulosic materials (hemp, flax, flax waste, cork, and straw) with five fiber conditions (loose, chopped, dust, pre-compressed, and tow) to investigate their properties and found that mycelium composites containing hemp, flax, and straw exhibited good thermal insulation properties, but not as good mechanical properties (Figure 2D). Furthermore, mycelium-based biocomposites showed a significantly reduced tendency to burn compared to those of polymethylmethacrylate (PMMA) and polylactic acid (PLA) materials, indicating that they are less prone to fire and thus safer to use (Jones et al., 2018). The mycelium-based composite biomaterials studied by Tanmay Bhat et al. were found to have good flame-retardant properties. Chitosan has been studied as a promising flame retardant additive (Hu et al., 2012), mainly relying on the substance being stable at high temperatures, with a peak value of 300°C. In addition, hydrophobin (Appels et al., 2018) and lignin (Yu et al., 2017) can also be used as natural flame-retardant additives, as they were shown to improve the flame-retardant properties of mycelium-based composites.

Acoustic performance is a physical property of sound that affects our quality of life. Mycelium-based composite materials can absorb sound by pressing the material and increasing its density. The higher the density, the better the noise reduction coefficient and sound insulation effect. M.G. Pelletier et al. (2017) grew a mycelium based on agricultural by-products such as

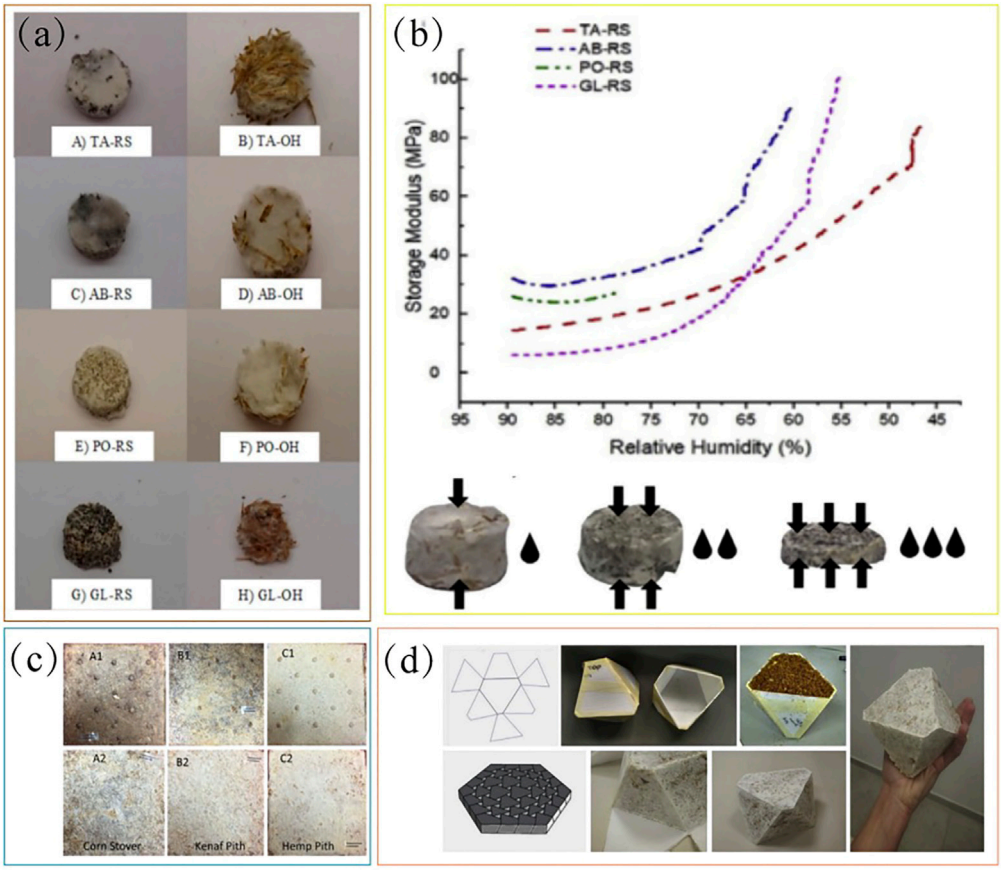

FIGURE 3
(A) Development of moisture-resistant composites based on different matrices (*Trichoderma asperellum* (TA) grown on A) rapeseed cake (RS) and B) oat husks (OH) as substrates; Agaricus bisporus (AB) grown on C) RS and D) OH; Pleurotus ostreatus (PO) grown on E) RS and F) OH; Ganoderma lucidum (GL) grown on G) RS and H) OH), **(B)** their dynamic moisture monitoring and schematic diagram of material changes (Tacer-Caba et al., 2020), **(C)** development of termite-resistant composite bio-boards (Bajwa et al., 2017), **(D)** specific models constructed based on CAD design and innovative molds (Attias et al., 2020).

cotton by-products, cotton burrs, straw, sorghum stems, and corn stalks, and then compressed the original products into high-density composite materials to form natural lightweight bio-composite panels that can be applied to acoustics. This mycelium absorbed 50%–70% of the sound. The results showed that the sound insulation performance gradually improved and almost reached 0.087 g/cc. Afterwards, increased density also does not enhance sound insulation. Unlike modern commercial acoustic insulation materials, this novel mycelium-based composite density material provides good sound insulation and is a promising bio-based composite alternative to sound shielding panels.

Different fungal strains have different hydrophobic properties. The stronger the hydrophobicity, the higher its potential to be used as a moisture-resistant material. However, a common problem with mycelium-based materials is their high-water absorption capacity, which has certain restrictions on the use of their materials. The properties of these materials can be adjusted by pressing them or finding suitable strains. Kirsi S. Mikkonen used *Agaricus bisporus*, *Trichoderma asperellum*, *Pleurotus ostreatus* and *Ganoderma lucidum* and compounded them with oat mixture and rapeseed cake (Figure 3A). They obtained eight types of fungal composites after oil pressure growth (Tacer-Caba et al., 2020). In contrast to EPS (50 kg/m^3), the density of foam-like material based on mycelia can range from 59 to 318 kg/m^3. In the present study, the RS-fed hyphal composite (561 kg/m^3) had a higher density than the OH-fed hyphal composite (230 kg/m^3). Therefore, the comprehensive results showed that the products of *A. bisporus* grown on rapeseed cakes had strong hydrophobic properties and can be used to produce moisture-resistant plastic products. This was the first study to measure the dynamic moisture-retaining properties of fungal composites (Figure 3B). To sum up, the heat, sound and moisture resistance of mycelium-based materials can be improved by increasing the density.

In addition to this, mycelium-based termite resistant composites were also investigated to resistant to termite. The mycelium-based degradable composite material studied by Dilpreet S. Bajwa was composed of fungal mycelium, lignocellulose, and termites. Biocomposite panels with two densities were fabricated using three different fungal strains (*Daedaleopsis confragosa*, *Ganoderma resinaceum*, and *Tramates versicolor*) based on kenaf, hemp, and corn stover fibers (Bajwa et al., 2017). The termite resistance of these bio composite panels was evaluated using four termiticides (vetiver oil, guayule resin, cedar oil, and borax). Comprehensive tests showed that resin-treated kenaf and hemp boards had the strongest repellency to termites and could be used as effective anti-termite bio-based composites (Figure 3C).

2.2 Summary

Further innovations and optimizations of the materials described above include the use of plant crop waste, design, and adjustment of molds according to CAD, construction of specific shapes, and achievement of mycelium-based self-fusion growth, so that such materials can meet different requirements and promote the sustainable development of bio-based fungal materials. For example, Yasha Grobman and Michael Weizman used a laser to cut and fold into 37 unique 3D molds that can be self-assembled to form suspended ceiling models, known as topologically interlocking mycelial bricks (Attias et al., 2020) (Figure 3D). In addition to this, many studies have evaluated other properties of mycelial materials. For example. Jones et al. (2020) and. Girometta et al. (2019) comprehensively evaluated the basic and engineering properties (including antibacterial properties and shape flexibility) of mycelial bio-based materials et al. (Kuribayashi et al., 2022).

The ability to develop low-cost and sustainable environmentally friendly composite materials has attracted commercial and academic interest. Such mycelium-based composites are constructed from complex network structures of fungal mycelia grown on natural or waste substrates (Jones et al., 2017). Filamentous hyphae grow and colonize the substrate, acting as a natural gum which provides mechanical support. Substrates for growing mycelial complexes can mainly be recovered from industrial or agricultural wastes at low prices, reduce the production costs and achieving economic benefits. The materials have the characteristics of reusability, diverse functions, and easy operation. To a certain extent, they can replace petroleum-based plastic products, thus effectively reducing environmental pollution and our negative impact on the ecological environment and human health, aiming to achieve environmental protection and sustainable use of resources. Although some basic research has been carried out on such materials, at this research stage, some problems still exist:

1) Few studies on these topics have investigated the fungi used for making these composite materials, even though researching the properties of different fungal strains is necessary to find more suitable strains to produce different composite materials (Hyde et al., 2019).
2) It is necessary to develop low-cost and sustainable substrates for industrial production.
3) The composite design is not its most important property; the process production and manufacturing also need to be optimized, which can be combined with other data technology.

In addition, the appearance of these materials is still not as appealing, as they are currently in rough processing.

3 Inorganic materials

Inorganic materials are divided into metal and non-metal materials, mainly including nano-metal and semiconductor materials. Nano-metal materials are metals and alloys that form nano-grains. They are characterized by large specific surface area and high adsorption capacity and used as good adsorbents in combination with fungal hyphae. The currently used application substrates mainly include nano-metal oxides, magnetic nanoparticles, and nano-gold particles, which are used in wastewater treatment, as catalysts, *etc.* (Rashid et al., 2020). Inorganic non-metallic materials are materials composed of oxides, carbides, aluminates, and other substances of certain elements. Inorganic non-metallic functional materials have many functions because of their semiconductor properties, adsorption properties, and radiation resistance. The materials compounded with mycelia include semiconductors, such as graphene oxide, which are used for the absorption of radioactive substances (Zhu et al., 2019).

3.1 Heavy metal absorbing and catalytic materials

Nano-metal sulfides have attracted extensive attention because of their simple fabrication process, low cost, and strong ion exchange capacity. Zhou et al. (2007) used sonochemical methods to synthesize ZnS nanostructures using microorganisms as templates. Pala and Brock. (2012) used ZnS nanoparticle gels to remove Pb^{2+} and Hg^{2+} from heavy metal sewage. Jaiswal et al. (2012) showed that ZnS quantum dots-chitosan films can be used to remove heavy metal ions from wastewater. Fang et al. (2018) used ZnS nanocrystals for the sequential removal of multicomponent heavy metals in aqueous solutions. Hu et al. (Qin et al., 2020) successfully synthesized ZnS nanoparticles on the cell surface of *P. chrysosporium*(BKMF-1767) cells using a sonochemical method, obtaining a high-

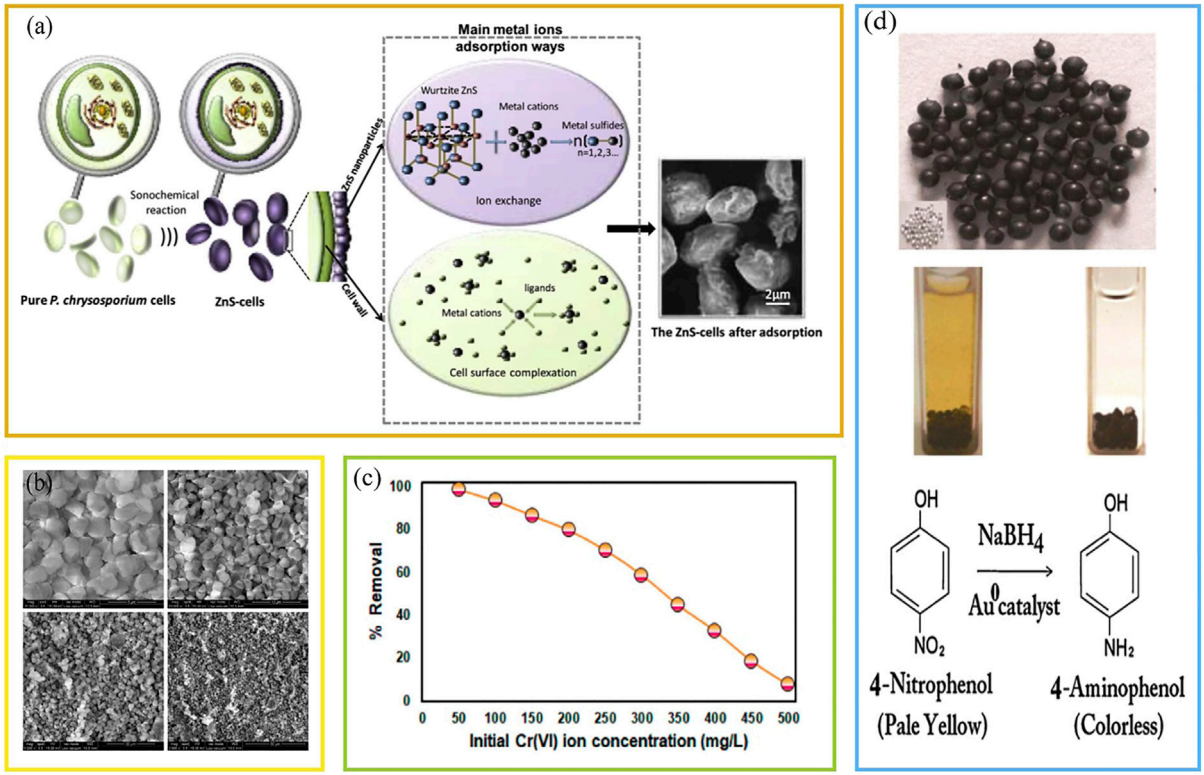

FIGURE 4
(A) High-performance adsorption of Pb^{2+} and Cd^{2+} by ZnS nanoparticle layer (Qin et al., 2020), **(B)** synthesis of magnetic nanoparticles coated mixed fungal biomass (MNP-FB), **(C)** adsorption of Cr(VI) ions (Saravanan et al., 2021), **(D)** nanocomposite biomass synthesis of materials and their heterogeneous catalysis to enable the recovery of AuNPs catalysts: schematic representation after catalytic adsorption (Narayanan and Sakthivel, 2011).

performance composite adsorbent. Compared with primitive fungal cells, the adsorption capacities of these developed materials for Pb^{2+} and Cd^{2+} were increased by 140% and 160%, respectively (Figure 4A). For removing Cr^{6+} from wastewater, P. Senthil Kumar used newly synthesized magnetic nanoparticles mixed with fungi (*Aspergillus niger* and *A. fumigatus*) to cultivate the MNP-FB material (Saravanan et al., 2021) (Figure 4B). The monolayer adsorption efficiency of Cr^{6+} by MNP-FB was 249.9 mg/g, making it an economically feasible material (Figure 4C). This mycelium-based composite study provided a feasible and novel method for preparing a heavy metal wastewater adsorbent by combining microorganisms and nanomaterials, which has great potential for practical wastewater treatments.

For the first time, Narayanan and Sakthivel. (2011) developed a green chemistry-stable spherical gold nanocomposite with high catalytic activity based on nano-gold material biocomposite with fungal mycelium (*Cylindrocladium floridanum*). This material can quantitatively and heterogeneously reduce 4-NP to 4-AP, reducing the environmental harm of toxic organic pollutants (Figure 4D). Heterogeneous catalysts, supported by fungal biomass, promote biocatalysis, and increase reaction rates. However, considering their economic feasibility and environmental friendliness, an in-depth understanding of sustainable green biocatalytic reduction of various nitro pollutants is required for their further use.

3.2 Radioactive absorbing materials

Graphene oxide (GO) plays an important role in wastewater treatment because of its high specific surface area and fast reaction kinetics. Zhu et al. (2019) successfully prepared hierarchical core-shell structured FH/Fe_3O_4/GO nanocomposite spheres (FFGS) by continuously culturing fungal hyphae (FH) in Fe_3O_4- or GO-containing media (Figure 5A). The bulk adsorption results showed that the composite FFGS was much better than FH, FH/GO, and FH/Fe_3O_4 in the adsorption of methyl violet (MV) and uranium (U), which may be attributed to its lower zeta potential (Figure 5B). Therefore, the core-shell structured FFGS is a promising adsorbent for the removal and recovery of MV or U(VI) from

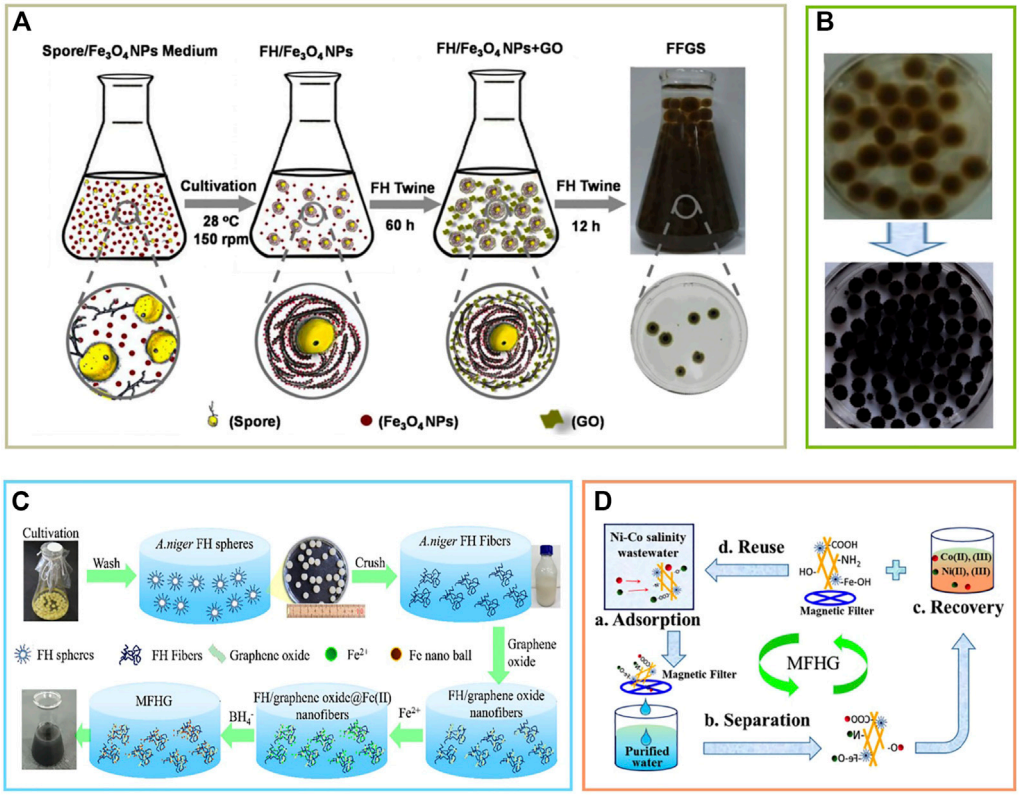

FIGURE 5
(A) Synthesis of layered core-shell structured fungus hyphae (FH)/Fe_3O_4/graphene oxide (GO) nanocomposite spheres (FFGS), **(B)** removal and recovery of methyl violet (MV) and uranium (U) (after 72 h) (Zhu et al., 2019), **(C)** preparation of three-dimensional magnetic fungal hyphal/graphene oxide nanofibers (MFHG), **(D)** capture and adsorption of metal ions Co (II) and Ni (II) (Li et al., 2019).

wastewater, and this strategy is low-cost and environmentally friendly. Nanosheets based on graphene oxide have also been developed. He et al. (Chen et al., 2021) used photodegradation to develop FH-graphene-MoS_2 hybrid nanosheets, which can effectively adsorb radioactive U ions. However, this nanomaterial has a low recovery rate and poor stability, which should also be considered in future research. Wang et al. (Li et al., 2019) assembled three-dimensional magnetic fungal hyphae/graphene oxide nanofibers (MFHG) using a self-assembly reduction (RSA) strategy for the purpose of efficient capture of Co and Ni from high-salinity aqueous solutions, improving the stability of the material (Figures 5C,D). Based on MFHG, a continuous recovery reactor (CFRR) for treating aqueous solutions was developed, which exhibited high efficiency in removal and regeneration. The combination of MFHG and CFRR is a promising and efficient method for wastewater treatment. For heavy metal adsorption and radioactive material absorption, the adsorption effect of mycelium-based materials can be judged by fitting adsorption kinetics.

Inorganic materials, including nanoparticles and semiconductors, have the advantages of strong self-assembly ability, high specificity, and good reactivity, which make them the preferred substrates for the treatment of water pollution and other harmful pollutants. Therefore, adsorbents formed by the composite of inorganic and biological materials can rapidly adsorb heavy metals and radioactive substances in wastewater. These materials can not only make up for the weak mechanical properties and limited adsorption capacity of microorganisms but can also neutralize the shortcomings of the difficult separation of inorganic materials, resulting in a significant increase in wastewater adsorption efficiency (Holkar et al., 2016).

The functional materials developed by composing such inorganic materials and fungal mycelia are promising treatment materials for the adsorption of harmful substances (Rashid et al., 2021). However, such mycelium-based composite functional materials are rarely studied and are currently only used in laboratories. Thus, more research on their industrial adaptability is needed to achieve the goal of low cost and high adsorption.

4 Concluding remarks and future perspectives

In the context of environmental pollution, this review discusses and summarizes the advantages of composite biomaterials, focusing on mycelium materials. Mycelium-based composite biomaterials can be used as packaging materials (Nawawi et al., 2020), building decoration materials, environmental restoration materials (Holkar et al., 2016), and for many other purposes. With the progress of research, the genome sequences of many species have been revealed, allowing them to be genetically modified. The research on mycelium-based composite biomaterials is still at the beginning, and it is a popular future research direction. With the crossover of multiple disciplines and diversification of research, the development of composite biomaterials progresses from ordinary simple compounding to gene editing synthesis, that is, synthetic biology is being used to transform mycelium-based composites and utilize chassis cells in biological systems to endow them with new functions (Wang Y. et al., 2022). By designing, transforming, and recombining biological cell systems, and then combining them with new functional elements, we can develop many efficient, safe, and environmentally friendly products for many purposes. Because of their diverse biological applications and advanced technical means, composite biomaterials have good application prospects in the fields of bioenergy, environmental improvement, medicine, food technology, and health care, and can thus provide many benefits for human social development and ecological health. Although there are still many problems that need to be addressed in the currently available mycelium-based composite materials, as cheap and degradable materials, their researching, and commercialization trend is increasing day by day. Their main advantages are their broad application potential and market prospects, and their potential in promoting sustainable development in the future.

Author contributions

KL and JJ determined the topic of the review and complete the manuscript writing, QX, and NW helped with the preparation of the material. All authors commented on the final manuscript.

Funding

This work was supported by the China Postdoctoral Science Foundation (2021M690081).

Conflict of interest

The authors declare that the research was conducted in the absence of any commercial or financial relationships that could be construed as a potential conflict of interest.

Publisher's note

All claims expressed in this article are solely those of the authors and do not necessarily represent those of their affiliated organizations, or those of the publisher, the editors and the reviewers. Any product that may be evaluated in this article, or claim that may be made by its manufacturer, is not guaranteed or endorsed by the publisher.

References

Alemu, D., Tafesse, M., and Mondal, A. K. (2022). Mycelium-based composite: The future sustainable biomaterial. *Int. J. Biomater.* 2022, 1–12. doi:10.1155/2022/8401528

Antinori, M. E., Ceseracciu, L., Mancini, G., Heredia-Guerrero, J. A., and Athanassiou, A. (2020). Fine-tuning of physicochemical properties and growth dynamics of mycelium-based materials. *ACS Appl. Bio Mat.* 3 (2), 1044–1051. doi:10.1021/acsabm.9b01031

Appels, F. V. W., Camere, S., Montalti, M., Karana, E., Jansen, K. M. B., Dijksterhuis, J., et al. (2019). Fabrication factors influencing mechanical, moisture- and water-related properties of mycelium-based composites. *Mater. Des.* 161, 64–71. doi:10.1016/j.matdes.2018.11.027

Appels, F. V. W., Dijksterhuis, J., Lukasiewicz, C. E., Jansen, K. M. B., Wosten, H. A. B., and Krijgsheld, P. (2018). Hydrophobin gene deletion and environmental growth conditions impact mechanical properties of mycelium by affecting the density of the material. *Sci. Rep.* 8 (1), 4703. doi:10.1038/s41598-018-23171-2

Attias, N., Danai, O., Abitbol, T., Tarazi, E., Ezov, N., Pereman, I., et al. (2020). Mycelium bio-composites in industrial design and architecture: Comparative review and experimental analysis. *J. Clean. Prod.* 246, 119037. doi:10.1016/j.jclepro.2019.119037

Bajwa, D. S., Holt, G. A., Bajwa, S. G., Duke, S. E., and McIntyre, G. (2017). Enhancement of termite (Reticulitermes flavipes L.) resistance in mycelium reinforced biofiber-composites. *Industrial Crops Prod.* 107, 420–426. doi:10.1016/j.indcrop.2017.06.032

Bruscato, C., Malvessi, E., Brandalise, R. N., and Camassola, M. (2019). High performance of macrofungi in the production of mycelium-based biofoams using sawdust — sustainable technology for waste reduction. *J. Clean. Prod.* 234, 225–232. doi:10.1016/j.jclepro.2019.06.150

Chen, R., Cheng, Y., Wang, P., Wang, Q., Wan, S., Huang, S., et al. (2021). Enhanced removal of Co(II) and Ni(II) from high-salinity aqueous solution using reductive self-assembly of three-dimensional magnetic fungal hyphal/graphene oxide nanofibers. *Sci. Total Environ.* 756, 143871. doi:10.1016/j.scitotenv.2020.143871

Duan, B., Huang, Y., Lu, A., and Zhang, L. (2018). Recent advances in chitin based materials constructed via physical methods. *Prog. Polym. Sci.* 82, 1–33. doi:10.1016/j.progpolymsci.2018.04.001

Elsacker, E., Vandelook, S., Van Wylick, A., Ruytinx, J., De Laet, L., and Peeters, E. (2020). A comprehensive framework for the production of mycelium-based lignocellulosic composites. *Sci. Total Environ.* 725, 138431. doi:10.1016/j.scitotenv.2020.138431

Fang, L., Li, L., Qu, Z., Xu, H., Xu, J., and Yan, N. (2018). A novel method for the sequential removal and separation of multiple heavy metals from wastewater. *J. Hazard. Mat.* 342, 617–624. doi:10.1016/j.jhazmat.2017.08.072

Gandia, A., van den Brandhof, J. G., Appels, F. V. W., and Jones, M. P. (2021). Flexible fungal materials: Shaping the future. *Trends Biotechnol.* 39 (12), 1321–1331. doi:10.1016/j.tibtech.2021.03.002

Girometta, C., Picco, A. M., Baiguera, R. M., Dondi, D., Babbini, S., Cartabia, M., et al. (2019). Physico-mechanical and thermodynamic properties of mycelium-based biocomposites: A review. *Sustainability* 11 (1), 281. doi:10.3390/su11010281

Holkar, C. R., Jadhav, A. J., Pinjari, D. V., Mahamuni, N. M., and Pandit, A. B. (2016). A critical review on textile wastewater treatments: Possible approaches. *J. Environ. Manage.* 182, 351–366. doi:10.1016/j.jenvman.2016.07.090

Holt, G. A., McIntyre, G., Flagg, D., Bayer, E., Wanjura, J. D., and Pelletier, M. G. (2012). Fungal mycelium and cotton plant materials in the manufacture of biodegradable molded packaging material: Evaluation study of select blends of cotton byproducts. *J. Biobased Mat. Bioenergy* 6 (4), 431–439. doi:10.1166/jbmb.2012.1241

Hori, C., Gaskell, J., Igarashi, K., Samejima, M., Hibbett, D., Henrissat, B., et al. (2013). Genomewide analysis of polysaccharides degrading enzymes in 11 white- and brown-rot Polyporales provides insight into mechanisms of wood decay. *Mycologia* 105 (6), 1412–1427. doi:10.3852/13-072

Hu, S., Song, L., Pan, H., and Hu, Y. (2012). Effect of a novel chitosan-based flame retardant on thermal and flammability properties of polyvinyl alcohol. *J. Therm. Anal. Calorim.* 112 (2), 859–864. doi:10.1007/s10973-012-2686-7

Huber, T., Müssig, J., Curnow, O., Pang, S., Bickerton, S., and Staiger, M. P. (2011). A critical review of all-cellulose composites. *J. Mat. Sci.* 47 (3), 1171–1186. doi:10.1007/s10853-011-5774-3

Hyde, K. D., Xu, J., Rapior, S., Jeewon, R., Lumyong, S., Niego, A. G. T., et al. (2019). The amazing potential of fungi: 50 ways we can exploit fungi industrially. *Fungal Divers.* 97 (1), 1–136. doi:10.1007/s13225-019-00430-9

Jaiswal, A., Ghsoh, S. S., and Chattopadhyay, A. (2012). Quantum dot impregnated-chitosan film for heavy metal ion sensing and removal. *Langmuir* 28 (44), 15687–15696. doi:10.1021/la3027573

Jones, M., Bhat, T., Kandare, E., Thomas, A., Joseph, P., Dekiwadia, C., et al. (2018). Thermal degradation and fire properties of fungal mycelium and mycelium - biomass composite materials. *Sci. Rep.* 8 (1), 17583. doi:10.1038/s41598-018-36032-9

Jones, M., Huynh, T., Dekiwadia, C., Daver, F., and John, S. (2017). Mycelium composites: A review of engineering characteristics and growth kinetics. *J. Bionanosci.* 11 (4), 241–257. doi:10.1166/jbns.2017.1440

Jones, M., Mautner, A., Luenco, S., Bismarck, A., and John, S. (2020). Engineered mycelium composite construction materials from fungal biorefineries: A critical review. *Mater. Des.* 187, 108397. doi:10.1016/j.matdes.2019.108397

Kuribayashi, T., Lankinen, P., Hietala, S., and Mikkonen, K. S. (2022). Dense and continuous networks of aerial hyphae improve flexibility and shape retention of mycelium composite in the wet state. *Compos. Part A Appl. Sci. Manuf.* 152, 106688. doi:10.1016/j.compositesa.2021.106688

Li, Y., Zou, G., Yang, S., Wang, Z., Chen, T., Yu, X., et al. (2019). Integration of bio-inspired adsorption and photodegradation for the treatment of organics-containing radioactive wastewater. *Chem. Eng. J.* 364, 139–145. doi:10.1016/j.cej.2019.01.169

Liu, R., Long, L., Sheng, Y., Xu, J., Qiu, H., Li, X., et al. (2019). Preparation of a kind of novel sustainable mycelium/cotton stalk composites and effects of pressing temperature on the properties. *Industrial Crops Prod.* 141, 111732. doi:10.1016/j.indcrop.2019.111732

Liu, S., Qin, S., He, M., Zhou, D., Qin, Q., and Wang, H. (2020). Current applications of poly(lactic acid) composites in tissue engineering and drug delivery. *Compos. Part B Eng.* 199, 108238. doi:10.1016/j.compositesb.2020.108238

López Nava, J. A., Méndez González, J., Ruelas Chacón, X., and Nájera Luna, J. A. (2015). Assessment of edible fungi and films bio-based material simulating expanded polystyrene. *Mater. Manuf. Process.* 31 (8), 1085–1090. doi:10.1080/10426914.2015.1070420

Matos, M. P., Teixeira, J. L., Nascimento, B. L., Griza, S., Holanda, F. S. R., and Marino, R. H. (2019). Production of biocomposites from the reuse of coconut powder colonized by Shiitake mushroom. *Cienc. Agrotec.* 43. doi:10.1590/1413-7054201943003819

Meyer, V., Basenko, E. Y., Benz, J. P., Braus, G. H., Caddick, M. X., Csukai, M., et al. (2020). Growing a circular economy with fungal biotechnology: A white paper. *Fungal Biol. Biotechnol.* 7, 5. doi:10.1186/s40694-020-00095-z

Meyer, V., Wu, B., and Ram, A. F. (2011). Aspergillus as a multi-purpose cell factory: Current status and perspectives. *Biotechnol. Lett.* 33 (3), 469–476. doi:10.1007/s10529-010-0473-8

Narayanan, K. B., and Sakthivel, N. (2011). Synthesis and characterization of nano-gold composite using Cylindrocladium floridanum and its heterogeneous catalysis in the degradation of 4-nitrophenol. *J. Hazard. Mat.* 189 (1-2), 519–525. doi:10.1016/j.jhazmat.2011.02.069

Nawawi, W., Jones, M., Murphy, R. J., Lee, K. Y., Kontturi, E., and Bismarck, A. (2020). Nanomaterials derived from fungal sources-is it the new hype? *Biomacromolecules* 21 (1), 30–55. doi:10.1021/acs.biomac.9b01141

Pala, I. R., and Brock, S. L. (2012). ZnS nanoparticle gels for remediation of Pb2+ and Hg2+ polluted water. *ACS Appl. Mat. Interfaces* 4 (4), 2160–2167. doi:10.1021/am3001538

Pelletier, M. G., Holt, G. A., Wanjura, J. D., Lara, A. J., Tapia-Carillo, A., McIntyre, G., et al. (2017). An evaluation study of pressure-compressed acoustic absorbers grown on agricultural by-products. *Industrial Crops Prod.* 95, 342–347. doi:10.1016/j.indcrop.2016.10.042

Qin, H., Hu, T., Zhai, Y., Lu, N., and Aliyeva, J. (2020). Sonochemical synthesis of ZnS nanolayers on the surface of microbial cells and their application in the removal of heavy metals. *J. Hazard. Mat.* 400, 123161. doi:10.1016/j.jhazmat.2020.123161

Qiu, M. Q., Liu, L. J., Ling, Q., Cai, Y. W., Yu, S. J., Wang, S. Q., et al. (2022). Biochar for the removal of contaminants from soil and water: A review. *Biochar* 4 (1), 19. doi:10.1007/s42773-022-00146-1

Rashid, R., Shafiq, I., Akhter, P., Iqbal, M. J., and Hussain, M. (2021). A state-of-the-art review on wastewater treatment techniques: The effectiveness of adsorption method. *Environ. Sci. Pollut. Res.* 28 (8), 9050–9066. doi:10.1007/s11356-021-12395-x

Rashid, T., Iqbal, D., Abu, H., Hussain, S., Sher, F., and Sher, F. (2020). Formulation of zeolite supported nano-metallic catalyst and applications in textile effluent treatment. *J. Environ. Chem. Eng.* 8 (4), 104023. doi:10.1016/j.jece.2020.104023

Sabantina, L., Kinzel, F., Hauser, T., Tobber, A., Klocker, M., Dopke, C., et al. (2019). Comparative study of Pleurotus ostreatus mushroom grown on modified PAN nanofiber mats. *Nanomater. (Basel)* 9 (3), 475. doi:10.3390/nano9030475

Saravanan, A., Kumar, P. S., Govarthanan, M., George, C. S., Vaishnavi, S., Moulishwaran, B., et al. (2021). Adsorption characteristics of magnetic nanoparticles coated mixed fungal biomass for toxic Cr(VI) ions in aquatic environment. *Chemosphere* 267, 129226. doi:10.1016/j.chemosphere.2020.129226

Shah, A. A., Hasan, F., Hameed, A., and Ahmed, S. (2008). Biological degradation of plastics: A comprehensive review. *Biotechnol. Adv.* 26 (3), 246–265. doi:10.1016/j.biotechadv.2007.12.005

Sharma, R., and Sumbria, R. (2022). Mycelium bricks and composites for sustainable construction industry: A state-of-the-art review. *Innov. Infrastruct. Solut.* 7 (5), 298. doi:10.1007/s41062-022-00903-y

Su, Y., Hu, X., Tang, H. J., Lu, K., Li, H. M., Liu, S. J., et al. (2022). Author Correction: Steam disinfection releases micro(nano)plastics from silicone-rubber baby teats as examined by optical photothermal infrared microspectroscopy. *Nat. Nanotechnol.* 17 (6), 672. doi:10.1038/s41565-022-01155-8

Sun, W., Tajvidi, M., Hunt, C. G., McIntyre, G., and Gardner, D. J. (2019). Fully bio-based hybrid composites made of wood, fungal mycelium and cellulose nanofibrils. *Sci. Rep.* 9 (1), 3766. doi:10.1038/s41598-019-40442-8

Tacer-Caba, Z., Varis, J. J., Lankinen, P., and Mikkonen, K. S. (2020). Comparison of novel fungal mycelia strains and sustainable growth substrates to produce humidity-resistant biocomposites. *Mater. Des.* 192, 108728. doi:10.1016/j.matdes.2020.108728

Tudryn, G. J., Smith, L. C., Freitag, J., Bucinell, R., and Schadler, L. S. (2018). Processing and morphology impacts on mechanical properties of fungal based biopolymer composites. *J. Polym. Environ.* 26 (4), 1473–1483. doi:10.1007/s10924-017-1047-9

Wang, B., Yu, B., Yuan, C., Guo, L., Liu, P., Gao, W., et al. (2022). An overview on plasticized biodegradable corn starch-based films: The physicochemical properties and gelatinization process. *Crit. Rev. Food Sci. Nutr.* 62 (10), 2569–2579. doi:10.1080/10408398.2020.1868971

Wang, Y., Liu, Y., Li, J., Chen, Y., Liu, S., and Zhong, C. (2022). Engineered living materials (ELMs) design: From function allocation to dynamic behavior modulation. *Curr. Opin. Chem. Biol.* 70, 102188. doi:10.1016/j.cbpa.2022.102188

Yang, L., Park, D., and Qin, Z. (2021). Material function of mycelium-based biocomposite: A review. *Front. Mat.* 8. doi:10.3389/fmats.2021.737377

Yu, J., Paterson, N., Blamey, J., and Millan, M. (2017). Cellulose, xylan and lignin interactions during pyrolysis of lignocellulosic biomass. *Fuel* 191, 140–149. doi:10.1016/j.fuel.2016.11.057

Zhang, X. J., Hu, J. Y., Fan, X. D., and Yu, X. (2022). Naturally grown mycelium-composite as sustainable building insulation materials. *J. Clean. Prod.* 342, 130784. doi:10.1016/j.jclepro.2022.130784

Zhou, H., Fan, T., Zhang, D., Guo, Q., and Ogawa, H. (2007). Novel bacteria-templated sonochemical route for the *in situ* one-step synthesis of ZnS hollow nanostructures. *Chem. Mat.* 19 (9), 2144–2146. doi:10.1021/cm0629311

Zhu, W., Lei, J., Li, Y., Dai, L., Chen, T., Bai, X., et al. (2019). Procedural growth of fungal hyphae/Fe3O4/graphene oxide as ordered-structure composites for water purification. *Chem. Eng. J.* 355, 777–783. doi:10.1016/j.cej.2018.08.215

frontiers | Frontiers in Bioengineering and Biotechnology

TYPE Original Research
PUBLISHED 25 January 2023
DOI 10.3389/fbioe.2022.1093402

OPEN ACCESS

EDITED BY
Xiao-Jun Ji,
Nanjing Tech University, China

REVIEWED BY
Chengwei Liu,
Northeast Forestry University, China
Asha Chaubey,
Indian Institute of Integrative Medicine (CSIR), India

*CORRESPONDENCE
Shaoxin Chen,
sxzlb@263.net
Xuenian Huang,
huangxn@qibebt.ac.cn

†These authors have contributed equally to this work and share first authorship.

SPECIALTY SECTION
This article was submitted to Industrial Biotechnology, a section of the journal Frontiers in Bioengineering and Biotechnology

RECEIVED 09 November 2022
ACCEPTED 28 December 2022
PUBLISHED 25 January 2023

CITATION
Hu M, Zhou Y, Du S, Zhang X, Tang S, Yang Y, Zhang W, Chen S, Huang X and Lu X (2023), Construction of an efficient *Claviceps paspali* cell factory for lysergic acid production.
Front. Bioeng. Biotechnol. 10:1093402.
doi: 10.3389/fbioe.2022.1093402

Construction of an efficient *Claviceps paspali* cell factory for lysergic acid production

Mingzhe Hu[1,2,3,4†], Yu Zhou[2,3,4,5†], Siyu Du[2,3,4], Xuan Zhang[2,3,4], Shen Tang[2,3,4], Yong Yang[6], Wei Zhang[2,3,4,7], Shaoxin Chen[8*], Xuenian Huang[2,3,4*] and Xuefeng Lu[2,3,4,7,9]

[1]College of Life Sciences, Qingdao University, Qingdao, China, [2]Shandong Provincial Key Laboratory of Synthetic Biology, Qingdao Institute of Bioenergy and Bioprocess Technology, Chinese Academy of Sciences, Qingdao, China, [3]Shandong Energy Institute, Qingdao, China, [4]Qingdao New Energy Shandong Laboratory, Qingdao, China, [5]Institute for Smart Materials and Engineering, University of Jinan, Jinan, China, [6]Shisenhai (Hangzhou) Biopharmaceutical Co., Ltd., Hangzhou, China, [7]University of Chinese Academy of Sciences, Beijing, China, [8]State Key Lab of New Drug and Pharmaceutical Process, Shanghai Institute of Pharmaceutical Industry, Shanghai, China, [9]Marine Biology and Biotechnology Laboratory, Qingdao National Laboratory for Marine Science and Technology, Qingdao, China

Lysergic acid (LA) is the key precursor of ergot alkaloids, and its derivatives have been used extensively for the treatment of neurological disorders. However, the poor fermentation efficiency limited its industrial application. At the same time, the hardship of genetic manipulation has hindered the metabolic engineering of *Claviceps* strains to improve the LA titer further. In this study, an efficient genetic manipulation system based on the protoplast-mediated transformation was established in the industrial strain *Claviceps paspali*. On this basis, the gene *lpsB* located in the ergot alkaloids biosynthetic gene cluster was deleted to construct the LA-producing cell factory. Plackett-Burman and Box-Behnken designs were used in shaking flasks, achieving an optimal fermentation medium composition. The final titer of LA and iso-lysergic acid (ILA) reached 3.7 g·L^{-1}, which was 4.6 times higher than that in the initial medium. Our work provides an efficient strategy for the biosynthesis of LA and ILA and lays the groundwork for its industrial production.

KEYWORDS

lysergic acid, *Claviceps paspali*, metabolic engineering, medium composition, fermentation optimization

1 Introduction

Ergot alkaloids (EA) are a class of natural products known for their extensive pharmacologic activities (Wallwey and Li, 2011; Hulvová et al., 2013; Jakubczyk et al., 2014). They are structurally similar to dopamine, serotonin and adrenaline, and exhibit neurotoxicity by acting on the neurotransmitter receptors of tryptamine derivatives (Mantegani et al., 1999; Liu and Jia, 2017). Many natural and semi-synthetic ergot alkaloids, such as ergometrine, nicergoline and cabergoline, have been developed as important clinical drugs to treat *postpartum* hemorrhages, Alzheimer's disease, Parkinson's disease and other disorders (Baskys and Hou, 2007; Perez-Lloret and Rascol, 2010; Robinson and Panaccione, 2015). As an important pharmaceutical intermediate, LA is applied to the industrial production of nicergoline, cabergoline and dihydroergotamine. And LA derivatives, such as lysergic acid diethylamide (LSD), have been widely used in the therapy of psychiatric diseases (Young et al., 2015; Chen et al., 2017). Due to high demand in the market, up to 10–15 tons of LA have been produced annually (Hulvová et al., 2013; Wong et al., 2022). However, the current industrial production of LA shows low production efficiency and high

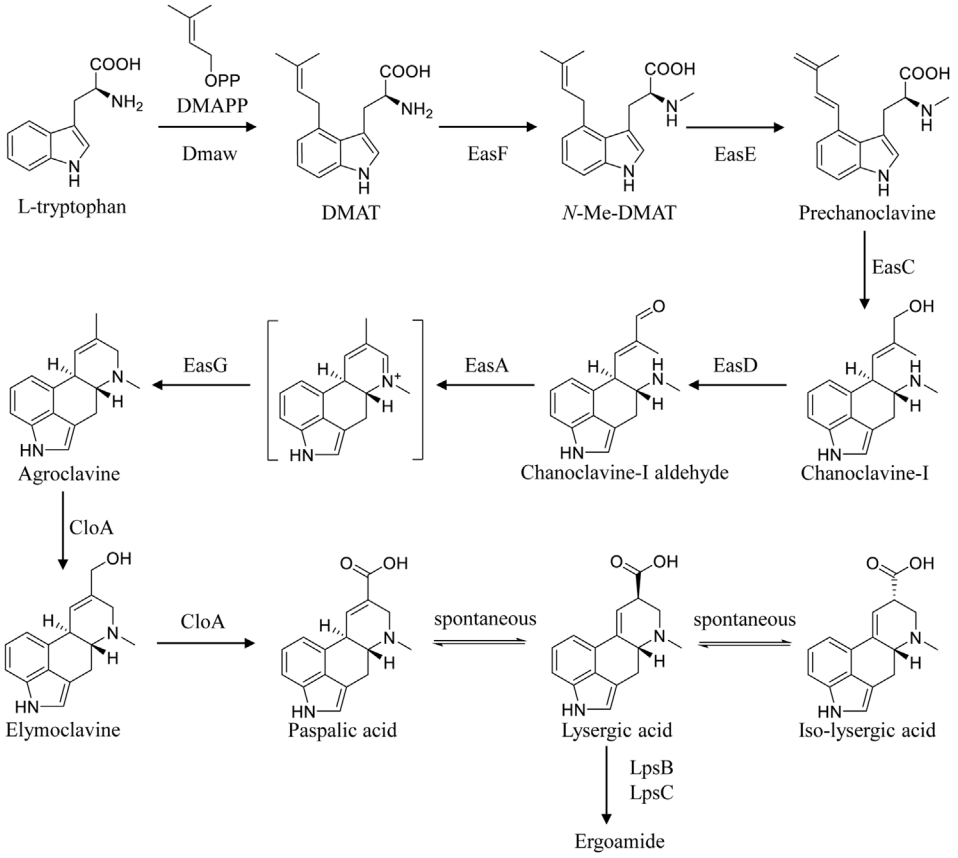

FIGURE 1
The complete biosynthetic and metabolic pathways of LA in *C. paspali*.

cost. There is no sophisticated scheme to directly produce LA in the current industry. All the LA is acquired from alkali hydrolysis of ergometrine. About 40%–50% of ergometrine is obtained from the parasitic production of ergot on rye (field cultivation), which highly depends on the climate and growth conditions of the host (Tudzynski et al., 2001). The rest of ergometrine has been contributed by the submerged fermentation using *Claviceps paspali* (Hulvová et al., 2013; Wong et al., 2022). Complicated post-processing and separation severely restrict the yield. Hence, efficient LA-producing cell factories are urgently needed to improve the production efficiency in industry.

In *Claviceps*, the biosynthetic pathway of EA is broadly classified into three parts (Chen et al., 2017). Firstly, the biosynthesis of chanoclavine-I-aldehyde, the common steps in all EA-producing species, requires five enzymes including DmaW, EasF, EasC, EasE, and EasD (Chen et al., 2017; Wong et al., 2022). Then, the introduction of EasA, EasG, and CloA can result in the formation of LA from chanoclavine-I-aldehyde (Robinson and Panaccione, 2014; Chen et al., 2017). Finally, LA is activated by LpsB and converted into ergoamides by LpsC (Correia et al., 2003; Ortel and Keller, 2009; Chen et al., 2017). Progress in ergot alkaloid biosynthesis provides new clues for the construction of LA-producing cell factories (Figure 1)(Chen et al., 2017). Wong *et al.* reconstituted the LA biosynthetic pathway in *Saccharomyces cerevisiae* and screened the key enzymes for functional expression from different sources, constructing a LA-producing strain with 1.7 mg·L^{-1} titer after 5 days culture in a 1 L bioreactor (Wong et al., 2022). Yao *et al.* expressed the key genes involved in EA biosynthesis in heterologous host *Aspergillus nidulans*, yielding trace amounts of LA (Yao et al., 2022). Besides, other engineered heterologous LA-producing strains, for instance, *Metarhizium brunneum*, *Neosartorya fumigate*, and *Aspergillus fumigatus*, were constructed with low titer (Robinson and Panaccione, 2014; Arnold and Panaccione, 2017; Davis et al., 2020; Yao et al., 2022). However, LA production in the above heterogeneous cell factories cannot meet actual industrial demand. It has been reported that some of the enzymes involved in the biosynthetic pathway of EA were poorly expressed in heterologous host (Coyle et al., 2010; Nielsen et al., 2014; Wong et al., 2022), hampering the improvement of the production. Thus, we turn to the metabolic engineering of industrial strains *C. paspali* MJXA-WT with high-yield ergometrine, which may avoid the incompatibility of expression elements and heterologous host. The genetic transformation method for the genus *Claviceps* has been reported over the past decades (Hulvová et al., 2013). Protoplast-mediated transformation is the most popular method for the genetic transformation of *Claviceps*. A successful transformation method for *Claviceps purpurea* based on the protoplast preparation was first described in 1989 (van Engelenburg et al., 1989). And the conditions of protoplast formation and regeneration were further optimized (Comino et al., 1989; Smit and Tudzynski, 1992; Mey et al., 2002; Wang et al., 2016). Besides, the *Agrobacterium tumefaciens*-mediated transformation method for *C. purpurea* has been attempted, but no successful procedure has been described

(Hulvová et al., 2013). However, there are few reports on the genetic transformation for *C. paspali*. Engelenburg *et al.* developed a protoplast-mediated transformation system for *C. purpurea*, while suffering from low protoplast regeneration efficiency when applied to *C. paspali* (van Engelenburg et al., 1989; Kozák et al., 2018). The *Agrobacterium tumefaciens*-mediated transformation system had been successfully applied in *C. paspali*, which is operational complexity and time consuming (Kozák et al., 2018).

The lack of genetic tools of *C. paspali* hindered the process of constructing high-yield strains through metabolic engineering. In this study, we established an effective system of genetic manipulation in the industrial strain of *C. paspali* MJXA-WT in the first step. Based on this, the *lpsB* gene was deleted in *C. paspali*, leading to the accumulation of LA and ILA in mutants. Finally, the fermentation process was developed and optimized for the engineered strain in shaking flasks.

2 Materials and methods

2.1 Microorganism and culture conditions

C. paspali MJXA-WT is an industrial ergometrine-producing strain frozen at −80°C in our lab at Qingdao Institute of Bioenergy and Bioprocess Technology, Chinese Academic of Science, China. The strains were maintained on PDA (39 g·L^{-1} PDA dry powder, BD company) at 25°C for 6 days, and then 3 cm^2 fresh mycelium from the PDA plates was transferred to a 250-mL flask containing 25 mL of seed medium (20 g·L^{-1} mannitol, 10 g·L^{-1} succinic acid, 2 g·L^{-1} soybean cake powder, 1 g·L^{-1} KH_2PO_4, 0.3 g·L^{-1} $MgSO_4{\cdot}7H_2O$, and pH 5.0) and cultured for 4 days at 25°C, 220 rpm. The seed liquid was inoculated into 250-mL flask containing 25 mL of fermentation medium (100 g·L^{-1} sorbitol, 35 g·L^{-1} succinic acid, 20 g·L^{-1} corn steep powder, 0.5 g·L^{-1} yeast extract powder, 0.022 g·L^{-1} $FeSO_4{\cdot}7H_2O$, 0.01 g·L^{-1} $ZnSO_4{\cdot}7H_2O$, 0.7 g·L^{-1} $MgSO_4{\cdot}7H_2O$, pH 5.5). The flasks were kept in the dark for 12 days at 25°C, 220 rpm. An inoculum ratio of 15% (v/v) was used in all bioprocess. All the experiments were repeated three times in this study.

2.2 DNA manipulation for cassettes construction

Primers used in this study are listed in Supplementary Table S1. To knock out gene *lpsB*, primer pairs Up-lpsB-F/Up-lpsB-hph-R and Down-lpsB-hph-F/Down-lpsB-R were used to amplify the flanking 5' and 3' DNA of the *lpsB* gene from the genome of *C. paspali* MJXA-WT. The resulting DNA fragments were fused with the *hph* marker by fusion PCR. Primers N-lpsB-F/N-lpsB-R were used to amplify the gene-targeting cassette.

2.3 Protoplast-mediated transformation

About 3 cm^2 of fresh mycelium from the PDA plates was crushed and inoculated into 100 mL of PDB medium and cultured for 3–4 days at 25°C, 220 rpm. The mycelium was collected by filtering with sterile 300 mesh nylon cloth, and washed twice with 0.7 M KCl solution. The mycelium was immersed in the enzymatic solution (0.1% of lywallzyme), and incubated at 30°C for 1 h to prepare protoplasts. The culture solution was filtered with 500 mesh nylon cloth and centrifuged for 12 min at 4,000 rpm to obtain protoplasts. The protoplasts were resuspended with 10 mL of STC solution (0.85 M sorbitol, 10 Tris-HCl pH 8.0, 50 mM $CaCl_2$), and centrifuged for 10 min at 3,400 rpm. The precipitation of protoplasts was diluted to 10^7 cells/mL. Then 2–4 μg of DNA fragments, 100 μL protoplast solution and 50 μL of ice-cold PSTC (25% PEG 6000, 1 M D-sorbitol, 10 mM Tris-HCl pH 8.0, and 50 mM $CaCl_2$) were mixed, and incubated on ice for 25 min. After that, 1 mL of PSTC was added and incubated for 20 min. Afterwards, 20 mL of liquid top agar (PDB with 0.5% agarose and 0.4 M D-sorbitol) was added and the mixture was spread on PDAS (PDA with 0.4 M D-sorbitol). The plates were cultured in the dark for 7 days at 30 C.

2.4 HPLC analysis

LA and ILA were analyzed by high-performance liquid chromatography (HPLC) equipped with a C18 reversed-phase column (Agilent, 4.6 × 150 mm, 5 μm). 1 mL of fermentation supernatant was extracted with 4 mL of mixed solvent containing acetonitrile and water (1:1, v/v) for HPLC and LC-MS measurement. The mobile phases were as follows: water with 0.1% $(NH_4)_2CO_3$ (solvent A); and 75% acetonitrile (solvent B). Chromatography was carried out over a flow rate of 1.2 mL/min, with a stepped gradient as follows: 13%–43% B from 0–12 min, 43% B for 1 min, 13% B for 1 min. LA and ILA were quantified by comparing peak areas to standard curves under 254 nm. The titers of LA and ILA were quantified by HPLC according to the calibration curves respectively. The calibration curves were presented as Supplementary Figure S1.

2.5 Plackett-Burman design (PBD) of the experiment

To determine the significant factors influencing the LA and ILA titer in submerged fermentation, six factors including inoculum amount (A), succinic acid (B), corn steep powder (C), yeast extract (D), sorbitol (E), and $MgSO_4{\cdot}7H_2O$ (F) were handpicked for PBD. The final titer of total lysergic acid (TLA), including LA and ILA, was chosen as the response. For each independent factor, there were high (+1) and low (−1) levels, which were determined based on the single factor experiment, and used to assess the influence of each factor. The coded level and actual level of each factor are listed in Table 1. All experiments were repeated three times.

2.6 Box-Behnken design (BBD) of the experiment

The most monumental factors were chosen to identify their optimal level with the LA and ILA titer as the response. Three significant factors identified by PBD were corn steep powder (A), succinic acid (B) and yeast extract (C). For each variable, there were low (−1), middle (0) and high (+1) levels. The coded level and actual

TABLE 1 PBD for the evaluation of the factors influencing TLA titer.

Code factors	Factors	Coded level and actual level	
		−1	+1
A	Inoculum amount (mL)	3	5
B	Succinic acid ($g{\cdot}L^{-1}$)	25	45
C	Corn steep powder ($g{\cdot}L^{-1}$)	10	30
D	Yeast extract ($g{\cdot}L^{-1}$)	0	0.5
E	Sorbitol ($g{\cdot}L^{-1}$)	100	140
F	$MgSO_4{\cdot}7H_2O$ ($g{\cdot}L^{-1}$)	1	2

TABLE 2 BBD for the evaluation of the factors influencing TLA titer.

Code factors	Factors	Coded level and actual level		
		-1	0	+1
A	Corn steep powder ($g{\cdot}L^{-1}$)	10	20	30
B	Succinic acid ($g{\cdot}L^{-1}$)	25	35	45
C	Yeast extract ($g{\cdot}L^{-1}$)	0	0.25	0.5

level of three factors is listed in Table 2. All the experiments were repeated three times.

3 Results and discussion

3.1 Development of genetic manipulation system in *C. paspali*

Inefficient genetic manipulation system restricted metabolic engineering of *C. paspali*. Protoplast-mediated transformation is widely and efficiently used in ascomycetes transformation. Therefore, we choose this method to establish the genetic manipulation system in *C. paspali*. As an industrial strain, *C. paspali* MJXA-WT lost the sporulation ability, the mycelium from PDA plates was used as seeds for cultivation of mycelium. Poor mycelium leads to difficulties in protoplast preparation and low efficiency of cell wall regeneration. Homologous recombination usually occurs in logarithmic growth period. The regeneration efficiency was mainly depended on the culture time of mycelia. We tried to apply the mycelia of non-sporulating *C. paspali* MJXA-WT cultured in original medium for different time to transformation. However, it showed very low regeneration efficiency probably due to the slow growth state. Luckily, we found that the mycelia of *C. paspali* MJXA-WT grew very fast only in the PDB medium, and the hyphae of *C. paspali* MJXA-WT cultivated in PDB medium for 3-days was applied to the enzymatic digestion in next step. Enzyme solution of 0.1% lywallzyme was used to digest cell wall, which produced 1.0×10^6 cells/mL at 30°C in an hour or so. STC solution was used to wash and resuspend the protoplasts at 1.0×10^7 cells/mL. In the PEG-$CaCl_2$ mediated transformation, 2–4 μg of DNA fragments, a cassette containing *PgpdAt* (constitutive promoter of glyceraldehyde-3-phosphate dehydrogenase from *Aspergillus terreus*), *sgfp* (synthetic green fluorescent protein), *TtrpC* (terminator of tryptophan synthetase from *Aspergillus nidulans*) and *hph* (hygromycin B phosphotransferase gene), was added in 100 μL protoplasts solution. The D-sorbitol concentration of regeneration medium was optimized, and the optimal concentration was 0.4 M (Supplementary Table S2). Beginning with 1.0×10^7 protoplasts, approximately 120–150 positive clones were obtained in a reaction (Supplementary Figure S2). Transformants were verified by genomic PCR. The representative mutant strains displayed significant green fluorescence under the fluorescence microscope, while the parental strain did not show any visible fluorescence (Figure 2). Consequently, an efficient genetic manipulation system, which was based on the

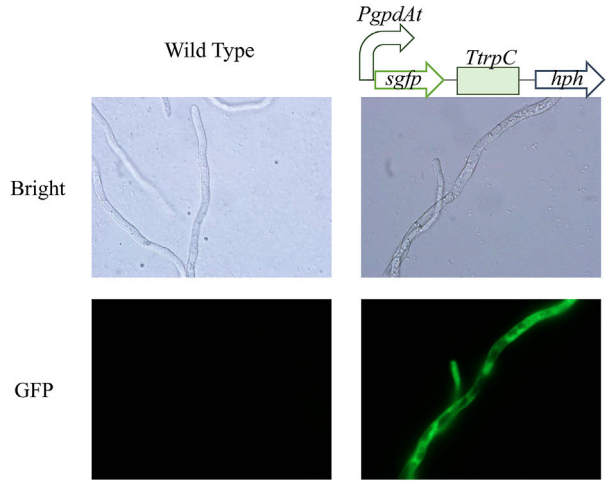

FIGURE 2
Microscopic features of wild-type and mutant strains. Bright: Bright-field images. GFP: Fluorescence images.

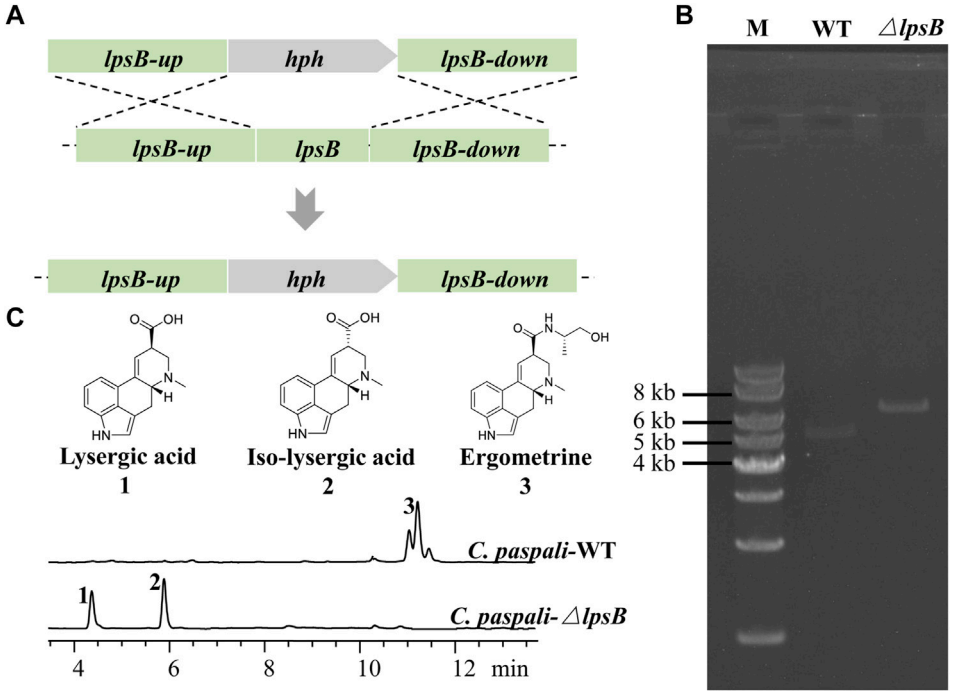

FIGURE 3
Construction of the LA-producing cell factory. **(A)** Strategy for deleting *lpsB* gene in *C. paspali* MJXA-WT. **(B)** Genotype verification. Lane M: 1 kb DNA marker; lane WT: *C. paspali* MJXA-WT; lane *ΔlpsB*: parent strain *C. paspali* MJXA-*ΔlpsB-hph*. **(C)** HPLC analysis of wild-type and mutant strains.

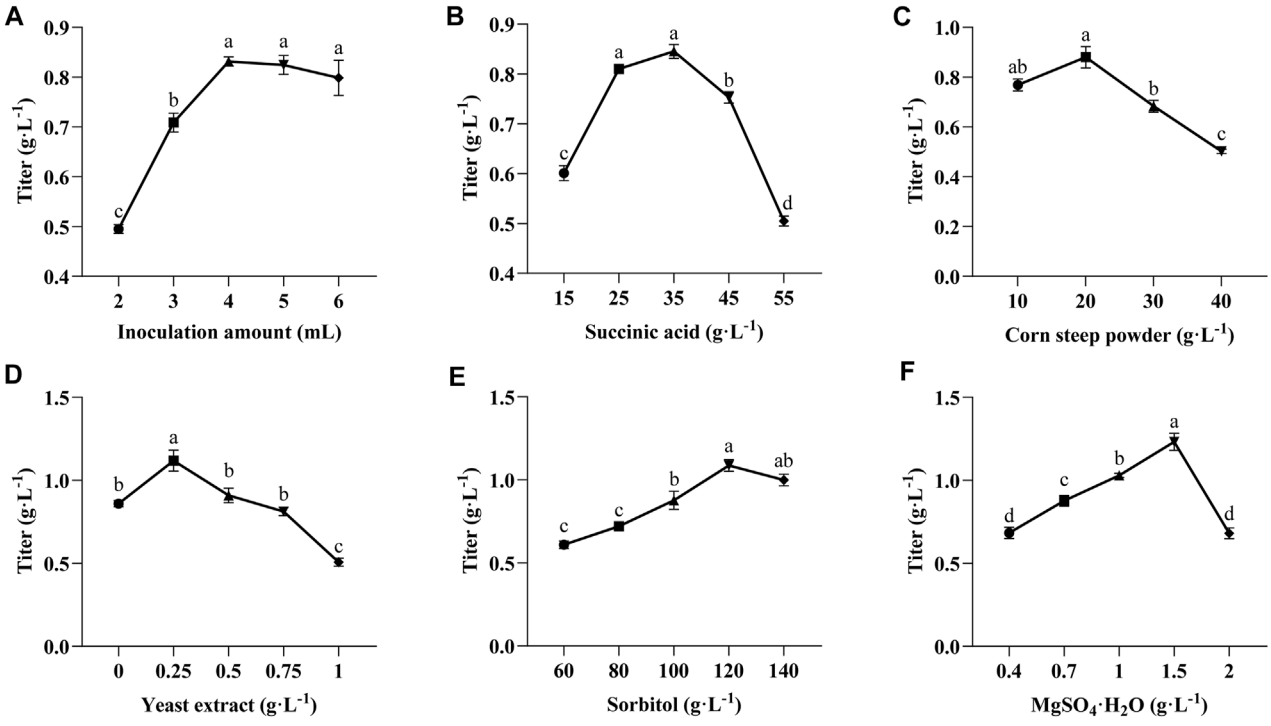

FIGURE 4
Effect of inoculation amount **(A)** and initial medium components of succinic acid **(B)**, corn steep powder **(C)**, yeast extract **(D)**, sorbitol **(E)** and $MgSO_4{\cdot}7H_2O$ **(F)** on LA and ILA accumulation. Lowercase alphabets indicate that the values are statistically significant with corresponding *p*-values less than 0.05.

TABLE 3 PBD factors affecting the titer of TLA.

Run order	A	B	C	D	E	F	Response
	Inoculum size	Succinic acid	Corn steep powder	Yeast extract	Sorbitol	$MgSO_4·7H_2O$	Titer of TLA ($g·L^{-1}$)
1	1	−1	1	1	−1	−1	1.36 ± 0.05
2	1	−1	1	1	−1	1	1.56 ± 0.01
3	−1	−1	−1	1	1	−1	2.19 ± 0.10
4	−1	−1	1	−1	1	1	1.08 ± 0.04
5	1	1	−1	1	1	−1	2.94 ± 0.05
6	1	1	−1	−1	−1	1	2.20 ± 0.01
7	−1	1	−1	1	−1	1	2.57 ± 0.02
8	1	−1	−1	−1	1	1	1.87 ± 0.02
9	−1	1	1	−1	−1	−1	1.60 ± 0.03
10	1	1	1	−1	1	−1	1.54 ± 0.01
11	−1	−1	−1	−1	−1	−1	1.82 ± 0.01
12	−1	1	1	1	1	1	2.10 ± 0.06

TABLE 4 ANOVA of PBD with F and *p* values.

Source	Sum of squares	Degrees of freedom	Mean square	F-value	*p*-value
Model	2.9624	6	0.4937	27.85	0.0011
A-Inoculum amount	0.0010	1	0.0010	0.06	0.8210
B-Succinic acid	0.7854	1	0.7854	44.30	0.0012
C-Corn steep powder	1.5769	1	1.5769	88.95	0.0002
D-Yeast extract	0.5677	1	0.5677	32.02	0.0024
E-Sorbitol	0.0310	1	0.0310	1.75	0.2433
F-$MgSO_4·7H_2O$	0.0004	1	0.0004	0.02	0.8853
Residual	0.0886	5	0.0177		
Total	3.0510	11			

protoplast-mediated transformation, was established in the industrial strain *C. paspali* MJXA-WT.

3.2 Construction of the LA-producing cell factory

The gene *lpsB* was involved in the modification of LA in the biosynthetic pathway of ergometrine (Figure 1). We tried to knock out *lpsB* to prevent the biosynthesis of ergometrine, resulting in the accumulation of LA. The targeting element was constructed using *hph* as a marker. About 1 kb region in *lpsB* gene was replaced by the *hph* (2.2 kb) (Figure 3A). As shown in Figure 3B, the *lpsB* gene was successfully disrupted in mutant strains (Figure 3B). Knocking out *lpsB* eliminated the production of ergometrine but accumulated two new products with identical molecular ion peaks ($[M + H]^+$ 269.1303) (Figure 3C; Supplementary Figure S3). The new products were identified as LA and ILA by further NMR analyses (Supplementary Figures S4, 5) (Liu and Jia, 2011). The ^1H and ^{13}C NMR data of ILA showed quite similar signals to those of LA. The noticeable differences were the occurrence of C-8 (δC 42.7, δH 3.54–3.50) in ILA, rather than C-8 (δC 44.4, δH 4.09–4.04) carbons in LA. Supplementary Table S3 indicated the attribution of ^1H and ^{13}C NMR data for LA and ILA. Due to its instability, LA could be partially converted to its isomer ILA (Stoll et al., 1949; Himmelsbach et al., 2014; Yao et al., 2022). The percentages of LA were stabilized at around 45%, while the percentages of ILA were stabilized at around 55%. Base on this, we used the titer of TLA to evaluate the change of production in the next step.

3.3 Effects of initial media components on LA and ILA accumulation

Since various factors in the fermentation medium affect the titer of TLA, an effective experimental approach, such as

TABLE 5 BBD for factors affecting the titer of TLA.

Run order	A	B	C	Response
	Corn steep powder	Succinic acid	Yeast extract	Titer of TLA ($g·L^{-1}$)
1	1	0	1	3.09 ± 0.00
2	−1	−1	0	1.49 ± 0.00
3	0	0	0	3.41 ± 0.00
4	−1	0	−1	1.48 ± 0.02
5	1	−1	0	2.02 ± 0.01
6	0	0	0	3.34 ± 0.04
7	0	1	−1	2.00 ± 0.03
8	0	−1	−1	1.63 ± 0.03
9	0	0	0	3.03 ± 0.13
10	1	1	0	2.74 ± 0.00
11	0	−1	1	2.25 ± 0.00
12	0	0	0	3.36 ± 0.00
13	0	1	1	3.07 ± 0.01
14	−1	1	0	1.99 ± 0.07
15	0	0	0	3.44 ± 0.05
16	−1	0	1	2.02 ± 0.03
17	1	0	−1	2.01 ± 0.02

TABLE 6 Analysis of variance for regression model of LA and ILA production.

Source	Sum of squares	Degrees of freedom	Mean square	F-value	*p*-value
Model	8.66	9	0.9623	271.56	<0.0001
A	1.04	1	1.04	292.59	<0.0001
B	0.726	1	0.726	204.88	<0.0001
C	1.37	1	1.37	386.48	<0.0001
AB	0.0121	1	0.0121	3.41	0.1071
AC	0.0729	1	0.0729	20.57	0.0027
BC	0.0506	1	0.0506	14.29	0.0069
A^2	2.08	1	2.08	586.81	<0.0001
B^2	1.59	1	1.59	449.78	<0.0001
C^2	1.16	1	1.16	327.81	<0.0001
Residual	0.0248	7	0.0035		
Lack of Fit	0.0135	3	0.0045	1.6	0.3227
Pure Error	0.0113	4	0.0028		
Cor Total	8.69	16			

Plackett-Burman and Box-Behnken design, is essential to achieve the optimal production. First, single-factor experiments were selected to assess the influence of inoculum amount and five key components of the medium (succinic acid, corn steep powder, yeast extract, sorbitol, and $MgSO_4·7H_2O$) on the titer of TLA. The influence of different inoculum amount on the titer of TLA

10.3389/fbioe.2022.1093402

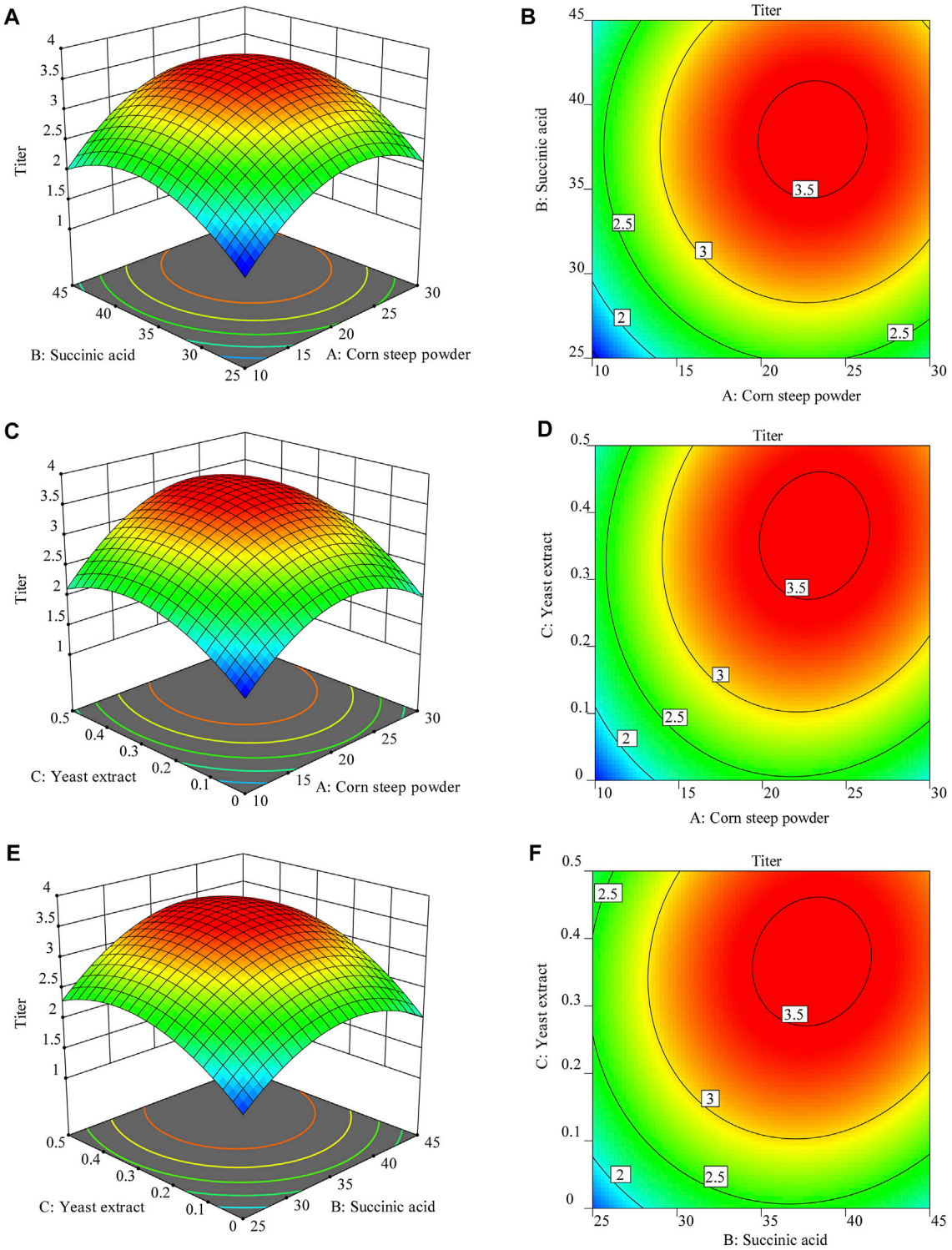

FIGURE 5
Three-dimensional response surfaces of **(A)** corn steep powder and succinic acid; **(C)** corn steep powder and yeast extract; **(E)** succinic acid and yeast extract, contour plots of **(B)** corn steep powder and succinic acid; **(D)** corn steep powder and yeast extract; **(F)** succinic acid and yeast extract.

was shown in Figure 4A. With the increase of inoculum amount, the titer of TLA improved. The highest titre was obtained when the inoculum amount was 4 mL, reaching 0.83 g·L^{-1}. The production curve of the titer of TLA tended to flatten when the inoculum amount was more than 4 mL. The effect of succinic acid with the addition between 25 g·L^{-1} to 45 g·L^{-1} was not significant (Figure 4B), the production was highest when the concentration was 35 g·L^{-1}. A high titer of TLA was obtained with 20 g·L^{-1} corn steep powder added, while the titer of TLA decreased when the corn steep powder concentration was

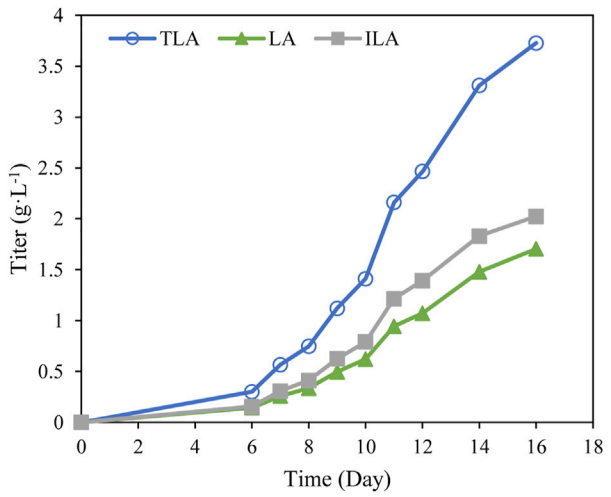

FIGURE 6
The time profile of the production of TLA using the optimal fermentation medium.

further increased (Figure 4C). When the concentration of yeast extract was 0.25 g·L^{-1}, the titer of TLA reached the maximum, and then decreased significantly with the increase of yeast extract content (Figure 4D). Increasing sorbitol and $MgSO_4{\cdot}7H_2O$ concentrations enhanced the titer of TLA. A maximum titer of TLA of 1.09 g·L^{-1} and 1.23 g·L^{-1} was achieved when sorbitol and $MgSO_4{\cdot}7H_2O$ were added in the medium with the concentration of 120 g·L^{-1} and 1.5 g L^{-1}, respectively (Figures 4E, F).

3.4 Identification of significant factors using PBD

PBD, a two-level experimental design (Abdel-Fattah et al., 2005; Abuhena et al., 2022), was further used to screen out the crucial factors which have a significant impact on the titer of TLA. The experimental data were shown in Table 3. And analysis of experimental results was listed in Table 4 using Design Expert 12.0 software. As the F-value was 27.85 and the *p*-value of 0.0011 was less than 0.05, the model was significant. Two factors, succinic acid and yeast extract were identified as the significant factors influencing the titer of TLA, with corresponding *p*-values less than 0.05. The corresponding *p*-values of corn steep powder was less than 0.001, implying that it was highly significant. Others factors, inoculum amount, sorbitol and $MgSO_4{\cdot}7H_2O$, with corresponding *p*-values more than 0.1, implied that they were not significant. Another important evaluation indicator of the model quality is R^2. The values of R^2, predicated R^2 and adjusted R^2 were 0.9709, 0.9361, and 0.8327, respectively, indicating that the predicted model was highly fit and effective. The final equation in terms of actual factors was derived as follows:

$$Y = 1.903 + 0.009A + 0.256B - 0.363C + 0.218D + 0.051E - 0.006F$$

According to the regression coefficient, four factors (inoculum amount, succinic acid, yeast extract and sorbitol) showed positive effects on the titer of TLA. Besides, succinic acid and $MgSO_4{\cdot}7H_2O$ showed negative effects. Succinic acid, corn steep powder, and yeast extract were chosen as key factors for further optimization. Succinic acid in the tricarboxylic acid cycle was usually used as a carbon source, which may promote the high level of oxidative metabolism in the *Claviceps* cells, promoting the biosynthesis of secondary metabolites (Hulvová et al., 2013). Fermentation nitrogen (corn steep powder and yeast extract) are particularly rich in protein and amino acid, such as tryptophan and methionine, which may promote the synthesis of ergot alkaloids (Hulvová et al., 2013; Chen et al., 2017).

3.5 Optimization of culture medium using BBD

BBD is a reliable method which is usually used to identify the optimum response region for significant factors (Hegazy et al., 2022). In this study, three significant factors (corn steep powder, (A); succinic acid, (B); yeast extract, (C)) were further explored at three levels. The experimental data were shown in Table 5. And analysis of experimental results was listed in Table 6 using Design Expert 12.0 software. As the F-value was 271.56 and the *p*-value was less than 0.0001, the model was highly significant. The corresponding *p*-values of A, B, and C were both less than 0.0001, suggesting that these factors were highly significant. In the same light, the corresponding *p*-values of A^2, B^2, and C^2 were both less than 0.0001. The values of R^2, predicated R^2 and adjusted R^2 were 0.9971, 0.9935, and 0.9731, respectively, indicating that the model was effective and reliable. To predict the optimal point, the final equation fitted to the experimental response results was represented below:

$$Y = 3.38 + 0.36A + 0.301B + 0.414C + 0.055AB + 0.135AC + 0.113BC - 0.703A^2 - 0.615B^2 - 0.525C^2$$

According to the equation, the predicted optimum of the cultural medium consisted of 37.2 g·L^{-1} succinic acid, 23.5 g·L^{-1} corn steep liquor powder, and 0.4 g·L^{-1} yeast extract powder, and the predicated titer was 3.6 g·L^{-1}. The value of R^2 was 0.997, indicating a great degree of correlation between the experimental and the predicted values.

To better evaluate the interaction effect between three key factors, three-dimensional response surfaces and contour plots were created in Figure 5. Based on the surface drawing and contour drawing of response surface model, Figures 5A, B showed the interaction effect of corn steep powder and succinic acid on the titer of TLA with the concentration of yeast extract was 0.4 g·L^{-1}. Increasing the corn steep powder and succinic acid to the optimal point improved the titer of TLA. However, the increased amount of both factors leaded to the decline of the titer. Figures 5C, D showed the interaction effect of corn steep powder and yeast extract on the titer of TLA with the concentration of succinic acid was 37.2 g·L^{-1}. Increasing the addition of corn steep powder and yeast extract to the optimal point improved the titer of TLA. However, improving concentration of both factors leaded to the decline of the titer. Figures 5E, F showed the interaction effect of succinic acid and yeast extract on the titer of TLA with the concentration of corn steep powder was 23.5 g·L^{-1}. Increasing the concentration of

succinic acid and yeast extract to the optimal point improved the titer of TLA. However, improving concentration of both factors leaded to the decline of the titer.

To verify the developed model, the time profile of TLA production under the optimal fermentation condition was analyzed. After 16 days culture, the final titer of TLA reached 3.7 $g{\cdot}L^{-1}$ using the optimal fermentation medium (Figure 6), which was close to the predicted value 3.6 $g{\cdot}L^{-1}$. Hence, the validity of this model was verified. Whereas, the titer of TLA reached 0.8 $g{\cdot}L^{-1}$ using the original fermentation medium. It indicates that an efficient microbial fermentation technology for LA production has been developed using an engineered *C. paspali* strain.

4 Conclusion

In this study, an efficient genetic manipulation system, which was based on the protoplast-mediated transformation, was established in the industrial strain *C. paspali*. Based on this, LA and ILA were accumulated in the *ΔlpsB* strain. By single factor optimization, PBD and BBD optimization in shaking flasks, an optimal fermentation medium composition was obtained. The final titer of TLA reached 3.7 $g{\cdot}L^{-1}$, which was 4.6-fold of that in the initial medium. Our work provides an efficient strategy for LA production, and lays the foundation for its industrial application in the future.

Data availability statement

The original contributions presented in the study are included in the article/Supplementary Material, further inquiries can be directed to the corresponding authors.

Author contributions

XH, SC, and XL conceived the project; SC provide the parent strain of *Claviceps paspali*. MH, ST, and XZ performed the fungal engineering; YZ, MH, SD, and YY performed the fermentation experiments and analysed the results with the help of WZ, MH, YZ, and XZ drafted the manuscript; XH, XZ, and XL revised the manuscript. All authors read the manuscript and agree to submit to Frontiers in Bioengineering and Biotechnology.

Funding

This work was supported by the National Key R&D Program of China (No. 2021YFC2102600), the National Natural Science Foundation of China (U2032139, 32170098, 81903483), Key R&D Program of Shandong Province (No. 2021ZDSYS02). XL and XH are supported by the Shandong Taishan Scholarship.

Conflict of interest

Author YY is employed by Shisenhai (Hangzhou) Biopharmaceutical Co., Ltd.

The remaining authors declare that the research was conducted in the absence of any commercial or financial relationships that could be construed as a potential conflict of interest.

Publisher's note

Supplementary material

The Supplementary Material for this article can be found online at: https://www.frontiersin.org/articles/10.3389/fbioe.2022.1093402/full#supplementary-material

References

Abdel-Fattah, Y. R., Saeed, H. M., Gohar, Y. M., and El-Baz, M. A. (2005). Improved production of *Pseudomonas aeruginosa* uricase by optimization of process parameters through statistical experimental designs. *Process. Biochem.* 40 (5), 1707–1714. doi:10.1016/j.procbio.2004.06.048

Abuhena, M., Al-Rashid, J., Azim, M. F., Khan, M. N. M., Kabir, M. G., Barman, N. C. B., et al. (2022). Optimization of industrial (3000 L) production of *Bacillus subtilis* CW-S and its novel application for minituber and industrial-grade potato cultivation. *Sci. Rep.* 12, 11153. doi:10.1038/s41598-022-15366-5

Arnold, S. L., and Panaccione, D. G. (2017). Biosynthesis of the pharmaceutically important fungal ergot alkaloid dihydrolysergic acid requires a specialized allele of *cloA*. *Appl. Environ. Microbiol.* 83 (14), e00805–e00817. doi:10.1128/AEM.00805-17

Baskys, A., and Hou, A. C. (2007). Vascular dementia: Pharmacological treatment approaches and perspectives. *Clin. Interv. Aging.* 2 (3), 327–335.

Chen, J.-J., Han, M.-Y., Gong, T., Yang, J.-L., and Zhu, P. (2017). Recent progress in ergot alkaloid research. *RSC Adv.* 7, 27384–27396. doi:10.1039/C7RA03152A

Comino, A., Kolar, M., Schwab, H., and Sočič, H. (1989). Heterologous transformation ofClaviceps purpurea. *Claviceps Purpurea. Biotechnol. Lett.* 11, 389–392. doi:10.1007/BF01089469

Correia, T., Grammel, N., Ortel, I., Keller, U., and Tudzynski, P. (2003). Molecular cloning and analysis of the ergopeptine assembly system in the ergot fungus *Claviceps purpurea*. *Chem. Biol.* 10 (12), 1281–1292. doi:10.1016/j.chembiol.2003.11.013

Coyle, C. M., Cheng, J. Z., O'Connor, S. E., and Panaccione, D. G. (2010). An old yellow enzyme gene controls the branch point between *Aspergillus fumigatus* and *Claviceps purpurea* ergot alkaloid pathways. *Appl. Environ. Microbiol.* 76 (12), 3898–3903. doi:10.1128/AEM.02914-09

Davis, K. A., Sampson, J. K., and Panaccione, D. G. (2020). Genetic reprogramming of the ergot alkaloid pathway of *Metarhizium brunneum*. *Appl. Environ. Microbiol.* 86 (19), 012511–e1320. doi:10.1128/AEM.01251-20

Hegazy, G. E., Abu-Serie, M. M., Abou-Elela, G. M., Ghozlan, H., Sabry, S. A., Soliman, N. A., et al. (2022). Bioprocess development for biosurfactant production by *Natrialba* sp. M6 with effective direct virucidal and anti-replicative potential against HCV and HSV. *Sci. Rep.* 12 (1), 16577. doi:10.1038/s41598-022-20091-0

Himmelsbach, M., Ferdig, M., and Rohrer, T. (2014). Analysis of paspalic acid, lysergic acid, and iso-lysergic acid by capillary zone electrophoresis with UV- and quadrupole time-of-flight mass spectrometric detection. *Electrophoresis* 35 (9), 1329–1333. doi:10.1002/elps.201300224

Hulvová, H., Galuszka, P., Frébortová, J., and Frébort, I. (2013). Parasitic fungus *Claviceps* as a source for biotechnological production of ergot alkaloids. *Biotechnol. Adv.* 31 (1), 79–89. doi:10.1016/j.biotechadv.2012.01.005

Jakubczyk, D., Cheng, J. Z., and O'Connor, S. E. (2014). Biosynthesis of the ergot alkaloids. *Nat. Prod. Rep.* 31 (10), 1328–1338. doi:10.1039/c4np00062e

Kozák, L., Szilágyi, Z., Vágó, B., Kakuk, A., Tóth, L., Molnár, I., et al. (2018). Inactivation of the indole-diterpene biosynthetic gene cluster of *Claviceps paspali* by *Agrobacterium-*

mediated gene replacement. *Appl. Microbiol. Biotechnol.* 102 (7), 3255–3266. doi:10.1007/s00253-018-8807-x

Liu, Q., and Jia, Y. (2011). Total synthesis of (+)-lysergic acid. *Org. Lett.* 13 (18), 4810–4813. doi:10.1021/ol2018467

Liu, H., and Jia, Y. (2017). Ergot alkaloids: Synthetic approaches to lysergic acid and clavine alkaloids. *Nat. Prod. Rep.* 34 (4), 411–432. doi:10.1039/c6np00110f

Mantegani, S., Brambilla, E., and Varasi, M. (1999). Ergoline derivatives: Receptor affinity and selectivity. *Farmaco* 54 (5), 288–296. doi:10.1016/s0014-827x(99)00028-2

Mey, G., Held, K., Scheffer, J., Tenberge, K. B., and Tudzynski, P. (2002). CPMK2, an SLT2-homologous mitogen-activated protein (MAP) kinase, is essential for pathogenesis of *Claviceps purpurea* on rye: evidence for a second conserved pathogenesis-related MAP kinase cascade in phytopathogenic fungi. *Mol. Microbiol.* 46 (2), 305–318. doi:10.1046/j.1365-2958.2002.03133.x

Nielsen, C. A. F., Folly, C., Hatsch, A., Molt, A., Schröder, H., O'Connor, S. E., et al. (2014). The important ergot alkaloid intermediate chanoclavine-I produced in the yeast *Saccharomyces cerevisiae* by the combined action of EasC and EasE from *Aspergillus japonicus*. *Microb. Cell Fact.* 13, 95. doi:10.1186/s12934-014-0095-2

Ortel, I., and Keller, U. (2009). Combinatorial assembly of simple and complex D-lysergic acid alkaloid peptide classes in the ergot fungus *Claviceps purpurea*. *J. Biol. Chem.* 284 (11), 6650–6660. doi:10.1074/jbc.M807168200

Perez-Lloret, S., and Rascol, O. (2010). Dopamine receptor agonists for the treatment of early or advanced Parkinson's disease. *CNS Drugs* 24 (11), 941–968. doi:10.2165/11537810-000000000-00000

Robinson, S. L., and Panaccione, D. G. (2014). Heterologous expression of lysergic acid and novel ergot alkaloids in *Aspergillus fumigatus*. *Appl. Environ. Microbiol.* 80 (20), 6465–6472. doi:10.1128/AEM.02137-14

Robinson, S. L., and Panaccione, D. G. (2015). Diversification of ergot alkaloids in natural and modified fungi. *Toxins* 7 (1), 201–218. doi:10.3390/toxins7010201

Smit, R., and Tudzynski, P. (1992). Efficient transformation of *Claviceps purpurea* using pyrimidine auxotrophic mutants: cloning of the OMP decarboxylase gene. *Mol. Gen. Genet.* 234 (2), 297–305. doi:10.1007/BF00283850

Stoll, A., Hofmann, A., and Troxler, F. (1949). Über die Isomerie von Lysergsäure und Isolysergsäure. 14. Mitteilung über Mutterkornalkaloide. *Helv. Chim. Acta.* 32 (2), 506–521. doi:10.1002/hlca.19490320219

Tudzynski, P., Correia, T., and Keller, U. (2001). Biotechnology and genetics of ergot alkaloids. *Appl. Microbiol. Biotechnol.* 57 (5-6), 593–605. doi:10.1007/s002530100801

van Engelenburg, F., Smit, R., Goosen, T., van den Broek, H., and Tudzynski, P. (1989). Transformation of *Claviceps purpurea* using a bleomycin resistance gene. *Appl. Microbiol. Biotechnol.* 30, 364–370. doi:10.1007/BF00296625

Wallwey, C., and Li, S.-M. (2011). Ergot alkaloids: Structure diversity, biosynthetic gene clusters and functional proof of biosynthetic genes. *Nat. Prod. Rep.* 28 (3), 496–510. doi:10.1039/c0np00060d

Wang, W.-B., Chen, J.-J., and Zhu, P. (2016). Establishment of transformation system of *Claviceps purpurea* Cp-1 strain. *Acta Pharm. Sin.* 51 (5), 828–833.

Wong, G., Lim, L. R., Tan, Y. Q., Go, M. K., Bell, D. J., Freemont, P. S., et al. (2022). Reconstituting the complete biosynthesis of D-lysergic acid in yeast. *Nat. Commun.* 13 (1), 712. doi:10.1038/s41467-022-28386-6

Yao, Y., Wang, W., Shi, W., Yan, R., Zhang, J., Wei, G., et al. (2022). Overproduction of medicinal ergot alkaloids based on a fungal platform. *Metab. Eng.* 69, 198–208. doi:10.1016/j.ymben.2021.12.002

Young, C. A., Schardl, C. L., Panaccione, D. G., Florea, S., Takach, J. E., Charlton, N. D., et al. (2015). Genetics, genomics and evolution of ergot alkaloid diversity. *Toxins* 7 (4), 1273–1302. doi:10.3390/toxins7041273

frontiers | Frontiers in Bioengineering and Biotechnology

TYPE Original Research
PUBLISHED 30 January 2023
DOI 10.3389/fbioe.2023.1117890

OPEN ACCESS

EDITED BY
Zhi-Qiang Liu,
Zhejiang University of Technology, China

REVIEWED BY
Feng Cheng,
Zhejiang University of Technology, China
Jinhui Feng,
Tianjin Institute of Industrial Biotechnology (CAS), China

*CORRESPONDENCE
Rongzhen Zhang,
rzzhang@jiangnan.edu.cn

SPECIALTY SECTION
This article was submitted to Industrial Biotechnology, a section of the journal Frontiers in Bioengineering and Biotechnology

RECEIVED 07 December 2022
ACCEPTED 19 January 2023
PUBLISHED 30 January 2023

CITATION
Li L, Zhang R, Xu Y and Zhang W (2023), Comprehensive screening strategy coupled with structure-guided engineering of L-threonine aldolase from *Pseudomonas putida* for enhanced catalytic efficiency towards L-*threo*-4-methylsulfonylphenylserine.
Front. Bioeng. Biotechnol. 11:1117890.
doi: 10.3389/fbioe.2023.1117890

Comprehensive screening strategy coupled with structure-guided engineering of L-threonine aldolase from *Pseudomonas putida* for enhanced catalytic efficiency towards L-*threo*-4-methylsulfonylphenylserine

Lihong Li[1], Rongzhen Zhang[1]*, Yan Xu[1] and Wenchi Zhang[2]

[1]Lab of Brewing Microbiology and Applied Enzymology, School of Biotechnology and Key Laboratory of Industrial Biotechnology of Ministry of Education, Jiangnan University, Wuxi, China, [2]Solomon H. Snyder Department of Neuroscience, Johns Hopkins University School of Medicine, Baltimore, MD, United States

L-Threonine aldolases (TAs) can catalyze aldol condensation reactions to form β-hydroxy-α-amino acids, but afford unsatisfactory conversion and poor stereoselectivity at the C_β position. In this study, a directed evolution coupling high-throughput screening method was developed to screen more efficient L-TA mutants based on their aldol condensation activity. A mutant library with over 4000 L-TA mutants from *Pseudomonas putida* were obtained by random mutagenesis. About 10% of mutants retained activity toward 4-methylsulfonylbenzaldehyde, with five site mutations (A9L, Y13K, H133N, E147D, and Y312E) showing higher activity. Iterative combinatorial mutant A9V/Y13K/Y312R catalyzed L-*threo*-4-methylsulfonylphenylserine with a 72% conversion and 86% diastereoselectivity, representing 2.3-fold and 5.1-fold improvements relative to the wild-type. Molecular dynamics simulations illustrated that additional hydrogen bonds, water bridge force, hydrophobic interactions, and π-cation interactions were present in the A9V/Y13K/Y312R mutant compared with the wild-type to reshape the substrate-binding pocket, resulting in a higher conversion and C_β stereoselectivity. This study provides a useful strategy for engineering TAs to resolve the low C_β stereoselectivity problem and contributes to the industrial application of TAs.

KEYWORDS

threonine aldolases, *Pseudomonas putida*, high-throughput screening, structure-guided engineering, product enantioselectivity

Introduction

Pyridoxal-5-phosphate (PLP)-dependent threonine aldolase (TA, EC 4.1.2.5) catalyzes the reversible aldol condensation reaction of glycine and aldehydes to form β-hydroxy-α-amino acids in a single step (Contestabile et al., 2001; Lypetska et al., 2014). β-Hydroxy-α-amino acids are important chiral building blocks for the preparation of agrochemicals and pharmaceuticals

Abbreviations: DNPH, 2,4-dinitrophenylhydrazine; HTS, high-throughput screening; ICM, iterative combinatorial mutagenesis; MSBA, 4-methylsulfonylbenzaldehyde; MSPS, l-threo-4-methylsulfonylphenylserine; PLP, pyridoxal-5-phosphate; SM, saturation mutation; TA, threonine aldolase.

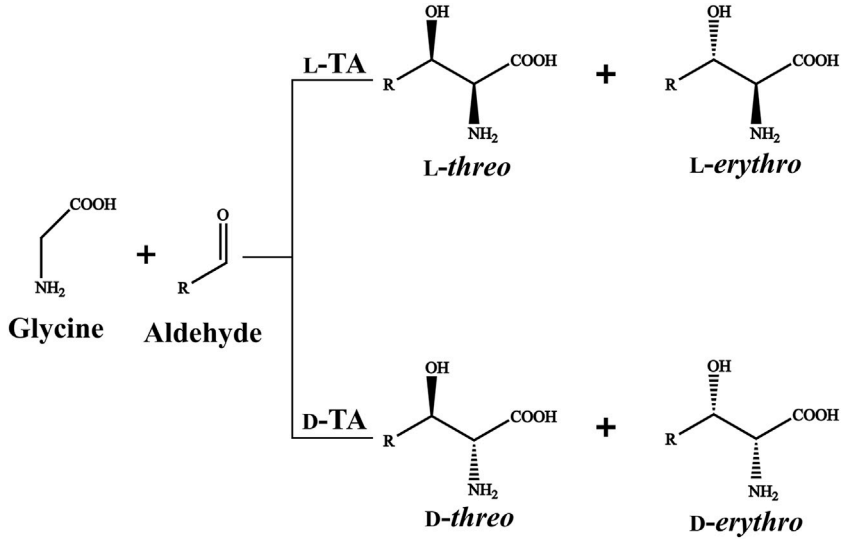

FIGURE 1
L-TA/D-TA catalyzed reaction.

bioactive products (Steinreiber et al., 2007; Hibi et al., 2015). For example, L-*threo*-4-methylsulfonylphenylserine (MSPS) is a key precursor for the production of antibiotics, thiamphenicol and florfenicol (Zhao et al., 2011), and L-*threo*-3,4-dihydroxyphenylserine is an anti-Parkinsonism drug approved by Food and Drug Administration (Zhao et al., 2021).

TA-mediated β-hydroxy-α-amino acids biosynthesis is regarded as a feasible alternative owing to their high stereoselectivity, uncomplicated reaction procedure and environmental friendliness. TAs consist of L-TA and D-TA based on the C_α stereospecificity of the products (Fesko et al., 2015). L-TAs generate the L-*threo* and L-*erythro* products, while D-TAs form D-*threo* and D-*erythro* products (Figure 1). Most of TAs have an excellent stereoselectivity towards C_α but exhibit poor stereoselectivity at the C_β (Duckers et al., 2010; Wang et al., 2021). The inadequate C_β stereoselectivity has limited the application of TAs in industrial production (Fesko et al., 2018). Thus, it is urgent to develop the novel TAs with good stereoselectivity at the C_α and C_β simultaneously using a rapid and reliable method.

Recently, substantial attempts have been devoted for engineering TAs to enhance the stereoselectivity at the C_β. Fesko et al. (2008) labeled 4 TAs with ^{13}C- distribution in the retro-aldol reaction and determined the formation of glycine–PLP quinonoid complex. (Liu Z. C. et al., 2020) found that residues external the catalytic pocket also affected the C_β stereoselectivity of TA from *Pseudomonas* sp. And Chen et al. (2019) developed a substrate-binding-guided mutagenesis and stepwise visual screening method to improve or invert C_β-stereoselectivity of TA from *Pseudomonas* sp. All reported methods represent the methodology to improve C_β stereoselectivity, while fundamentally resolve the "C_β" problem requires more efforts.

Directed evolution is considered as a common means to modify the enzymes performance (Ali et al., 2020; Qu et al., 2020), such as expanding substrate spectrum (Zheng et al., 2017), enhancing catalytic functions (Wu et al., 2020), and improving stereoselectivity (Li et al., 2021). Site-directed saturation mutagenesis (SM) strategies are commonly used to mutate residues lining or adjacent the catalytic pocket, such as structure-based combinatorial protein engineering (Wang et al., 2021), combinatorial active site saturation test (Reetz et al., 2005) and iterative combinatorial mutagenesis (ICM) (Liu Y. F. et al., 2020). The directed evolution and site-mutagenesis ideally in combination might be a useful strategy for improving TAs-catalyzed reaction efficiency.

Moreover, traditional enzyme activity of TAs was determined according to the retro-aldol reaction (Steinreiber et al., 2007; Fesko, 2016). In this assay, threonine is transformed into glycine and acetaldehyde by TAs. Then, yeast alcohol dehydrogenase reduces acetaldehyde to ethanol and simultaneously oxidizes NADH to NAD^+, monitoring the decrease of absorbance at 340 nm. However, in this method, retro-aldol reaction replaced aldol reaction for β-hydroxy-α-amino acids synthesis, and threonine as model substrate substituted the actually used substrate. In view of the application, the properties of variants on the product synthesis are far more relevant (Giger et al., 2012; Liu et al., 2014). Thus, TA evolution coupling with a high-throughput screening (HTS) method is required to be developed, which can monitor synthesis efficiency of β-hydroxy-α-amino acids by aldol reaction.

Previously, we identified an aldolase L-PpTA from *Pseudomonas putida* KT2440, which could synthesize L-*threo*-4-methylsulfonylphenylserine with glycine and 4-methylsulfonylbenzaldehyde as substrates (Li et al., 2019). In this work, we evolved L-PpTA to construct a high-quality library, and developed an efficient and sensitive HTS method basing visual color reaction of 2,4-dinitrophenylhydrazine (DNPH). The mutants with improved L-*threo*-4-methylsulfonylphenylserine biotransformation were screened basing the enzyme activity in aldol reaction direction. Then, we employed SM/ICM strategy to combine beneficial site mutations to obtain the best variant. This work will supply good protein engineering strategy for improving C_β-stereoselectivity of TA enzymes.

Experimental sections

Microorganisms and chemicals

Escherichia coli BL21 (DE3) stored in our laboratory served as host strain. NADH, PLP and acetonitrile were purchased from Sigma-

Aldrich (Shanghai, China). The PrimeSTAR DNA polymerase and restriction enzymes were purchased from Takara (Dalian, China). The ClonExpress MultiS One Step Cloning Kit was purchased from Vazyme (Nanjing, China). L-*threo*-4-methylsulfonylphenylserine was purchased from Baishansheng Bio-Technology Co., Ltd (Hangzhou, China). All other chemicals used were of the highest grade and commercially available.

Construction of recombinant strain with L-PpTA

The gene *latE* (GenBank accession no. AE015451.2) coding for L-TA from *Pseudomonas putida* KT2440 (L-PpTA) was chemically synthesized by Shenggong Co. Ltd. (Shanghai, China). It was cloned into the vector pET28a in *E. coli* BL21 (DE3). Recombinant *E. coli* BL21/pET28a-L-PpTA was acquired after DNA sequencing.

Construct mutant library by error prone PCR

Error-prone PCR of L-PpTA was carried out using the recombinant plasmid pET28a-L-PpTA as a template. The reaction mixture (50 μl) contains reaction buffer, 2.5 mM dNTP mixture, 100 μM $MnSO_4$, 500 μM $MgCl_2$, 0.1 μM per primer pair, 10 ng template and 1.25 U rTaq polymerase and ultra-pure water. Forward primers were 5′- AGCAAATGGGTCGCGGATCCATGA CCGATAAAAGCCAGCAG-3′ and reverse primers were 5′-GGT GGTGGTGGTGCTCGAGTTAGCCACCGATGATG GTACG-3′. PCR was performed at 98 °C for 30 s, 55°C for 30 s, and 72°C for 60 s for 34 cycles. The PCR products were cloned into the pET28a vector between *Bam*H I and *Xho* I sites using Exnase ClonExpress MultiS One Step Cloning Kit, followed by transformation into the competent cells of *E. coli* BL21 (DE3). The recombinant *E. coli* cells were cultured on LB plates added with 50 μg·ml^{-1} kanamycin and incubated overnight at 37°C to obtain the mutant library.

The colonies on LB plates were displaced into 96-well plates (each containing 500 μl LB medium and 50 μg·ml^{-1} kanamycin), and incubated at 37°C for 3 h. 0.1 mM IPTG was added to induce the protein expression at 25°C for 14 h. The cells were collected by centrifugation with 6,000 × g for 5 min.

HTS of the mutant library by DNPH screening method

The enzyme assay mixture (200 μl) contained 100 mM HEPES-NaOH buffer (pH 8.0), appropriate amount of enzyme solution, 150 μl of 2.5 mM 4-methylsulfonylbenzaldehyde (MSBA) dissolved with 10% DMSO, 30 μl of 25 mM glycine and 10 μl of 50 μM PLP. The reaction mixture was shaken at 200 rpm, 30°C for 5 min. Color reaction was carried out as follows: 10 μl of the above-mentioned reaction mixture was added into 90 μl of 20 mM 2,4-dinitrophenylhydrazine (DNPH) dissolved in 10% HCl, and the reaction was performed for 1 min to obtain the white sediment. And 100 μl of 4 M NaOH was added into the white sediment, resulting in the red-brown solution. The absorbance of the red-brown solution was determined at 470 nm by spectrophotometer (Biotek, Vermont, United States). To achieve high detection sensitivity, the effect of incubation time (1, 2, 3, 4, 5, 10, 20 and 30 min) and alkalis (NaOH, KOH, Na_2CO_3, K_2CO_3, Na_2SO_4, K_2SO_4, $NaHCO_3$, and $KHCO_3$) with different pK_b values were determined.

The standard curve of MSBA using DNPH screening method was made with different concentrations of MSBA (0.25–5.0 mM) dissolved with 10% DMSO in 100 mM HEPES-NaOH buffer (pH 8.0) at 30°C and with a shaken at 200 rpm for 5 min. Then, the absorbance is determined by color reaction method.

The collected cells were suspended in 1 ml of HEPES-NaOH buffer (100 mM, pH 8.0) and screened using DNPH method. The absorbance of the red-brown solution was determined at 470 nm by a spectrophotometer. One unit of the aldol activity (U) was defined as the amount of enzyme needed to consume 1 μmol MSBA per minute. *E. coli* BL21/pET28a was regarded as a control.

Saturation mutations and combinatorial mutations

Five amino acid residues, A9, Y13, H133, E147, and Y312 lining the substrate-binding pocket were selected. The SM libraries of L-PpTA were constructed to encode 20 canonical amino acids using the degenerate codons NNK. The short fragments include the target mutations were amplified using the primers S-F and S-R. The long fragments were amplified using the primers L-F and primers L-R. Then, the short fragments and long fragments were connected using the ClonExpress MultiS One Step Cloning Kit through homologous recombination (Supplementary Figure S1). The primers used are listed in Supplementary Table S1. The beneficial mutants were screened using the DNPH screening methods from saturation mutation library. Then the double site combined mutants (A9V/Y13K, A9V/H133N, A9V/E147D, A9V/Y312R, Y13K/H133N, Y13K/E147D, Y13K/Y312R, H133N/E147D, H133N/Y312R, and E147D/Y312R) and the triple site combined mutants (A9V/Y13K/H133N, A9V/Y13K/E147D, A9V/Y13K/Y312R, Y13K/H133N/E147D, Y13K/E147D/Y312R, and H133N/E147D/Y312R) were also constructed using the homologous recombination approach.

Protein expression and purification

The recombinant *E. coli* was cultured in LB medium added with 50 μg·ml^{-1} kanamycin at 37°C and shaken at 200 rpm. When the OD_{600} value of the culture reached 0.6–0.8, 0.1 mM IPTG was supplemented to induce protein expression at 25°C for 14 h. The cells were harvested by centrifugation and suspended in buffer (20 mM Tris–HCl and 150 mM NaCl, pH 8.0) and lysed by an ultrasonic oscillator (Sonic Materials Co., Piscataway, USA). The supernatant was gathered by centrifugation (12,000 × g, 30 min) at 4°C.

The collected supernatant was loaded on a HisTrap affinity column equilibrated with buffer (20 mM Tris–HCl and 150 mM NaCl, pH 8.0), and then it was eluted with buffer (20 mM Tris–HCl, 150 mM NaCl, 1 M imidazole, pH 8.0). Afterwards the pooled fractions were applied to a Resource Q column equilibrated with buffer (20 mM Tris–HCl, pH 8.0). Finally, the fractions were loaded on a Superdex 200 (10/300 GL) gel column for chromatography. The purified L-PpTA was assayed by sodium dodecyl sulfate-polyacrylamide gel electrophoresis (SDS-PAGE).

10.3389/fbioe.2023.1117890

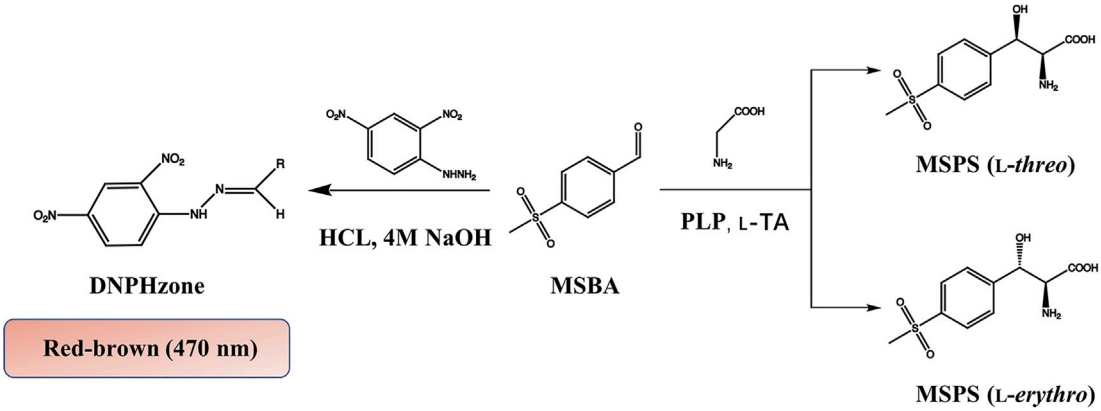

FIGURE 2
HTS colorimetric method for determining MSBA comsuption by L-PpTA.

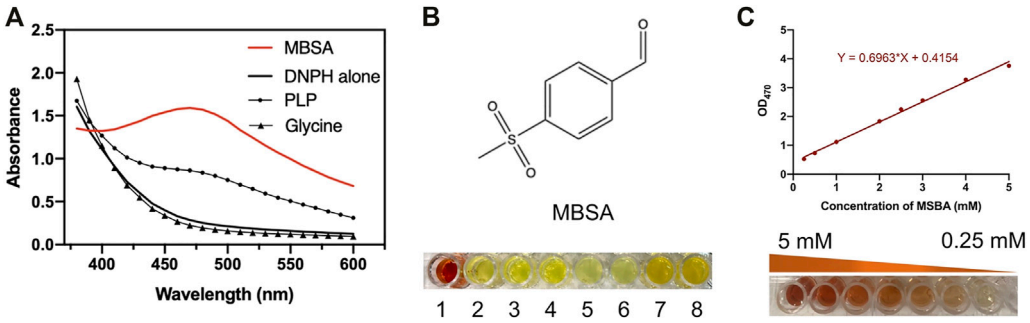

FIGURE 3
(A) Absorbance spectra of MSBA, PLP, Glycine, and DNPH; **(B)** Red-brown color formation between different alkalis including NaOH, KOH, Na_2CO_3, K_2CO_3, Na_2SO_4, K_2SO_4, $NaHCO_3$, and $KHCO_3$; **(C)** The standard curve of MSBA determined DNPH methods at OD_{470}.

Enzyme assay and kinetic determination

The enzyme activities in aldol reaction were measured on the basis of DNPH screening method. The kinetic parameters were measured at different glycine concentrations (2.5–50 mM). The K_M and k_{cat} values were determined by fitting the data to Michaelis–Menten equation using GraphPad Prism for non-linear regression. Each measurement was repeated for three times.

Biotransformation and analytical methods

The asymmetric reaction was performed in 2 mL volume consisted of 50 mM potassium dihydrogen phosphate buffer (pH 8.0), 100 mM MSBA, 1 M glycine, 50 μM PLP, 10% DMSO and an appropriate amount of enzyme solution. The reactions were performed at 30°C for 8 h with shaking at 200 rpm. At the end of reaction, the reaction solution was boiled for 10 min, and then it was diluted with 50 mM potassium dihydrogen phosphate buffer (pH 8.0). The conversion and stereospecificity of product were determined by High Performance Liquid Chromatography after its derivatization with ortho-phthaldialdehyde/N-acetyl cysteine (OPA/NAC) (Steinreiber et al., 2007) on an achiral RP18 column (250 mm/5 μm). The OPA/NAC derivative reagent was acquired by dissolving 20 mg NAC in 4 mL buffer (0.2 M boric acid, pH 10.2) and then 20 mg OPA in 1 mL acetonitrile was added. The chromatographic analysis was carried out using Agilent 1260 high performance liquid chromatography system (Agilent Technologies Inc., Palo Alto, USA) with an UV detector at 338 nm. The detection conditions were performed in the mobile phase: 50 mM KH_2PO_4, pH 8.0/acetonitrile = (81/19); flow rate: 0.8 mL·min^{-1}; temperature: 40°C; run time: 30 min.

Molecular docking and molecular dynamic simulations

P. putida L-TA (PDB ID: 5VYE) shared the similarity of 98.26% with L-PpTA in amino acid sequence. Molecular docking of L-PpTA and its variants were built with Discovery Studio using crystal structure of *P. putida* L-TA (PDB ID: 5VYE) as template. The ligands were optimized and docked into L-PpTA and its variants by using flexible docking. Molecular dynamic (MD) simulations were carried out as follows: firstly, the CHARMm force field was applied to the protein, and the system was constructed in a cubic box composed of TIP3P water molecules that stretched 10 Å away from the protein

10.3389/fbioe.2023.1117890

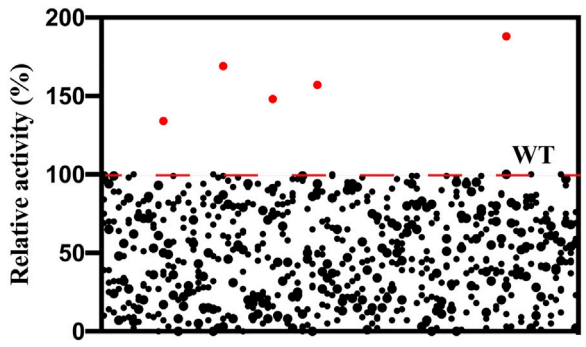

FIGURE 4
Screening of the random mutagenesis library of L-PpTA. Red dots represent the selected mutants.

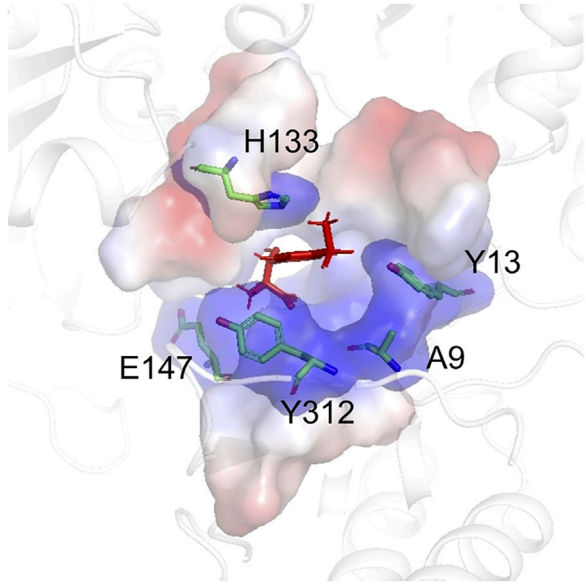

FIGURE 5
The model structure of WT L-PpTA. The enzyme backbone is represented as a cartoon in white. The substrate binding pocket is represented as a surface. The MSPS is indicated by red sticks.

surface to create a buffer zone between them; Secondly, sodium ions as counterions were added to the system to build a neutral system; Thirdly, the step of energy minimization was carried out using the conjugate gradient algorithms; Finally, the protein-ligand complex simulations with 50 ns were carried out, gradually heat the system from 0 to 300 K.

Results and discussion

Establishment of HTS method based on aldol reaction activity of L-PpTA

Recombinant *E. coli* BL21/pET28a-L-PpTA was constructed and the recombinant L-PpTA enzyme was purified. This enzyme

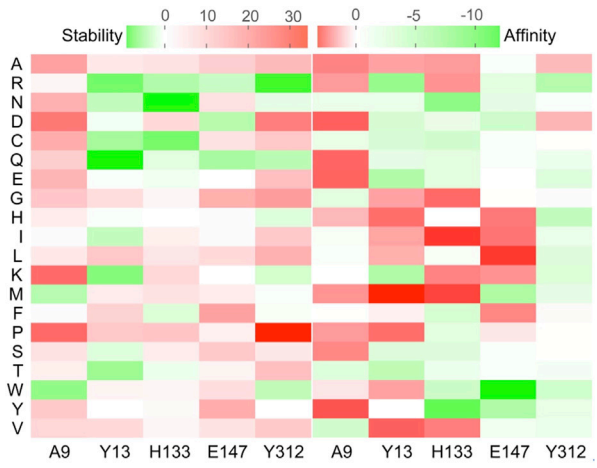

FIGURE 6
Virtual mutation of A9, Y13, H133, E147, and Y312 residues in L-PpTA.

catalyzed the transformation of substrates glycine and MSBA into MSPS owing to its aldol condensation reaction activity. MSBA is a non-natural aromatic aldehyde, whose aldehyde group can react with DNPH-zine under basic conditions to produce red-brown product DNPH-zone (Figure 2). In the L-PpTA-catalyzed aldol reaction, four potential components, namely, MSBA, DNPH, PLP, and glycine, possibly affected the absorbance. Substrate MSBA exhibited an absorbance peak at 470 nm, which was distinct from those of DNPH, PLP, and glycine (Figure 3A), indicating that the DNPH screening method was feasible for MSBA determination.

The effects of incubation time and base type on the colorimetric reaction between DNPH-zine and MSBA were investigated. Incubation for 1 min at 30°C was sufficient to produce DNPH-zone with a distinct red-brown color. Several bases with different pK_b values, including NaOH, KOH, Na_2CO_3, K_2CO_3, Na_2SO_4, K_2SO_4, $NaHCO_3$, and $KHCO_3$, were used as chromogenic reagents. The results showed that only NaOH produced the clear red-brown color (Figure 3B).

A calibration curve and detection limit were required for quantitative determination of MSBA concentration in the DNPH screening method. As shown in (Figure 3C), a linear relationship was observed in the MSBA concentration range of 0.25–5.0 mM at OD_{470}, indicating the feasibility of the DNPH screening method for low-concentration MSBA. The color became light red-brown with an increase in MSBA concentration (Figure 3C). These results demonstrated that the DNPH screening method was sufficiently sensitive for the quantification of MSBA in L-PpTA screening.

Screening five potential sites with higher aldol condensation activity using directed-evolution coupling HTS method

To obtain variants with improved aldol activity, a random mutagenesis library of L-PpTA containing 4280 variants was

10.3389/fbioe.2023.1117890

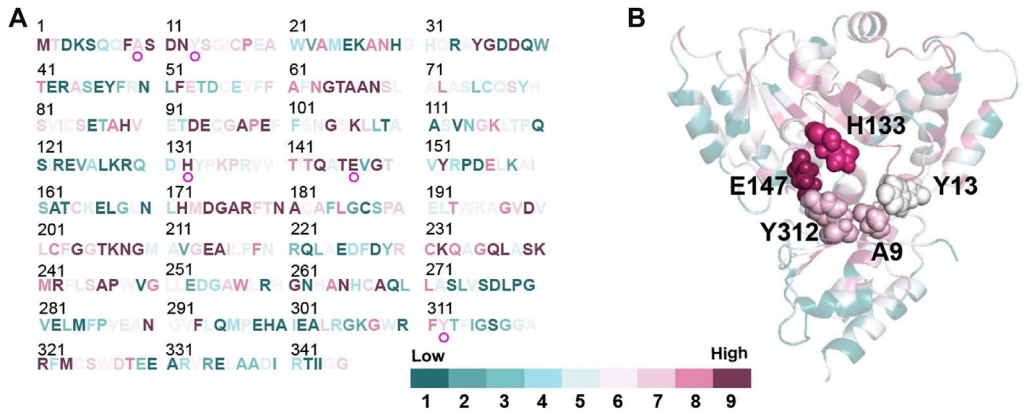

FIGURE 7
Conservation analysis of L-PpTA by ConSurf (https://consurf.tau.ac.il/). Amino acids are colored by their conservation grades. **(A)** Conservation of each amino acids residue in the protein sequence; **(B)** The protein structure of the monomer represented as a cartoon. A9, Y13, H133, E147, and Y312 are highlighted by spheres.

TABLE 1 Kinetic parameters of L-PpTA and its variants in aldol direction.

Enzymes	K_M (mM)	k_{cat} (s^{-1})	k_{cat}/K_M (s^{-1} mM^{-1})
WT	17.4	7.1	0.41
A9L	14.6	7.7	0.53
A9V	13.8	7.2	0.52
Y13C	24.7	13.9	0.56
Y13K	19.6	10.4	0.53
Y13Q	30.8	15.4	0.50
Y13R	34.4	16.8	0.49
H133N	12.8	12.7	0.99
H133Y	22.6	12.5	0.55
H133W	12.9	12.3	0.95
E147D	15.1	6.5	0.43
Y312R	20.1	12.2	0.61
Y312E	25.3	15.3	0.60
Y312K	26.3	11.04	0.42

TABLE 2 The conversion and *de* value of positive variants produced in SM and ICM.

Enzymes	Library	*de* (%)	conv (%)
WT	—	17	32
A9V	SM	51	57
Y13K	SM	50	61
H133N	SM	47	54
E147D	SM	52	35
Y312R	SM	61	58
A9V/Y13K	ICM	65	64
A9V/Y312R	ICM	71	59
Y13K/Y312R	ICM	79	61
A9V/Y13K/Y312R	ICM	86	72

constructed by the error-prone PCR technique. Selection of the beneficial mutations was attempted using the DNPH screening method (Supplementary Figure S2). The supernatant of most mutants showed reduced activity, with some completely losing activity. About 10% of the mutants retained aldol reaction activity with glycine and MSBA as substrates (Figure 4). Only five variants showed higher aldol reaction activity. After DNA sequencing, mutations A9L, Y13K, H133N, E147D, and Y312E were identified, and all were expressed as soluble forms in the recombinant *E. coli* (SupplementaryFigure S3).

The structure model of L-PpTA was built based on the known crystal structure (PDB: 5VYE) and docked with product MSPS using Discovery Studio (DS) 4.1. In the modelled L-PpTA structure, residues A9, Y13, H133, E147, and Y312 were located in the catalytic pocket area (Figure 5). The stability and affinity of protein–product complexes were calculated using the DS binding mutation energy after the five amino acids were mutated to 19 other amino acid residues (Petukh et al., 2016; Zheng et al., 2020). Lower values indicated variants with more stable protein–product complexes and higher affinities. The DS algorithm results indicated that Y13 and Y312 exhibited higher stability and affinity (Figure 6). Sequence conservation analysis showed that the five residues had moderate to high conservation. H133 and E147 were the most highly conserved (Figure 7), which might provide high evolutionary selective pressure and significantly impact protein function (Chen et al., 2019). Lee et al. found that mutations at conserved positions during evolution had a greater effect on enzyme functions than those at non-conserved positions (Lee and Goodey, 2011).

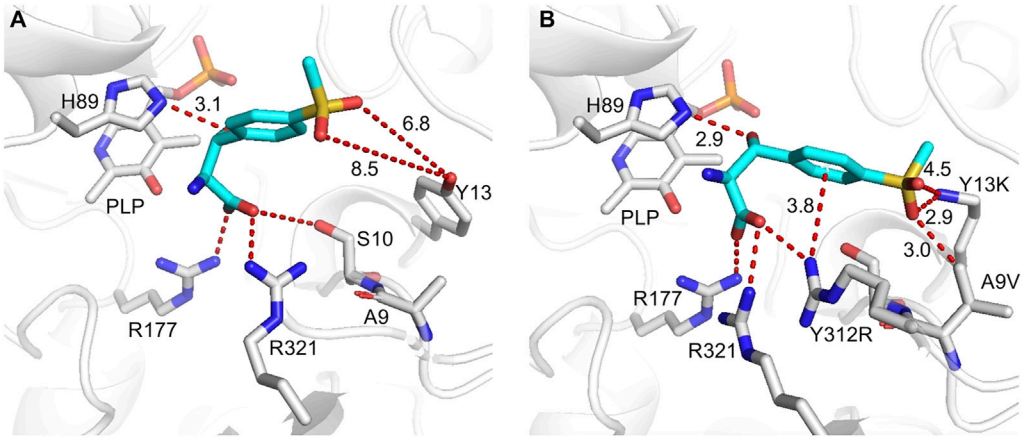

FIGURE 8
Flexible docking results of MSPS (cyan) in WT **(A)** and A9V/Y13K/Y312R **(B)**. Active sites and PLP are displayed in grey, the interactions are indicated by red dashes.

Identified beneficial mutants from saturation mutation library of five potential sites

To further improve the catalytic efficiency, an SM library of the five potential sites, A9, Y13, H133, E147, and Y312, was constructed. Thirteen positive variants, A9L, A9V, Y13C, Y13K, Y13Q, Y13R, H133N, H133Y, H133W, E147D, Y312R, Y312E, and Y312K, were obtained (Supplementary Figure S4). All variants showed a certain degree of improvement of k_{cat}/K_M values in the aldol reaction direction. The A9V, Y13K, H133N, E147D, and Y312R mutants showed higher k_{cat}/K_M values compared with the WT. Among all mutations, H133N resulted in the highest k_{cat}/K_M value (2.4-fold higher than that of the WT (Table 1), suggesting that H133N had a favorable effect on the aldol reaction. Chen et al. (2019) suspected the H133 participated in regulating the C_β stereoselectivity by adjusting protonation of the aldehyde group in the aldol reaction. Salvo et al. (2014) found that mutations of H126 in *E. coli* L-TA (corresponding to H133 in L-PpTA) had an effect on establishing or destroying the hydrogen bond between H126 and the substrate hydroxyl group. Fesko mutated H128Y in *Aeromonas jandaei* L-TA (corresponding to H133 in L-PpTA), which improved the conversion efficiency of L-β-phenylserine in the aldol addition reaction (Fesko, 2019). As complementary experiments, H133N and H133F enhanced activity in both the retro-aldol cleavage and aldol reaction directions. Other variants clearly decreased retro-aldol cleavage activity, but improved the aldol reaction activity (data not shown). These results suggested that the traditional activity assay corresponding to retro-aldol activity could not calibrate the aldol reaction activity for the biotransformation of β-hydroxy-α-amino acids.

Using WT, A9V, Y13K, H133N, E147D, and Y312R as catalysts, the MSPS conversion and diastereomeric excess (*de*) were measured by HPLC (Table 2, Fig. S5). Y312R exhibited the highest catalytic efficiency, affording a 58% conversion and 61% *de*, which were 1.8–3.6-fold higher than those of the WT. Variants A9V and Y13K achieved a conversion of 57%–61% and 50%–51% *de* in MSPS production. H133N and E147D increased the conversion to 54% and 35%, and the *de* values to 47% and 52%, representing increases of 1.1–1.7-fold and 2.8–3.1-fold compared with the WT, respectively.

Significantly improved catalytic efficiency of MSPS by combinatorial mutagenesis

To further enhance the catalytic efficiency of L-PpTA, the iterative combinatorial mutagenesis strategy was conducted on the five single mutants (A9V, Y13K, H133N, E147D, and Y312R). Three high-performing double-site combined mutants, A9V/Y13K, A9V/Y312R, and Y13K/Y312R with improved catalytic efficiency were identified (Table 2). Among them, variant Y13K/Y312R exhibited the highest catalytic efficiency, with a conversion of 61% and 79% *de*, representing 1.9-fold and 4.6-fold improvements, respectively. Furthermore, A9V/Y13K and A9V/Y312R catalyzed the synthesis of MSPS with conversion of 59%–64% and *de* values of 65%–71%, while the WT only afforded the product with a 32% conversion and 17% *de*. The other variants with double-site combined mutations, namely, A9V/H133N, A9V/E147D, Y13K/H133N, Y13K/E147D, H133N/E147D, H133N/Y312R, and E147D/Y312R improved the conversion 1.3–1.8-fold and the *de* value 2.6–3.5-fold (Supplementary Figure S5).

Among the triple-site combined mutants, A9V/Y13K/Y312R achieved the highest catalytic efficiency, which converted 100 mM MSBA and 1 M glycine to MSPS after reacted 30°C for 8 h in pH 8.0 with a conversion of 72% and 86% *de*, (Supplementary Figure S6), representing 2.3-fold and 5.1-fold improvements, respectively (Table 2).

The combined mutants involving E147D (A9V/Y13K/E147D, Y13K/H133N/E147D, Y13K/E147D/Y312R, and H133N/E147D/Y312R) did not lead to obviously enhanced efficiency, with conversion of 51%–58% and *de* values of 56%–71%. Furthermore, combination A9V/Y13K/H133N showed a conversion of 61% and 69% *de*, which were 1.9-fold and 4.1-fold higher than those of the WT, respectively. Among all combinatorial mutations, A9V/Y13K/Y312R resulted in the highest values of 86% *de* with a 72% yield, which were also higher than previously reported results (Liu Z. C. et al., 2020).

10.3389/fbioe.2023.1117890

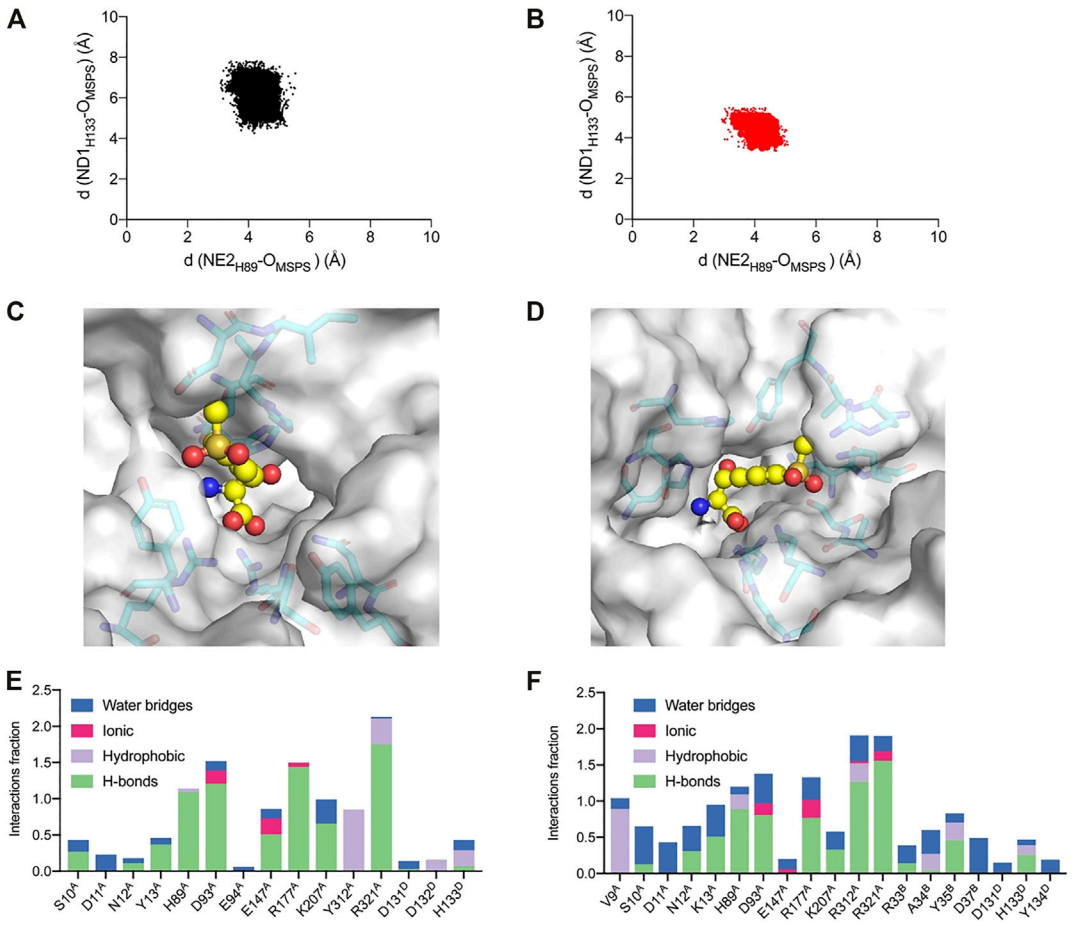

FIGURE 9
Analysis of the MD simulations. Conformation distribution of **(A)** WT and **(B)** A9V/Y13K/Y312R. The active sites adjacent to the MSPS of **(C)** WT and **(D)** A9V/Y13K/Y312R. The protein is represented as a surface in gray. The active sites are represented as sticks. The ligand MSPS is indicated by sphere. Protein interactions with the MSPS of **(E)** WT and **(F)** A9V/Y13K/Y312R. The protein-ligand interactions are categorized into four types: water bridges (blue), ionic (rosy), hydrophobic (purple) and hydrogen bonds (green).

Mechanism of improved catalytic efficiency from molecular dynamics simulations

To gain molecular insight into the enhanced catalytic efficiency produced by A9V/Y13K/Y312R mutations, the L-PpTA structure was modeled using the *P. putida* L-TA complexed structure with PLP (PDB ID: 5VYE) as a template, and product MSPS was docked into the active center of the WT and its variants. In all docked structures, a conserved H89 stack was parallel to the PLP ring, forming a π–π interaction with cofactor PLP. The distance between H89-NE2 and the hydroxyl group of MSPS was 2.9–3.1 Å, which was within hydrogen-bonding distance, suggesting that H89 acted as the catalytic base to initiate the aldol reaction (Wang et al., 2021). The carboxylate group of MSPS formed a salt bridge with the side chains of highly conserved R177, R321, and S10 (Figure 8; Supplementary Figure S7) to anchor the carboxylate of MSPS and equilibrate the transient state generated during the reaction (Salvo et al., 2014). In the WT docking conformation, the benzene ring and sulfonyl group of MSPS were free, without direct and strong anchoring forces (Figure 8A), while the A9V variant formed a powerful hydrophobic interaction between the methyl group of V9 and sulfonyl group of MSPS (Supplementary Figure S8A). The Y13K mutation in the substrate binding pocket showed a shortened distance (decreased from 6.8 to 8.5 Å to 2.8–4.7 Å) between its amino group and the two oxygen atoms of MSPS-RSO_2 (Supplementary Figure S8B). Furthermore, the Y312R mutation resulted in a newly formed π-cation interaction between the guanidine group of R312 and the benzene ring of MSPS, and a salt bridge between the guanidine group of R312 and the carboxylate group of MSPS, which enhanced their attractive charge interaction and conformation stability (Supplementary Figure S8C). In the mutant A9V/Y13K/Y312R structure model (Figure 8B), three amino acids were adjacent to the benzene ring and sulfonyl group of the ligand. Among them, K13 and R312 were polar amino acids with big side chain, which dramatically shrank the binding-pocket and enhanced the electrostatic interactions with the ligand. Simultaneously, the mutant V9 supplemented the hydrophobic interaction with the ligand. Therefore, the binding pocket was reshaped after the mutation, which would contribute to improve the catalytic efficiency.

To further explore the catalytic mechanism and interactions between protein and ligand, MD simulations were conducted using the WT and A9V/Y13K/Y312R complexed with MSPS for 50 ns. The root-mean-square deviation (RMSD) showed that the C_α and side

chains had a relatively small fluctuation range, indicating that the simulation system was stable (Fig. S9). Furthermore, the RMSD of A9V/Y13K/Y312R was lower than that of the WT, suggesting that A9V/Y13K/Y312R exhibited less structural deviation than the WT during the simulation. According to the reported mechanism, the two conserved H89 and H133 residues in L-PpTA might abstract a proton from the substrate hydroxyl group to form a C–C bond and initiate aldol reactions, providing flexibility in recognition of the C_β configuration. The $NE2_{H89}$–O_{MSPS} distance in the WT and A9V/Y13K/Y312R complexed with MSPS fluctuated in the range of 2.9–5.4 Å and 2.8–5.1 Å, respectively, while the $ND1_{H133}$–O_{MSPS} distance fluctuated at a much greater length (4.1–7.8 Å and 3.2–5.7 Å, respectively) (Figure 9). These results suggested that H89 was more likely to abstract the proton compared with H133. Furthermore, the $ND1_{H133}$–O_{MSPS} distance in A9V/Y13K/Y312R was much shorter than that in the WT, indicating that the H133 residue in the former had a strong interaction with the MSPS oxygen atom. The interactions among residue side chains and MSPS were further monitored during the MD simulations (Supplementary Figure S10). The A9V/Y13K/Y312R mutant exhibited a reshaped catalytic pocket, changing from a spacious catalytic pocket to a smaller and narrower pocket (Figure 9C; Figure 9D), which resulted in the phenyl and sulfonyl groups of MSPS being firmly anchored in the binding pocket and enhanced more interactions between enzyme and MSPS. Compared with the WT (Figure 9E), residues V9, S10, D11, N12, K13, D93, R177, R312, and R321 showed different degrees of improvement in hydrogen bonding, hydrophobic interactions, and water bridge forces in A9V/Y13K/Y312R (Figure 9F). Furthermore, R312 formed additional hydrogen bonds with the carboxylate groups of MSPS to form a π-cation interaction between the enzyme and benzene ring of MSPS (Supplementary Figure S10B). Therefore, A9V/Y13K/Y312R conferred a higher conversion and C_β-stereoselectivity toward MSPS compared with the WT.

Conclusion

To improve the efficiency of the L-PpTA-catalyzed production of MSPS using directed evolution, a simple and fast HTS screening method was constructed by calibrating the aldol reaction activity to detect substrate consumption. The error PCR technique was used to construct the mutant library and a color rendering method with DNPH to screen potential mutations was explored. Five amino acids lining the catalytic pocket were found to improve catalytic efficiency in the aldol reaction direction. Structure-guided SM and ICM were used to increase the catalytic efficiency, and variant A9V/Y13K/Y312R increased the conversion and *de* values by about 2.3-fold and 5.1-fold compared with the WT. Molecular modeling results suggested that the additional hydrogen bonds, hydrophobic interactions, and π-cation interaction between A9V/Y13K/Y312R and MSPS promoted the improved conversion and stereoselectivity. This study provides a promising method for addressing the challenge of engineering TA enzymes to efficiently prepare β-hydroxy-α-amino acids with two chiral sites by monitoring the aldol condensation activity.

Data availability statement

The datasets presented in this study can be found in online repositories. The names of the repository/repositories and accession number(s) can be found in the article/Supplementary Material.

Author contributions

LH: conducted the experiments and wrote the original draft. RZ: guided the project and edited the manuscript. WC and YX: provided advice and assistance for data analysis.

Funding

This work was supported by the National Key research and Development Program of China (2018YFA0900302), the National Science Foundation of China (32271487, 31970045), the National First-class Discipline Program of Light Industry Technology and Engineering (LITE 2018-12), the Program of Introducing Talents of Discipline to Universities (111-2-06).

Conflict of interest

The authors declare that the research was conducted in the absence of any commercial or financial relationships that could be construed as a potential conflict of interest.

Publisher's note

Supplementary material

The Supplementary Material for this article can be found online at: https://www.frontiersin.org/articles/10.3389/fbioe.2023.1117890/full#supplementary-material

References

Ali, M., Ishqi, H. M., and Husain, Q. (2020). Enzyme engineering: Reshaping the biocatalytic functions. *Biotechnol. Bioeng.* 117, 1877–1894. doi:10.1002/bit.27329

Chen, Q. J., Chen, X., Feng, J. H., Wu, Q. Q., Zhu, D. M., and Ma, Y. H. (2019). Improving and inverting C-beta-stereoselectivity of threonine aldolase via substrate-binding-guided mutagenesis and a stepwise visual screening. *Acs Catal.* 9, 4462–4469. doi:10.1021/acscatal.9b00859

Contestabile, R., Paiardini, A., Pascarella, S., Di Salvo, M. L., D'aguanno, S., and Bossa, F. (2001). L-Threonine aldolase, serine hydroxymethyltransferase and fungal alanine

racemase - a subgroup of strictly related enzymes specialized for different functions. *Euro J. Biochem.* 268, 6508–6525. doi:10.1046/j.0014-2956.2001.02606.x

Duckers, N., Baer, K., Simon, S., Groger, H., and Hummel, W. (2010). Threonine aldolases-screening, properties and applications in the synthesis of non-proteinogenic beta-hydroxy-alpha-amino acids. *Appl. Microbiol. Biotechnol.* 88, 409–424. doi:10.1007/s00253-010-2751-8

Fesko, K. (2019). Comparison of L-threonine aldolase variants in the aldol and retro-aldol reactions. *Front. Bioeng. Biotechnol.* 7, 119–130. doi:10.3389/fbioe.2019.00119

Fesko, K., Reisinger, C., Steinreiber, J., Weber, H., Schurmann, M., and Griengl, H. (2008). Four types of threonine aldolases: Similarities and differences in kinetics/thermodynamics. *J. Mol. Catal. B-Enzym* 52-53, 19–26. doi:10.1016/j.molcatb.2007.10.010

Fesko, K., Strohmeier, G. A., and Breinbauer, R. (2015). Expanding the threonine aldolase toolbox for the asymmetric synthesis of tertiary alpha-amino acids. *Appl. Microbiol. Biotechnol.* 99, 9651–9661. doi:10.1007/s00253-015-6803-y

Fesko, K., Suplatov, D., and Svedas, V. (2018). Bioinformatic analysis of the fold type I PLP-dependent enzymes reveals determinants of reaction specificity in L-threonine aldolase from *Aeromonas jandaei*. *FEBS Open Bio* 8, 1013–1028. doi:10.1002/2211-5463.12441

Fesko, K. (2016). Threonine aldolases: Perspectives in engineering and screening the enzymes with enhanced substrate and stereo specificities. *Appl. Microbiol. Biotechnol.* 100, 2579–2590. doi:10.1007/s00253-015-7218-5

Giger, L., Toscano, M. D., Bouzon, M., Marliere, P., and Hilvert, D. (2012). A novel genetic selection system for PLP-dependent threonine aldolases. *Tetrahedron* 68, 7549–7557. doi:10.1016/j.tet.2012.05.097

Hibi, M., Kasahara, T., Kawashima, T., Yajima, H., Kozono, S., Smirnov, S. V., et al. (2015). Multi-enzymatic synthesis of optically pure β-hydroxy α-amino acids. *Adv Syn Catal* 357, 767–774. doi:10.1002/adsc.201400672

Lee, J., and Goodey, N. M. (2011). Catalytic contributions from remote regions of enzyme structure. *Chem. Rev.* 111, 7595–7624. doi:10.1021/cr100042n

Li, A., Wang, T., Tian, Q., Yang, X., Yin, D., Qin, Y., et al. (2021). Single-point mutant inverts the stereoselectivity of a carbonyl reductase toward beta-ketoesters with enhanced activity. *Chemistry* 27, 6283–6294. doi:10.1002/chem.202005195

Li, L., Zhang, R., Zhou, L., Liu, Z., Xuan, K., Junchao, R., et al. (2019). Expression, characterization and thermostability improvement of low-specificity L-threonine aldolase from *Pseudomonas putida* KT2440. *Acta Microbiol. Sin.* 59, 2013–2023. doi:10.13343/j.cnki.wsxb.20180546

Liu, Y. F., Li, F. R., Zhang, X. R., Cao, G. Q., Jiang, W. X., Sun, Y. X., et al. (2014). A fast and sensitive coupled enzyme assay for the measurement of L-threonine and application to high-throughput screening of threonine-overproducing strains. *Enzym Microb. Technol.* 67, 1–7. doi:10.1016/j.enzmictec.2014.08.008

Liu, Y. F., Xu, G. C., Zhou, J. Y., Ni, J., Zhang, L., Hou, X. D., et al. (2020). Structure-guided engineering of D-carbamoylase reveals a key loop at substrate entrance tunnel. *Acs Catal.* 10, 12393–12402. doi:10.1021/acscatal.0c02942

Liu, Z. C., Chen, X., Chen, Q. J., Feng, J. H., Wang, M., Wu, Q. Q., et al. (2020). Engineering of L-threonine aldolase for the preparation of 4-(methylsulfonyl) phenylserine, an important intermediate for the synthesis of florfenicol and thiamphenicol. *Enzym Microb. Technol.* 137, 109551–109557. doi:10.1016/j.enzmictec.2020.109551

Lypetska, K., Strohmeier, G., and Breinbauer, R. (2014). Exploring the new threonine aldolases with broad donor specificity. *New Biotechnol.* 31, S87. doi:10.1016/j.nbt.2014.05.1813

Petukh, M., Dai, L. G., and Alexov, E. (2016). Saambe: Webserver to predict the charge of binding free energy caused by amino acids mutations. *Int. J. Mol. Sci.* 17, 547–557. doi:10.3390/ijms17040547

Qu, G., Li, A., Acevedo-Rocha, C. G., Sun, Z., and Reetz, M. T. (2020). The Crucial role of methodology development in directed evolution of selective enzymes. *Angew. Chem. Int. Ed. Engl.* 59, 13204–13231. doi:10.1002/anie.201901491

Reetz, M. T., Bocola, M., Carballeira, J. D., Zha, D., and Vogel, A. (2005). Expanding the range of substrate acceptance of enzymes: Combinatorial active-site saturation test. *Angew. Chem. Int. Ed. Engl.* 44, 4192–4196. doi:10.1002/anie.200500767

Salvo, M. L. D., Remesh, S. G., Vivoli, M., Ghatge, M. S., Paiardini, A., D'aguanno, S., et al. (2014). On the catalytic mechanism and stereospecificity of *Escherichia coli* L-threonine aldolase. *FEBS J.* 281, 129–145. doi:10.1111/febs.12581

Steinreiber, J., Fesko, K., Reisinger, C., Schurmann, M., Van Assema, F., Wolberg, M., et al. (2007). Threonine aldolases - an emerging tool for organic synthesis. *Tetrahedron* 63, 918–926. doi:10.1016/j.tet.2006.11.035

Wang, L. C., Xu, L., Su, B. M., Lin, W., Xu, X. Q., and Lin, J. (2021). Improving the C-beta stereoselectivity of L-threonine aldolase for the synthesis of L-*threo*-4-methylsulfonylphenylserine by modulating the substrate-binding pocket to control the rrientation of the substrate entrance. *Chem-a Euro J.* 27, 9654–9660. doi:10.1002/chem.202100752

Wu, K., Yang, Z. J., Meng, X. G., Chen, R., Huang, J. K., and Shao, L. (2020). Engineering an alcohol dehydrogenase with enhanced activity and stereoselectivity toward diaryl ketones: Reduction of steric hindrance and change of the stereocontrol element. *Catal. Sci. Technol.* 10, 1650–1660. doi:10.1039/C9CY02444A

Zhao, G. H., Li, H., Liu, W., Zhang, W. G., Zhang, F., Liu, Q., et al. (2011). Preparation of optically active beta-hydroxy-alpha-amino acid by immobilized *Escherichia coli* cells with serine hydroxymethyl transferase activity. *Amino Acids* 40, 215–220. doi:10.1007/s00726-010-0637-9

Zhao, W. Y., Yang, B. L., Zha, R. F., Zhang, Z., Tang, S. J., Pan, Y. P., et al. (2021). A recombinant L-threonine aldolase with high diastereoselectivity in the synthesis of L-*threo*-dihydroxyphenylserine. *Biochem. Engin J.* 166, 107852–107858. doi:10.1016/j.bej.2020.107852

Zheng, G. W., Liu, Y. Y., Chen, Q., Huang, L., Yu, H. L., Lou, W. Y., et al. (2017). Preparation of structurally diverse chiral alcohols by engineering ketoreductase CgKR1. *Acs Catal.* 7, 7174–7181. doi:10.1021/acscatal.7b01933

Zheng, W. L., Chen, K. T., Wang, Z., Cheng, X. L., Xu, G., Yang, L. R., et al. (2020). Construction of a highly diastereoselective aldol reaction system with L-threonine aldolase by computer-assisted rational molecular modification and medium engineering. *Org. Lett.* 22, 5763–5767. doi:10.1021/acs.orglett.0c01792

Frontiers in
Bioengineering and Biotechnology

Accelerates the development of therapies, devices, and technologies to improve our lives

A multidisciplinary journal that accelerates the development of biological therapies, devices, processes and technologies to improve our lives by bridging the gap between discoveries and their application.

Discover the latest Research Topics

See more →

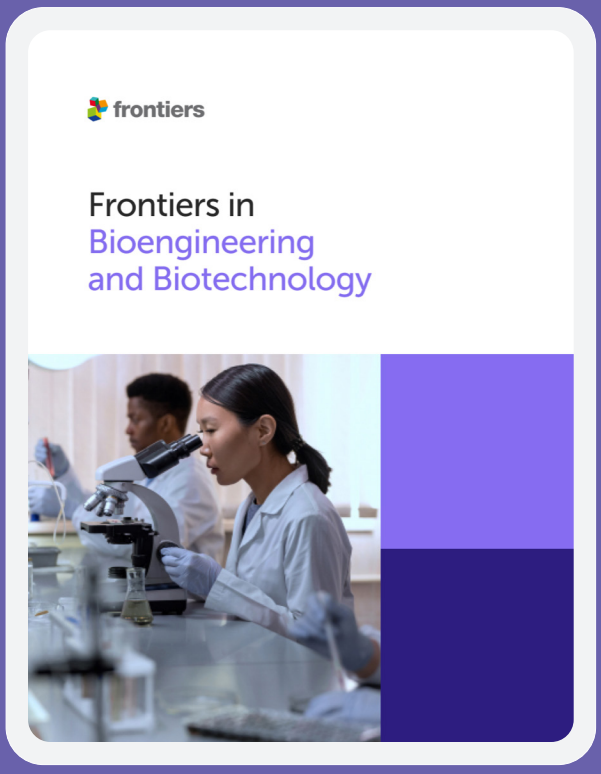

Frontiers

Avenue du Tribunal-Fédéral 34
1005 Lausanne, Switzerland
frontiersin.org

Contact us

+41 (0)21 510 17 00
frontiersin.org/about/contact